DEVELOPMENT AND IMPLEMENTATION OF SOME CONTROLLERS FOR PERFORMANCE ENHANCEMENT AND EFFECTIVE UTILIZATION OF INDUCTION MOTOR DRIVE

RABI NARAYAN MISHRA

July 2018

Department of Electrical Engineering

National Institute of Technology Rourkela

Rourkela-769008, INDIA

DEVELOPMENT AND IMPLEMENTATION OF SOME CONTROLLERS FOR PERFORMANCE ENHANCEMENT AND EFFECTIVE UTILIZATION OF INDUCTION MOTOR DRIVE

Dissertation submitted

in partial fulfillment of the requirements

for the degree of

Doctor of Philosophy

in

Electrical Engineering

by

Rabi Narayan Mishra

(Roll Number: 514EE7020)

Under the supervision of

Prof. Kanungo Barada Mohanty

July 2018

Department of Electrical Engineering

National Institute of Technology Rourkela

Rourkela-769008, INDIA

Electrical Engineering

National Institute of Technology Rourkela

July 2018

Certificate of Examination

Roll Number: 514EE7020

Name: Rabi Narayan Mishra

Title of Dissertation: Development and implementation of some controllers for performance enhancement and effective utilization of induction motor drive

We the below signed, after checking the dissertation mentioned above and the official record book(s) of the student, hereby state our approval of the dissertation submitted in partial fulfillment of the requirements of the degree of Doctor of Philosophy in Electrical Engineering at National Institute of Technology Rourkela. We are satisfied with the volume, quality, correctness, and originality of the work.

Kanungo Barada Mohanty

Principal Supervisor

S. Gopalakrishna

Member (DSC)

Monalisa Patnaik

Member (DSC)

S. Ari

Member (DSC)

Examiner

Anup Kumar Panda

Chairman (DSC)

Electrical Engineering

National Institute of Technology Rourkela

Dr. Kanungo Barada Mohanty

Professor

July 2018

Supervisor's Certificate

This is to certify that the work presented in this dissertation entitled "*Development and implementation of some controllers for performance enhancement and effective utilization of induction motor drive*" by "*Rabi Narayan Mishra*", Roll Number: 514EE7020, is a record of original research carried out by him under my supervision and guidance in partial fulfilment of the requirements of the degree of *Doctor of Philosophy* in *Electrical Engineering*. Neither this dissertation nor any part of it has been submitted for any degree or diploma to any institute or university in India or abroad.

Prof. Kanungo Barada Mohanty

Dedicated

to

My Family Members

and

Well-Wishers

...Rabi Narayan Mishra

Declaration of Originality

I, Rabi Narayan Mishra, Roll Number 514EE7020 hereby declare that this dissertation entitled "*Development and implementation of some controllers for performance enhancement and effective utilization of induction motor drive*" represents my original work carried out as a doctoral student of NIT Rourkela and, to the best of my knowledge, it contains no material previously published or written by another person, nor any material presented for the award of any other degree or diploma of NIT Rourkela or any other institution. Any contribution made to this research by others, with whom I have worked at NIT Rourkela or elsewhere, is explicitly acknowledged in the dissertation. The works of other authors cited in this dissertation have been duly acknowledged under the Section "References". I have also submitted my original research records to the doctoral scrutiny committee for evaluation of my dissertation.

I am fully aware that in case of any non-compliance detected in the future, the Senate of NIT Rourkela may withdraw the degree awarded to me on the basis of the present dissertation.

July 2018

NIT Rourkela *Rabi Narayan Mishra*

Acknowledgement

First and foremost, I would like to convey my deep sense of gratitude to Prof. Kanungo Barada Mohanty, Department of Electrical Engineering for accepting me as a student in the Power Electronics and Drives group and suggesting me the research topic. I am deeply indebted for his continuous support and encouragement given throughout the research work. I consider myself fortunate to have worked under his guidance. I am indebted to him for providing all official and laboratory facilities. I look at him with great respect for his profound knowledge and relentless pursuit for perfection.

I am grateful to the Director, Prof. A. Biswas, Ex-Director, Prof. S. K. Sarangi, and Prof. J. K. Satpathy, Head of Electrical Engineering Department, National Institute of Technology Rourkela, for their kind support and concern regarding my academic requirements.

I gratefully thank my Doctoral Scrutiny Committee members, Prof. Anup Kumar Panda, Prof. S. Gopala Krishna, Prof. Monalisa Pattnaik, and Prof. Samit Ari for their valuable suggestions and contributions to this dissertation. I express my thankfulness to the faculty and staff members of the Electrical Engineering Department for their continuous encouragement and suggestions.

I gratefully acknowledge Prof. Anup Kumar Panda**,** the Ex-Head of the Department, for his gentle and supportive attitude and providing all possible facilities in the Power Electronics and Drive laboratory while pursuing the research work.

Specifically, I wish to express my sincere gratitude to Prof. Kanungo Barada Mohanty for all the help, encouragement, and generous support, particularly at my hard times. His guidance and insight encouraged me to proceed with confidence towards publishing in the reputed journals of this field.

I extend my sincere gratitude to the reviewers and editors of various journals for their valuable comments and suggestions for publishing paper, which encouraged me to carry out the research work in a proper direction.

I also wish to record my sincere thanks to Silicon Institute of Technology, Bhubaneswar for granting me leave under QIP scheme and providing constant financial support to carry out this work at National Institute of Technology Rourkela.

I am especially indebted to all my research colleagues and friends in the power electronics group Mr. Kishor Thakre, Mr. Ashwini Kumar Nayak, Ms. Aditi Chatterjee, Mr. K. Vinay Sagar, Ms. Jyotismita, Mr. Nishant Patnaik, Ms. Ranjeeta Patel, Mr. Pratap, Mr. Trilochan,

Mr Asis, Mr. Amit Kumar, Mr. Shiva Kumar for their help and support in different form throughout my research work.

My thanks are also due to the Laboratory staff Mr. Rabindra Nayak, Mr. Rama Prasad Samantaray, and Mr. Rama Hari Swain for their kind cooperation during this research work.

It would have been impossible to achieve anything without the blessings of my parents, parents-in-law, uncle, and aunty. I express my deep sense of gratitude and reverence to my beloved father Sri. Srikanta Mishra, mother Smt. Shantilata Mishra. My special thanks to my brothers-in-law and sisters who took care of my parents during my absence and supported and encouraged me a lot, no matter what difficulties I confronted. I would like to express my greatest admiration to all my family members and relatives for their positive encouragement that they showered on me throughout this research work. This research work would not have been possible without my family's sacrifice and support.

I especially thank my wife Sagarika Mishra for her support, encouragement, patience and unwavering love, provided strength to make my dream come true. I also do not forget to acknowledge my adorable little son Ram who always made me smile and relax whenever I got depressed during my work. It is a great pleasure for me to acknowledge and express my appreciation to all my well-wishers for their understanding, relentless supports, and encouragement during my research work.

Last but not the least, I wish to express my sincere thanks to all those who helped me directly or indirectly at various stages of my work and above all, I would like to thank The Almighty God for the wisdom and perseverance that has been bestowed upon me during this research work, and indeed, throughout my life.

July 2018 *Rabi Narayan Mishra*

NIT Rourkela Roll Number: 514EE7020

Contents

Abstract

The technological development in the field of power electronics and DSP technology is rapidly changing the aspect of drive technology. Implementations of advanced control strategies like field oriented control, linearization control, etc. to AC drives with variable voltage, and variable frequency source is possible because of the advent of high modulating frequency PWM inverters. The modeling complexity in the drive system and the subsequent requirement for modern control algorithms are being easily taken care by high computational power, low-cost DSP controllers. The present work is directed to study, design, development, and implementation of various controllers and their comparative evaluations to identify the proper controller for high-performance induction motor (IM) drives.

The dynamic modeling for decoupling control of IM is developed by making the flux and torque decoupled. The simulation is carried out in the stationary reference frame with linearized control based on state-space linearization technique. Further, comprehensive and systematic design procedures are derived to tune the PI controllers for both electrical and mechanical subsystems. However, the PI-controller performance is not satisfactory under various disturbances and system uncertainties. Also, precise mathematical model, gain values, and continuous tuning are required for the controller design to obtain high performance. Thus, to overcome these drawbacks, an adapted control strategy based on Adaptive Neuro-Fuzzy Inference System (ANFIS) based controller is developed and implemented in real-time to validate different control strategies. The superiority of the proposed controller is analyzed and is contrasted with the conventional PI controller-based linearized IM drive.

The simplified neuro-fuzzy control (NFC) integrates the concept of fuzzy logic and neural network structure like conventional NFC, but it has the advantages of simplicity and improved computational efficiency over conventional NFC as the single input introduced here is an error instead of two inputs error and change in error as in conventional NFC. This structure makes the proposed NFC robust and simple as compared to conventional NFC and thus, can be easily applied to real-time industrial applications. The proposed system incorporated with different control methods is also validated with extensive experimental results using DSP2812. The effectiveness of the proposed method using feedback linearization of IM drive is investigated in simulation as well as in experiment with different working modes. It is evident from the comparative results that the system performance is not

deteriorated using proposed simplified NFC as compared to the conventional NFC, rather it shows superior performance over PI-controller-based drive.

A hybrid fuel cell (FC) supply system to deliver the power demanded by the feedback linearization (FBL) based IM drive is designed and implemented. The modified simple hybrid neuro-fuzzy sliding-mode control (NFSMC) incorporated with the intuitive FBL substantially reduces torque chattering and improves speed response, giving optimal drive performance under system uncertainties and disturbances. This novel technique also has the benefit of reduced computational burden over conventional NFSMC and thus, suitable for real-time industrial applications. The parameters of the modified NFC is tuned by an adaptive mechanism based on sliding-mode control (SMC). A FC stack with a dc/dc boost converter is considered here as a separate external source during interruption of main supply for maintaining the supply to the motor drive control through the inverter, thereby reducing the burden and average rating of the inverter. A rechargeable battery used as an energy storage supplements the FC during different operating conditions of the drive system. The effectiveness of the proposed method using FC-based linearized IM drive is investigated in simulation, and the efficacy of the proposed controller is validated in real-time. It is evident from the results that the system provides optimal dynamic performance in terms of ripples, overshoot, and settling time responses and is robust in terms of parameters variation and external load.

Keywords*: *Induction motor drive; Feedback linearization; ANFIS controller; Simplified neuro-fuzzy control; Neuro-fuzzy sliding-mode control; Fuel cell.

List of Symbols

B	Rotor friction coefficient
C_{dc}	DC link capacitance
$D(x)$	Decoupling matrix
d-q	Direct axis and quadrature axis stationary (stator oriented) reference frame
E_{oc}	Fuel cell stack open circuit voltage
$e(t)$	Error signal
$\Delta e(t)$	Change in error signal
G_{ol1}	Open loop gain for the electrical subsystem
$G_{PI1}(S)$	Transfer function of PI-flux controller
$G_{f1}(S)$	Transfer function of the feed-forward path for the electrical subsystem
$G_{cl1}(S)$	Closed-loop transfer function for the electrical subsystem
$G_{ol2}(S)$	Open-loop transfer function for the mechanical subsystem
$G_{PI2}(S)$	Transfer function of PI-speed controller
$G_{f1}(S)$	Transfer function of the feed-forward path for the mechanical subsystem
$G_{cl2}(S)$	Closed-loop transfer function for the mechanical subsystem
i_a,i_b,i_c	Three-phase stator current
i_a^*, i_b^*, and i_c^*	Motor reference currents
i_{ds}, i_{qs}	Stator current space vector components in d-q stationary reference frame
i_{dr}, i_{qr}	Rotor current space vector components in d-q stationary reference frame
i_{fc}	Fuel cell stack output current
i_o	Fuel cell exchange current
J	Rotor inertia coefficient
K_i	Integral gain
K_p	Proportional gain
K_T	Torque constant
k	Sampling instant
$k_{\omega r}$	Uncertain speed dynamics
$\hat{k}_{\omega r}$	Estimated dynamics of the uncertainties
L_m	Magnetizing inductance
L_r	Rotor self-inductance

L_s	Stator self-inductance
M_{1i} and M_{2i}	Antecedent fuzzy sets for i^{th} rule
m	No of rows for input control vector
m_{1i}, m_{2i}, and r_i	Design parameters for i^{th} rule
N	Number of cells in the fuel cell stack
n	No of rows for state vector
O_i	Output corresponding to the i^{th} node number and superscript (1, 2, 3) denotes the number of layers
P	Number of pole pairs
p	Differential operator $\frac{d}{dt}$
R_{br}	Braking resistance
R_s ,R_r	Stator and rotor resistances per phase
R_{int}	Fuel cell internal resistance
r	Relative degree of the system
S	Sliding surface
S_1, S_2, and S_3	Switching signals
T	Sampling time
T_e	Motor electromagnetic torque
T_l	Load torque
T_r	Rotor time constant
T_{rf}	Flux time constant
T_{rs}	Mechanical time constant
$\hat{u}$	Estimated input control vector
V_a, V_b, V_c	Three-phase stator voltage
V_{act}	Activation voltage
V_{cell}	Actual operating voltage of the single cell
V_{dc}	DC link voltage
V_{ds}, V_{qs}	Stator voltage space vector components in *d-q* stationary reference frame
V_{dr}, V_{qr}	Rotor voltage space vector components in *d-q* stationary reference frame
V_{fc}	Fuel cell stack output voltage
v_i	Output singleton membership functions (MFs) for i^{th} rule
V_{sh}	Shutdown voltage
w_i	Firing strength (weight) of rules

$\overline{w_i}$	Normalized firing strength
X	State vector matrix
x_i^1	Input corresponding to the i^{th} node of the first layer
Y	Output control vector
ψ_r	Rotor flux
ψ_r^*	Reference rotor flux
ψ_{ds}, ψ_{qs}	Stator flux linkage space vector components in *d-q* stationary reference frame
ψ_{dr}, ψ_{qr}	Rotor flux linkage space vector components in *d-q* stationary reference frame
ω_n	Natural frequency of oscillation
ω_0	Cut-off frequency
ω_r	Rotor mechanical speed in rad/s
ω_r^*	Reference/target speed
σ	Leakage coefficient
ξ	Damping factor
μ	MF value
(η_{ai}, η_{bi}, η_{wi})	Fixed learning rate of corresponding parameters (a_i, b_i, w_i)
(∇_{ai}, ∇_{bi}, ∇_{wi})	Gradient of cost function E corresponding to parameters (a_i, b_i, w_i)
$\lambda_{\omega r}$	Design parameters for sliding-mode control (SMC)
$\beta_{\omega r}$	Switching control gain
$\beta_{\omega r}\,\mathrm{sgn}(S)$	corrective switching control gain
$\eta_{\omega r}$	Positive constant which controls the convergence speed to the SMC
$\phi_{\omega r}$	Boundary layer thickness around the sliding surface
η_{fc}	Nominal efficiency of the fuel cell stack

List of Abbreviations

A/D	Analog to Digital Converter
ANN	Artificial Neural Network
ANFIS	Adaptive Neuro-Fuzzy Inference System
D/A	Digital to Analog Converter
DSP	Digital Signal Processor
DTC	Direct Torque Control
ESS	Energy Storage System
FOC	Field Oriented Control
FBL	Feedback Linearization
FLC	Fuzzy logic control
FSMC	Fuzzy Sliding-Mode Control
IM	Induction Motor
IGBT	Insulated-Gate Bipolar Transistor
ITAE	Integral Time Absolute Error
LHV	Low Heating Value
MRAS	Model Reference Adaptive System
MF	Membership Functions
MSE	Mean Square Error
NN	Neural Network
NFSMC	Neuro-Fuzzy Sliding-Mode Control
PWM	Pulse Width Modulation
PEM	Proton Exchange Membrane
RNFN	Recurrent Neuro-Fuzzy Network
SISO	Single Input Single Output
SMC	Sliding-Mode control
THD	Total Harmonic Distortion
VSI	Voltage Source Inverter

List of Figures

List of Tables

Chapter 1

INTRODUCTION

CHAPTER-1

INTRODUCTION

1.1 Research Background

Nowadays industrial requirements are high precision and high-performance drives for better products in terms of good quality with minimal effort, low cost, and less maintenance. Implementations of converter fed DC motors with simple controller structure had evolved as the traditional selection for high-performance and most industrial applications. But, there were several drawbacks due to commutation problem, bulky structure, and high maintenance cost. Additionally, DC motors have the disadvantages of low torque-to-weight ratio and reduced unity capacity. There is a great revolution in AC drives, especially induction motor (IM) drives which have been the vital part of industrial drives because of their robust and simple structure, compactness, low inertia, low cost, high efficiency, higher reliability, and suitability for use in volatile environment with less maintenance. However, their control approaches are quite complex because of coupling effect due to nonlinear dynamics and parameter sensitivity under various working modes. On the other hand, in DC motors, the control of torque and flux is done independently by inherent decoupling of armature and field currents. In IM, the space angle between rotating stator field and rotor field changes with different load resulting in a complex control strategy, whereas this does not happen in the DC motor as the stationary field winding and the commutator-brush position decides the orientation of field mmf and armature mmf. The IM dynamics can be made equivalent to that of DC motors by controlling the flux producing and torque producing components of the stator current independently. This becomes possible by the rapid technological development of power semiconductor devices mostly IGBT, digital signal processor (DSP), and VLSI technology. This has led to a cost economic power electronic control method, application of microprocessor technology, implementation of modern control theory approach, etc. The real-time implementations of modern control approach have been tremendous interest area of the researchers for performance enhancement of the AC drive system with different controllers such as fuzzy logic, neural network, backstepping approach, model reference adaptive system (MRAS), sliding-mode control, and neuro-fuzzy sliding-

mode control. In the present dissertation, an attempt has been made for a comprehensive and systematic study, development, and implementation of some controllers for IM drive and their comparative performance analysis with simulation as well as real-time implementation.

1.2 Literature Survey

With the rapid technological development in design and fabrication of semiconductor devices and microelectronics, the initial investigation works on IM drive have been initiated long before [1]. Many investigations have been reported by the researchers to enhance the performance of the inverter-fed IM drive. The revolution of the semiconductor switching devices-based power electronic circuits and DSP technology make it easy for implementation of complex control approach for IM drive. Over the years, extensive research has been going on to update the IM drive system performance using various controllers which details are described in the literature survey.

The promising implementation of nonlinear control [2] in the IM drive has been evolving as an emerging area of investigation work. The industrial standards for implementation of high-performance adjustable speed drive need extensive torque ripple minimization, fast dynamic response, good load disturbance rejection, working under different modes of operations, and insensitivity to parameter variations and plant uncertainties [3], [4]. IMs have been broadly utilized for industrial purpose because of their simple and robust structure, rugged, least cost, higher reliability, suitability to work in a hazardous environment, and they are essentially maintenance free. However, it includes complex control approach as it has three unavoidable disadvantages [4]. (a) It has nonlinear dynamics with higher order mathematical equations, (b) Inaccessible rotor quantities, and (c) Parameters uncertainties like variations of rotor resistance and inductance under different operating modes.

Many attempts have been made earlier to upgrade the performance of IM drive control strategy through different control techniques like field oriented control (FOC) by Hasse and Blaschke [4], [5]. FOC is a very popular method and in fact, has a tremendous impact on industrial applications by replacing costly, heavy DC motor drive. But, FOC methods require coordinate transformations and the implementation of controllers are very difficult as the decoupling behavior is obtained by proper state coordinates selection and only under the assumption of constant rotor flux. This leads to asymptotically decoupling of rotor flux and torque, i.e., decoupling is achieved in steady-state. Further, the decoupling behavior is not completely obtained in the higher speed zone when the flux is weakened or when flux varies

to achieve maximum efficiency [6]-[8]. The several robust control schemes like variable structure control, feedback linearization (FBL) are also discussed broadly in the area of power electronics and drives [9]-[14]. However, from a theoretical perspective, other coordinates can be chosen to obtain decoupling and linearization equations of the IM. This has led to nonlinear differential geometric control theory which develops the control strategies for the decoupling linearized control [9], [15]-[17].

Many investigations based on feedback linearized decoupling control have been reported in past few decades [6]-[8], [18]-[34]. The differential geometric control approach recommended by Krezminski in [18] is based on a new multi-scalar motor model where static state feedback controller decouples the rotor torque and flux completely by selecting new state variables which are different than that of FOC. However, there was no experimental analysis conducted and reported in this regard. Further, the system response in terms of variations of rotor resistance was not considered, and the design procedure of controllers for the linearized drive is not properly explained. De Luca in [35] implemented first time the dynamic state feedback control concept in the IM, where the electrical dynamics of IM was made fully linearized by considering rotor speed as a constant parameter. Again, in [20], it was shown that IM dynamics could be made input-output linearized and stable zero dynamics were possible as indicated by the simulation.

In the articles [29], [30], [36], [21]-[27], it was depicted that systems with multi-input can be made static feedback linearizable from input to state when an extra integrator is introduced to one of the inputs. An adaptive nonlinear decoupling feedback input-output linearizing control for both electrical and mechanical dynamics of IM drive was modeled in [25]. Here, the magnetic circuit of IM is assumed to be linear, and rotor resistance and load torque are considered to be unknown fixed parameters. Also, a nonlinear identification technique in the control algorithm follows the actual load torque and rotor resistance asymptotically which is presented in this article. The power efficiency without altering the speed regulation is improved by performing control task of decoupling of rotor speed and flux. However, the main drawback associated with this controller is to measure all the state of the system. The approach of adding an integrator is considered in [29], where IM model is made static feedback linearizable by converting fifth order IM state-space model to a sixth order model. Here, the fifth order IM state space-model is considered in *a-b* coordinate system where two stator voltages are considered as inputs and two stator currents, two rotor fluxes, and speed are considered as state variables. However, this had certain constraints that make feedback

linearization dynamically infeasible. These are (1) if the motor torque is zero, feedback linearizing transformation is singular, (2) to avoid this singularity, the control structure needs to be switched between two distinct transformations, and (3) computational prohibition of the required coordinate transformations and cancellation of feedback. So, to overcome this in [30], a single dynamic feedback linearization and controller are proposed where the issue of singularity can be easily avoided, and there is no computational prohibition as the required computations are well within the limits of contemporary microprocessor technology. The main concept behind this is consideration of IM in the *d-q* coordinate system instead of *a-b* coordinates. Here, one control quantity is transformed into two linearization schemes. However, the dynamic controller is quite complex to implement, and large computations are required for the feedback cancellations. Further, the proposed feedback linearization controller loses its property, when an integrator is introduced in the *q*- axis instead of *d*-axis and position as a state variable is included in the model. In [31], [32], partial state feedback of IM is presented with a globally stable controller. The response obtained here is under the assumption that the parameters of IM are known and that both the command and load torques are constant. The machine dynamics shown here is of fifth-order state-space model in the stationary *d-q* reference frame and is dynamic feedback linearizable. In [11], [37], the decoupling of torque and flux control of current controlled induction motor is obtained by two nonlinear feedback controllers. This is mainly based on input-output linearization of the nonlinear system through dynamic state feedback control.

In [38], for another type of machine like switched reluctance motors; feedback linearization approach is successfully developed for robot manipulators. In [39]-[46], the linearizing theory is implemented for synchronous motor drives. A linearized model of IM based on input-output feedback linearization technique is used in [34], where the torque and flux loops are decoupled. The required transient, as well as steady-state response, are achieved by state feedback controllers which are designed for feedback linearization using pole placement method.

1.2.1 Requirement of Robust Control Technique

The linearization technique based FBL is a nonlinear approach where it uses a nonlinear change of system variables to another appropriate coordinate system that facilitates equivalent linear system, and thus, it simplifies the controller design. The FBL IM drive effectively sorted out the problem of coupling, causing a quick dynamic response. But, they are very much sensitive to modeling errors, parameter uncertainties, and external

disturbances. The detuning of rotor parameters reduces the motor efficiency owing to the reduction of torque producing capacity and the magnetic saturation because of overexcitation. This led to the incorporation of different controllers in the IM drive. In traditional control systems, the precise and accurate control of system largely depends on the system or plant modeling, which is generally complex, affected by parameter variations, and based various assumptions for simplicity purpose. This leads to inaccuracies in the system model. Traditionally, the PI and PID controllers of fixed gain type and their adaptive versions have been broadly proposed for motor drives. Conclusively, the model-based controllers like a PI-controller incorporated with the IM drive have the disadvantages of steady-state ripple, parametric uncertainties, and load perturbation leading to weak decoupling of flux and torque and poor dynamic response [47]-[51]. In, [11], one control quantity is transformed into two linearization schemes. Further, in [52], the control performance may degrade due to perturbations, detuning parameters, and measurement error, which are observed from the sensitivity analysis. To deal with these problems, variable structure control techniques like sliding-mode control (SMC) [53], fuzzy logic control [54], and hybrid neuro-fuzzy control [55], [56] are used over the years. SMC technique has been applied effectively in the IM drives, which exhibits robust performance with the system uncertainties and outer disturbances [42], [57]-[59]. SMC has the main advantage of switching control law that ensures the stability of the system [61]. In later stage, SMC in conjunction with various adaptive controls is reported to be better control technique in many literatures [62]-[71]. However, the main disadvantage in SMC is the chattering effect in control variables due to switching control law which is introduced in the system steady-state. Further, it may be observed that this chattering effect added with the chattering phenomena occurred naturally due to the presence of PWM switching in real-time implementation leads to high stress for the system to be controlled. These issues can be fixed by applying intelligent control approaches as the controllers are constructed using human experience while handling the IM in every working mode and thereby, making the system robust and independent of system model [71]-[76].

Fuzzy logic control (FLC) [77], [78], can handle the plant uncertainties and deviations of system parameter well, but it has the issue of instability, uncertainty, and optimal fuzzy logic control cannot be figured out by trial and error. The FLC used for adjustable speed drive requires membership functions (MFs) of asymmetric type, i.e., adjusted manually by trial and error if the optimal system performance is needed [47], [76], [79], [80]. On the other hand,

acquisition of training data for a neural network (NN) to handle every working mode of IM drive is a tough task [73], [74]. Thus, to overcome these drawbacks, the hybrid neuro-fuzzy control (NFC) systems have been implemented for IM drive [76], [81]-[83]. The adaptive neuro-fuzzy hybrid intelligent system builds up a more effective system, which overcomes the drawbacks of FLC and NN and generates optimized rules for the controller [75], [76] [84]. However, many industries are still reluctant to implement this controller for the commercial drive as it has more computational burden due to a large number of MFs, rules, especially on auto-tuning condition [75], [83]. Low sampling frequency due to this high computational burden leads to greater torque ripple, which is not acceptable for real-time industrial applications. A quick processor may be required for this high computational control algorithms, which may be a costly affair and another concern for industries. In [75], the NFC uses only three MFs for two inputs, and no MFs are used at the output side to reduce the computational burden and thus, suitable for industrial applications. Further, with the knowledge of control requirements of motor and intelligent control algorithms, an improved auto-tuning method is introduced here for this proposed NFC. Based on the back-propagation algorithm, only parameters of output layer are online updated in order to minimize the error square and reduce the computational burden. As less number of input MFs have to be chosen, minimum trial and error is required to design the proposed NFC. However, the computational burden is kept at a reasonable level by online tuning of weights only. But, the MFs are not tuned, and adjusted by trial and error method in the simulation.

1.2.1.1 Neuro-Fuzzy Control Technique based Controller

Over the years, researchers and scientists have done extensive research on different control theories and techniques. Intelligent control techniques are some of those adaptive, robust, and versatile control techniques, and generally considered as the aggregation of fuzzy logic control, neural network control, genetic algorithm, and expert system, which have performed certain superior control tasks [86]. By using low-cost efficient microprocessor, it is possible to implement such intelligent controllers. However, both fuzzy logic and neural network have their own merits and demerits, which can not be overlooked. In recent years, the approach of incorporating fuzzy logic into the neural network has been evolving into a highly adopted research field [87], [88]. As compared to individual fuzzy network and neural network system, the fuzzy-neural network system consists of both of their advantages, i.e., it integrates the fuzzy reasoning capability with its transparent linguistic representation in

handling the information that has uncertainty [89] and the ability of neural network in process learning system [90]. It has been proven that the neuro-fuzzy hybrid system to build more powerful intelligent technique in the area of system control with improved design and performance features, particularly in the control design, which is model-free [87], [88]. The choice of training algorithm of neuro-fuzzy network plays a key role for many neuro-fuzzy implementations. The sensitivity of the system to be controlled requires online training process in the conventional gradient descent algorithm [91], [92]. However, it is very tough to acquire data from highly nonlinear or unknown dynamics of the system. Also, the stability of the system is a latent issue to be encountered [93]. Although many fuzzy neural network concepts have been verified by Lyapunov stability theorem for ensuring the control system stability [94]-[100], it is necessary to satisfy some limiting conditions, and large computation burden and prior knowledge about the system to be controlled may be required. It is very hard to meet those requirements in real-time control applications. For example, an adaptive robust neuro-fuzzy controller was investigated in [98]. The neuro-fuzzy inference system based error compensator attenuates the impact of modeling errors, external perturbations, and unmodeled system dynamics on the tracking error. However, some constraints still exist in this complex system. A control system based on hybrid recurrent neuro-fuzzy network (RNFN) for a linear induction motor servo drive is proposed in [99]. In this scheme, the main tracking controller RNFN is tuned to adapt suitable control rules, and the compensated controller is designed to compensate the error between the control laws and the RNFN controller. However, the position of a simplified second-order dynamic model of linear IM is dealt here with the assumption of field orientation. The implementation of a hybrid neuro-fuzzy in a motor-toggle servomechanism is explained in [100], where a proper tracking could be offered for this nonlinear mechanism. But, a compensated controller is still needed to track the system trajectory in a stable region. In real practice, a comprehensive control design methodology with simple inference system is required to guarantee the robustness and stability of the overall system configuration. Further, in [101], the concept of Petri net incorporated into a classical fuzzy neural network to construct a robust Petri fuzzy neural network control system for the linear IM drive control. This reduces the computational burden of the classical fuzzy neural technique [91]-[93]. Here, the stability of the control system can be ensured without auxiliary controllers compensation and system information.

Over the last few decades, various works on implementations of neuro-fuzzy controller for adjustable speed drives like interior permanent magnet synchronous motor drive, brush-less

drive, IM drive, etc., [74], [102]-[105] have been reported by the researchers. In [81], a novel, simple direct-torque NFC scheme is implemented for PWM fed IM drive, which provides high performance decoupled flux and torque control of IM drive. It has been demonstrated that the behavior of simple direct-torque NFC is improved in terms of rapid torque and flux response, speed operation at lower range, and simple tuning capability. A Sugeno type fuzzy neural network controller is proposed for position control of vector controlled IM drive in [55], where the fuzzy neural network controller behaves like a robust nonlinear IP controller. In [106], the implementation of adaptive neuro-fuzzy inference based angular rotor speed estimator to vector or scalar drives is presented. In [101], a robust Petri-fuzzy-neural network control system is performed based on the design of model-free control in order to retain the decoupling controlled behavior of the feedback linearized IM drive for high-performance applications. An adaptive neuro-fuzzy control for IM drive based on model reference adaptive flux observer is presented in [107]. A novel NFC for speed control of IM is presented in [75]. The main objective of this paper is to increase the computational efficiency by introducing low computational burdened NFC for performance enhancement of the indirect field oriented control IM drive. Thus, this can be easily implemented for real-time applications. Further, an improved intelligent self-tuning algorithm for NFC is developed here for high-performance drive applications. In [108], a modified self-tuned NFC for direct torque control of IM drive is used to achieve high dynamic performance, and hysteresis band limits for torque controller are adjusted online to minimize the torque ripple.

1.2.1.2 Sliding-Mode Technique based Controller

Sliding-mode control (SMC) is a suitable robust control technique for a particular type of nonlinear system [2], [109]. This control method is applied to the control mechanism with system uncertainties, modeling errors, and external perturbations provided that the absolute values of upper bounds are known. Some system uncertainties like unknown parameters or selection of simplified system dynamics may give rise to modeling errors. SMC is useful for certain type of systems, and it gives satisfactory execution in terms of modeling imperfections and a proper way to maintain the stability of the system. SMC is particularly suitable for the tracking performance of the robot manipulators and motor drives, where variable mechanical loads are frequently applied.

The control mechanism based on the sliding-mode concept is not restricted to giving satisfactory performances to only step input, which is considered as one of the major strength

whereas, fixed control gain is a major weakness of SMC. The computation of control algorithm for SMC is simple compared to the adaptive controllers. It also has robustness with deviation of plant parameters. On the other side, the disadvantage associated with the SMC is the chattering introduced in system state variables because of sudden variations of the control variable.

Implementations of SMC to IM drive have been proposed by Utkin [110] and Soto and Yeung [111]. A novel switching surface based SMC for speed control of IM drive is presented in [112], where the stability is ensured with this switching surface. Further, resistant to external disturbances, and plant and system uncertainties are achieved using the switching control surface of SMC. In [113], the sliding-mode approach is applied to position control of indirect field oriented controlled IM. A variable structured controller with the discrete integral concept is presented in [114] to obtain zero steady-state error and to enhance the robustness of the system. Based on the IM dynamics in the synchronously rotating reference frame, an SMC method is proposed in [113]. An adaptive input-output linearizing concept with the sliding-mode approach is presented in [115] for IM drives, where the flux and speed are independently controlled by SMC with variable switching gains. In [116], the nonlinear SMC using state coordinate transformations with torque and flux dynamics is modeled to follow a reference linear model. In [42], a robust SMC is proposed as the exact input-output feedback linearization technique based rectifier/inverter fed IM drive is sensitive to the system parametric uncertainties. By this method, the DC link voltage is not affected by the impact of load. Consequently, DC link voltage profile could be stabilized with a small size DC link capacitor. Apart from IM drive, SMC incorporated with the feedback linearization concept has been successfully applied in other type of AC machines like synchronous wind turbines, permanent magnet synchronous machines, etc. including different power electronics applications such as active filter, synchronous buck converter, etc. [14], [117]-[119]. In [58], a new concept of feedback linearization approach is proposed where two states: stator flux and torque of linear IM model are perfectly decoupled. This intuitive linearization model is successfully proposed in a direct torque control (DTC) type controller, which preserves all the advantages of the conventional DTC along with the ripple-free torque and flux.

1.2.1.3 Neuro-Fuzzy Sliding-Mode based Controller

Fuzzy sliding-mode control (FSMC) is powerful hybrid intelligent control technique which is based on the human expert without having the knowledge of parameters and control system structure [120]. On the other hand, the lack of design methodology for the fuzzy rules and its MFs is one of the major drawbacks of this method [121]. So, adaptive FSMC have been developed to handle this problem [122]. In recent years, many investigations have been reported on adaptive FSMC algorithms of IM control to enhance the performance [123]-[125]. Lyapunov stability criteria is applied in this algorithm of adapting rules. It provides the automatic tuning of fuzzy rules according to the Lyapunov stability criteria. The robustness of conventional sliding-mode control and the online tuning feature of adaptive fuzzy logic control have led to an effective hybrid adaptive FSMC. Therefore, this control technique has been effectively implemented in many fields of industries like robotics, adjustable speed drives, etc. [3], [126]-[129]. However, the demerits of both sliding-mode control and fuzzy logic control particularly for variable speed drives motivate many researchers to develop SMC-based neuro-fuzzy control. The collective advantages of the adaptive neuro-fuzzy control and robustness of SMC are combined to overcome the system and parameter uncertainties that appear in motor drive control [148]. Further, no major work regarding the applications of effective hybrid self-tuned neuro-fuzzy sliding-mode based feedback linearized IM drive is reported yet.

1.2.2 Use of Non-Conventional Energy Source in IM Drive Control

Usually, variable speed IM takes power from a grid followed by a rectifier and an inverter. But, to make the system more reliable during power failure and voltage outages, the power is delivered to inverter fed IM drive directly on DC form in a stand-alone application which shows a big advantage. Over the years, photovoltaic systems have been reported as most frequently used non-conventional power supply in stand-alone applications [130]-[132]. In [3], the design of photovoltaic-energy storage electrical system integrated with an asynchronous motor drive using fuzzy sliding-mode control is presented. However, in spite of having many advantages, the major drawbacks are uneven irradiation and temperature of the solar system. It also has the problem of handling fuel-based electrical appliances. Therefore, to overcome these issues, a fuel cell (FC) with its energy storage system (ESS) used with IM

drive control strategies have been proposed in a stand-alone application [132], [133]. The requirement of induction machines with its inverter control is one of the vital stand-alone applications. But, industrial norms for implementation of high-performance adjustable speed drive need extensive torque ripple minimization, fast dynamic response, good load disturbance rejection, working under different modes of operations, and insensitivity to parameter variations and plant uncertainties [3], [133]. A hybrid FC with its ESS (battery) based drive system has the advantages of providing fast, additional power during acceleration, recovering of energy during regenerative braking through a braking chopper, which improves the drive efficiency [133], [134]. The FC system as a clean and continuous source of electricity provides an effective and eco-friendly approach to be used as a separate external source.

1.3 Motivation and Objectives of the Thesis

The presence of new converter topologies with fast switching semiconductor devices and availability of fast processors have developed tremendous interest in the researchers for design and implementation of high-performance AC drives, especially IM drives. Further, low cost, and maintenance-free drive systems are the major criteria for industrial applications. Various contemporary control techniques for IM drives and its implementation in real-time industrial purpose have been the key focus area of investigations. It may be observed from the literature survey that still some scopes are there for performance enhancement of the inverter-fed IM drive by using different control strategies. The present research work focuses on performance improvement and comparative analysis of various aspects of different controllers, with objectives formulated as follows.

- Study of different controllers and their comparative analysis for high-performance IM drive.

  The dynamic and steady-state performances of IM drive system are deteriorated as motor parameters vary during various operations. Because of this detuned parameter conditions, the system dynamic responses and steady-state characteristics of torque control degrade from the instantaneous torque control characteristic of a properly tuned controller. So efforts have been made to improve the drive system performance by making it insensitive to parameter variations. Adequate attention with regard to the implementation of hybrid neuro-fuzzy controller to feedback linearized IM drives needs to be given.

- Design and implementation of PI controllers and adaptive neuro-fuzzy inference system (ANFIS) on IM drive based on feedback linearization approach and their comparative evaluations.

  The mathematical modeling of ANFIS torque compensator for Feedback linearized IM drive with a speed sensor is developed. A systematic tuning algorithm is developed for the mechanical subsystem. The design of the proposed feedback linearized IM drive system is modeled and extensively simulated in the MATLAB/SIMULINK environment and is experimentally investigated in the real-time hardware setup using DSP TMS320F2812 processor. The simulated and experimental performance analysis has been carried out under different operating conditions.

- Development and implementation of computationally less burdened adaptive simplified neuro-fuzzy compensator on feedback linearized IM drive.

  No major work has been reported on implementation of auto-tuned NFC for adaptive linearized IM drive. Further, conventional NFCs generally require large number of membership functions as speed error and acceleration are used as two inputs. The controller's robustness can be improved by the adoption of input acceleration ($\dot{\omega}$) [135], [136]. However, the accurate measurement of acceleration is not required [135], [137] as it deteriorates the ability and even makes utilization of acceleration useless. Therefore, the design of the particular type neuro-fuzzy compensator as proposed for the linearized modeled sensorless IM drive is presented in order to reduce the computational burden. Comprehensive and unsupervised algorithm is systematically developed, and the stepwise procedure is followed for self-tuning of the proposed NFC. The proposed NFC incorporated with the intuitive FBL based IM drive system is designed and modeled in MATLAB software and experimentally investigated in the real-time hardware setup using DSP TMS320F2812 processor. A comparative performance analysis with conventional neuro-fuzzy controller and PI controller based linearized IM drive has been done to show the superiority of the proposed controller.

- Design and experimental investigation of the robust adaptive hybrid simplified neuro-fuzzy sliding-mode controller for feedback linearized IM drive, and its application to fuel cell-energy storage system operated drive system.

A hybrid intelligent technique based on simplified neuro-fuzzy sliding-mode control (NFSMC) technique for linearized IM drive is introduced with an aim to enhance some system performances further. It is expected that the hybrid intelligent simplified NFSMC would be a good selection for linearized IM drive as it is claimed to be adaptive and robust. Also, these controllers do not have any drawbacks of the fuzzy controller, i.e., uncertain, unoptimized, and asymmetric MFs especially used for adjustable speed drives, and drawbacks of the sliding-mode controller, i.e., chattering of the control states and inputs. The performance of the drive system is investigated in parallel by integrating fuel cell-energy storage system (FC-ESS) with the NFSMC-based FBL IM drive system. This has the main advantage for the stand-alone application of the drive system during voltage disruption and outages and thereby, making the system more efficient. The application of FC-ESS (battery) hybrid power system based FBL modeled IM driven by using a new adaptive NFSMC technique has not yet been investigated to the best of our knowledge. Apart from being resistant to the motor parameter variations, system uncertainties, and load impact, the proposed controller has the benefit of decreasing the computational burden by reducing the rules and MFs compared to the conventional NFC. Hence, the main objective of this work is to develop robust, computationally less burdened, speed and torque regulator that can achieve excellent dynamic, as well as steady-state performance of linearized IM drive system.

1.4 Scope and Organization of the Thesis

The work reported in the dissertation is related to the study, development, and implementation of some controllers and their comparative evaluation for performance improvement of IM drive. Different types of controllers like PI, neuro-fuzzy, and neuro-fuzzy sliding-mode have been taken up for the performance analysis of the linearized drive system. Simulink model has been developed, and an extensive simulation for the proposed controller has been carried out in MATLAB/SIMULINK environment. Subsequently, prototype development and experimental implementations of the controllers have been done in the laboratory. The brief outline of the work as presented in the dissertation is given as follows.

Chapter 1:

This Chapter presents general survey of literature on various control aspects and their implementations for IM drive performance improvement, stating their limitations,

advantages, and disadvantages. Extensive literature review is presented on linearization control, robust control, and different hybrid soft computing based control techniques. The applications of neuro-fuzzy control, sliding-mode control and their combination, i.e., neuro-fuzzy sliding-mode control to IM drive are presented. A brief description of literature has also been given on the application of non-conventional energy systems to the IM drive using various controllers. Finally, the objectives of the present dissertation followed by its scope and organization are outlined.

Chapter 2:

In this Chapter, the dynamic modeling of the IM in the stationary reference frame with rotor speed, rotor current, and rotor flux as state variables are presented which are the basic requirements for controller design. Implementation of feedback linearization control based on the input-output linearization technique with the nonlinear dynamics of the induction motor drive is described. The IM drive system model based on the linearization concept is divided into two linear subsystems, i.e., electrical subsystem and mechanical subsystem. Further, the gains of the PI controllers for both the subsystems are obtained by comprehensive and systematic design procedures.

Chapter 3:

The design of adaptive neuro-fuzzy inference system (ANFIS) based controller for linearized IM drive is reviewed in this Chapter. A systematic tuning algorithm of the ANFIS controller is introduced for the system. A sensorless flux and torque observer has also been presented. As simulation study predicts the dynamic response and performance of the linearized drive system, a systematic simulation study of the drive system is carried out prior to the experimental study. The different model blocks of the proposed drive system are designed and developed in the MATLAB software and are experimentally realized in the real-time prototype hardware setup using DSP TMS320F2812 processor. A comparative performance analysis of simulated and experimental results has been carried out under different operating conditions.

Chapter 4:

The design of specific types of NFCs as implemented on the linearized IM drive is presented in this Chapter. A comprehensive and systematic step-wise self-tuning procedure is developed for the proposed NFC. The proposed NFC incorporated with the linearized IM drive system is designed and modeled in MATLAB and experimentally implemented in the laboratory. A comparative analysis is carried out to show the advantages of the proposed

method for feedback linearized of IM drive in various modes of operations. The sensitivity and robustness of the controller are verified experimentally in terms of parameter variations and external load disturbances. Further, the robustness and adaptability of the proposed controller are validated experimentally by altering the gains of PI-speed controller.

Chapter 5:

In this Chapter, some efforts have been made to improve the system performance further by using simplified neuro-fuzzy sliding-mode controllers (NFSMC). The design methodology of the simplified NFC pertaining to sliding-mode approach for a speed sensorless linearized IM drive is presented. The self-tuning algorithm and the steps employed for updating parameters are presented for the proposed controller. Further, the proposed controller integrated with the fuel cell-energy storage system for the linearized drive is developed to expand its applications. This is used as a stand-alone application, which shows big advantage during interruption of main power supply and voltage outages and thus, making the system more efficient. The modeling of the overall drive system is done in MATLAB software, and the proposed controller is experimentally investigated in prototype hardware setup using low cost, high computational DSP TMS320F2812 processor. Based on simulation and experimental results, a thorough comparative study is carried out with the conventional controller in order to show the superiority of the proposed controller.

Chapter 6:

Finally, some concluding remarks of overall research work summarizing various aspects of development and implementation of the proposed controllers are presented in this Chapter. Few suggestions are also included in this Chapter to extend this research work in future.

Chapter 2

INDUCTION MOTOR DRIVE BASED ON FEEDBACK LINEARIZATION APPROACH WITH PI CONTROLLERS

CHAPTER-2

INDUCTION MOTOR DRIVE BASED ON FEEDBACK LINEARIZATION APPROACH WITH PI CONTROLLERS

2.1 Introduction

This Chapter focuses on the modeling of the induction motor (IM) in the stationary reference frame with rotor speed, stator current, and rotor flux as state variables which are required for the controller design. Using this model, feedback linearization control can be implemented efficiently for performance improvement of the IM drive as described in Section 2.2. The feedback linearized IM drive system consists of two linear subsystems, i.e., electrical subsystem and mechanical subsystem. Further, systematic and comprehensive procedures are adapted to obtain the gain of the PI controllers for both the subsystems.

2.2 Modeling of Induction Motor

An accurate model for the three-phase induction motor is required to simulate and analyze the overall drive system. The induction motor model is derived in the stationary *d-q* reference frame [4] with the following assumptions.

- The stator winding is considered to be distributed in order to produce a sinusoidal mmf along the airgap, i.e., space harmonics are negligible.
- The stator and rotor slots produce negligible variation in corresponding inductances.
- Mutual inductances are equal.
- Voltage and current harmonics are negligible.
- The saturation of the magnetic circuit is neglected.
- Skin effect and hysteresis and eddy current losses are neglected.

The voltage equations for the three-phase induction motor in *d-q* stationary reference frame can be written as [4]

$$V_{ds} = R_s i_{ds} + p\psi_{ds} \tag{2.1}$$

$$V_{qs} = R_s i_{qs} + p\psi_{qs} \tag{2.2}$$

$$V_{dr} = R_r i_{dr} + P\omega_r \psi_{qr} + p\psi_{dr} \tag{2.3}$$

$$V_{qr} = R_r i_{qr} - P\omega_r \psi_{dr} + p\psi_{qr} \tag{2.4}$$

The instantaneous developed electromagnetic torque equation and torque balance equation are given by

$$T_e = \frac{3}{2}\frac{L_m}{L_r} P\left(\psi_{dr} i_{qs} - \psi_{qr} i_{ds}\right) \tag{2.5}$$

$$\frac{d\omega_r}{dt} = -\frac{B}{J}\omega_r + \frac{1}{J}\left(T_e - T_l\right) \tag{2.6}$$

where V, i, and ψ represent voltage, current, and flux linkage, in that order. Their subscripts (*ds*, *qs*) and (*dr*, *qr*) correspond to the stator and rotor components along the *d-q* axes. R_s and R_r are the stator and rotor resistances per phase. p is the differential operator $\frac{d}{dt}.\omega_r$, P, T_e, T_l, J, and B are the rotor mechanical speed, number of pole pairs, electromagnetic torque, load torque, rotor inertia coefficient, and friction coefficient, in that order.

Since an induction motor is normally fed with the stator side supply and windings of the rotor side are short-circuited,

$$\begin{bmatrix} V_{dr} \\ V_{qr} \end{bmatrix} = \begin{bmatrix} 0 \\ 0 \end{bmatrix} \tag{2.7}$$

By considering equal mutual inductances, linear magnetic circuit, and negligible iron losses, the stator and rotor flux linkage components in the *d-q* stationary reference frame are given by: [85]

$$\begin{bmatrix} \psi_{ds} \\ \psi_{qs} \end{bmatrix} = \begin{bmatrix} L_s & 0 \\ 0 & L_s \end{bmatrix} \begin{bmatrix} i_{ds} \\ i_{qs} \end{bmatrix} + \begin{bmatrix} L_m & 0 \\ 0 & L_m \end{bmatrix} \begin{bmatrix} i_{dr} \\ i_{qr} \end{bmatrix} \tag{2.8}$$

$$\begin{bmatrix} \psi_{dr} \\ \psi_{qr} \end{bmatrix} = \begin{bmatrix} L_m & 0 \\ 0 & L_m \end{bmatrix} \begin{bmatrix} i_{ds} \\ i_{qs} \end{bmatrix} + \begin{bmatrix} L_r & 0 \\ 0 & L_r \end{bmatrix} \begin{bmatrix} i_{dr} \\ i_{qr} \end{bmatrix} \tag{2.9}$$

where L_s and L_r are the stator and rotor self-inductances and L_m is the magnetizing inductance. From (2.9), we obtain

$$\begin{bmatrix} i_{dr} \\ i_{qr} \end{bmatrix} = \begin{bmatrix} \frac{1}{L_r} & 0 \\ 0 & \frac{1}{L_{r\,r}} \end{bmatrix} \begin{bmatrix} \psi_{dr} \\ \psi_{qr} \end{bmatrix} - \begin{bmatrix} \frac{L_m}{L_r} & 0 \\ 0 & \frac{L_m}{L_r} \end{bmatrix} \begin{bmatrix} i_{ds} \\ i_{qs} \end{bmatrix} \tag{2.10}$$

Substituting (2.10) in (2.8), we get

$$\begin{aligned} \begin{bmatrix} \psi_{ds} \\ \psi_{qs} \end{bmatrix} &= \begin{bmatrix} L_s - \frac{L_m^{\,2}}{L_r} & 0 \\ 0 & L_s - \frac{L_m^{\,2}}{L_r} \end{bmatrix} \begin{bmatrix} i_{ds} \\ i_{qs} \end{bmatrix} + \begin{bmatrix} \frac{L_m}{L_r} & 0 \\ 0 & \frac{L_m}{L_r} \end{bmatrix} \begin{bmatrix} \psi_{dr} \\ \psi_{qr} \end{bmatrix} \\ &= \begin{bmatrix} \sigma L_s & 0 \\ 0 & \sigma L_s \end{bmatrix} \begin{bmatrix} i_{ds} \\ i_{qs} \end{bmatrix} + \begin{bmatrix} \frac{L_m}{L_r} & 0 \\ 0 & \frac{L_m}{L_r} \end{bmatrix} \begin{bmatrix} \psi_{dr} \\ \psi_{qr} \end{bmatrix} \end{aligned} \tag{2.11}$$

where $\sigma = \left(1 - \frac{L_m^{\,2}}{L_s L_r}\right)$ is the leakage coefficient.

Substituting (2.10) in (2.3) and (2.4) and using (2.7) and then reorganizing, we get

$$\begin{bmatrix} p\psi_{dr} \\ p\psi_{qr} \end{bmatrix} = \begin{bmatrix} R_r \frac{L_m}{L_r} & 0 \\ 0 & R_r \frac{L_m}{L_r} \end{bmatrix} \begin{bmatrix} i_{ds} \\ i_{qs} \end{bmatrix} + \begin{bmatrix} -\frac{R_r}{L_r} & 0 \\ 0 & -\frac{R_r}{L_r} \end{bmatrix} \begin{bmatrix} \psi_{dr} \\ \psi_{qr} \end{bmatrix} + \begin{bmatrix} 0 & -P\omega_r \\ P\omega_r & 0 \end{bmatrix} \begin{bmatrix} \psi_{dr} \\ \psi_{qr} \end{bmatrix} \tag{2.12}$$

Further, substituting (2.11) in (2.1) and (2.2) and using (2.12), the simplified equation is obtained as

$$\begin{aligned} \begin{bmatrix} pi_{ds} \\ pi_{qs} \end{bmatrix} = {} & \begin{bmatrix} -\frac{1}{\sigma L_s}\left(R_s + R_r \frac{L_m^{\,2}}{L_r^{\,2}}\right) & 0 \\ 0 & -\frac{1}{\sigma L_s}\left(R_s + R_r \frac{L_m^{\,2}}{L_r^{\,2}}\right) \end{bmatrix} \begin{bmatrix} i_{ds} \\ i_{qs} \end{bmatrix} + \begin{bmatrix} \left(\frac{1}{\sigma L_s} R_r \frac{L_m}{L_r^{\,2}}\right) & \left(P \frac{1}{\sigma L_s} \frac{L_m}{L_r} \omega_r\right) \\ \left(-P \frac{1}{\sigma L_s} \frac{L_m}{L_r} \omega_r\right) & \left(\frac{1}{\sigma L_s} R_r \frac{L_m}{L_r^{\,2}}\right) \end{bmatrix} \begin{bmatrix} \psi_{dr} \\ \psi_{qr} \end{bmatrix} \\ & + \begin{bmatrix} \frac{1}{\sigma L_s} & 0 \\ 0 & \frac{1}{\sigma L_s} \end{bmatrix} \begin{bmatrix} V_{ds} \\ V_{qs} \end{bmatrix} \end{aligned} \tag{2.13}$$

Differentiating (2.11), we get

$$\begin{bmatrix} p\psi_{ds} \\ p\psi_{qs} \end{bmatrix} = \begin{bmatrix} \sigma L_s & 0 \\ 0 & \sigma L_s \end{bmatrix} \begin{bmatrix} pi_{ds} \\ pi_{qs} \end{bmatrix} + \begin{bmatrix} \frac{L_m}{L_r} & 0 \\ 0 & \frac{L_m}{L_r} \end{bmatrix} \begin{bmatrix} p\psi_{dr} \\ p\psi_{qr} \end{bmatrix} \tag{2.14}$$

Then, substituting (2.14) in (2.1) and (2.2), we get

$$\begin{bmatrix} V_{ds} \\ V_{qs} \end{bmatrix} = \begin{bmatrix} R+\sigma L_s p & 0 \\ 0 & R+\sigma L_s p \end{bmatrix} \begin{bmatrix} i_{ds} \\ i_{qs} \end{bmatrix} + \begin{bmatrix} \frac{L_m}{L_r} & 0 \\ 0 & \frac{L_m}{L_r} \end{bmatrix} \begin{bmatrix} p\psi_{dr} \\ p\psi_{qr} \end{bmatrix} \tag{2.15}$$

Rewriting (2.12), (2.13), (2.5), and (2.6) together, the following equations characterize the dynamic mathematical modeling of induction motor drive in the *d-q* stationary reference frame.

$$\frac{di_{ds}}{dt} = -\frac{1}{\sigma L_s}\left(R_s + \frac{L_m^{\,2}}{L_r^{\,2}} R_r\right) i_{ds} + \frac{1}{\sigma L_s}\frac{L_m R_r}{L_r^{\,2}}\psi_{dr} + \frac{PL_m}{\sigma L_s L_r}\omega_r \psi_{qr} + \frac{V_{ds}}{\sigma L_s} \tag{2.16}$$

$$\frac{di_{qs}}{dt} = -\frac{1}{\sigma L_s}\left(R_s + \frac{L_m^{\,2}}{L_r^{\,2}} R_r\right) i_{qs} + \frac{1}{\sigma L_s}\frac{L_m R_r}{L_r^{\,2}}\psi_{qr} - \frac{PL_m}{\sigma L_s L_r}\omega_r \psi_{dr} + \frac{V_{qs}}{\sigma L_s} \tag{2.17}$$

$$\frac{d\psi_{dr}}{dt} = -\frac{R_r}{L_r}\psi_{dr} - P\omega_r \psi_{qr} + \frac{L_m R_r}{L_r} i_{ds} \tag{2.18}$$

$$\frac{d\psi_{qr}}{dt} = -\frac{R_r}{L_r}\psi_{qr} + P\omega_r \psi_{dr} + \frac{L_m R_r}{L_r} i_{qs} \tag{2.19}$$

$$\frac{d\omega_r}{dt} = -\frac{B}{J}\omega_r + \frac{1}{J}\left(T_e - T_l\right) \tag{2.20}$$

$$T_e = \frac{3}{2}\frac{L_m}{L_r} P\left(\psi_{dr} i_{qs} - \psi_{qr} i_{ds}\right) \tag{2.21}$$

2.3 Feedback Linearization Approach of IM Drive

Conventional linearization of a nonlinear system depends on a first-order approximation of the system dynamics at a selected working point while ignoring high-order elements. This linearization is acceptable in numerous applications where typical system operation stays in the region of a stable or gradually shifting equilibrium, but it is generally inappropriate. Specifically, this linearization is appropriate for IM drives working at fixed rotor speed. Otherwise, IM behavior is characteristically nonlinear and different methodologies must be utilized.

Feedback linearization (FBL) control is an approach to apply nonlinear control strategy in which many investigations have been going on recent years. The main idea about the approach is to change over methodically nonlinear mathematical equations into a totally or partially linear equation so that linear control technique can be applied. This contrasts absolutely from conventional linearization frameworks as this linearization technique is satisfied universally, rather than the neighborhood of an equilibrium point [2], [58]. The feedback linearization is distinguished by a specific state coordinate change. Thus, it uses a

nonlinear transformation of system variables to another appropriate coordinate system that facilitates feedback linearization. The theoretical approach and a deliberate methodology are given in [85].

The nonlinear dynamics of induction motor considered here is of fifth order with the chosen state variables as

$$X^T = \begin{bmatrix} i_{ds} & i_{qs} & \psi_{dr} & \psi_{qr} & \omega_r \end{bmatrix} \tag{2.22}$$

and the input variables as

$$\hat{u}^T = \begin{bmatrix} \hat{u}_1 & \hat{u}_2 \end{bmatrix} = \begin{bmatrix} i_{ds}^* & i_{qs}^* \end{bmatrix} \tag{2.23}$$

where X is the 5×1 state vector and $\hat{u}$ is the 2×1 input control vector.

The controller output parameter should be so chosen that the induction motor behaves like a DC motor making the rotor speed and flux decoupled. Therefore, output of control parameter to be chosen as

$$Y^T = \begin{bmatrix} h_1(x) & h_2(x) \end{bmatrix} = \begin{bmatrix} \omega_r & \psi_r \end{bmatrix} \tag{2.24}$$

where Y^T is the 2×1 system output vector. ω_r and ψ_r are the rotor speed and flux, respectively.

The above nonlinear state space equation for the multivariable system [9] can be written as

$$\dot{X} = f(x) + \sum_{i=1}^{m} g_i(x)\hat{u}_i \text{ and } Y_i = h_i(x) \text{ for } 1 \le i \le m. \tag{2.25}$$

Then, from the induction motor modeling equations (2.16) – (2.21)

$$f(x) = \begin{bmatrix} -\frac{1}{\sigma L_s}\left(R_s + \frac{L_m^2}{L_r^2}R_r\right) i_{ds} + \frac{1}{\sigma L_s}\frac{L_m R_r}{L_r^2}\psi_{dr} + \frac{PL_m}{\sigma L_s L_r}\omega_r\psi_{qr} + \frac{V_{ds}}{\sigma L_s} \\ -\frac{1}{\sigma L_s}\left(R_s + \frac{L_m^2}{L_r^2}R_r\right) i_{qs} + \frac{1}{\sigma L_s}\frac{L_m R_r}{L_r^2}\psi_{qr} - \frac{PL_m}{\sigma L_s L_r}\omega_r\psi_{dr} + \frac{V_{qs}}{\sigma L_s} \\ -\frac{R_r}{L_r}\psi_{dr} - P\omega_r\psi_{qr} \\ -\frac{R_r}{L_r}\psi_{qr} + P\omega_r\psi_{dr} \\ -\frac{B}{J}\omega_r - \frac{1}{J}T_l \end{bmatrix} \tag{2.26}$$

$$g_1(x) = \begin{bmatrix} 0 & 0 & \frac{L_m}{T_r} & 0 & -\frac{K_T}{J}\psi_{qr} \end{bmatrix}^T,\ g_2(x) = \begin{bmatrix} 0 & 0 & 0 & \frac{L_m}{T_r} & \frac{K_T}{J}\psi_{dr} \end{bmatrix}^T \tag{2.27}$$

where $K_T = \frac{3}{2}\frac{L_m}{L_r}P$ is known as torque constant and $T_r = \frac{L_r}{R_r}$ is known as rotor time constant.

If ψ_{dr} and ψ_{qr} are considered as nonzero values altogether, the relative degree of the system $r = r_1 + r_2 = 4$, provided that it satisfies the involutive condition which is the necessary condition for FBL, i.e., the Lie bracket of $g_1(x)$ and $g_2(x)$ exists [30].

The Lie bracket of $g_1(x)$ and $g_2(x)$ is given as

$$[g_1, g_2](x) = \frac{\partial g_2}{\partial x} g_1(x) - \frac{\partial g_1}{\partial x} g_2(x) = \frac{2K_T L_m}{JT_r} \neq 0 \tag{2.28}$$

So, it satisfies the involutive condition for the values of P, L_m, R_r, J, and L_r, which are mentioned in Appendix A.1.

Now the total rotor flux in terms of *d-q* component is expressed as

$$\psi_r^{\,2} = \psi_{dr}^{\,2} + \psi_{qr}^{\,2} \tag{2.29}$$

and $$\frac{d\psi_r}{dt} = \frac{1}{\psi_r}\left(\psi_{dr}\frac{d\psi_{dr}}{dt} + \psi_{qr}\frac{d\psi_{qr}}{dt}\right) \tag{2.30}$$

When the stator currents are directly controlled by the hysteresis current controller, the dynamic modeling equations (2.18), (2.19), and (2.20) of the IM can be approached as

$$\frac{d\psi_{dr}}{dt} = -\frac{R_r}{L_r}\psi_{dr} - P\omega_r\psi_{qr} + \frac{L_m R_r}{L_r}\hat{u}_1 \tag{2.31}$$

$$\frac{d\psi_{qr}}{dt} = -\frac{R_r}{L_r}\psi_{qr} + P\omega_r\psi_{dr} + \frac{L_m R_r}{L_r}\hat{u}_2 \tag{2.32}$$

$$\frac{d\omega_r}{dt} = -\frac{B}{J}\omega_r + \frac{1}{J}\frac{3}{2}\frac{L_m}{L_r}P\left(\hat{u}_2\psi_{dr} - \hat{u}_1\psi_{qr}\right) - \frac{1}{J}T_l \tag{2.33}$$

Now substituting $\frac{d\psi_{dr}}{dt}$ and $\frac{d\psi_{qr}}{dt}$ from equations (2.31) and (2.32) in equation (2.30) the linearized state-space equations of rotor flux and speed are obtained as

$$\frac{d\psi_r}{dt} = -\frac{R_r}{L_r}\psi_r + \frac{L_m R_r}{L_r}u_1 \tag{2.34}$$

$$\frac{d\omega_r}{dt} = -\frac{B}{J}\omega_r + \frac{1}{J}\frac{3}{2}\frac{L_m}{L_r}Pu_2 - \frac{1}{J}T_l \tag{2.35}$$

where u_1 and u_2 are considered as new control inputs that make state equations (2.31) - (2.33) feedback linearized and is redefined as

$$\begin{bmatrix} u_1 \\ u_2 \end{bmatrix} = \begin{bmatrix} \frac{\psi_{dr}}{\psi_r} & \frac{\psi_{qr}}{\psi_r} \\ -\psi_{qr} & \psi_{dr} \end{bmatrix} \begin{bmatrix} \hat{u}_1 \\ \hat{u}_2 \end{bmatrix} \tag{2.36}$$

where the matrix $\begin{bmatrix} \frac{\psi_{dr}}{\psi_r} & \frac{\psi_{qr}}{\psi_r} \\ -\psi_{qr} & \psi_{dr} \end{bmatrix}$ is defined as decoupling matrix $D(x)$. The matrix $D(x)$ is non-singular except in the trivial condition when the rotor flux is zero which occurs during start-up of the motor. However, in the regular operation of the motor, this condition never happens in the practical drive as the flux is set up prior to starting the induction motor drive. Since the left plane poles are evident from the dynamics of ω_r and ψ_r, the closed loop input-output stability of the remaining state variables can be assured provided that the rotor flux has a nonzero value.

The equations (2.34) and (2.35) represent induction motor model with feedback linearization which is of the second order, with the rotor flux and speed as decoupled state variables. Consequently, the new model is intuitively linear and simplifying the designing of the controller. The nonlinear state feedback controller is obtained from (2.36), and it decouples the system, which is given by (2.37) if and only if the decoupling matrix is non-singular. The block diagram of the feedback linearized controller is givenin Fig. 2.1.

$$\begin{bmatrix} \hat{u}_1 \\ \hat{u}_2 \end{bmatrix} = \begin{bmatrix} i_{ds}^* \\ i_{qs}^* \end{bmatrix} = \frac{1}{\psi_r} \begin{bmatrix} \psi_{dr} & -\psi_{qr} \\ \psi_{qr} & \psi_{dr} \end{bmatrix} \begin{bmatrix} 1 & 0 \\ 0 & \frac{1}{\psi_r} \end{bmatrix} \begin{bmatrix} u_1 \\ u_2 \end{bmatrix} \tag{2.37}$$

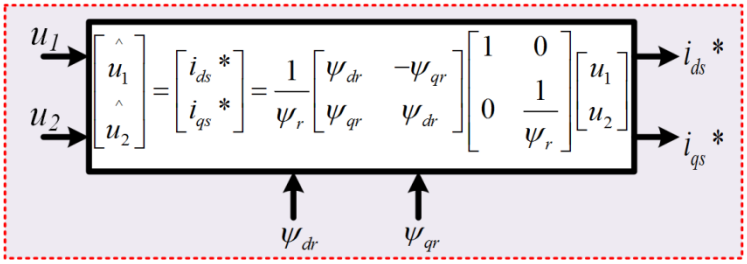

Fig. 2.1 Decoupling feedback linearized controller

The equations (2.34) and (2.35) define the electrical subsystem and mechanical sub system with (i_{ds}^*, i_{qs}^*) and (ψ_r, ω_r) as control input and output, respectively. So, it describes a framework that is decoupled as the outputs and inputs are not directly related. Thus, the nonlinear control theory [35] is utilized to wipe out this coupled relation and makes the system inputs i_{ds}, i_{qs} and the outputs ψ_r, ω_r totally decoupled. The feedback decoupled systems with (2.34) and (2.35) are represented in the schematic block diagram as shown in Fig. 2.2 (a) and (b).

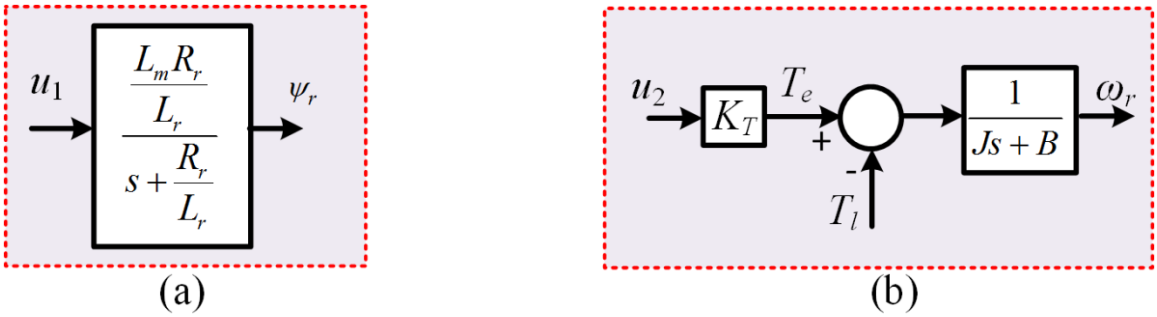

Fig. 2.2 Open loop block diagram of (a) electrical system (b) mechanical system

2.4 Design of PI Controllers

The performance of the FBL IM drive system is largely dependent on the selection of the controllers. As the FBL model of IM obtained is decoupled one, the developed torque and the rotor flux are controlled independently. The controllers have been designed, so as to achieve the desired steady-state as well as transient performance. Thus, the FBL approach facilitates the controller design of IM with highly nonlinear dynamics. The electrical and mechanical subsystems as shown in Fig. 2.2 are type zero systems as there is no integral term. So, a step input gives rise to a steady-state error. This leads to incorporation of PI controllers for both the subsystems. For stable error dynamics and exact tracking of target rotor flux and speed, the derived inputs u_1 and u_2 are the outputs of PI-controller, which are given by

$$u_1 = K_{p1}\left(\psi_r{}^* - \psi_r\right) + K_{i1}\int_0^t \left(\psi_r{}^* - \psi_r\right) dt \tag{2.38}$$

$$u_2 = K_{p2}\left(\omega_r{}^* - \omega_r\right) + K_{i2}\int_0^t \left(\omega_r{}^* - \omega_r\right) dt \tag{2.39}$$

Further, the determination of constant gain values of these PI controllers is vital for controller design in the drive system. An improper choice of gains may lead to undesirable and unstable response. Therefore, precise selection of gains is required in order to get a drive with high performance. The transfer functions of the electrical and mechanical subsystems are derivedin order to verify the factors affecting the gains of the PI controllers in particular and to have a feel of the influence of controller gains on the drive characteristic in general. Electrical system using PI-controller is validated and is verified that the drive characteristic using the designed controller is satisfactory. Mechanical system with one PI-controller is also validated, but the response obtained is not satisfactory enough. This is due to the fact that two state variables such as speed and torque present in the mechanical subsystem. The speed as a mechanical quantity has higher time constant or settling time compared to the developed

torque, which is a product of ψ_d and i_q, has smaller time constant or settling time. It means that the speed transients die down too slowly compared to the torque or current transients. Again, the overshoot of torque and current responses is increased if the speed response is improved by the controller and vice versa. Therefore, in order to achieve improved response of both speed and current, two PI controllers are incorporated in the mechanical subsystem [85]. One is used in inner loop known as PI-torque controller and other is the PI-controller used in the outer loop known as PI-speed controller. With both PI controllers, the system becomes faster and better at the expense of more complexity. PI controllers design for both the subsystems is given in the following subsections.

Two different methods are used to design PI controllers. In one method known as pole-zero cancellation technique, the zero of the PI-controller is selected to cancel one of the system poles in the open loop. This is used for both electrical as well as mechanical subsystems. In the other method, PI controllers tuning was done by using the conventional second-order single-variable linear system theory as it provides simple mathematical analysis approach. The gains of the PI controller are obtained by using SISO (single input single output) tool in MATLAB environment [139], [140]. This technique is used for the mechanical subsystem

2.4.1 Design of PI-Flux Controller

The schematic model of the closed-loop electrical subsystem with unity feedback and PI-controller is shown in Fig. 2.3.

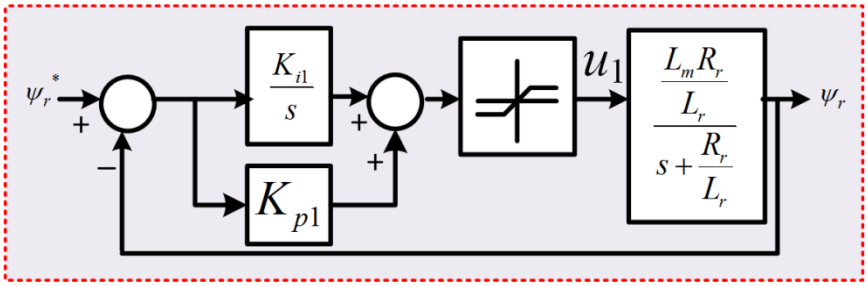

Fig. 2.3 Block diagram of the closed-loop electrical sub-system

The open loop transfer function for the electrical subsystem as in Fig. 2.2 (a) can be written as

$$G_{ol1}(s)=\frac{\psi_r(s)}{u_1(s)}=\frac{\frac{L_m R_r}{L_r}}{s+\frac{R_r}{L_r}}=\frac{5.42}{s+10.82} \tag{2.40}$$

where the values of the IM parameters R_r, L_r, and L_m are given in Appendix A.1.

The above equation is a transfer function of first order where the time constant of the open loop system response is given by

$$T_{rf} = \frac{L_r}{R_r} = \frac{1}{10.82} = 0.092 \text{ s.} \tag{2.41}$$

If the input is unit step, 90% rise time of flux = $2.3T_{rf}$ = 0.21s. Also, the response is slow as only one pole at -10.82 exists. So, to improve the system response for accurately tracking the command flux ψ_r^*, a properly designed PI-controller is introduced in the open loop with unity feedback as shown in Fig. 2.3.

The transfer function of PI-flux controller is given by

$$G_{PI1}(s) = \frac{K_{p1}s + K_{i1}}{s} \tag{2.42}$$

The transfer function $G_{f1}(s)$ of the forward path with the PI-controller is given by

$$\begin{aligned} G_{f1}(s) &= G_{PI1}(s).G_{ol1}(s) \\ &= \frac{K_{p1}s + K_{i1}}{s} \cdot \frac{5.41}{s + 10.82} \\ &= \frac{5.41(K_{p1}s + K_{i1})}{s(s + 10.82)} \end{aligned} \tag{2.43}$$

Then, the transfer function of the closed-loop subsystem with the unity feedback is

$$\begin{aligned} G_{cl1}(s) = \frac{\psi_r(s)}{\psi_r^*(s)} = \frac{G_{f1}(s)}{1 + G_{f1}(s)} &= \frac{\dfrac{5.41(K_{p1}s + K_{i1})}{s(s + 10.82)}}{1 + \dfrac{5.41(K_{p1}s + K_{i1})}{s(s + 10.82)}} \\ &= \frac{5.41(K_{p1}s + K_{i1})}{s^2 + s(5.41K_{p1} + 10.82) + 5.41K_{i1}} \end{aligned} \tag{2.44}$$

The characteristic polynomial of (2.44) is of second order which is given as

$$s^2 + (5.41K_{p1} + 10.82)s + 5.41K_{i1} \tag{2.45}$$

This can be compared with the standard form

$$s^2 + 2\xi\omega_n s + \omega_n^2 \tag{2.46}$$

where ω_n is the natural frequency of oscillation and ξ is the damping factor.

If ω_n is assumed to be 50 rad/s,

$$5.41K_{i1} = \omega_n{}^2 = 2500$$
$$K_{i1} = 461.25$$

Again, if the system response is considered to be critically damped, K_{p1} is obtained as

$$(5.41K_{p1} + 10.82) = 100$$
$$K_{p1} = 16.45$$

The control law for this closed-loop system with these values of K_{p1} and K_{i1} is given as follows:

$$u_1 = 16.45(\psi_r{}^* - \psi_r) + 461.25\int_0^t (\psi_r{}^* - \psi_r)\, dt \tag{2.47}$$

The characteristic polynomial as given by (2.45) with these K_{p1} and K_{i1} values can be expressed as

$$s^2 + 100s + 2500 = (s + 50)(s + 50) \tag{2.48}$$

The roots of the characteristic polynomial are in the left half of the complex frequency plane (*s*-plane). Both the poles are present at -50, being far from the origin of *s*-plane than the pole at -10.8. The above gains are acceptable as the dynamic response of the closed-loop system is satisfactory. Further, for step input, the rise time = $2.3 \times \frac{1}{50} = 0.04$ s, which makes the system dynamic response faster and stable. For different value of assumed ω_n, the drive system is simulated, and the most acceptable ω_n from the simulated response is observed to be ω_n = 50 rad/s.

2.4.2 Design of PI-Speed Controller

The mechanical subsystem of state feedback linearized IM drive system with only PI-speed controller is shown in Fig. 2.4.

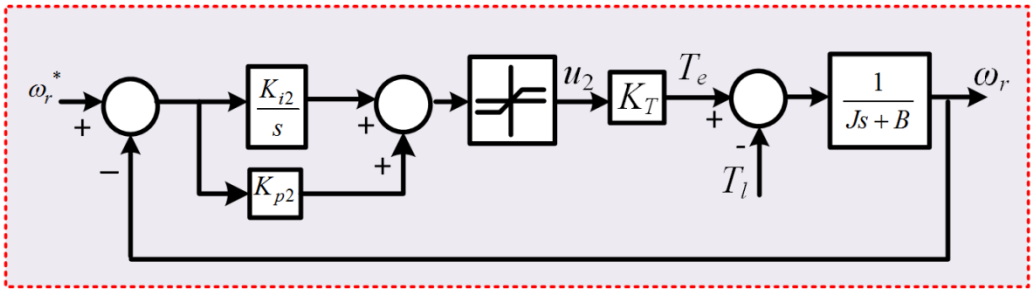

Fig. 2.4 Block diagram of the closed-loop mechanical subsystem with one PI-controller

The open loop speed transfer function of the system as shown in Fig. 2.2 (b) can be written as

$$G_{ol2}(s) = \frac{\omega_r(s)}{u_2(s)} = \frac{K_T}{Js+B} = \frac{18}{s+0.22} \tag{2.49}$$

where the values of the of the IM parameters R_r, L_r, L_m, P, J, and B are mentioned in Appendix A.1. Here, the load torque T_l is assumed to be zero for simplicity.

The above equation is a first order transfer function and the constant for rotor speed (mechanical time constant) is

$$T_{rs} = \frac{1}{0.22} = 4.55 \text{ s}$$

For a step input in u_2, the rise time of speed is $2.3T_{rs}$ = 10.46 s. The speed response is sluggish as it has one pole at -0.22. So, to follow the command speed ω_r^* and to enhance the dynamic response, a PI-controller is introduced in the forward path as shown in Fig. 2.4.

The transfer function of the PI-speed controller is

$$G_{PI2}(s) = \frac{K_{p2}s + K_{i2}}{s} \tag{2.50}$$

The transfer function of the forward path including speed controller is given by

$$\begin{aligned} G_{f2}(s) &= G_{PI2}(s).G_{ol2}(s) \\ &= \frac{(K_{p2}s + K_{i2})}{s} \cdot \frac{18}{(s+0.22)} \\ &= \frac{(K_{p2}s + K_{i2})18}{s^2 + 0.22s} \end{aligned} \tag{2.51}$$

The transfer function of the closed-loop mechanical subsystem with the unity feedback as shown in Fig. 2.4 is given by

$$G_{cl2}(s)=\frac{\omega_r(s)}{\omega_r^*(s)}=\frac{G_{f2}(s)}{1+G_{f2}(s)}$$

$$=\frac{(K_{p2}s+K_{i2})18}{s^2+(0.22+18K_{p2})s+18K_{i2}} \tag{2.52}$$

The characteristic polynomial of (2.52) is of second order and can be written in the standard form

$$s^2+2\xi\omega_n s+\omega_n{}^2 \tag{2.53}$$

Assuming the natural frequency of oscillation ω_n to be 50 rad/s,

$$18K_{i2}=2500$$
$$K_{i2}=138.8$$

Again, assuming the system response to be critically damped, K_{p2} is obtained as

$$18K_{p2}+0.22=100$$
$$K_{p2}=5.54$$

The control law for the closed-loop mechanical subsystem with these above gain values of PI-speed controller is given by

$$u_2=5.54(\omega_r*-\omega_r)+138.8\int_0^t(\omega_r*-\omega_r)\,dt \tag{2.54}$$

The dynamic speed response with PI-speed controller is not good enough. The transient responses of speed and torque are better if two PI controllers: one in speed loop (outer loop) and another in torque or current loop (inner loop) are incorporated in the drive system. This is because of the significant difference in the time constant of speed and torque.

2.4.3 Design of Both PI Speed and Torque Controller

With both PI controllers (speed and torque controller) incorporated in the mechanical subsystem, the state FBL IM drive system is shown in Fig. 2.5.

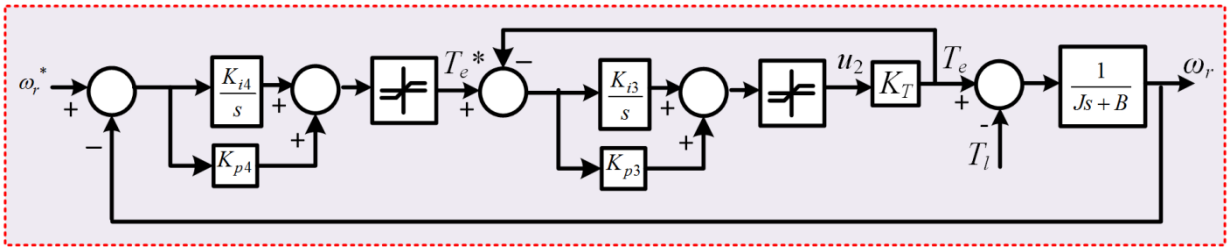

Fig. 2.5 Block diagram of the mechanical subsystem with two PI controllers

The transfer function of the torque controller (inner loop controller) is given by

$$G_{PI3}(s) = \frac{K_{p3}s + K_{i3}}{s} \tag{2.55}$$

The overall transfer function of the forward path is represented by

$$G_{f3}(s) = G_{PI3}(s)K_T = \frac{(K_{p3}s + K_{i3})K_T}{s} = \frac{(K_{p3}s + K_{i3})2.87}{s} \tag{2.56}$$

The transfer function of the torque loop with the unity feedback is

$$G_{cl3}(s) = \frac{T_e(s)}{T_e^*(s)} = \frac{G_{f3}(s)}{1 + G_{f3}(s)}$$

$$= \frac{(K_{p3}s + K_{i3})2.87}{s(1 + 2.87K_{p3}) + 2.87K_{i3}} \tag{2.57}$$

This is a first-order transfer function. In order to have instantaneous torque response, i.e., for a step input of reference torque T_e^*, the developed torque T_e tracks T_e^* instantaneously, K_{p3} and K_{i3} are chosen to be 10 and 0.01, respectively. So in this case, $\frac{T_e(s)}{T_e^*(s)}$ becomes unity and the simplified closed-loop subsystem is shown in Fig. 2.6.

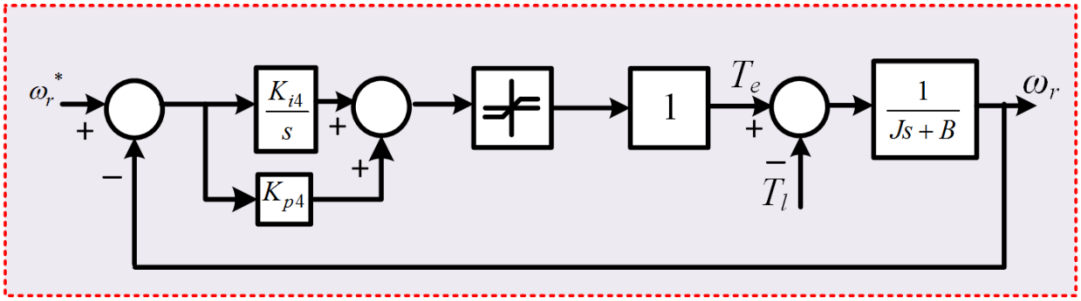

Fig. 2.6 Simplified block diagram of the mechanical subsystem

The transfer function of the outer loop speed controller is given by

$$G_{PI4}(s) = \frac{K_{p4}s + K_{i4}}{s} \tag{2.58}$$

The overall transfer function of the forward path including the speed controller is represented by

$$G_{f4}(s) = G_{PI4}(s)\frac{1}{Js + B}$$

$$= \frac{K_{p4}s + K_{i4}}{s} . \frac{6.25}{s + 0.22}$$

$$= \frac{(K_{p4}s + K_{i4})6.25}{s^2 + 0.22s} \tag{2.59}$$

Then, the transfer function of the overall outer speed loop with the unity feedback is expressed as

$$G_{cl4}(s) = \frac{\omega_r(s)}{\omega_r^*(s)} = \frac{G_{f4}(s)}{1 + G_{f4}(s)}$$

$$= \frac{(K_{p4}s + K_{i4})6.25}{s^2 + (0.22 + 6.25K_{p4})s + 6.25K_{i4}} \tag{2.60}$$

This is a second-order transfer function whose characteristic polynomial can be expressed in the standard form as

$$s^2 + 2\xi\omega_n s + \omega_n^2 \tag{2.61}$$

Assuming the natural frequency of oscillation ω_n to be 50 rad/s,

$$6.25K_{i4} = 2500$$
$$K_{i4} = 400$$

Assuming the system response to be critically damped, K_{p4} is obtained as

$$6.25K_{p4} + 0.22 = 100$$
$$K_{p4} = 15.96$$

Now, with all these gain values K_{p3}, K_{i3}, K_{p4}, and K_{i4}, the control law for both the speed and torque controller can be stated as

$$T_e^* = 15.96\left(\omega_r^* - \omega_r\right) + 400\int_0^t \left(\omega_r^* - \omega_r\right) dt \tag{2.62}$$

$$u_2 = 10\left(T_e^* - T_e\right) + 0.01\int_0^t \left(T_e^* - T_e\right) dt \tag{2.63}$$

The simulation of the mechanical subsystem with both the speed and torque controller was performed for the different value of gain. It is observed from the results that the assumptions of K_{p3}, K_{i3}, ω_n, and ξ are acceptable.

2.5 Conclusion

Modeling of the IM drive in the *d-q* stationary reference frame with stator current components, rotor flux components, and speed as state variables are briefly reviewed in this Chapter. Further, the feedback linearization technique based IM drive is developed and designed. Using this control approach, the IM drive system is decoupled into two linear subsystems – electrical and mechanical systems. Systematic procedures are derived to design the PI controllers for both the electrical and mechanical subsystems. With the PI-controllers, the system provides satisfactory performance over a large range of ideal operation. However, under various disturbance cases like sudden change in speed and load torque, the PI-controller performance is not satisfactory. Again, the controller design needs accurate and precise mathematical model, gain values, and tuning continuously to achieve high performance even under parameter variation cases. Thus, to overcome these demerits, hybrid intelligent control approaches are highly adaptable to enhance the performance of the FBL IM drive system further even at various disturbances. These controllers are discussed in the subsequent chapters. In Chapter 3, development and implementation of an adaptive neuro-fuzzy inference system (ANFIS) based controller is presented to enhance the performance and disturbance rejection of the feedback linearized IM drive system.

Chapter 3

IMPLEMENTATION OF AN ANFIS-BASED INDUCTION MOTOR DRIVE USING FEEDBACK LINEARIZATION

CHAPTER 3
IMPLEMENTATION OF AN ANFIS-BASED INDUCTION MOTOR DRIVE USING FEEDBACK LINEARIZATION

3.1 Introduction

As the feedback linearization (FBL) based induction motor (IM) drive is represented by time-varying dynamics and is sensitive to parameter variations, system uncertainties, and outer disturbances, an adaptive control strategy based adaptive neuro-fuzzy inference system (ANFIS) controller is implemented which is a combined methodology. It yields ideal results by selecting appropriate rule base, unlike fuzzy logic control procedure. The ANFIS control incorporated with the FBL IM drive preserves quick response of conventional PI-controller-based linearized IM drive with robustness to parameter variations and uncertainties. Additionally, it remarkably reduces the torque ripple and improves the system dynamic performance. In order to design the proposed FBL-based IM drive, the rotor flux needs to be known accurately. When an IM of large speed range operates with precision control for better dynamic performance, the flux should be measured by installing a flux sensor. In contrast, the sensorless control without sensing the rotor flux has been evolving as industrial standards because of cost-effectiveness and reliability. As a result, alot of research work has been going on over sensorless drive over past few decades [4]. A systematic simulation study of FBL IM drive system is carried out prior to the experimental study as it predicts the dynamic response and performance of the linearized drive system.

The second Section of this Chapter presents a brief description of the system. Flux and torque observer based on an estimation method is developed in the third Section. The fourth Section presents a design of an adaptive neuro-fuzzy torque controller technique applied to an IM drive via decoupling FBL for enhancing the dynamic as well as the steady-state performance of the IM drive. The fifth Section describes the tuning algorithm of the ANFIS controller. In the sixth Section, the execution and effectiveness of the proposed control technique based linearized IM drive is investigated in MATLAB environment in various operating conditions. The superiority of the proposed controller is analyzed and contrasted with the conventional PI-controller-based linearized IM drive in seventh Section. The eighth

and ninth Sections present the experimental implementation in a real-time using DSP 2812 to validate the different control strategies. Finally, concluding remarks are provided in the last Section.

3.2 Description of the Proposed System Configuration

The proposed ANFIS torque controller-based FBL IM drive system is demonstrated in Fig. 3.1. It consists of a rotor torque and flux observer to estimate torque and flux from the sensed input stator currents and voltages. The estimated flux is compared with the command flux which is generated from the estimated speed. Then, the flux error signal is processed through a PI-controller to produce signal u_1 which is input to the FBL controller. Similarly, another input u_2 to the FBL is generated by comparing the estimated torque and generated command torque followed by a torque controller which can be either ANFIS or PI controller. Further, the output of PI-flux controller, ANFIS, and rotor *d-q* flux components estimated from voltage model [4] are inputs to the FBL controller. The signal generated from the FBL scheme is fed to hysteresis current controller to generate the desired gate pulses for PWM voltage source inverter, which tracks the motor reference current to produce the desired torque.

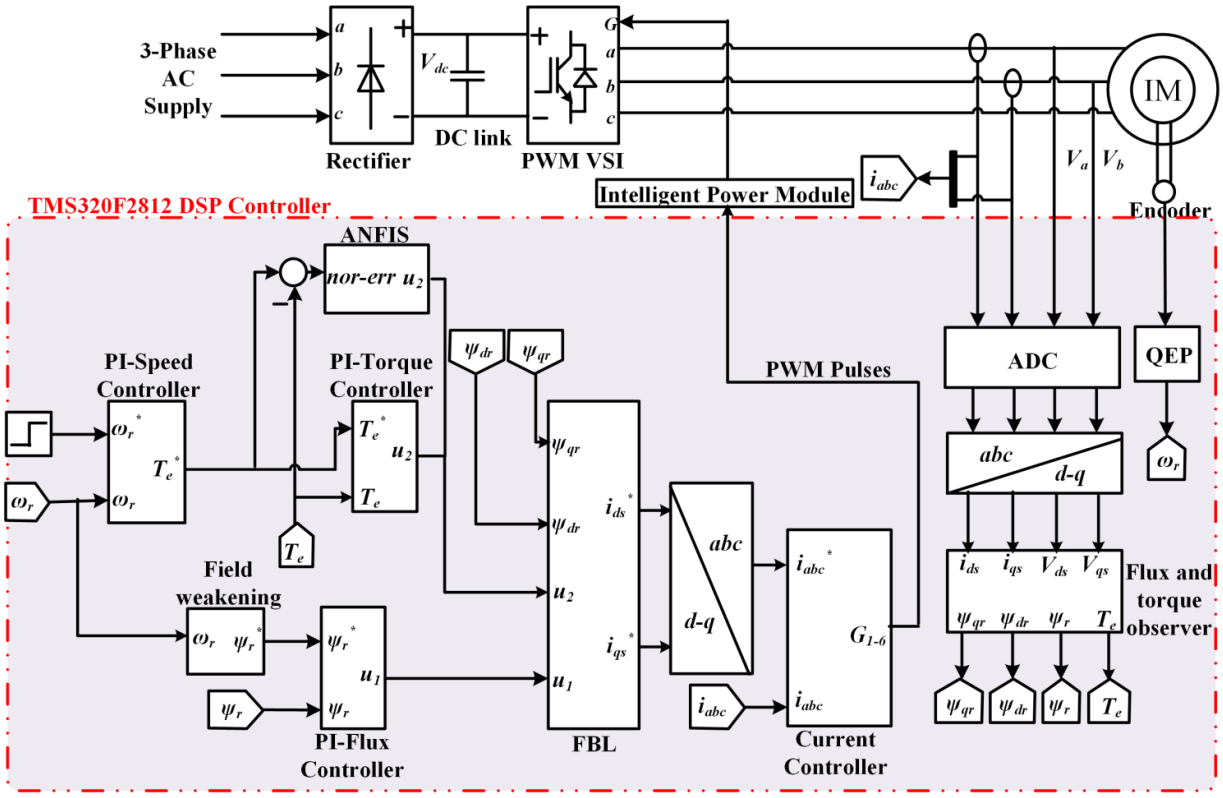

Fig. 3.1 Schematic diagram of an ANFIS torque controller-based linearized IM drive.

3.3 Rotor Flux and Torque Observer based on Estimation Strategy

An accurate estimation of flux is required to successfully implement the FBL scheme on IM drive system. A deterministic approach based enhanced method of flux estimation has been proposed in [140] which is known as Luenberger observer without the consideration of noise signal. Although the flux estimation accuracy is improved by the observer, there is a finite parameter variation effect. This estimation error tends to be more prominent as the speed approaches to zero. This observer-based flux-sensorless drive [4] has the demerits of noise sensitivity, modeling inaccuracies, and poor accuracy at low speeds. Due to extreme simplicity and ease of implementation, an estimation strategy based on voltage model [4] is adopted, where the stator voltages and currents are sensed, and the flux components are estimated in the *d-q* stationary reference frame. The *d-q* stator voltage and current components are calculated as follows:

$$\begin{bmatrix} V_{qs} \\ V_{ds} \end{bmatrix} = \frac{2}{3}\begin{bmatrix} 1 & -\frac{1}{2} & -\frac{1}{2} \\ 0 & -\frac{\sqrt{3}}{2} & \frac{\sqrt{3}}{2} \end{bmatrix}\begin{bmatrix} V_a \\ V_b \\ V_c \end{bmatrix} \tag{3.1}$$

$$\begin{bmatrix} i_{qs} \\ i_{ds} \end{bmatrix} = \frac{2}{3}\begin{bmatrix} 1 & -\frac{1}{2} & -\frac{1}{2} \\ 0 & -\frac{\sqrt{3}}{2} & \frac{\sqrt{3}}{2} \end{bmatrix}\begin{bmatrix} i_a \\ i_b \\ i_c \end{bmatrix} \tag{3.2}$$

where (V_a, V_b, V_c) and (i_a,i_b,i_c) are three-phase stator voltages and stator currents, respectively.

From (2.15), the following equations in the stationary reference frame are obtained.

$$V_{ds} = \left(R_s + \sigma L_s p\right) i_{ds} + \frac{L_m}{L_r} p\psi_{dr} \tag{3.3}$$

$$V_{qs} = \left(R_s + \sigma L_s p\right) i_{qs} + \frac{L_m}{L_r} p\psi_{qr} \tag{3.4}$$

The rotor flux components and then the torque can be obtained by using equations (3.3), (3.4), and (2.5).

From equations (3.3) and (3.4), the *d-q* components of flux ψ_{dr} and ψ_{qr} are obtained after integration operation which introduces DC offsets. This DC component leads to an error in the estimated flux during low-speed operations and it also severely affects motor operation.

Though this DC components are very small, they drive the integrators to saturation [141]. So to overcome this problem, a simple high pass filter is introduced here after integration operation to eliminate DC offset that arises due to the integration. The cut-off frequency ω_0 must be selected properly to remove the DC component so that the flux observer gives fast and accurate results at low speeds. When the machine is operated at the low-speed range, the cutoff frequency should be so selected that it avoid filtering the actual sinusoids. In this thesis, the ω_0 is chosen to be 5 rad/s.

The linearized model of IM drive formed by FBL technique is sensitive to parameter variations and plant uncertainties. As a result, a robust ANFIS control scheme is designed for confronting these challenges in real-time applications of the IM drive.

3.4 Design of ANFIS-Torque Controller

The knowledge representation of fuzzy logic controller (FLC) combining with the learning power of artificial neural network (ANN) system gives adaptive neuro-fuzzy inference (ANFIS) based controller. Since ANFIS design starts with a prestructured system, the degree of freedom for knowledge is constrained, i.e., the input and output membership functions (MFs) comprise of more information that a neural system needs to get from a test pair of data. Data concerning a system under an arrangement can be used right from the start. Some part of the system can be removed from training; therefore making the process more efficient. The intermediate results can be examined effortlessly as the rules are in linguistic form. ANFIS implements a first order Sugeno fuzzy system as a result of its computational efficiency and versatile procedures [4], [81], [82]. To start ANFIS tuning, a training data pair which contains necessary input-output data set of the target system to be designed is required. The objective is picked taking into account the best response of the system.

The schematic diagram of the proposed ANFIS based drive is demonstrated in Fig. 3.1. The ANFIS controller structural design integrates fuzzy logic and learning algorithm with a five-level artificial neural network arrangement [82] as portrayed in Fig. 3.2 (a). The parameter of the fourth layer is modified by tuning to control any deviation of control effort. The two inputs of the ANFIS controller are given by

error, $e(t)=T_e^* - T_e$

change in error, $\Delta e(t) = \dfrac{e(t)_k - e(t)_{k-1}}{T} \times 100$

where T_e^* is the reference torque, T is the sampling time, and k is the sampling instant.

In the proposed Sugeno fuzzy model [4] depicted in Fig. 3.2 (b), the typical rule set with fuzzy rules can be expressed as:

Rule i (i = 1, 2...7): if $e(t)$ is M_{1i} AND $\Delta e(t)$ is M_{2i} then $v_i = m_{1i}e(t) + m_{2i}\Delta e(t) + r_i$

Where M_{1i} and M_{2i} are the antecedent fuzzy sets and m_{1i}, m_{2i}, and r_i are the design parameters evaluated in training. Here v_i is the output singleton membership functions as shown in Fig. 3.2 (b).

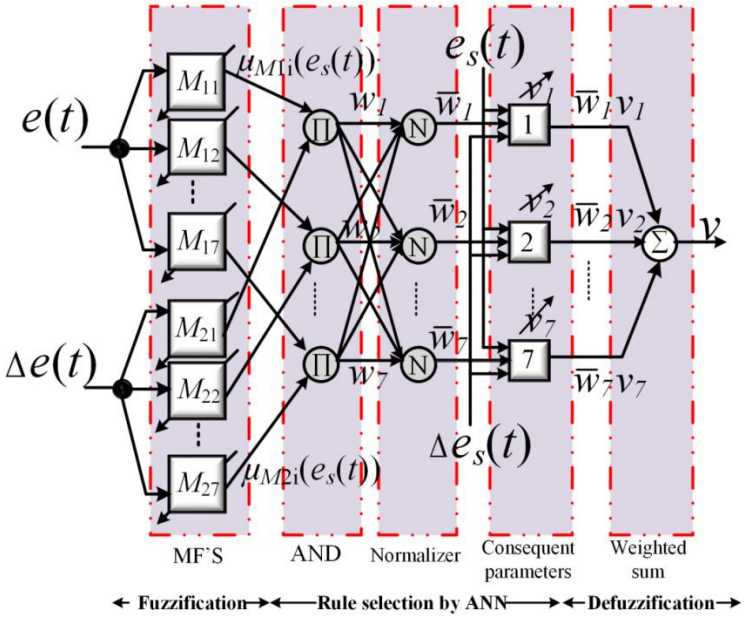

(a)

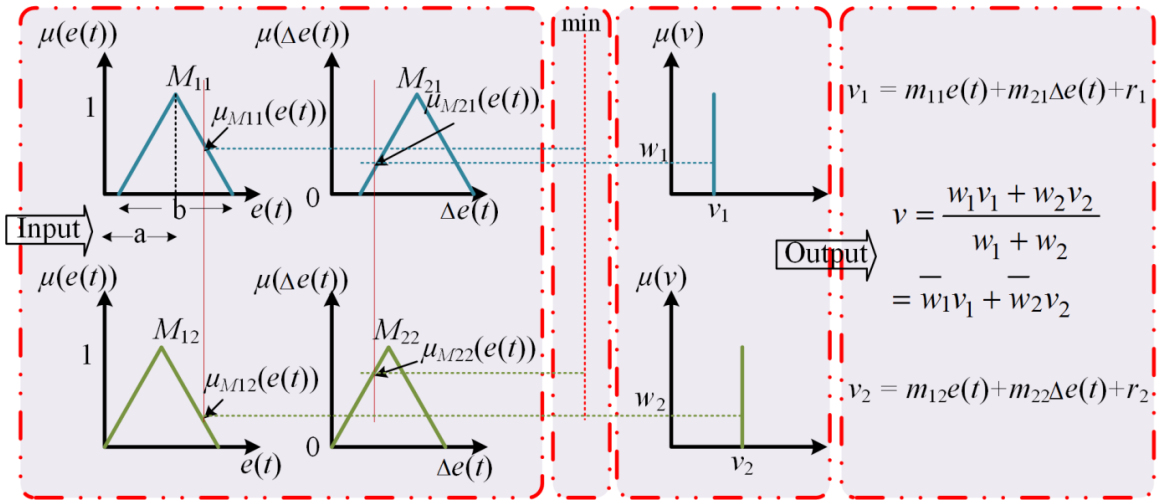

(b)

Fig. 3.2 (a) ANFIS controller structure with seven rules (b) Sugeno fuzzy model with two rules

Layer 1: Every adaptive node in this fuzzification layer contains node membership function.

$$O_i^1 = \mu_{M1i}(e(t)) \text{ , } i = 1, 2,\ldots 7 \tag{3.5}$$

$$O_i^1 = \mu_{M2i}(\Delta e(t)) \text{ , } i = 1, 2,\ldots 7 \tag{3.6}$$

where μ_{M1i} and μ_{M2i} are chosen to be a linear triangular symmetrical MFs as shown in Fig. 3.3 known as activation function which is specified by parameter $\{a, b\}$ as shown in Fig. 3.2 (b) as follows.

$$O_i^1 = \begin{cases} 0, & x_i^1 \le a - \dfrac{b}{2} \\ 1 - \dfrac{2\left|x_i^1 - a\right|}{b}, & a - \dfrac{b}{2} < x_i^1 < a + \dfrac{b}{2} \\ 0, & x_i^1 \ge a + \dfrac{b}{2} \end{cases} \tag{3.7}$$

Here O_i^j is the output corresponding to the i^{th} node number, and superscript 'j' denotes the j^{th} number of layer. x_i^1 is the input corresponding to the i^{th} node number of the first layer.

Layer 2: In this layer, the minimum of two input weights error or change in error value is picked up as firing strength of rules by the product operator 'AND' which is symbolized by $\prod$.

$$O_i^2 = w_i = \mu_{M1i}(e(t)).\mu_{M2i}(\Delta e(t)) = \min(\mu_{M1i}(e(t)),\mu_{M2i}(\Delta e(t)), \; i = 1, 2,\ldots 7 \tag{3.8}$$

Layer 3: This layer is symbolized by N where the weight is calculated by every node. As there are i number of weights in terms of firing strength of the rules, the normalized value with firing strength of $\overline{w_i}$ can be represented as

$$O_i^3 = \overline{w_i} = \frac{w_i}{\sum_i w_i} \text{ , } i = 1, 2,\ldots 7 \tag{3.9}$$

Layer 4: Every adaptive node i in this defuzzification layer determines the consequent value v_i and the output of this layer comprisesof a linear function given by

$$O_i^4 = \overline{w_i} v_i = \overline{w_i}(m_{1i} e(t) + m_{2i} \Delta e(t) + r_i) \text{ , } i = 1, 2\ldots 7 \tag{3.10}$$

where $\overline{w_i}$ is the output of layer 3, and (m_{1i}, m_{2i}, r_i) is the parameter set which is reflected to be the consequent parameters of the linear output function.

Layer 5: This is the output layer of ANFIS where the output *v* is estimated by the center-of-gravity method as specified below.

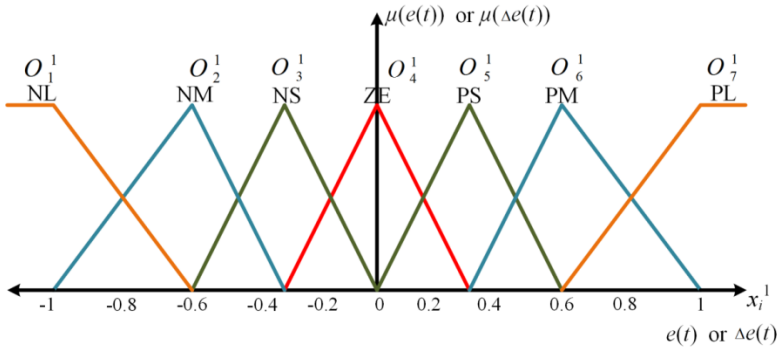

Fig. 3.3 Membership functions of torque error and change in torque error for the proposed ANFIS controller.

$$O_i^5 = \frac{\sum_i w_i v_i}{\sum_i w_i} = \sum_i \overline{w_i} v_i \qquad i = 1, 2,\ldots.7 \qquad (3.11)$$

The output *v* of which gives the predicted ANFIS value (u_2 of Fig. 3.1) can be written as

$$v = \sum_i (\overline{w_i} e(t)) m_{1i} + (\overline{w_i} \Delta e(t)) m_{2i} + (\overline{w_i}) r_i), \qquad i = 1, 2,\ldots.7 \qquad (3.12)$$

Fig. 3.4 signifies the surface view of the change in control output of ANFIS torque controller. The dependency of the output on two inputs, error (E) and change in error (CE) is displayed by using the surface viewer. Also, it is defined as the change in control output surface mapping of the system. Fig. 3.5 represents phase plot (vector plot) of the E and CE of the proposed controller which ensures the stability of the system controller [2]. In order to update the membership function parameters and weights, the ANFIS controller needs to be tuned.

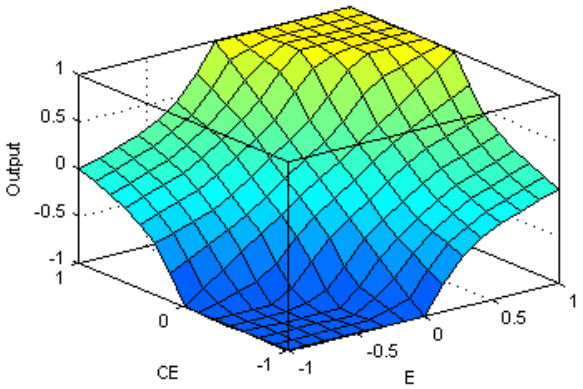

Fig. 3.4 Surface view of the proposed ANFIS controller

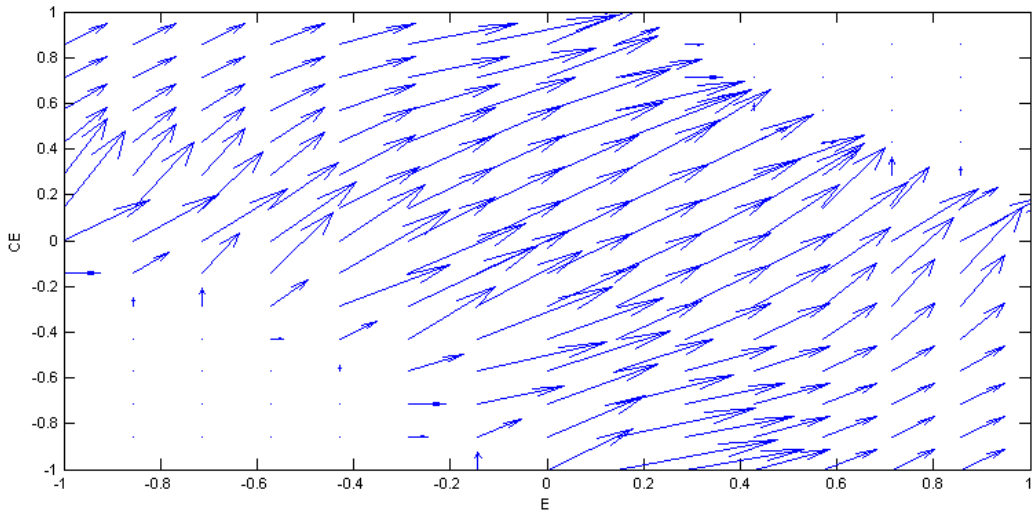

Fig. 3.5 Phase plot of the proposed ANFIS controller

3.5 Tuning Algorithm for ANFIS Controller

Back-propagation algorithm is developed here in this Section for the ANFIS controller which is automatically tuned by least square estimation strategy [81]. Back-propagation algorithm is very fast where the weight is updated by gradient descent rule which has salient features like locating global minimum of the cost function, fast convergence, good generalization, and less computational complexity [142], [143].

The cost function of the proposed work is defined as

$$E = \frac{1}{2}\sum_{p=1}^{n}(v_p^d - v_p)^2 \tag{3.13}$$

where v_p^d stands for desired output for p^{th} specific pattern and v_p is the actual output predicted by ANFIS. n is the number of pattern for the controller. According to the network error ξ, the data is tuned by back-propagation training algorithm.

Rather than employing the desired controller output v as a target, an error signal e which studies the performance of the controller and assesses the present condition of the system is utilized to manage the control activity by changing it in right directions and also to deliver the desired response [83]. So the objective function to be minimized is redefined as follows.

$$E = \frac{1}{2}(T_e^* - T_e)^2 = \frac{1}{2}e^2 \tag{3.14}$$

where T_e^* is the reference torque, and T_e is the actual or estimated torque. To achieve the desired control performance, the back-propagation parameter adaptation rules for instantaneous parameter update can be derived as

$$a_i(k+1) = a_i(k) - \eta_{ai} \nabla_{ai} E(k) \tag{3.15}$$

$$b_i(k+1) = b_i(k) - \eta_{bi} \nabla_{bi} E(k) \tag{3.16}$$

$$w_i(k+1) = w_i(k) - \eta_{wi} \nabla_{wi} E(k) \tag{3.17}$$

where (a_i, b_i) is the value of (a, b) corresponding to i^{th} node, (η_{ai}, η_{bi}, η_{wi}) is the set of fixed learning rates of corresponding parameters (a_i, b_i, w_i), and ($\nabla_{ai}, \nabla_{bi}, \nabla_{wi}$) is the set of gradients of cost function E corresponding to parameters (a_i, b_i, w_i). These are described by the following equations.

$$\nabla_{ai} E = \frac{\partial E}{\partial e} \frac{\partial e}{\partial T_e} \frac{\partial T_e}{\partial v} \frac{\partial v}{\partial O_i^1} \frac{\partial O_i^1}{\partial a_i} \tag{3.18}$$

$$\nabla_{bi} E = \frac{\partial E}{\partial e} \frac{\partial e}{\partial T_e} \frac{\partial T_e}{\partial v} \frac{\partial v}{\partial O_i^1} \frac{\partial O_i^1}{\partial b_i} \tag{3.19}$$

$$\nabla_{wi} E = \frac{\partial E}{\partial e} \frac{\partial e}{\partial T_e} \frac{\partial T_e}{\partial v} \frac{\partial v}{\partial w_i} \tag{3.20}$$

The common differential terms of aforesaid equations are determined as follows:

$$\frac{\partial E}{\partial e} = T_e^* - T_e \tag{3.21}$$

$$\frac{\partial e}{\partial T_e} = -1 \tag{3.22}$$

$$\frac{\partial T_e}{\partial v} = \text{constant } K \tag{3.33}$$

The value of K is greater than zero for the proposed induction motor drive scheme [74], [137]. The other terms of equations (3.18) – (3.20) are determined from equations (3.7) – (3.12) as

$$\frac{\partial v}{\partial O_i^1} = \frac{v_i(k)}{\sum w_i(k)} \tag{3.34}$$

$$\frac{\partial O_i^1}{\partial a_i} = \frac{2}{b_i(k)} \tag{3.35}$$

$$\frac{\partial O_i^1}{\partial b_i} = \frac{1 - O_i^1(k)}{b_i(k)} \tag{3.36}$$

$$\frac{\partial v}{\partial w_i} = \frac{v_i(k)}{\sum o_i^2(k)} \tag{3.37}$$

Error tolerance is used to create stopping criterion which is related to the error size. These errors are displayed for 30 epochs but, prior to five iterations, the controllers settled down to the minimum error as shown in Fig. 3.6. The MFs designed by parameter $\{a, b\}$ is updated according to the error propagated in a backward manner and thus changing the shape of the triangular MFs. So after tuning, the error tolerance is close to zero as shown in Fig. 3.6 and the shape of the MFs is also altered. The MFs before tuning and by using grid method, the MFs after tuning are shown in Fig. 3.7 (a) and (b).

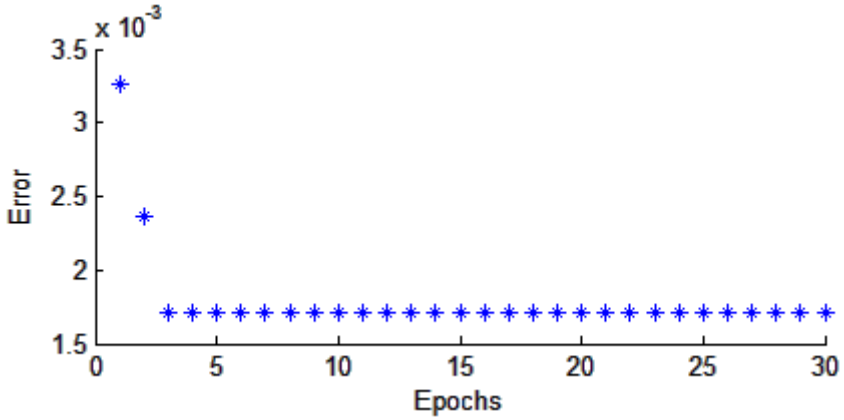

Fig. 3.6 Error of the proposed ANFIS controller

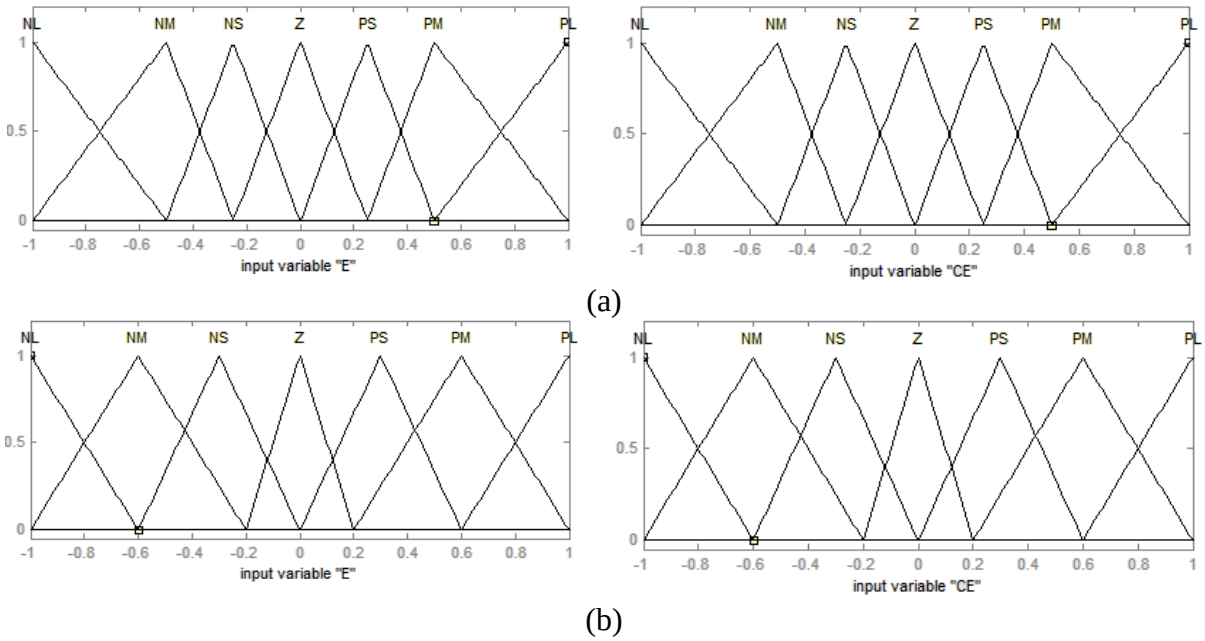

Fig. 3.7 MFs of error (E) and change in error (CE): (a) before tuning and (b) after tuning.

3.6 Simulation of the FBL IM Drive System

The simulation of the FBL IM drive system has been performed by using MATLAB software which is used to verify the reliability and versatility of the developed model using various controllers. The different sub-model blocks of MATLAB are explained in the following subsections.

3.6.1 Field Weakening Controller

The FBL IM drive with this field weakening operation is equivalent to the field controlled separately excited DC motor. When the drive speed goes above the base speed, this operation is applied. The input to the field weakening controller is the sensed speed of the IM drive, and the output is the reference rotor flux (ψ_r^*) as obtained in equations (3.38) and (3.39) given below. The rotor flux remains constant below the base speed, and it changes inversely above the base speed. Thus the main operation of the field weakening controller is to generate a flux command according to the actual sensed speed of the drive.

If $\omega_r \leq \omega_b$, $\psi_r^* = \psi_r$ (3.38)

If $\omega_r > \omega_b$, $\psi_r^* = \left(\frac{\omega_b}{\omega_r}\right)\psi_r$ (3.39)

where ψ_r and ψ_r^* are the rated (nominal) flux and reference rotor flux, respectively. ω_r and ω_b are the rotor speed and rotor base speed of the IM drive, respectively.

3.6.2 PI Controllers

The proportional integral (PI) controllers in the FBL IM drive system are simulated in the discrete time domain as

$$u(k) = u(k-1) + K_p[e(k) - e(k-1)] + K_i e(k)T \quad (3.40)$$

where

$u(k)$ = output of the controller at the k^{th} sampling instant

$e(k)$ = input error to the controller at the k^{th} sampling instant

T = sampling time

K_p and K_i are the proportional and the integral gains of the PI controllers, respectively.

3.6.2.1 PI-Speed Controller

The command speed ω_r^* and the actual sensed speed ω_r are compared, and the error is fed to the speed controller. This speed error at k^{th} instant is given by

$$e_s(k) = \omega_r^*(k) - \omega_r(k) \tag{3.41}$$

As the input to the PI-speed controller is discretized, the equation of the PI controller requires to be discretized as follows:

$$T_e^*(k) = T_e^*(k-1) + K_{p4}[e_s(k) - e_s(k-1)] + K_{i4}e_s(k)T \tag{3.42}$$

3.6.2.2 PI-Torque Controller

Like PI-speed controller, the equations of the PI-torque controller of the mechanical subsystem are given by

$$e_T(k) = T_e^*(k) - T_e(k) \tag{3.43}$$

$$u_2(k) = u_2(k-1) + K_{p3}[e_T(k) - e_T(k-1)] + K_{i3}e_T(k)T \tag{3.44}$$

3.6.2.3 PI-Flux Controller

The equations of the PI-flux controller of the electrical subsystem at k^{th} instant are given by

$$e_\psi(k) = \psi_r^*(k) - \psi_r(k) \tag{3.45}$$

$$u_1(k) = u_1(k-1) + K_{p1}[e_\psi(k) - e_\psi(k-1)] + K_{i1}e_\psi(k)T \tag{3.46}$$

The outputs of the PI controllers are restricted to predefined maximum and minimum values according to the type of controller used. In case of step change in speed, speed reversal, and load perturbation, the motor torque goes beyond the breakdown torque which may produce overcurrent and lead to instability. So, to make the motor torque within the reasonable value, the output of the speed controller (T_e^*) is fed to a limiter. Finally, the torque producing component of the current is calculated on the basis of the reference torque.

3.6.3 PWM Voltage Source Inverter

A hysteresis current controlled PWM voltage source inverter (VSI) as shown in Fig. 3.8 is implemented for the closed-loop drive system. The required switching signals for the inverters are produced using hysteresis band current controlled PWM method. A constant voltage source is applied at the inverter input, and the output 3-phase currents (i_a, i_b, and i_c) track the motor reference currents (i_a^*, i_b^*, and i_c^*) to produce the desired torque. The output currents of the VSI have variable frequency depending upon different operating modes. The switching state of the IGBTs of three arms determines the output voltage of the inverter. The

switching signals S_1, S_2, and S_3 are 0 for ON state of the lower switches and are 1 for ON state of the upper switches.

The equations of the three phase voltages in terms of the DC link voltage and switching signals are given by [4]

$$V_a = \frac{V_{dc}}{3}(2S_1 - S_2 - S_3) \tag{3.47}$$

$$V_b = \frac{V_{dc}}{3}(-S_1 + 2S_2 - S_3) \tag{3.48}$$

$$V_c = \frac{V_{dc}}{3}(-S_1 - S_2 + 2S_3) \tag{3.49}$$

Here, the following assumptions are made for the simulation of the VSI.

- The switching device drop and the effect of switching network are neglected.
- The switching delay of the individual switches along with the delay time between the switching instants in the same arm of the inverter is negligible.

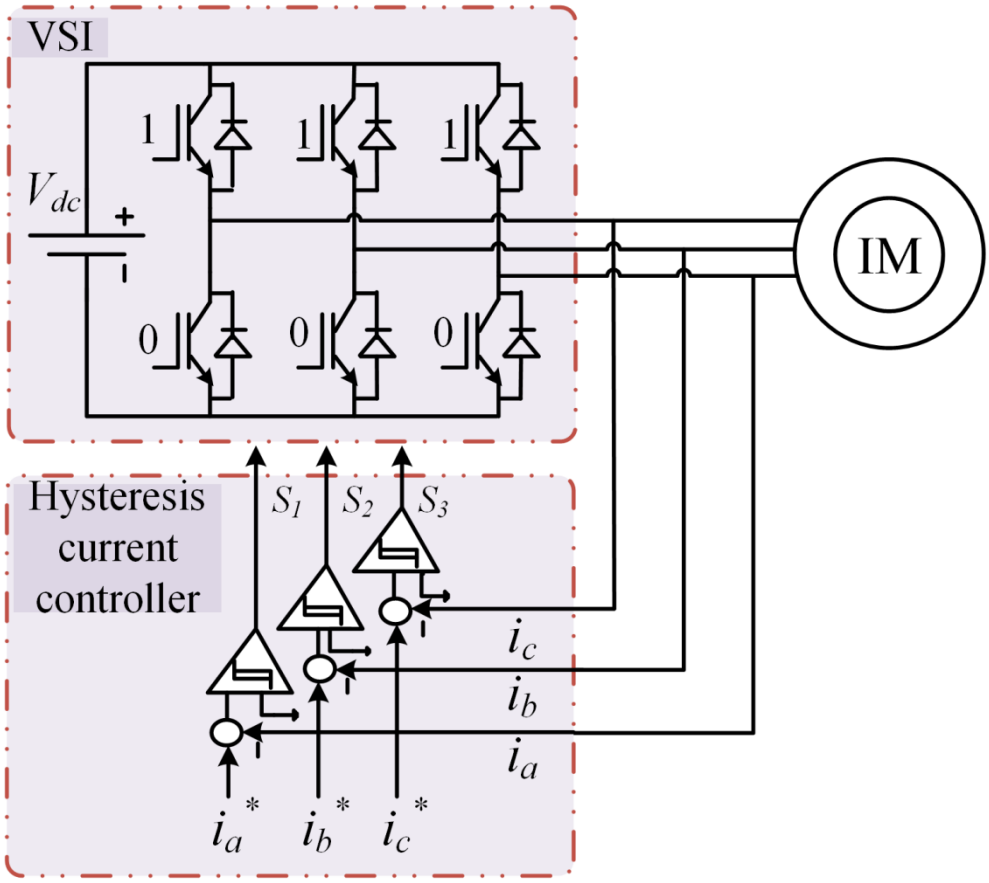

Fig. 3.8 Schematic diagram of hysteresis current controlled PWM VSI

3.6.4 Hysteresis PWM Current Controller

The function of the hysteresis current controller as shown in Fig. 3.8 is to produce the desired switching signals for the PWM VSI by comparing the reference current with the actual motor current within the hysteresis band. The proper selection of hysteresis band limit is required for the improved performance of the current controller [144]. The principle of generation of switching pulses of the hysteresis PWM is demonstrated in Fig. 3.9.

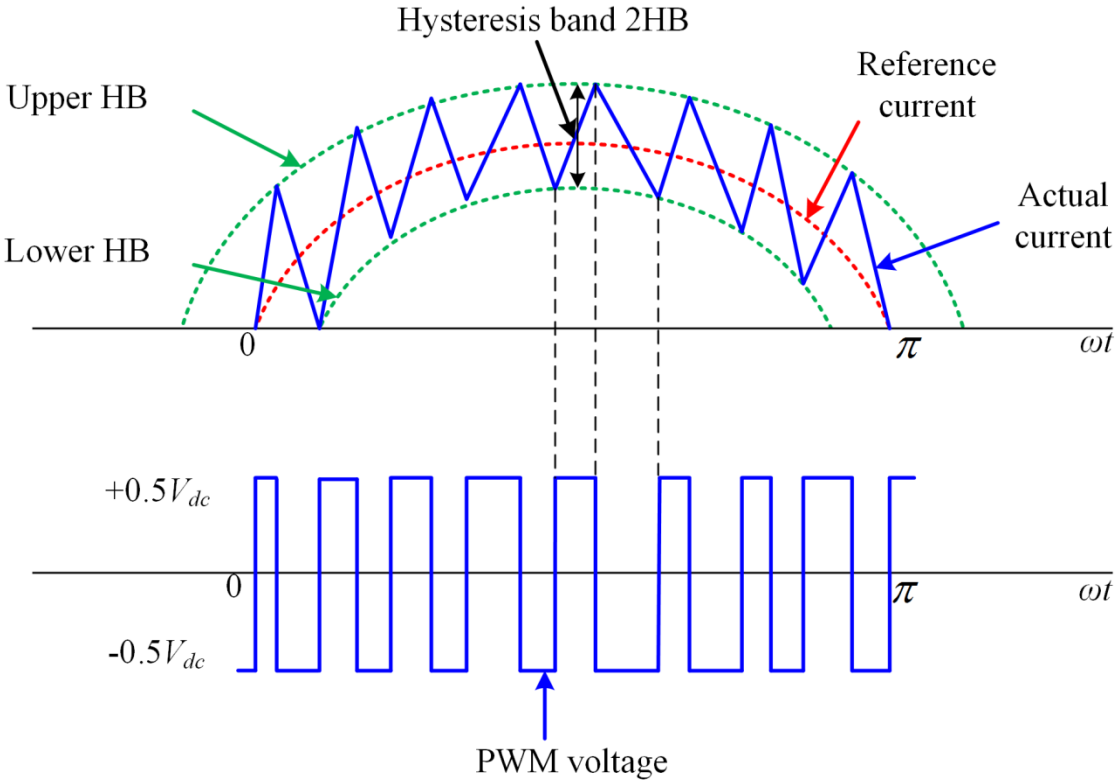

Fig. 3.9 Hysteresis band current controlled PWM

3.6.5 Feedback Linearization IM drive

The feedback linearization (FBL) controlled IM drive is simulated in the stationary reference frame whose details are described in Chapter 2.

3.7 Simulation Results and Analysis

The effectiveness and feasibility of proposed linearization concept with PI-torque controller and ANFIS torque controller are verified in MATLAB/Simulink environment using hysteresis PWM inverter for 3.7 kW IM. The performance results corresponding to various responses of speed, torque, rotor flux, and stator current are presented in Figs. 3.10 - 3.13 and a comparative analysis is demonstrated in Table 3.1 and Table 3.2.

3.7.1 Results with PI-Torque Controller

Case1: *Starting and forward motoring*

In this case, motor accelerates at a constant rate and reaches its set point speed of 400 rpm in 0.4 s with applied DC link voltage of 646 V as shown in Fig. 3.10 (i). The line voltage, line voltage with current, and gate pulses during starting are shown as in Fig. 3.10 (i). The current, torque and speed of the IM are settled at 0.4 s, and the flux amplitude is almost uniform from starting to steady state. However, the sudden increase in capacitor voltage V_{dc} is observed at starting as the capacitor charges and settles down later within 5 to 6 cycles by discharging through properly selected switching path as shown in Fig. 3.13 (i). Also, the capacitor voltage is reduced during the sudden increase of stator current at 3 s as the energy stored in the capacitor gets released when the large current is drawn by motor through the capacitor and comes to the steady state after one cycle (0.02 s). Substantial ripple and chattering in torque appear in the torque response with this PI-controller.

Case2: *Load perturbation*

A sudden load torque of 10 N-m is applied from 1 s to 1.5 s while the motor operating at steady-state of 400 rpm as depicted in Fig. 3.11 (i). It leads to undershoot and overshoot in speed of about 1.7 rpm at 1s and 1.5 s, respectively with settling period of around 10 to 11 cycles (0.2 s), accompanied by an increase in stator current amplitude to 8.5 A and sudden decrease of capacitor voltage to 644 V (as shown in Fig. 3.13) settled at 1.02 s. Likewise, the capacitor starts discharging and charging during application and removal of the load, which is evident from Fig. 3.13 (i). However, all through the operations, the flux amplitude is maintained uniform. The line voltage behavior during application and withdrawn of load is shown in Fig. 3.11 (i).

Case3: Speed reversal and reverse motoring

Subsequently, speed reversal is taking place at 2 s, motor decelerates at a uniform rate to zero speed and then settled at -400 rpm at 2.73 s as shown in Fig. 3.12 (b) (i). The line voltage responses at different points are shown in Fig. 3.12 (a) (i). This is accompanied by large stator current due to large negative motor torque and reversal of current takes place when speed crosses zero. During reversing, the frequency of the current is getting reduced first by the controller displaying regenerative braking followed by phase reversal. Again, the motor operates in the forward direction at 3 s and the speed, torque, and currents are steady at 4.4 s. Furthermore, the responses demonstrate the replica of the previous one.

3.7.2 Results with ANFIS-Torque Controller

Similar operating conditions as described above for the PI-torque controller were carried out for ANFIS-torque controller during starting, loading, and speed reversing and results are shown in Figs. 3.10 (ii) - 3.13 (ii). The line voltage behavior and gate signals during starting are shown in Fig. 3.10 (ii). At starting, the current drawn by stator is less, i.e., 18 A, settles rapidly at 0.39 s with less peak capacitor voltage V_{dc} and less flux ripple as compared to PI-torque controller. The torque response during starting is significantly improved as the torque ripple is remarkably reduced. Further, the line voltage responses at different points during reversal of speed are shown in Fig. 3.12 (a) (ii). During reversing the speed in both forward and reverse direction, the motor settles down faster at 2.7 s and 4.33 s. Moreover, this ANFIS controller based linearized induction motor has less dip in capacitor voltage with less torque distortion. The line voltage characteristic during loading of IM is shown in Fig. 3.11 (ii). During load perturbation at the same instant of PI-torque controller-based linearized IM, it was observed that the use of ANFIS-torque controller improves the speed response by a good load disturbance rejection with less undershoot and overshoot of 1.4 rpm and less settling time of around 3 to 4 cycles (0.07 s) as compared to PI-torque controller. It has also remarkably less ripple than that of PI-torque controller. The torque ripple is substantially reduced as compared to PI controller leading to less distorted motor current. Also, it is evident from the result of Fig. 3.13 (ii) that the proposed ANFIS controller improves the system performance considerably as far as the decoupling at all level is concerned. It also demonstrates overall superior dynamic and steady-state performance as compared to the conventional PI-torque controller.

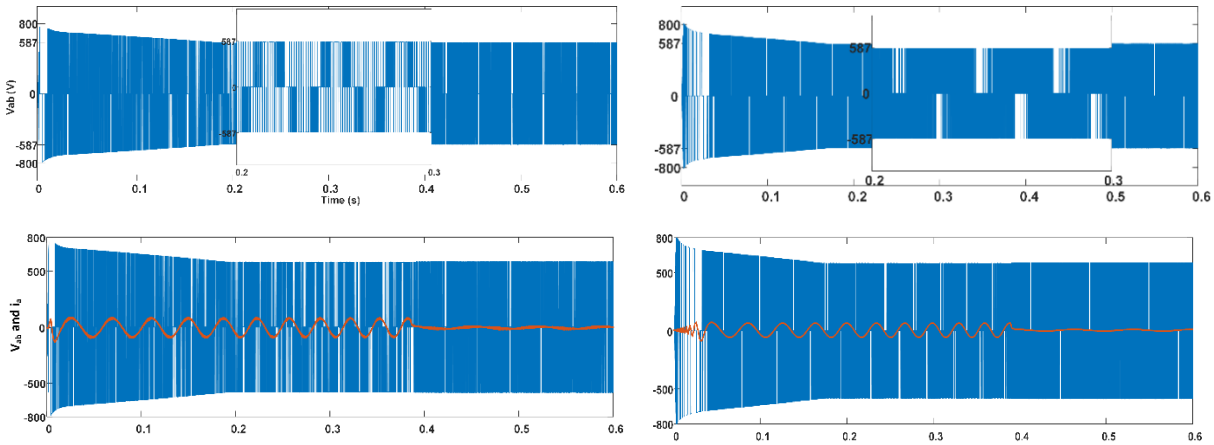

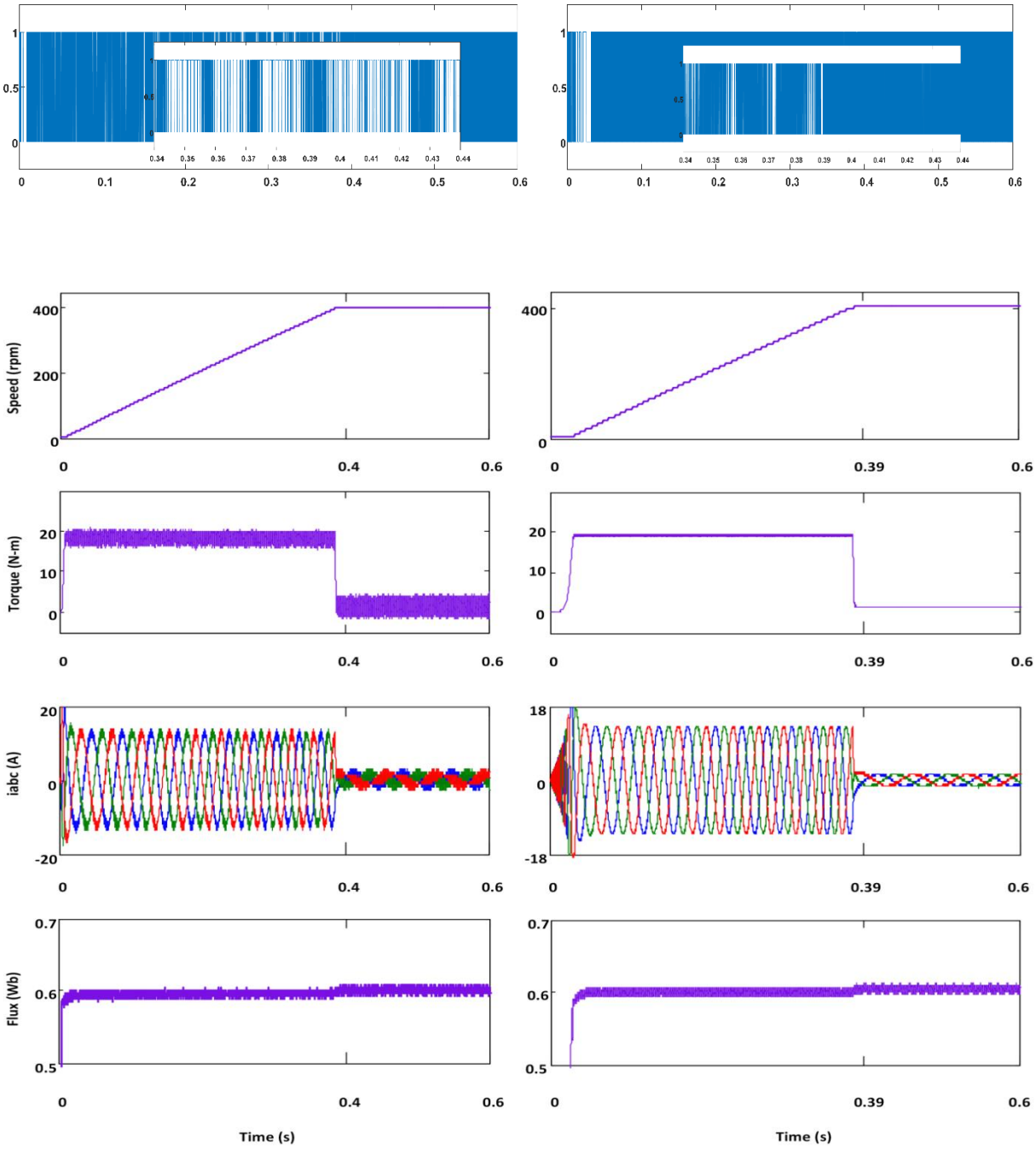

(i) (ii)

Fig. 3.10 Dynamic and steady-state performance characteristics (line voltage (V_{ab}), line voltage and current (V_{ab} and i_a), gate signals, speed (n_r), motor torque (T_e), 3-phase stator current (i_{abc}), and rotor flux (ψ_r)) of linearized decoupling controlled drive scheme during starting: (i) PI-torque controller and (ii) ANFIS-torque controller.

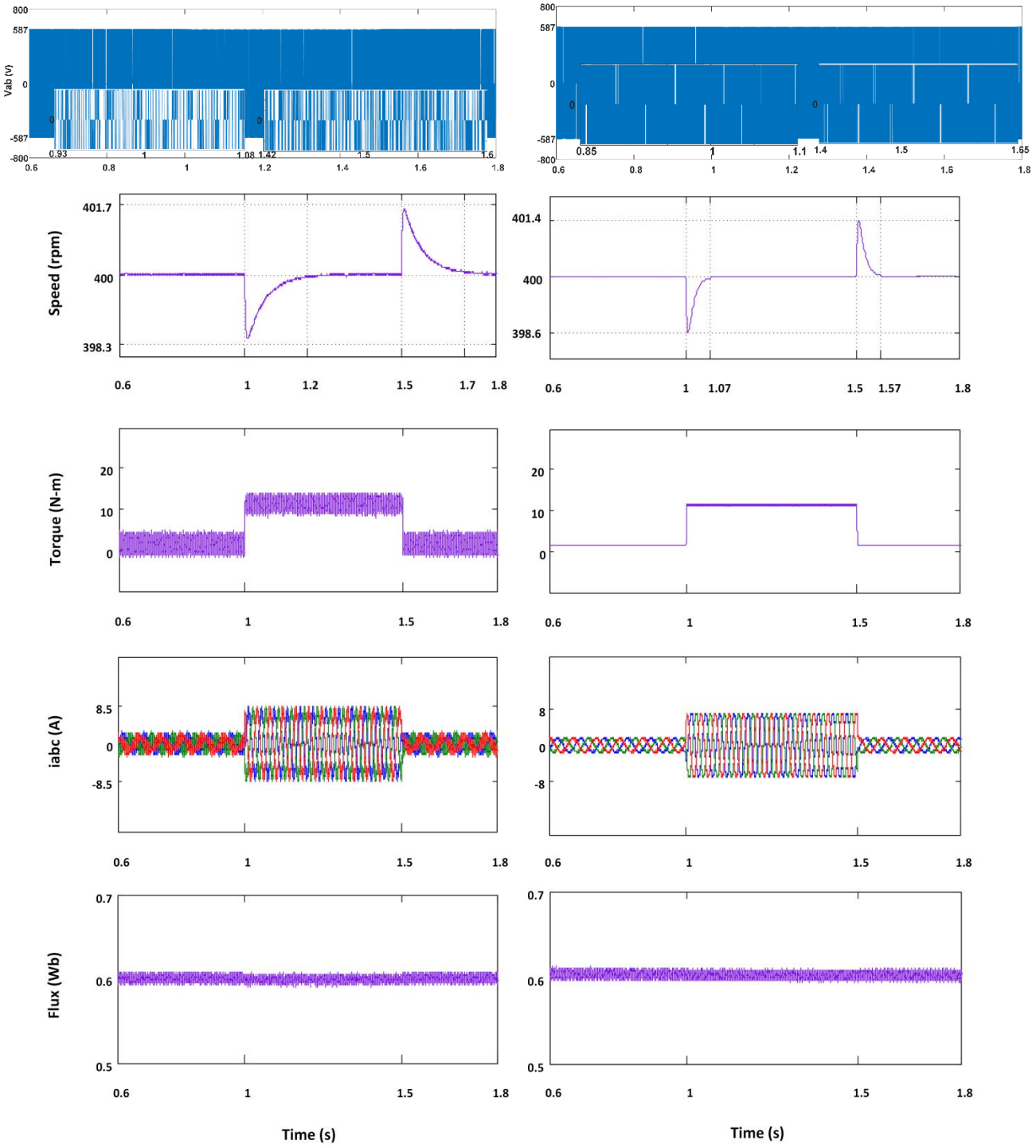

(i) (ii)

Fig. 3.11 Dynamic and steady-state performance characteristics (line voltage (V_{ab}), speed (n_r), motor torque (T_e), 3-phase stator current (i_{abc}), and rotor flux (ψ_r)) of linearized decoupling controlled drive scheme during load perturbation (10 N-m): (i) PI-torque controller and (ii) ANFIS-torque controller.

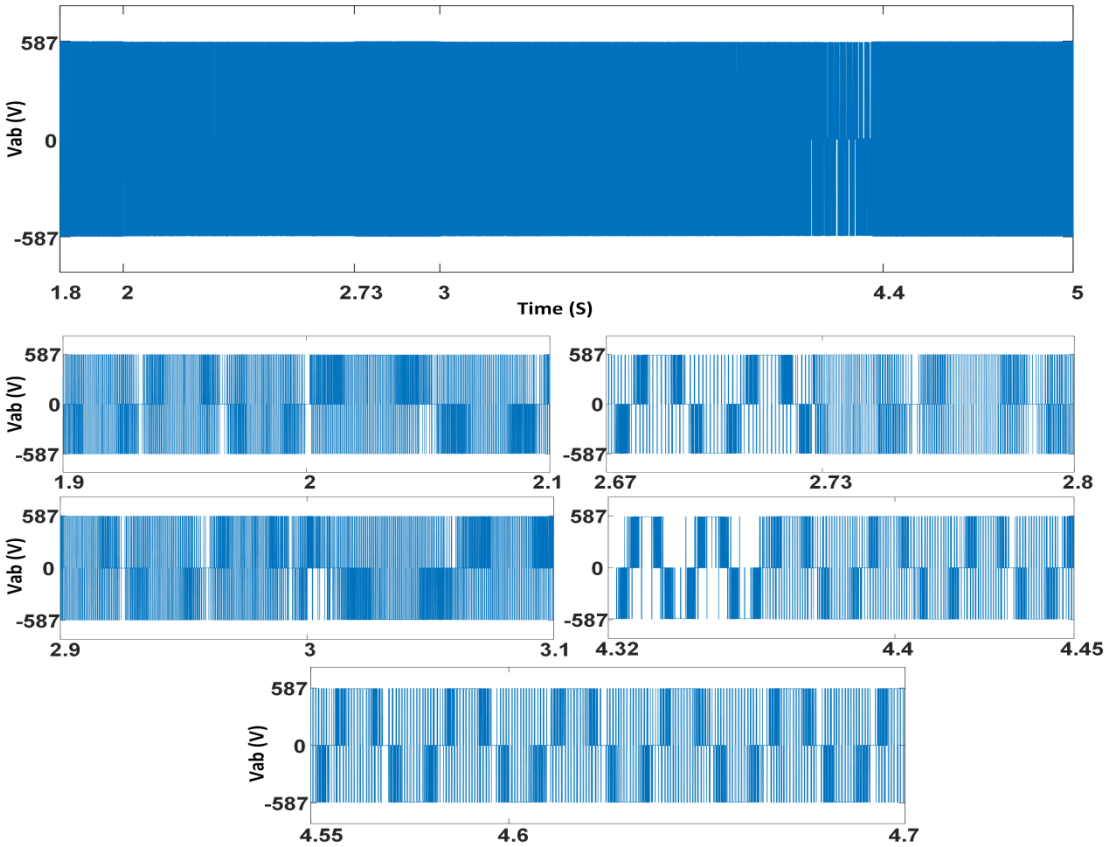

(i)

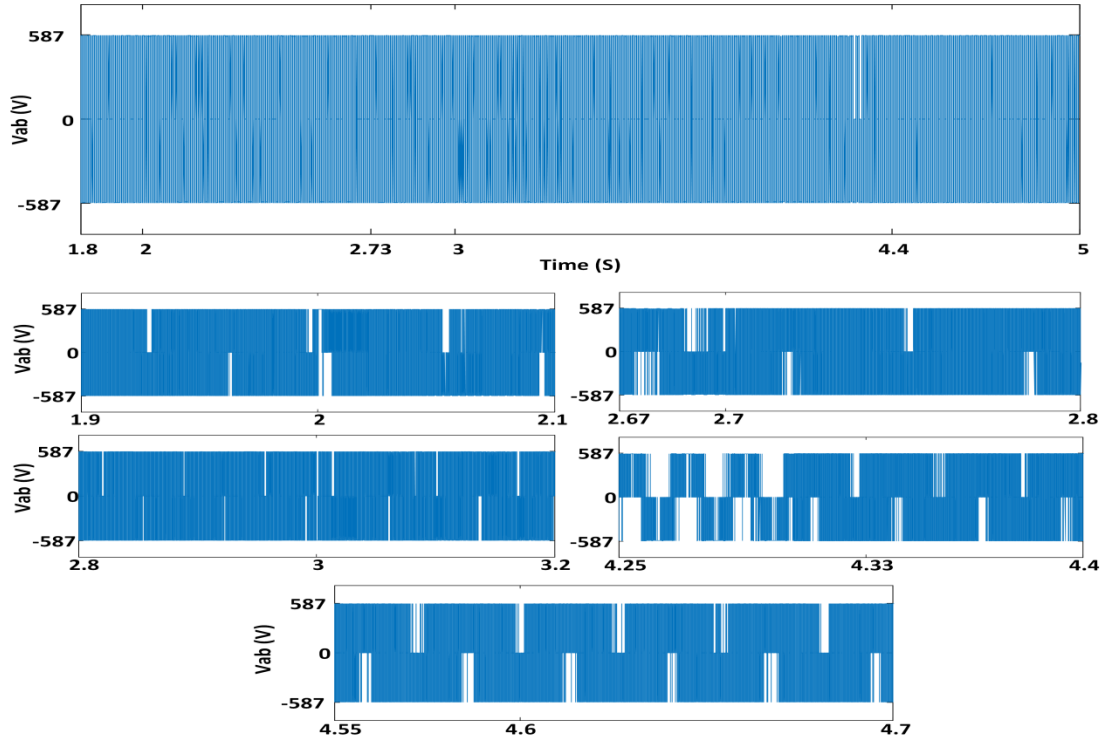

(ii)

Fig. 3.12 (a) Line voltage (V_{ab}) response of FBL controlled IM drive during speed reversal and forward again using (i) PI controller and (ii) ANFIS controller.

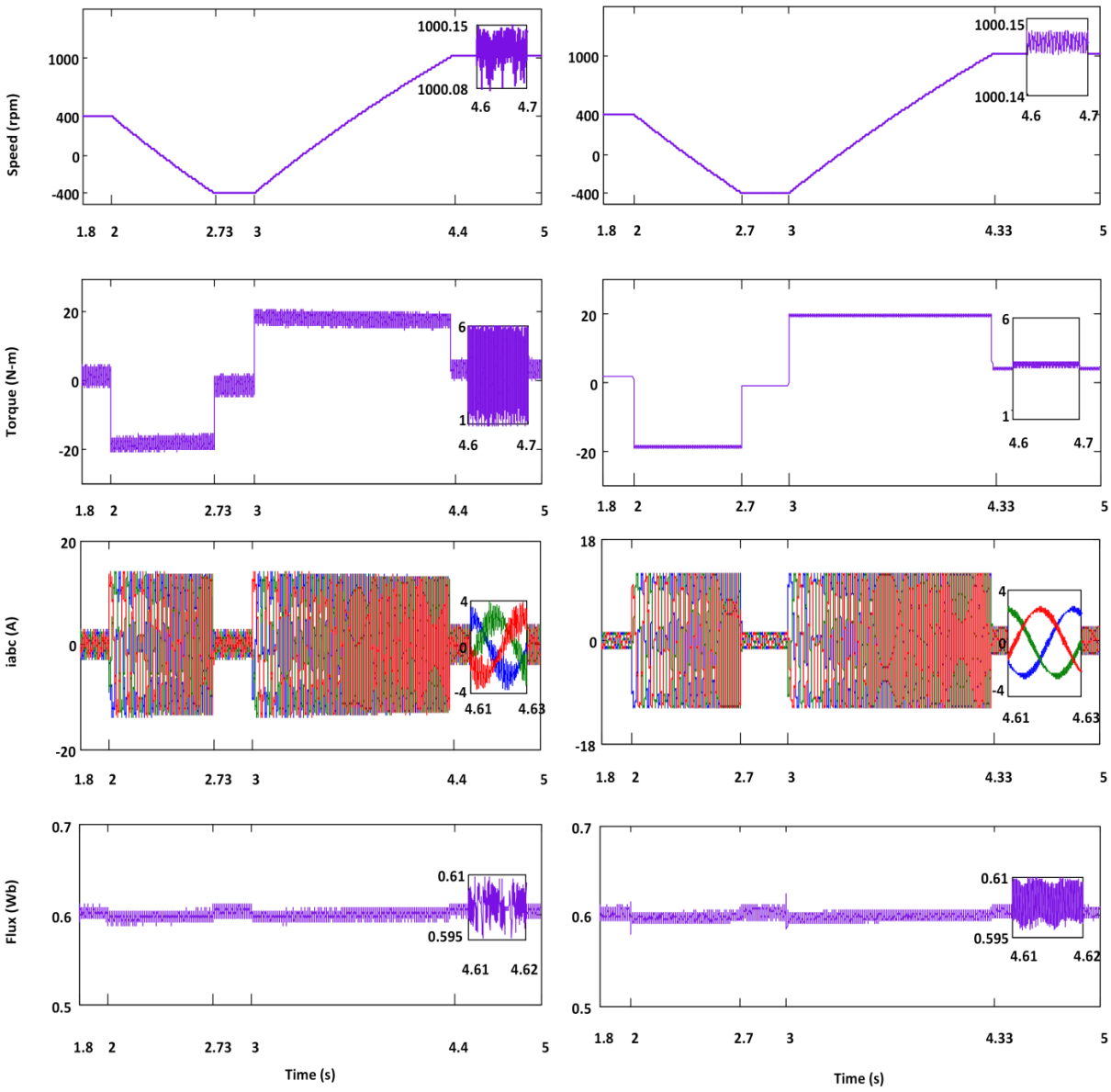

Fig. 3.12 (b) Dynamic and steady-state performance characteristics (speed (n_r), motor torque (T_e), 3-phase stator current (i_{abc}), and rotor flux (ψ_r)) of linearized decoupling controlled drive scheme during speed reversal: (i) PI-torque controller and (ii) ANFIS-torque controller.

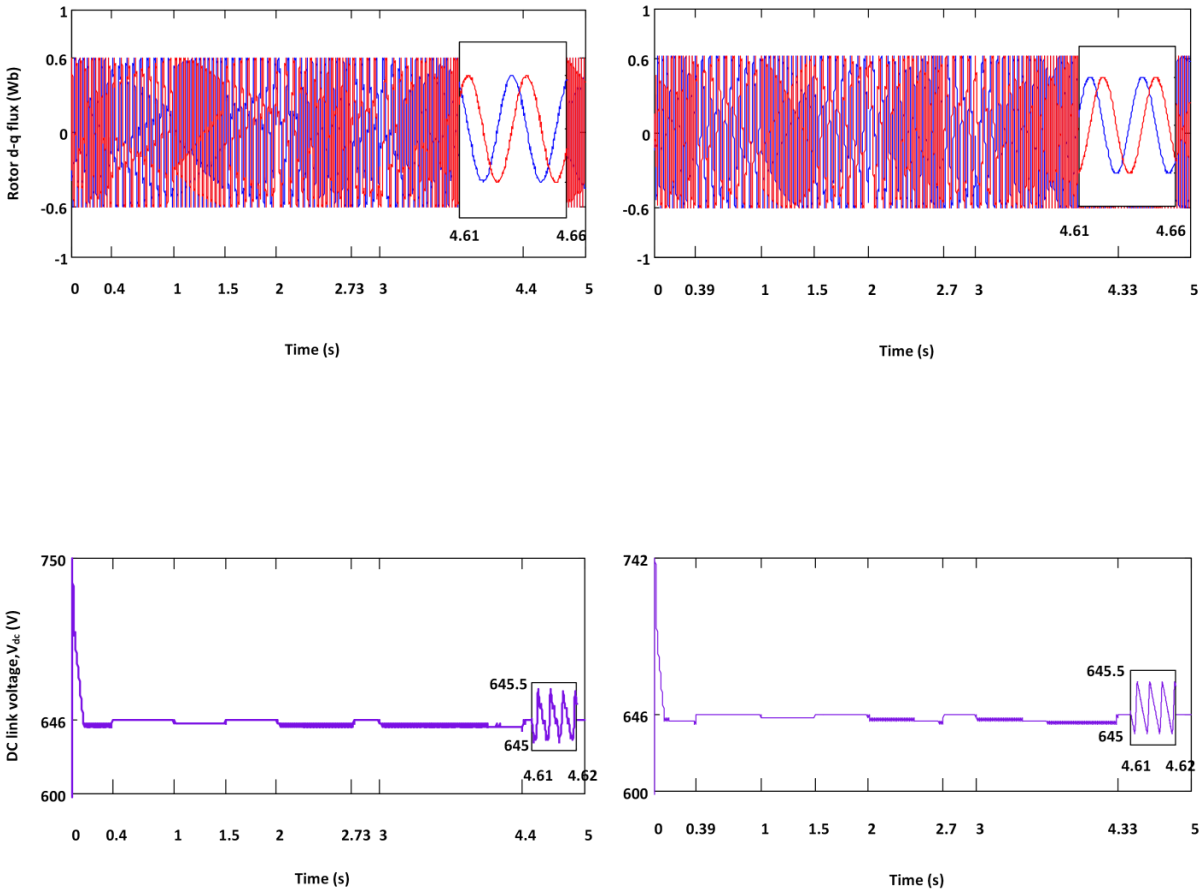

(i) (ii)

Fig. 3.13 Dynamic and steady-state performance characteristics (rotor *d-q* flux (ψ_{dqr}) and DC link or capacitor voltage (V_{dc})) of linearized decoupling controlled drive scheme during starting, loading (10 N-m), and speed reversing: (i) PI-torque controller and (ii) ANFIS-torque controller.

3.8 Experimental Setup

The proposed auto-tuned ANFIS-based feedback linearized IM drive system was validated in real-time using the platform of 32-bit fixed point DSP TMS320F2812 [145]. The real-time with a prototype FBL IM drive and an experimental setup are illustrated in Fig. 3.14 (a) and (b). The motor specifications are same as given in Appendix A.1. Hall-effect voltage sensor (LEM LV 25-P) and current sensor (LEM LTS 25-NP) sense the actual motor line voltages and currents, which are fed to the DSP board through A/D channels. The hysteresis current controlled PWM signals are generated by the DSP board which are required to be fed to the switches of 3-phase voltage source inverter. In order to get the load perturbation for torque analysis, IM is coupled to a DC machine shaft. Then by introducing resistance on armature circuit of DC generator, the load torque is varied. Other than the current, all the variables of this test are observed through a D/A converter, and these are displayed on a digital oscilloscope.

The developed real-time Simulink model of the proposed controller with the auto-tuning algorithm is compiled and dumped into DSP board using a JTAG emulator. A PI-controller based linearized IM drive system is also validated experimentally in order to have a fair comparison. In order to have a fair comparison with the proposed controller, the PI controller tuning was done by using the conventional second-order single-variable linear system theory as it provides simple mathematical analysis approach [138]. The details of PI tuning are described in Chapter 2.

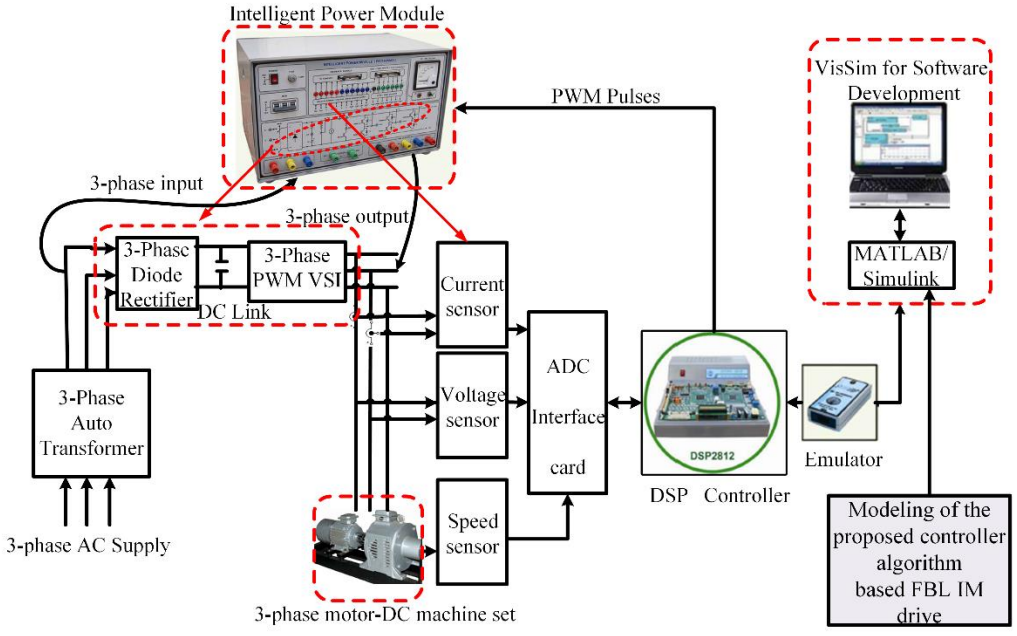

(a)

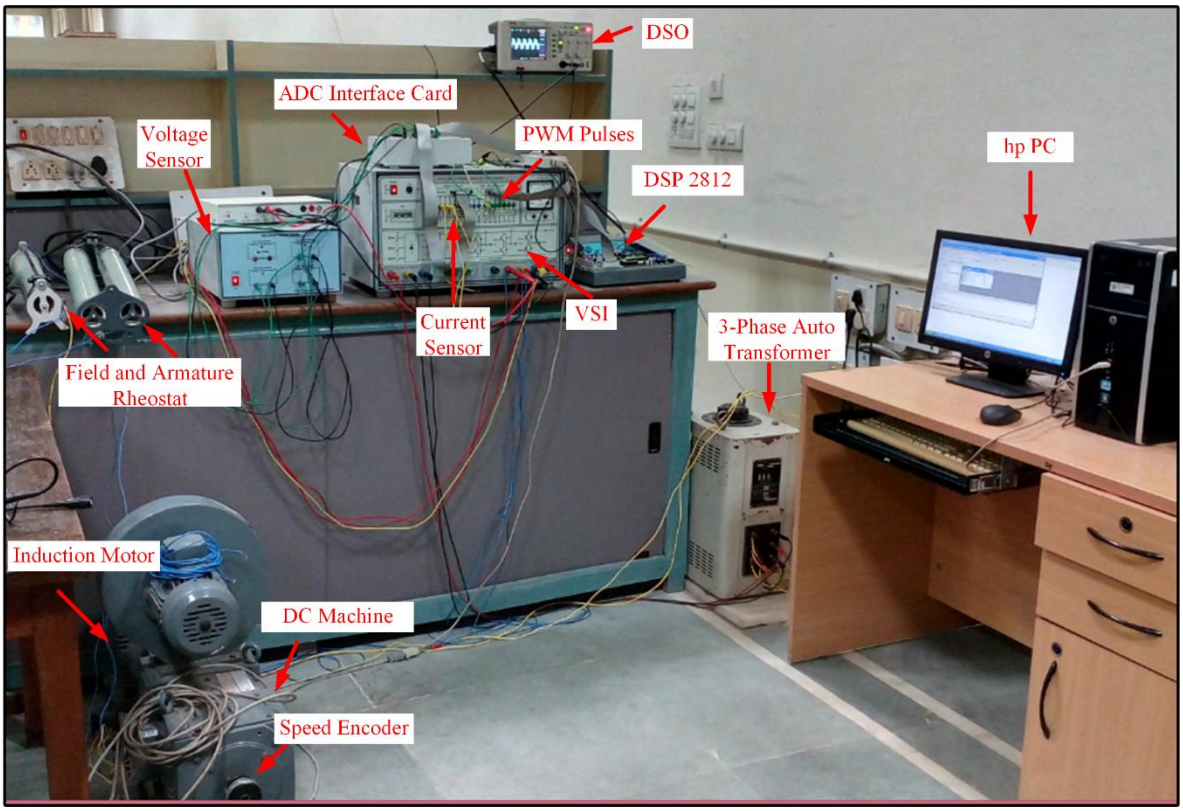

(b)

Fig. 3.14 Experimental prototype: (a) block diagram (b) laboratory setup.

3.9 Experimental Validation

With the real-time experimental setup shown in Fig. 3.14, the linearized IM drive with PI and ANFIS torque controller are verified under various operating mode. Subsequently, in order to show the robustness of the controllers, the linearized IM drive is investigated with the different gain values of speed-PI controller under the step change in load torque of 5 N-m as shown in Fig. 3.18 at steady-state speed by varying the armature resistance of DC machine connected to IM. The details of the experimental performance under various operating conditions are mentioned in Table 3.1 and Table 3.2.

Case1: Initially, the experimental performance of starting dynamics and forward motoring is carried out under 400 rpm without any load perturbation as illustrated in Fig. 3.15 (a) and (b). The linearized IM accelerates from rest condition to steady state speed 400 rpm in 0.51 s using PI-torque controller, whereas it settles rapidly at 0.4 s using an ANFIS torque controller. Also, the torque ripple is remarkably reduced to 0.34 N-m using ANFIS-torque controller, which improves the steady-state torque response significantly compared to the PI-torque controller where the ripple is found to be 5.5 N-m as shown in Fig. 3.15 (ii). The stator

current responses using both controllers are shown in Fig. 3.15 (iii). The peak starting current is 21 A using PI-torque controller and using ANFIS controller; it is 19.2 A along with less distorted and less magnitude steady state current. However, the rotor *d-q* components of flux are observed as a constant peak magnitude of 0.6 Wb from starting to steady-state without losing its decoupling behavior which is evident from Fig. 3.15 (iv).

Case2: While induction motor operating at steady-state speed of 400 rpm, sudden load 10 N-m is applied and taken out at instants 1 s and 1.5 s, respectively as shown in Fig. 3.16 (a). This leads to a speed undershoot and overshoot of 1.8 rpm at the instants mentioned above and settles down at 1.25 s and 1.75 s, respectively using PI-torque controller. The load perturbation makes the motor peak current to increase to 9.8 A at 1.01 s and decrease down at 1.51 s. The responses with the ANFIS-torque controller though look similar to PI-torque controller based drive, there is a remarkable improvement of torque ripple, and improvement of speed undershoot/overshoot by around 94% and 10%, respectively over PI-torque controller-based drive during load perturbation which is shown in Fig. 3.16 (b) (i) and (ii). Apart from these, the settling time of speed during load is 0.1 s which is decreased by 60% from PI-torque controller. Nevertheless, the flux components for both types of controllers remain constant throughout the operation.

Case3: Subsequently, the experimental performance in reversal mode of IM was observed in Fig. 3.17 (a) and (b). It takes place at 2 s with uniform deceleration reaching steady-state of -400 rpm at 2.8 s and 2.6 s using PI and ANFIS torque controller, respectively as shown in Fig. 3.17 (i). Further, the rotor gets back to forward mode at 3 s and settles at 1000 rpm at 4.6 s and 4 s using PI and ANFIS torque controller, respectively. Fig. 3.17 (ii) and (iii) also reveal that the distortion of current and ripple contents in torque are drastically reduced by using an ANFIS-torque controller. The rotor flux components shown in Fig. 3.17 (iv) are observed as constant throughout the operations.

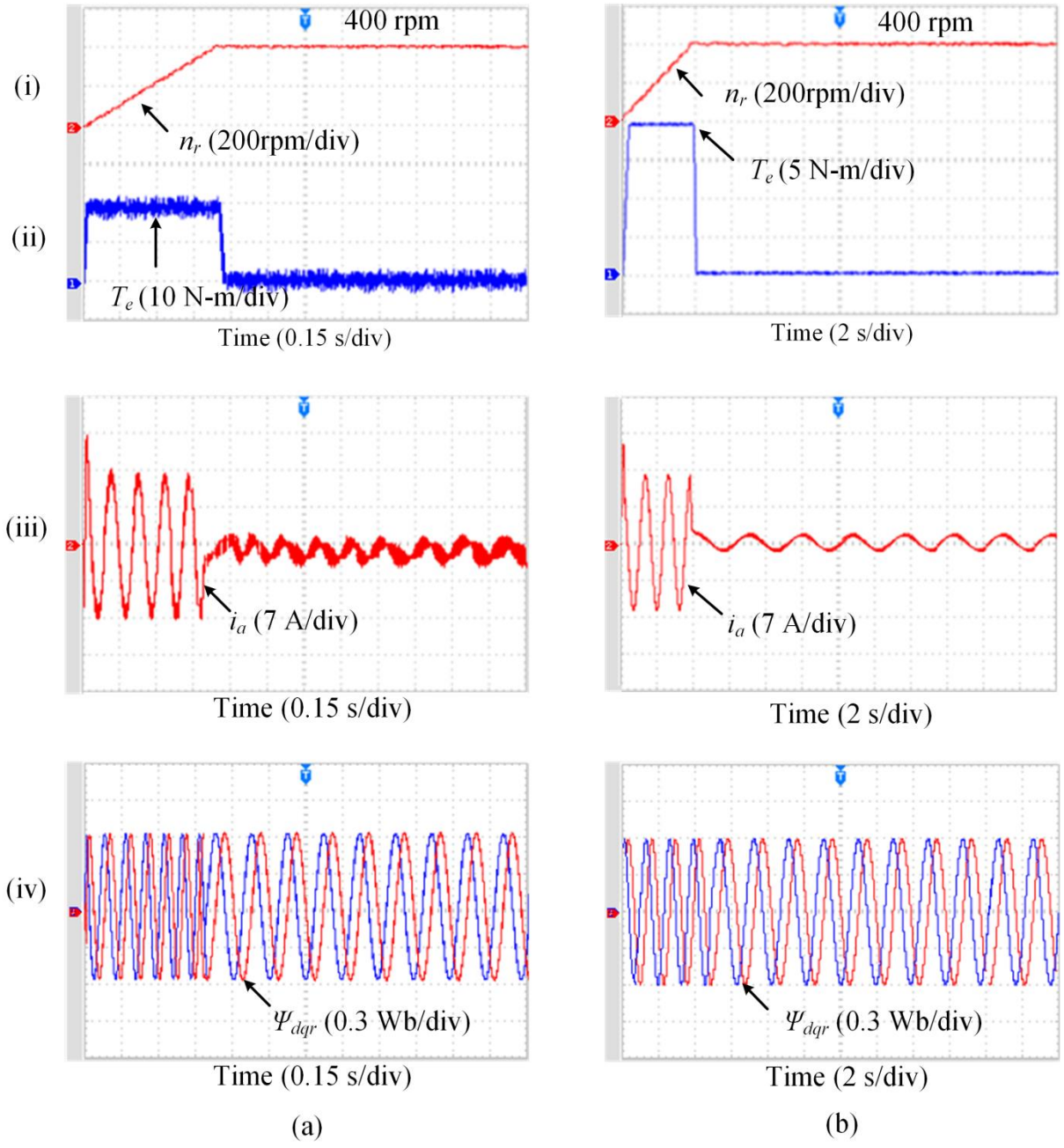

Fig. 3.15 The experimental starting characteristics of linearized IM drive scheme without any load disturbance for (a) PI-torque controller: (i) Speed (n_r), (ii) torque (T_e) (iii) stator current (i_a), and (iv) rotor *d-q* flux (ψ_{dqr}), (b) ANFIS torque controller (i) n_r, (ii) T_e, (iii) i_a, and (iv) ψ_{dqr}.

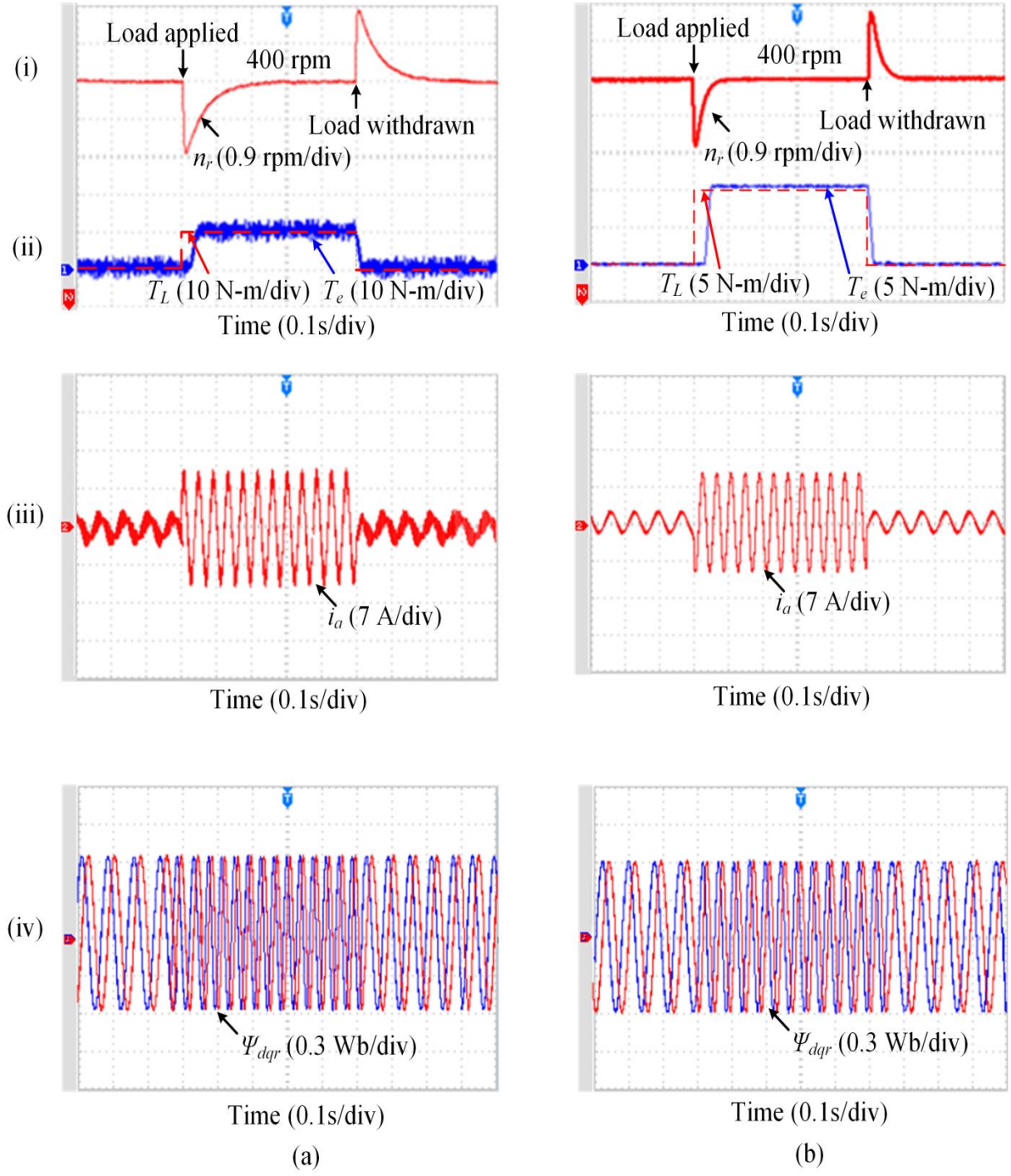

Fig. 3.16 The experimental characteristics of linearized IM drive scheme with a load disturbance of 10 N-m for (a) PI-torque controller: (i) Speed (n_r), (ii) torque (T_e) (iii) stator current (i_a), and (iv) rotor *d-q* flux (ψ_{dqr}), (b) ANFIS torque controller (i) n_r, (ii) T_e, (iii) i_a, and (iv) ψ_{dqr}.

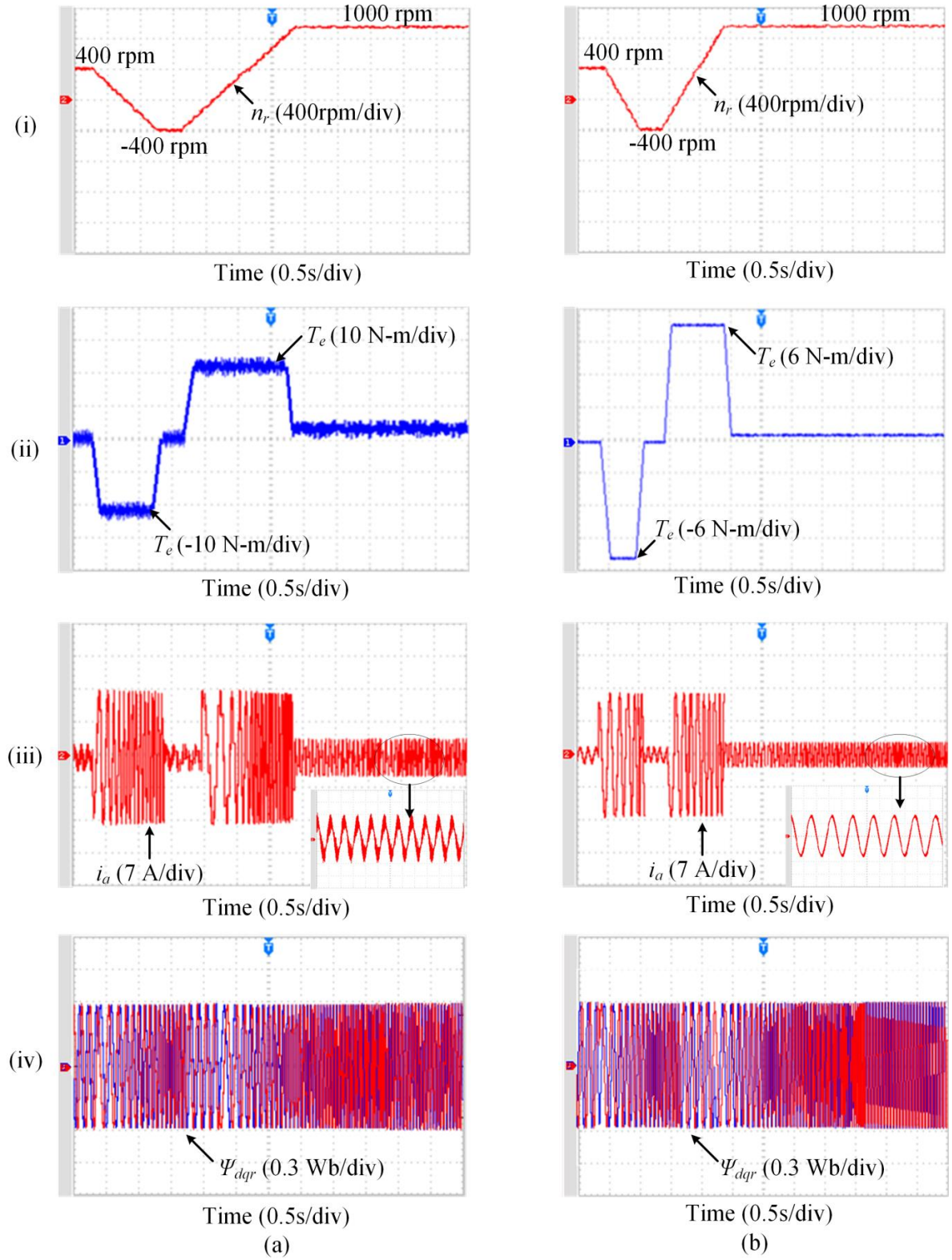

Fig. 3.17 The experimental characteristics of linearized IM drive scheme under speed reversal for (a) PI-torque controller: (i) Speed (n_r), (ii) torque (T_e) (iii) stator current (i_a), and (iv) rotor *d-q* flux (ψ_{dqr}), (b) ANFIS torque controller (i) n_r, (ii) T_e, (iii) i_a, and (iv) ψ_{dqr}.

Table 3.1 Comparative analysis of performance for different controllers

Controller	Speed (rpm)			Torque ripples (N-m)		Integral Time Absolute Error (ITAE) under load
	Ripples	% Undershoot and Overshoot during load of 10 N-m from 1 s to 1.5 s		Simulation	Experiment	
		Simulation	Experiment			
PI Torque Controller	0.07	1.7	1.8	5	5.5	1.7
ANFIS Torque Controller	**0.002**	**1.4**	**1.6**	**0.3**	**0.34**	**0.8**

Table 3.2 Comparison of Settling time of responses for PI and ANFIS controllers

Controller	Settling time (s)						
	Different initiated time (s)	Simulation			Experiment		
		$t_s(n_r)$	$t_s(T_e)$	$t_s(i)$	$t_s(n_r)$	$t_s(T_e)$	$t_s(i)$
PI Torque Controller	Starting	0.4	0.4	0.4	0.51	0.57	0.57
	Load applied at t = 1 s	0.2	0.01	0.01	0.25	0.02	0.02
	Load released at t = 1.5 s	0.2	0.01	0.01	0.25	0.02	0.02
	Speed reversal starts at t = 2 s	0.73	0.73	0.73	0.8	0.9	0.9
	Speed reversal from -400 rpm to 1000 rpm starts at t = 3 s	1.4	1.4	1.4	1.6	1.7	1.7
ANFIS Torque Controller	Starting	**0.39**	**0.39**	**0.39**	**0.4**	**0.44**	**0.44**
	Load applied at t = 1 s	**0.07**	**0**	**0**	**0.1**	**0.02**	**0.02**
	Load released at t = 1.5 s	**0.07**	**0**	**0**	**0.1**	**0.02**	**0.02**
	Speed reversal starts at t = 2 s	**0.7**	**0.7**	**0.7**	**0.6**	**0.7**	**0.7**
	Speed reversal from -400 rpm to 1000 rpm starts at t = 3 s	**1.33**	**1.33**	**1.33**	**1**	**1.1**	**1.1**

Table 3.1 and Table 3.2 show the comparative analysis of performance of the proposed ANFIS-torque controller-based linearized IM drive with the conventional PI-torque controller. The responses of the ANFIS torque controller obtained from the results corresponding to ripple in speed with or without load, % undershoot and overshoot of speed, and torque ripples are found to be superior compared to the classical PI-torque controller. The integral time absolute error which is defined by $ITAE = \int_0^\infty t\left|e(t)\right| dt$ is found to be 0.8 in case of ANFIS controller, which is almost half of that for PI-torque controller. It indicates as a good performance index for designing of controller. Further, the settling times for rotor speed, torque, and stator current obtained from the simulation as well as experiment under different operating conditions are depicted in Table 3.2. This reveals that the system shows very good performance for the load perturbation and sudden speed changes with ANFIS-torque controller-based drive as compared to the PI-torque controller.

The experimental results are found to be slightly poorer than that of simulated results because of some constraints like dead band, fluctuation of temperature, hard switching effect, variation of supply, electromagnetic interference phenomena, etc.

3.9.1 Robustness Studies of Controllers

The load torque is further reduced to 5 N-m for the same time instants of 1 s to 1.5 s and experimental analysis is carried out by altering the gain of PI-speed controller: K_p: 20 to 18 and K_i: 0.02 to 0.01 as shown in Fig. 3.18. It reveals that even if the K_p and K_i values of the PI-speed controller are changed, unlike with PI-torque controller as in Fig. 3.18 (a) (i) and (b) (i), there is no such difference of speed response in terms of undershoot/overshoot and settling time with ANFIS-torque controller-based linearized drive as presented in Fig. 3.18(a) (ii) and (b) (ii). Therefore, ANFIS-torque controller provides substantial torque ripple minimization, less deviation from reference speed, and quick speed response than that of the PI-torque controller-based drive with robustness to variation in PI-speed controller gains. This shows robustness because of the fact that the gains of PI controllers are tuned with proper optimization of rule by ANFIS controller using the center-of-gravity method. Apart from that, the system shows robustness with ANFIS-based torque controller over PI-torque controller so far as speed transition and load disturbance are concerned which is evident experimentally and from simulated performance results depicted in Table 3.1 and Table 3.2. Furthermore, at variable speed operations, the torque and speed ripples for ANFIS-torque

controller based drive are found to be substantially reduced with well-controlled rotor flux as shown in the results which prove the robustness of the controller.

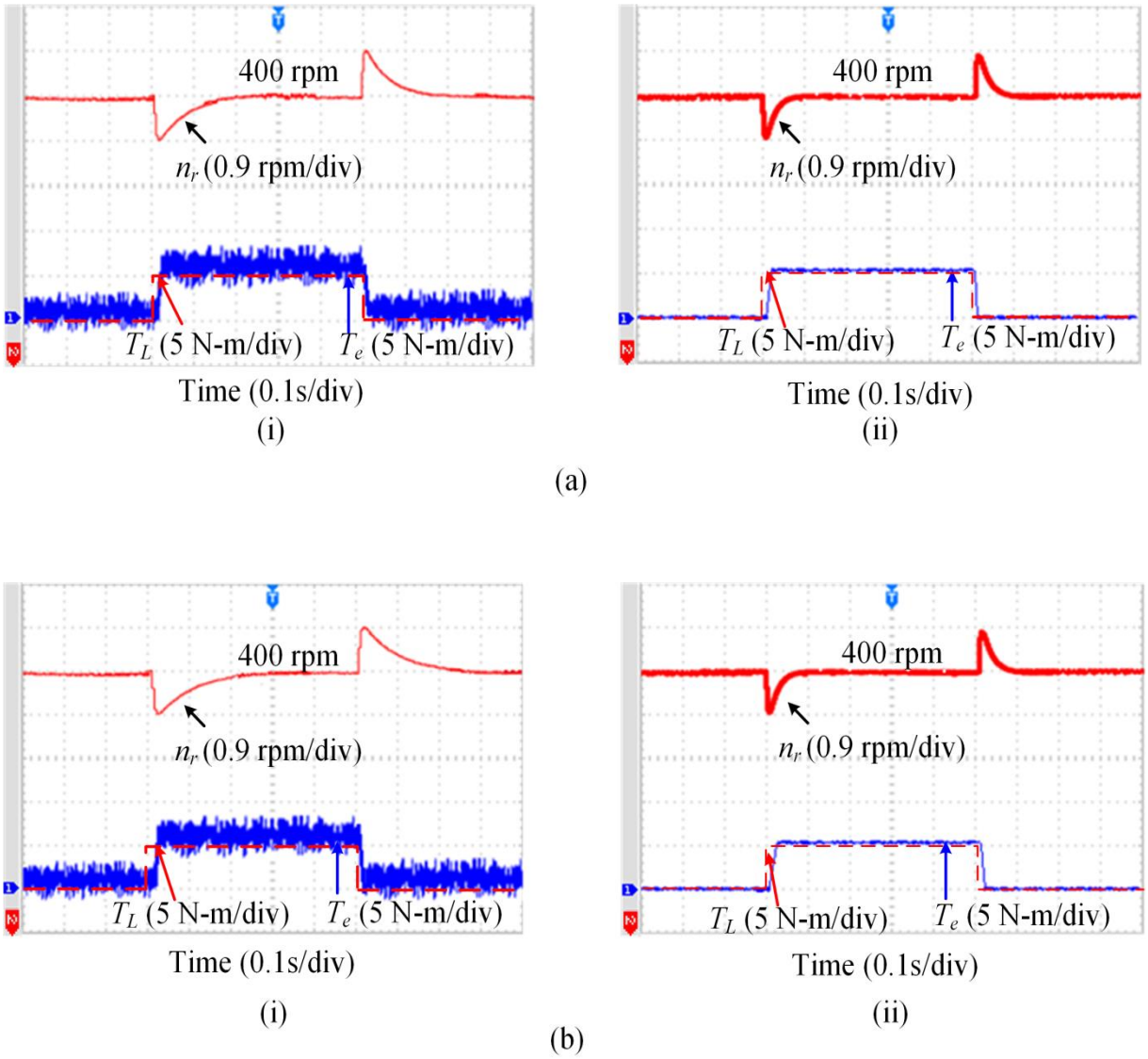

Fig. 3.18 The experimental characteristics at load perturbation of 5 N-m from 1 s to 1.5 s for different gains of speed PI-controller with (a) K_p = 20 and K_i = 0.02: (i) PI-torque controller-based drive and (ii) ANFIS-torque-controller-based drive: (b) K_p = 18 and K_i = 0.01, (i) PI-torque controller-based drive and (ii) ANFIS-torque controller-based drive.

3.10 Conclusion

The theory and design of ANFIS controller incorporated with the FBL IM drive are briefly reviewed in this Chapter. A systematic auto-tuning algorithm of the ANFIS controller is developed for the mechanical subsystem. A sensorless flux and torque observer based on the estimation strategy has also been presented. The design of different sub-model blocks of the proposed FBL IM drive system is designed and modeled in the MATLAB software and is experimentally investigated in the real-time hardware setup using DSP TMS320F2812 processor.

The feedback linearized IM drive with the ANFIS controller proves the robust and fast response with significantly reduced torque ripple compared to that of the PI-torque controller as far as starting, load perturbation, and speed reversal are concerned. However, the DC link capacitor voltage is well balanced all through these operations without using any extra controller. The flux responses throughout these operations are maintained almost constant. The performance index on ITAE indicates good responses in case of ANFIS-torque controller which can replace the conventional PI-torque controller.

An extensive experimental analysis has been carried out and the results provided and shown are closer to the simulated results. The adaptability and robustness of ANFIS scheme are proved experimentally by changing the gain of the speed-PI controller. Also, the results demonstrate the superior response of flux and perfect decoupling when the proposed ANFIS controller is implemented. A comparative performance analysis based on simulation as well as experiment has been carried out under different operating conditions as given in Table 3.1 and Table 3.2 which show the ANFIS controller provides a robust and excellent performance over PI-torque controller-based linearized IM without losing its decoupling characteristics. Thus, the proposed controller as a torque regulator is found to be suitable for high-performance industrial IM drive applications with a torque-sensitive load. The comparative study on PI and ANFIS controllers presented in this Chapter has revealed some salient features for the ANFIS controller which may be useful for implementation in high-performance or precision drive applications.

In spite of adequate advantages of this intelligent hybrid controller, various industries have still tendency not to accept these controllers for commercial drives because of high computational burden due to more number of MFs, weights, and rules, exclusively on auto-tuning condition [146]. Low sampling frequency due to this high computational burden is not acceptable for real-time application as it shows large torque ripples. Thus, a simple modified

version of single-input, reduced membership function based NFC method in conjunction with an intuitively flux-speed decoupled FBL approach of induction motor model is presented in Chapter 4. The proposed NFC with FBL remarkably suppresses the torque and speed ripple and improves the performance of the IM drive.

Chapter 4

DEVELOPMENT AND IMPLEMENTATION OF A SIMPLIFIED NEURO-FUZZY CONTROLLER FOR INDUCTION MOTOR DRIVE USING LINEARIZATION APPROACH

CHAPTER 4
DEVELOPMENT AND IMPLEMENTATION OF A SIMPLIFIED NEURO-FUZZY CONTROLLER FOR INDUCTION MOTOR DRIVE USING LINEARIZATION APPROACH

4.1 Introduction

Many industries are still reluctant to implement the conventional NFC for the commercial drive as it has more computational burden due to a large number of membership functions (MFs), rules, especially on auto-tuning condition [75], [83]. Low sampling frequency (high sampling rate) due to this high computational burden leads to greater torque ripple, which is not acceptable for industrial applications. Also, a fast processor may be required for this high computational control algorithms, which may be a costly affair. The modified simple structured neuro-fuzzy controller (NFC) proposed in this Chapter integrates the concept of fuzzy logic and neural network structure like conventional NFC, but it has the advantage of reduced computational burden. This is achieved by improving computational efficiency over conventional NFC as the single input introduced here is an error instead of two inputs error and change in error as in conventional NFC. This structure makes the proposed NFC simple as compared to the conventional NFC and thus, can be easily applied to real-time industrial applications. Apart from being resistant to the motor parameter variations, system uncertainties, and load impact, the proposed simplified single-input based NFC decreases the computational burden by reducing the rules and MFs compared to the conventional two-input NFC.

The theory and design of the proposed NFC as applied to the FBL controlled IM drive is described in Section 4.2. In Section 4.3, the auto-tuning algorithm for the proposed NFC is developed and the stepwise procedure is described for parameters tuning using the update rules. In sections 4.4-4.6, extensive simulation and experimental results are validated and comparative analysis is carried out to show the potentiality of the proposed method using feedback linearization of IM drive with different working modes. Robustness study of the controlleris discussed in Section 4.7 followed by the conclusion Section.

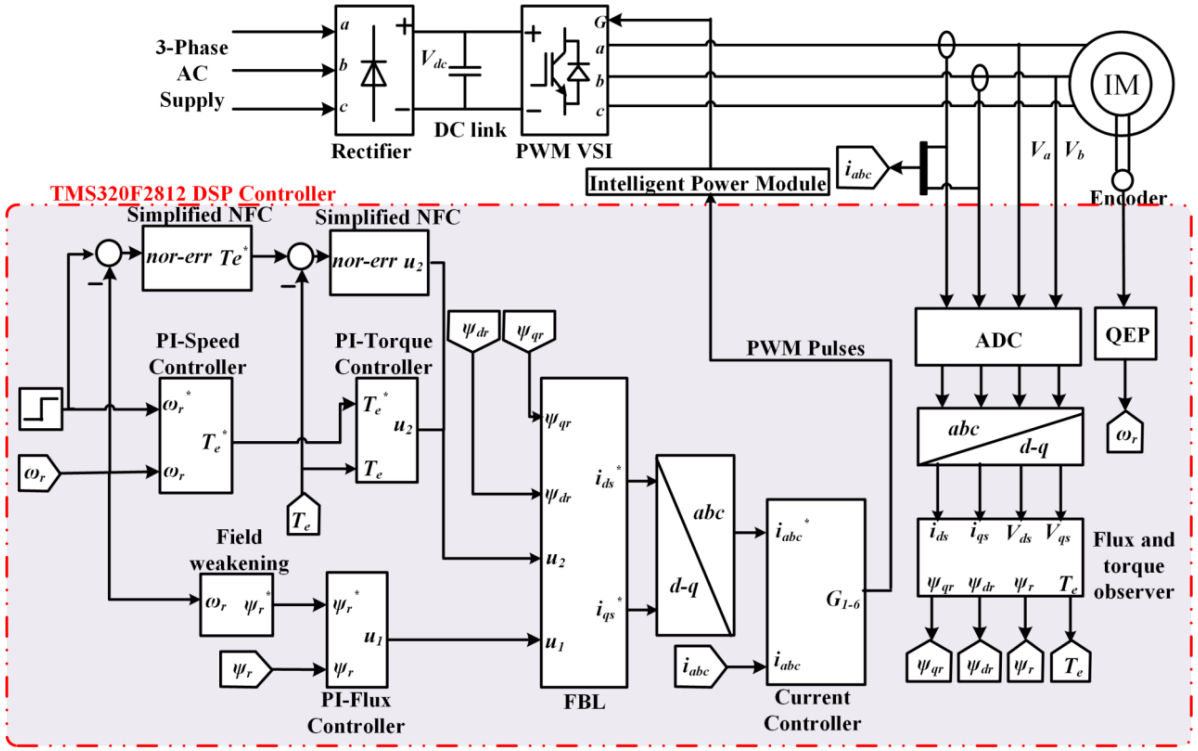

Fig. 4.1 Proposed NFC-based IM drive using feedback linearization

4.2 Design of Proposed Neuro-fuzzy Controllers

The unoptimized and uncertain fuzzy logic control as well as the computational burden imposed by conventional NFC (as illustrated later in Fig. 4.3) led to the development of a simplified NFC. The overall schematic model of the proposed NFC-based FBL IM drive is demonstrated in Fig. 4.1.

4.2.1 Conventional NFC

In order to have a fair comparative evaluation, the MFs of both conventional NFC and proposed simplified NFC are kept identical as depicted in Fig. 4.2 (b). The two inputs of this NFC are normalized speed error and change in speed error as shown in Fig. 4.3. Both NFCs are also tuned by the same auto-tuning methods as described in Section 4.3. The two inputs are as follows:

$$\%e_s(t) = \frac{\omega_r^* - \omega_r}{\omega_r^*} \times 100 \tag{4.1}$$

$$\%\Delta e_s(t) = \frac{e_s(t)_k - e_s(t)_{k-1}}{T} \times 100 \tag{4.2}$$

where T is the sampling time, k is the sampling instant, and $e_s(t)_k$ and $e_s(t)_{k-1}$ represent present and previous speed error, respectively.

The neuro-fuzzy controller structural design integrates fuzzy logic and learning algorithm with a five-level artificial neural network arrangement [82] as depicted in Fig. 4.2. In the proposed Sugeno fuzzy model [4] depicted in Fig. 3.2 (a) of Chapter 3, the typical rule set with fuzzy rules can be expressed as

Rule i (i = 1, 2, and 3): if e (t) is M_{1i} AND $\Delta e(t)$ is M_{2i} then $v_i = m_{1i}e(t) + m_{2i}\Delta e(t) + r_i$

where M_{1i} and M_{2i} are the antecedent fuzzy sets and m_{1i}, m_{2i}, and r_i are the design parameters evaluated in training. Here, v_i is the output singleton membership functions as shown in Fig.4. In the extra layer introduced here, the minimum of error or change in error value of two input weights are picked up as firing strength of rules by the product operator 'AND' which is symbolized by $\prod$ as shown in Fig. 4.2.

$$O_i^2 = w_i = \mu_{M1i}(e(t)).\mu_{M2i}(\Delta e(t)) = \min(\mu_{M1i}(e(t), \mu_{M2i}(\Delta e(t)), i = 1, 2, 3 \quad (4.3)$$

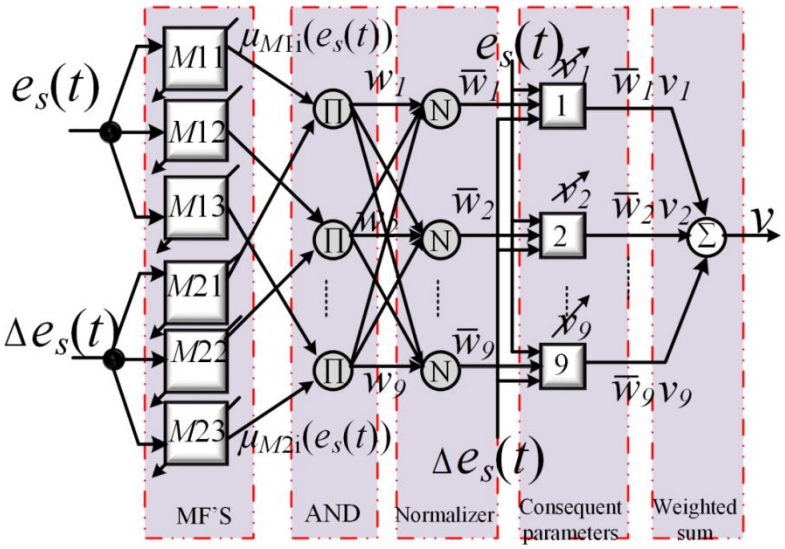

Fig. 4.2 Conventional NFC architecture with three MFs.

4.2.2 Proposed Simplified NFC

The proposed simplified NFC design integrates fuzzy logic control (FLC) with a four-level artificial neural network (ANN) organization, as described in Fig. 4.3 (a). However, the accurate measurement of change in error is not required [137] like conventional NFC as it deteriorates the ability of NFC by increasing the computational burden. The proposed NFC is modified by a simple control algorithmin order to achieve the required performance of the IM

drive system. The parameter of the third layer is modified by tuning to control any deviation of control effort. The single input speed error due to the difference between desired speed ω_r^* and the actual speed ω_r of the NFC is as follows.

$$\%e_s(t) = \frac{\omega_r^* - \omega_r}{\omega_r^*} \times 100 \tag{4.4}$$

Layer 1: The output equation of this fuzzification layer having adaptive nodes of three-speed error membership functions (MFs) as negative (N), zero (Z), and positive (P) speed errors are given by

$$O_1^1 = \mu_{M1}(e_s(t)) = \begin{cases} 1, & x_i^1 \le b_1 \\ \dfrac{x_i^1 - a_1}{b_1 - a_1}, & b_1 < x_i^1 < a_1 \\ 0, & x_i^1 \ge a_1 \end{cases} \tag{4.5}$$

$$O_2^1 = \mu_{M2}(e_s(t)) = \begin{cases} 0, & \left|x_i^1\right| \ge b_2 \\ 1 - \dfrac{\left|x_i^1 - a_2\right|}{b_2}, & \left|x_i^1 - a_2\right| \le b_2 \end{cases} \tag{4.6}$$

$$O_3^1 = \mu_{M3}(e_s(t)) = \begin{cases} 0, & x_i^1 \le a_3 \\ \dfrac{x_i^1 - a_3}{b_3 - a_3}, & a_3 < x_i^1 < b_3 \\ 1, & x_i^1 \ge b_3 \end{cases} \tag{4.7}$$

where $\mu_{M1}(e_s(t)), \mu_{M2}(e_s(t)), \mu_{M3}(e_s(t))$ are chosen to be symmetrical (a_2 = 0) linear MFs as in Fig. 4.3 (b) rather than any exponential function in order to lessen the computational burden and make it more efficient. Here *x* and *O* correspond to input and output, and their superscript and subscript denote layer and node number, respectively.

Layer 2: The "AND" logic operator is not used in this layer for the calculation of the weight of rules w_i since only one input is present here unlike conventional two-input NFC. The normalized $\overline{w_i}$ can be written as

$$O_i^2 = \overline{w_i} = \frac{w_i}{\sum_i w_i}, \; i = 1, 2, 3 \tag{4.8}$$

Layer 3: The consequent value v_i is calculated in this layer as node equation, whose output is specified as

$$O_i^3 = \overline{w_i} v_i, \; i = 1, 2, 3 \tag{4.9}$$

Layer 4: This is the defuzzification layer, where the NFC output is determined by center-of-gravity method and is specified as

$$v = O_i^4 = \frac{\sum_i w_i v_i}{\sum_i w_i} = \sum_i \overline{w_i} v_i \,,\ i = 1, 2, 3 \tag{4.10}$$

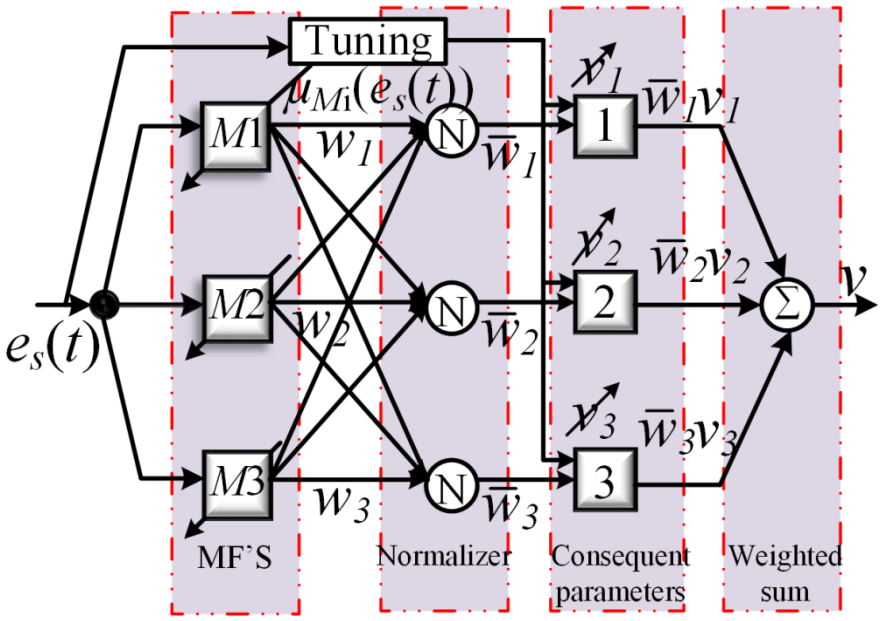

(a)

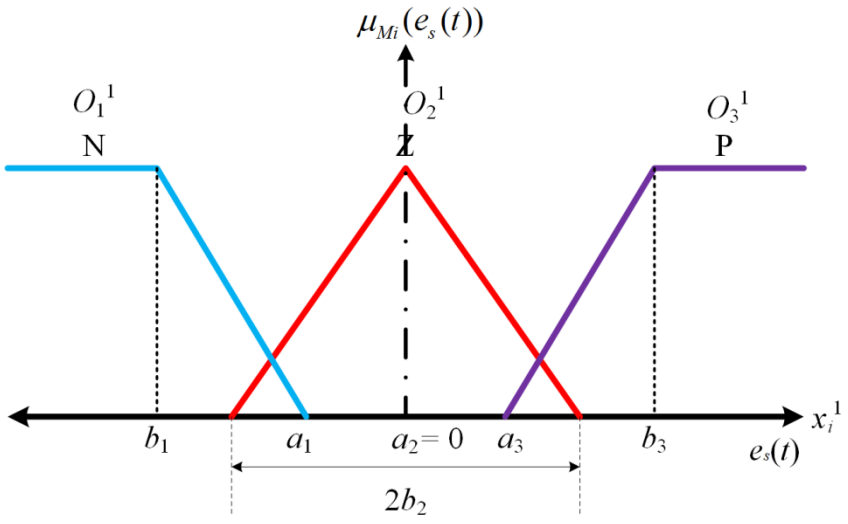

(b)

Fig. 4.3 Neuro-fuzzy controller: (a) proposed simplified architecture and (b) input MFs.

Likewise, the neuro-fuzzy torque controller is designed in the same approach of the neuro-fuzzy speed controller. Moreover, the MFs of the neuro-fuzzy torque controller is kept same as the neuro-fuzzy speed controller as depicted in Fig. 4.3 (b), but it has different input and output crisp values as in Fig. 4.1.

Fig. 4.4 (a) represents the MFs of single-input error (E) for the proposed Simplified NFC. Fig. 4.4 (a) and (b) represent the MFs of input error (E) and change in error (CE), respectively for the conventional NFC. Fig. 4.5 (a) shows the surface view in MATLAB plot based on the rules which is plotted between the change in control output and single-input error for the proposed NFC. Fig. 4.5 (b) represents the surface view plot between change in control output and two inputs error and change in error for the conventional NFC. The dependency of the output on a single input, E or two inputs, E and CE is displayed by using the surface viewer.

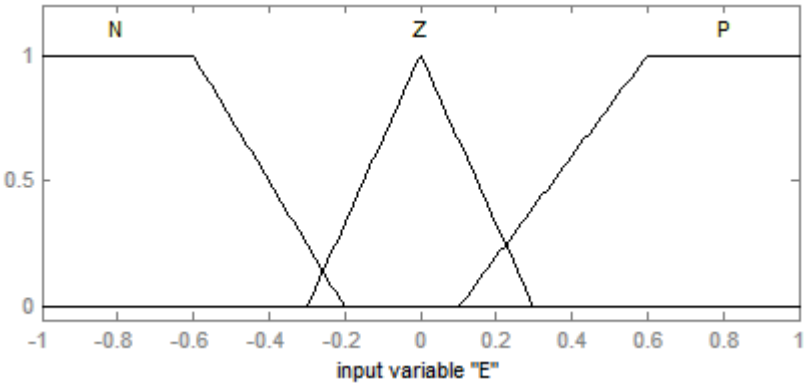

(a)

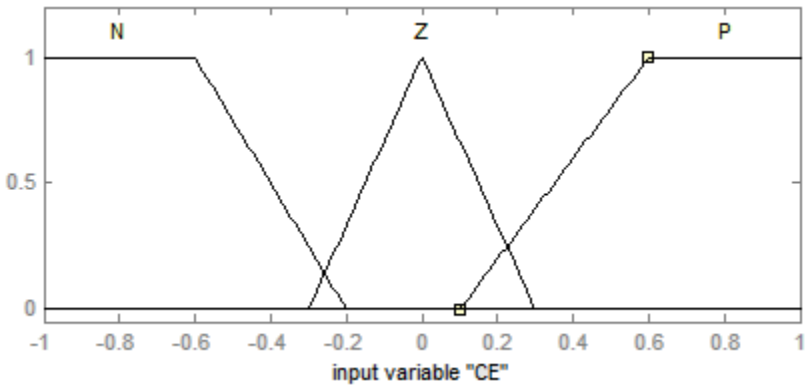

(b)

Fig. 4.4 Input membership functions: (a) error (E) of the proposed Simplified NFC and error (E) of conventional NFC, (b) change in error (CE) of conventional NFC.

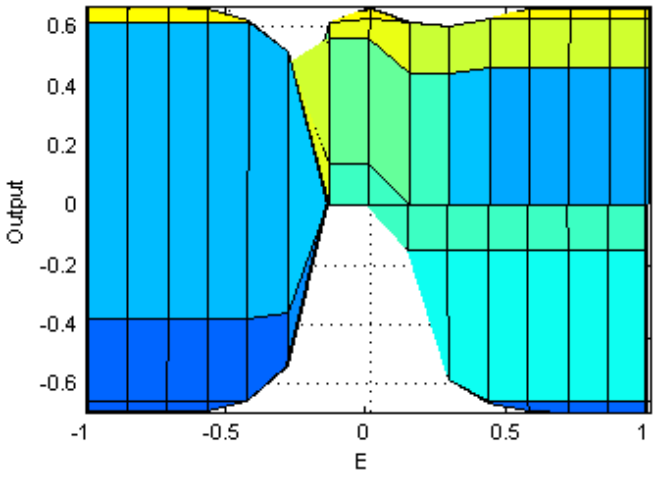

(a)

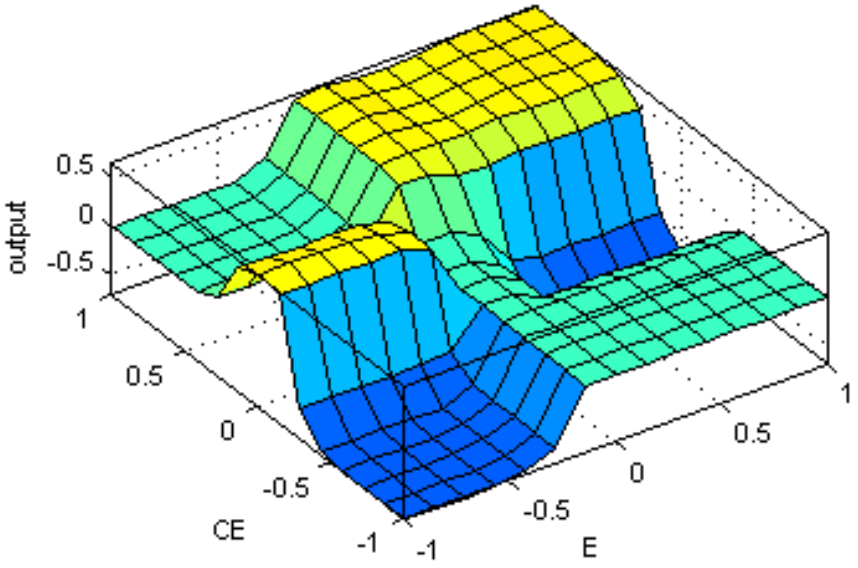

(b)

Fig. 4.5 Surface view of (a) proposed single-input NFC and (b) conventional two-input NFC.

4.3 Auto-tuning Algorithm for the Proposed NFC

Instead of employing the desired controller output *'v'* as a target, an error signal *'e'* which evaluates the execution of the controller and calculates the current state of the framework, is used to deal with the control action by changing it in right directions so as to deliver the desired response [83]. However, it is a very tough task to find out the required NFC output and offline trained data under different dynamic operating conditions. Therefore, an unsupervised online auto-tuning method based on back-propagation algorithm is developed

here [81], [142], [143], whose assignment is to upgrade the MFs parameters and weight in order to have minimized error signal which is considered underneath as a fitness function.

$$E = \frac{1}{2}(\omega_r^* - \omega_r)^2 = \frac{1}{2}e^2 \tag{4.11}$$

where ω_r^* is the reference speed and ω_r is the actual or measured speed. To achieve the desired control performance, the back-propagation parameter adaptation rules for instantaneous parameter update are derived as:

$$a_i(k+1) = a_i(k) - \eta_{ai}\nabla_{ai}E(k) \tag{4.12}$$

$$b_i(k+1) = b_i(k) - \eta_{bi}\nabla_{bi}E(k) \tag{4.13}$$

$$w_i(k+1) = w_i(k) - \eta_{wi}\nabla_{wi}E(k) \tag{4.14}$$

where a_i and b_i are the i^{th} node values of a and b, k is the sampling instant. η_{ai} , η_{bi} , and η_{wi} are the fixed learning rate of parameters a_i, b_i, and w_i. Gradient set $\left(\nabla_{ai}, \nabla_{bi}, \nabla_{wi}\right)$ is denoted as $\left(\frac{\partial E}{\partial a_i}, \frac{\partial E}{\partial b_i}, \frac{\partial E}{\partial w_i}\right)$ being the gradient of cost function E corresponding to parameters (a_i,b_i, w_i) and described by the following equations.

$$\nabla_{ai}E = \frac{\partial E}{\partial e}\frac{\partial e}{\partial \omega_r}\frac{\partial \omega_r}{\partial v}\frac{\partial v}{\partial O_i^1}\frac{\partial O_i^1}{\partial a_i} \tag{4.15}$$

$$\nabla_{bi}E = \frac{\partial E}{\partial e}\frac{\partial e}{\partial \omega_r}\frac{\partial \omega_r}{\partial v}\frac{\partial v}{\partial O_i^1}\frac{\partial O_i^1}{\partial b_i} \tag{4.16}$$

$$\nabla_{wi}E = \frac{\partial E}{\partial e}\frac{\partial e}{\partial \omega_r}\frac{\partial \omega_r}{\partial v}\frac{\partial v}{\partial w_i} \tag{4.17}$$

The common differential terms of equations (4.15) – (4.17) are determined as follows:

$$\frac{\partial E}{\partial e} = \omega_r^* - \omega_r = e \tag{4.18}$$

$$\frac{\partial e}{\partial \omega_r} = -1 \tag{4.19}$$

$$\frac{\partial \omega_r}{\partial v} = \text{constant } K \tag{4.20}$$

The value of *K* is greater than zero for the proposed IM drive scheme as the drive system is viewed as a single-input single-output system [74], [137]. The other terms of equations (4.15) – (4.17) are determined from equations (4.5) – (4.10) as

$$\frac{\partial v}{\partial O_i^1} = \frac{v_i(k)}{\sum w_i(k)} \tag{4.21}$$

$$\left.\begin{aligned} &\frac{\partial O_i^1}{\partial a_i} = \frac{\partial O_1^1}{\partial a_1} = \frac{x_1^{\,1} - b_1}{\left(b_1 - \mathrm{a}_1\right)^2} = -\frac{1 - O_1^1(k)}{b_1(k) - a_1(k)} \text{ for } i = 1 \\ &\text{Similarly, } \frac{\partial O_3^1}{\partial a_3} = -\frac{1 - O_3^1(k)}{b_3(k) - a_3(k)} \text{ for } i = 3 \end{aligned}\right\} \tag{4.22}$$

$$\left.\begin{aligned} &\frac{\partial O_i^1}{\partial b_i} = \frac{\partial O_1^1}{\partial b_1} = -\frac{x_1^{\,1} - a_1}{\left(b_1 - a_1\right)^2} = -\frac{O_1^1(k)}{b_1(k) - \mathrm{a}_1(k)} \text{ for } i = 1 \\ &\text{Similarly, } \frac{\partial O_2^1}{\partial b_2} = \frac{\left(x_2^{\,1} - a_2\right)}{b_2^{\,2}} = \frac{1 - O_2^1(k)}{b_2(k)} \text{ for } i = 2 \\ &\text{and } \frac{\partial O_3^1}{\partial b_3} = -\frac{O_3^1(k)}{b_3(k) - a_3(k)} \text{ for } i = 3 \end{aligned}\right\} \tag{4.23}$$

$$\frac{\partial v}{\partial w_i} = \frac{v_i(k)}{\sum w_i(k)} \tag{4.24}$$

Substituting (4.21) – (4.24) in (4.12) – (4.14) the following update rules are obtained.

$$a_1(k+1) = a_1(k) - \eta_{a1} e(k) K \frac{v_1(k)}{\sum w_i(k)} \frac{1 - O_1^1(k)}{b_1(k) - a_1(k)} \tag{4.25}$$

$$a_3(k+1) = a_3(k) - \eta_{a3} e(k) K \frac{v_3(k)}{\sum w_i(k)} \frac{1 - O_3^1(k)}{b_3(k) - a_3(k)} \tag{4.26}$$

$$b_1(k+1) = b_1(k) - \eta_{b1} e(k) K \frac{v_1(k)}{\sum w_i(k)} \frac{O_1^1(k)}{b_1(k) - a_1(k)} \tag{4.27}$$

$$b_2(k+1) = b_2(k) + \eta_{b2} e(k) K \frac{v_2(k)}{\sum w_i(k)} \frac{1 - O_2^1(k)}{b_2(k)} \tag{4.28}$$

$$b_3(k+1) = b_3(k) - \eta_{b3} e(k) K \frac{v_3(k)}{\sum w_i(k)} \frac{O_3^1(k)}{b_3(k) - a_3(k)} \tag{4.29}$$

$$w_i(k+1) = w_i(k) + \eta_{wi} e(k) K \frac{v_i(k)}{\sum w_i(k)} \tag{4.30}$$

The step-wise procedure followed for parameter tuning using the update rules given by equations (4.25) – (4.30) is shown in Fig. 4.6. Similarly, the same auto-tuning method is performed to update the proposed simplified neuro-fuzzy-torque control, where the error signal is defined as

$$E = \frac{1}{2}(T_e^* - T_e)^2 = \frac{1}{2}e^2 \tag{4.31}$$

where T_e^* is the reference torque which is the output of the neuro-fuzzy speed controller, and T_e is the actual or estimated torque.

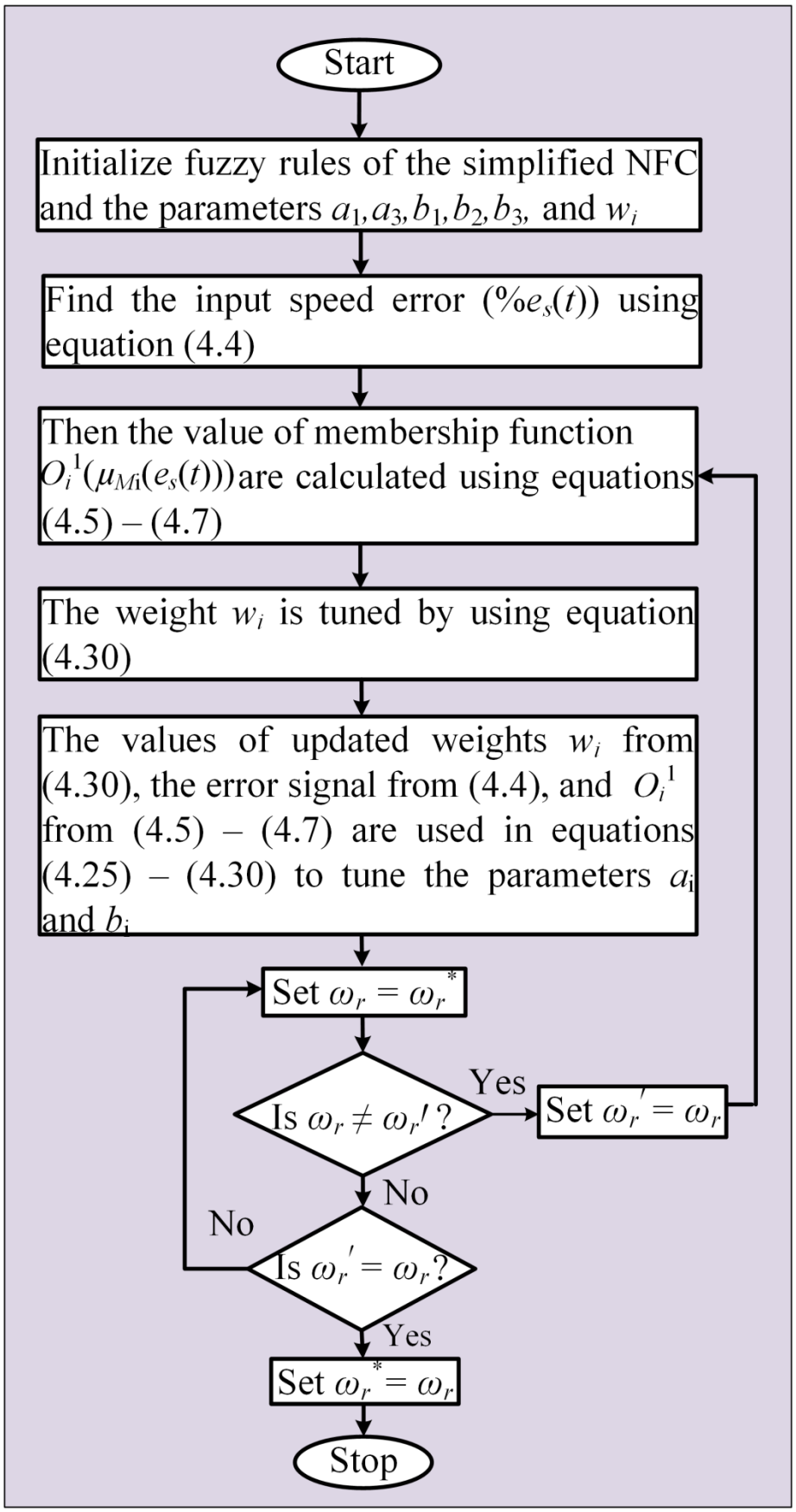

Fig. 4.6 Flowchart for tuning of the parameters to optimize the error signal.

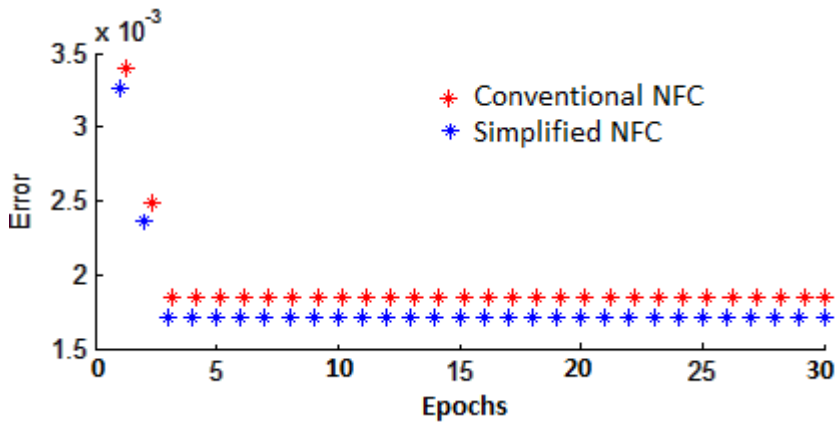

Fig. 4.7 Mean square error of the proposed simplified NFC and the conventional NFC.

The mean square error (MSE) of the simplified NFC is found to be the least value 0.00175 as shown in Fig. 4.7. These errors were displayed by taking 30 iterations but, prior to five iterations, the controllers are settled down to the minimum error of 0.00187 and 0.00175 for the conventional NFC and the proposed simplified NFC, respectively.

4.4 Simulation Results and Analysis

The effectiveness of proposed modified NFC-based control of linearized IM drive is investigated in MATLAB/Simulink using current controlled voltage source PWM inverter for 3.7 kW IM under various modes of operations. Figs. 4.8-4.12 represent the comparison of responses of the proposed NFC-based drive with conventional NFC and PI controller based drive under different working modes. It is observed that the results of the proposed simplified NFC-based drive is found to be similar to that of conventional NFC. Simultaneously, it is observed to be the enhanced performance from that of conventional PI-controller, which is evident from Table 4.1. IM specifications are illustrated in the Appendix A.1.

4.4.1 Results with PI-controller

Case1: This illustrates that motor accelerates from rest at a constant rate and reaches its target speed of 800 rpm at 1.1 s with an overshoot and applied DC link voltage of 646 V as shown in Fig. 4.8 and Fig. 4.11. The gate signal, line voltage and power characteristics are shown in Fig. 4.8 (i), (ii) and (iii). The current, torque, and speed of induction motor are settled at 1.1 s. However, the spike in capacitor voltage V_{dc} is observed at starting as the capacitor charges and settles down later within 5 to 6 cycles by discharging through properly selected switching path as in Fig. 4.11 (a) (iii). Substantial ripple and chattering in torque and speed appear with this PI-controller.

Case2: The dynamics of load disturbance is studied by a step increase in load from 0 to 50% at 1.5 s while the motor operating at steady-state speed of 800 rpm as depicted in Fig. 4.9. The gate signal and line voltage are shown in Fig. 4.9 (i) and (ii). The load is released and brought to zero at 2 s. It leads to undershoot and overshoot in the speed of about 1.7 rpm at 1.5 s and 2 s, respectively with settling period of around 14 to 15 cycles (0.3 s), accompanied by an increase in peak stator current to 10 A. Also, the capacitor voltage is reduced to 644 V during the sudden increase of stator current at 1.5 s as the energy stored in the capacitor gets released when the large current is drawn by motor through the capacitor and comes to the steady state after one cycle (0.02 s). Likewise, the capacitor gets charged to a higher voltage during removal of the load, which is evident from Fig. 4.11 (a) (iii). With this PI controller, anextensive ripple in torque and speed are evident from Fig. 4.9 (a).

Case3: Speed reversal starts at 2.5 s, at a uniform rate from 800 rpm to zero speed and then to -400 rpm at 3.8 s as shown in Fig. 4.10 (a). This is accompanied by large stator current due to large negative motor torque and the frequency of the current reduces initially due to regenerative braking followed by phase reversal for getting the motor reversed. The gate signal and line voltage are shown in Fig. 4.10 (i) and (ii). Further, it is evident from Fig. 4.10 that the responses replicate those of the start-up operation as shown in Fig. 4.8. The detailed comparative analysis is performed and illustrated in Table 4.1. However, all through these three operations, the flux is maintained uniform as evident from Fig. 4.11 (a) (ii).

4.4.2 Results with NFCs

Operating condition changes similar to those for PI-controller were carried out with NFCs for starting, loading, and speed reversing as shown in Figs. 4.8-4.12. At starting, the maximum peak stator current is less with less distortion, reduced settling time, less peak capacitor voltage V_{dc} and reduced torque ripple using proposed NFC and conventional NFC based linearized drive over PI-controller-based drive. The torque response during starting is significantly improved as the torque ripple is remarkably reduced from about 4.5 Nm in PI-controller to about 0.5 Nm in conventional NFC and 0.3 Nm in the proposed simplified NFC. It is evident from Table 4.1 that the proposed low computational simplified NFC bears a resemblance to that of conventional NFC and, simultaneously, it shows better performance over the traditional PI-controller-based drive with respect to ripple, rise time, settling time, and overshoot. It is seen that the implementation of the proposed NFC enhances the speed tracking performance during load perturbation with significantly less ripple, less fluctuation, and less settling time of around 5 to 6 cycles, which is superior to the PI-controller. The

torque ripple with the proposed NFC is significantly reduced compared to the PI-controller thereby decreasing the magnitude and distortion of the motor current as evident from Fig. 4.9 (v). In fact, the oscillation in speed has almost disappeared with the proposed NFC-based drive as compared to the conventional NFC which still has a tiny oscillation as in Fig. 4.9 (c) (iii). Subsequently, while reversing the speed, the motor settles down faster within 0.6 s for the proposed NFC-based drive as compared to the PI-controller-based drive. Moreover, the linearized IM with the proposed controller has less dip in capacitor voltage, less flux, and torque distortion. Also, Fig. 4.11 reveals that the rotor flux is steady throughout every operating mode regardless of the speed. Thus the proposed low computational NFC establishes the perfect decoupling without compromising the system behavior. Additionally, it exhibits superior performance as compared to the classical PI-controller.

The robustness of the proposed NFC-based feedback linearization controller in face of the motor parameter detuning is examined with the rotor inertia doubled as shown in Fig. 4.12. The settling time response is almost doubled as the rotor inertia is doubled. The responses demonstrate the robust stability of the proposed NFC as compared to the PI-controller-based drive.

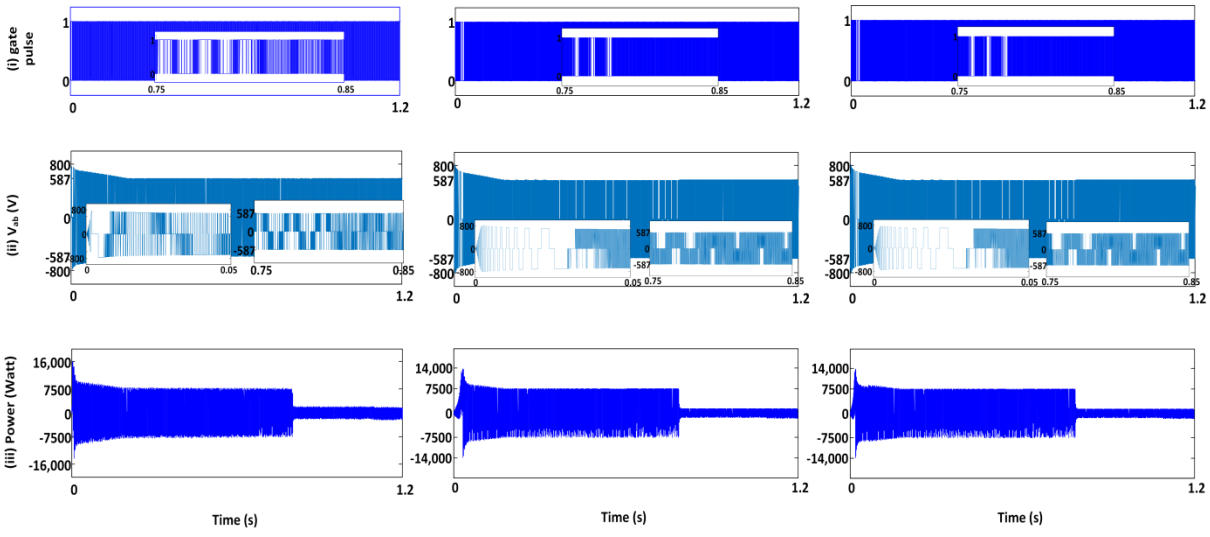

Fig. 4.8 Simulation response during starting of FBL controlled IM drive using (a) PI-controller: (i) gate signal, (ii) line voltage (V_{ab}), (iii) active power (P) (iv) speed (n_r), (v) torque (T_e), (vi) stator current (i_{abc}), (b) conventional NFC: (i) gate signal, (ii) V_{ab}, (iii) P (iv) n_r, (v) T_e, (vi) i_{abc}, (c) proposed simplified NFC (SNFC): (i) gate signal, (ii) V_{ab}, (iii) P (iv) n_r, (v) T_e, (vi) i_{abc}.

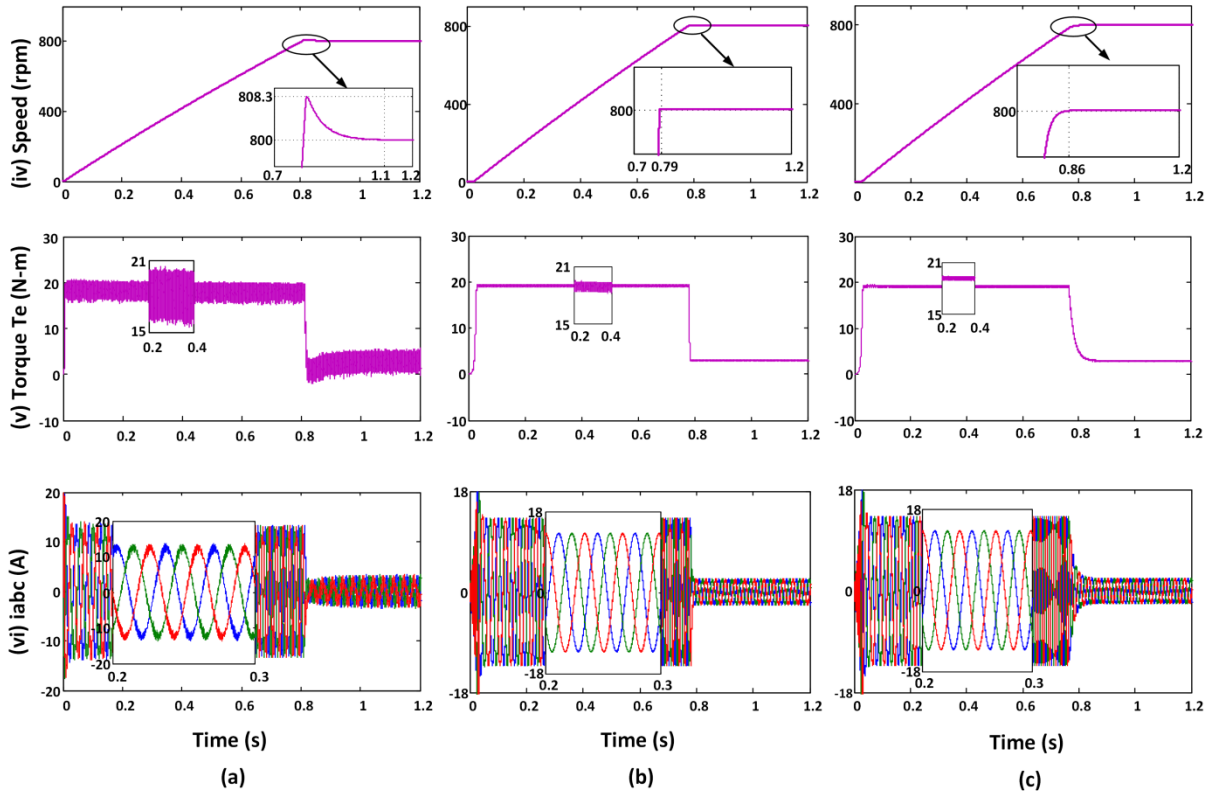

Fig. 4.8 continued.

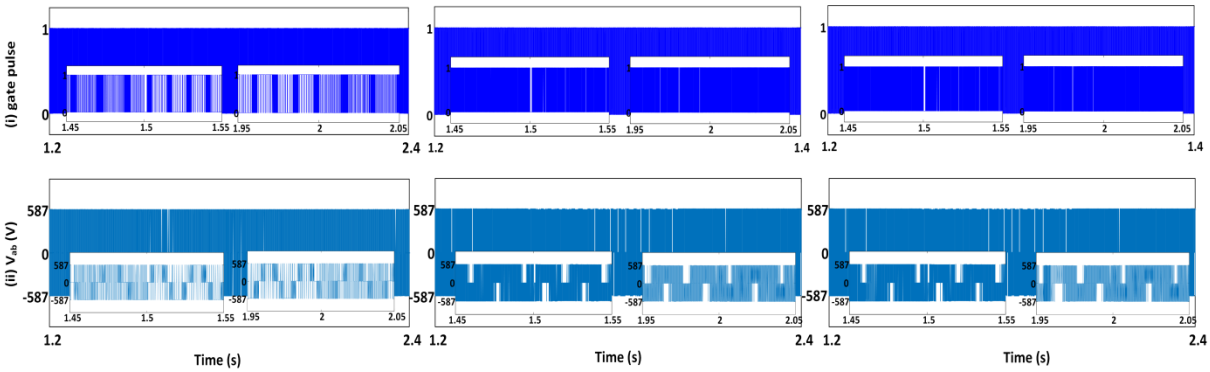

Fig. 4.9 Simulation responses of FBL controlled IM drive during 50% step change in load torque from 1.5 s to 2 s using (a) PI-controller: (i) gate signal, (ii) line voltage (V_{ab}), (iii) speed (n_r), (iv) torque (T_e), (v) stator current (i_{abc}), (b) conventional NFC: (i) gate signal, (ii) V_{ab}, (iii) n_r, (iv) T_e, (v) i_{abc}, (c) proposed simplified NFC (SNFC): (i) gate signal, (ii) V_{ab}, (iii) n_r, (iv) T_e, (v) i_{abc}.

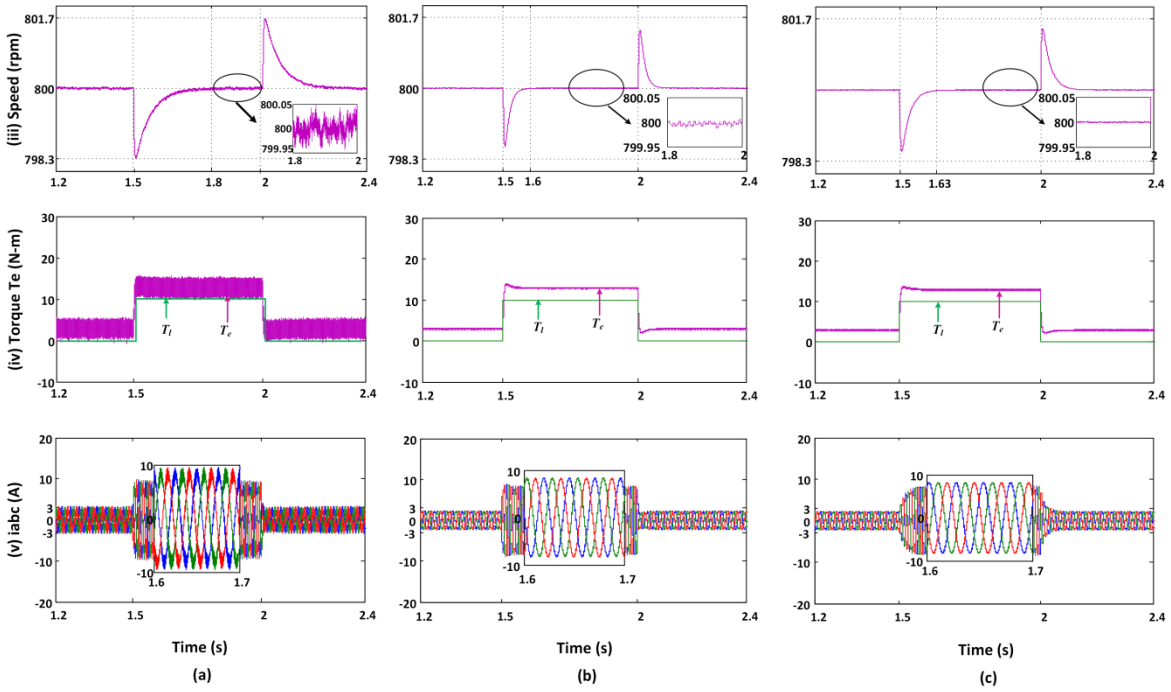

Fig. 4.9 continued.

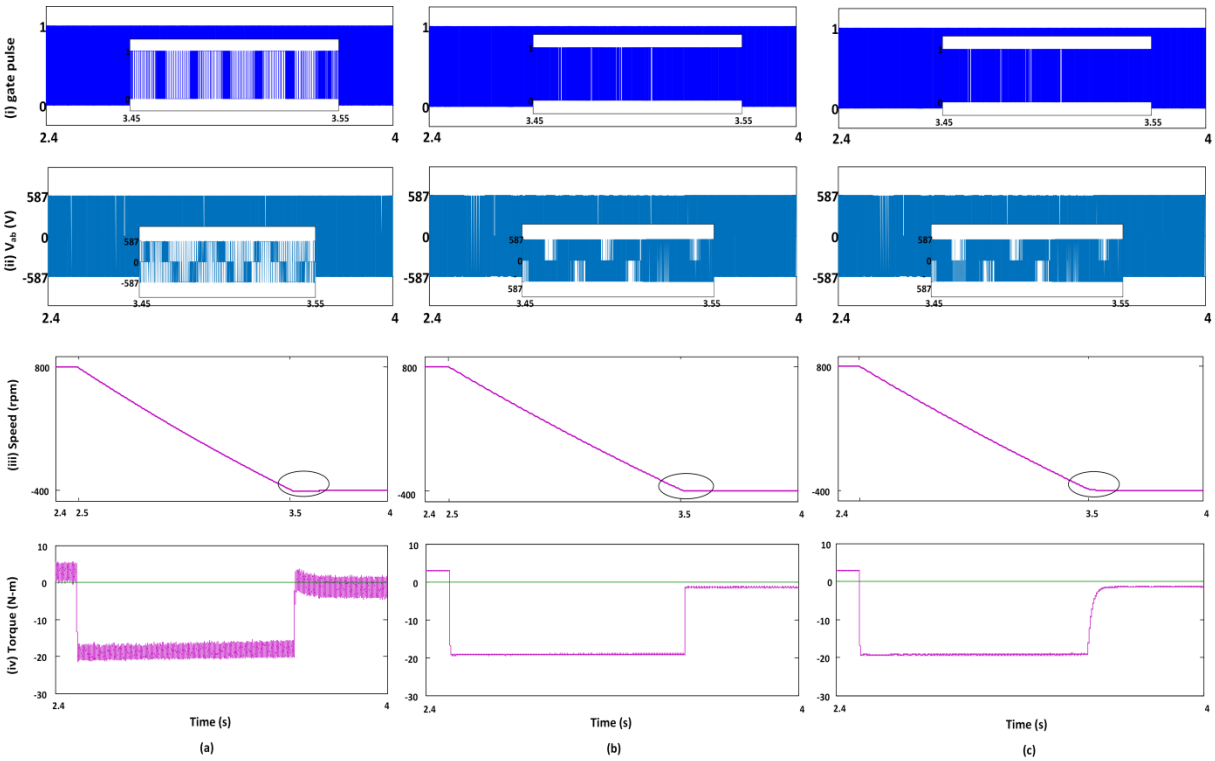

Fig. 4.10 Simulation response during speed reversal characteristics of FBL controlled IM drive using (a) PI-controller: (i) gate signal, (ii) line voltage (V_{ab}), (iii) speed (n_r), (iv) torque (T_e), (b) conventional NFC: (i) gate signal, (ii) V_{ab}, (iii) n_r, (iv) T_e, (c) proposed simplified NFC (SNFC): (i) gate signal, (ii) V_{ab}, (iii) n_r, (iv) T_e.

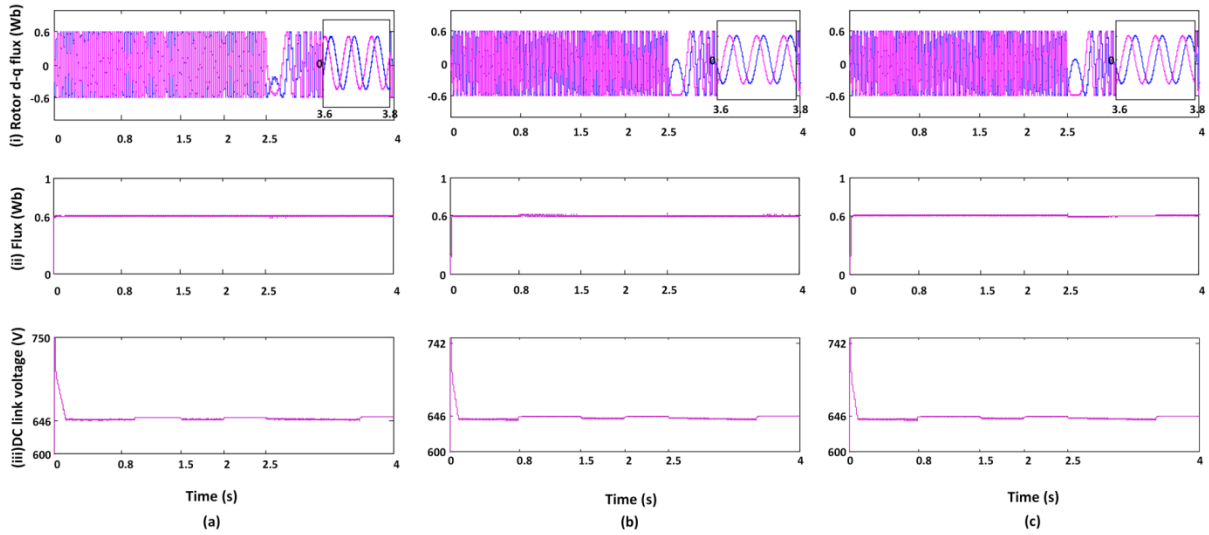

Fig. 4.11 Simulation responses (Starting, 50% loading from 1.5 s to 2 s and then speed reversal) of FBL controlled IM drive with (a) PI-controller: (i) rotor *d-q* flux (ψ_{dqr}), (ii) flux, and (iii) DC link voltage (V_{dc}), (b) conventional NFC: (i) rotor *d-q* flux (ψ_{dqr}), (ii) flux, and (iii) DC link voltage (V_{dc}), (c) proposed NFC: (i) rotor *d-q* flux (ψ_{dqr}),(ii) flux, and (iii) DC link voltage (V_{dc}).

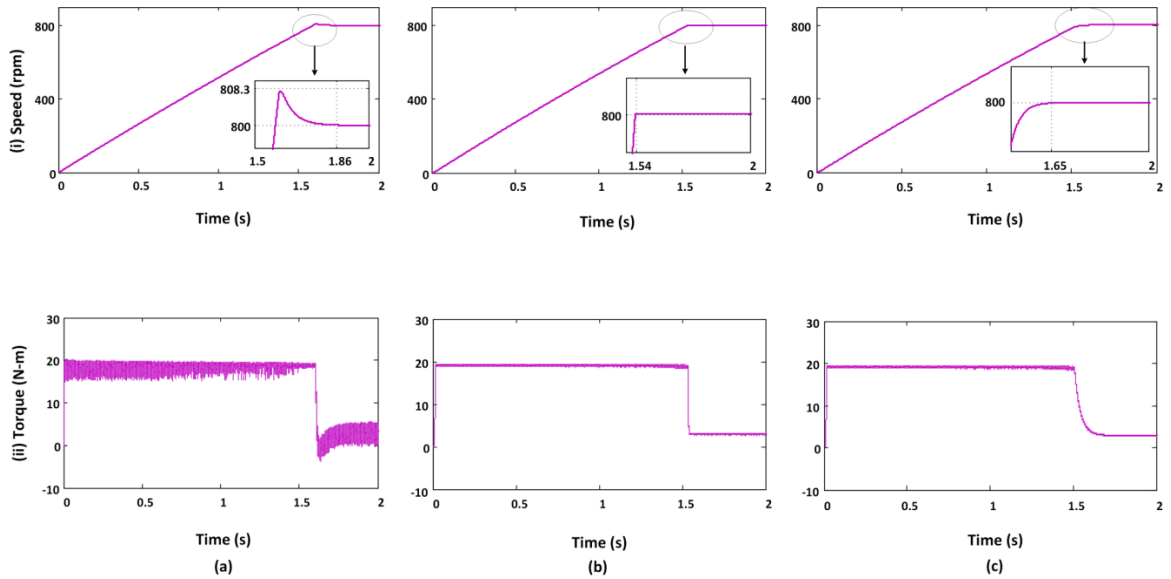

Fig. 4.12 Simulation response of FBL-based IM drive during starting with doubled rotor inertia using (a) PI-controller: (i) speed (n_r), (ii) torque (T_e), (b) conventional NFC: (i) n_r, (ii) T_e, (c) proposed simplified NFC (SNFC): (i) n_r, (ii) T_e.

Table 4.1 Comparative analysis of simulation responses using different controllers

Controller	**Modes of operations of IM**									**Integral Time Absolute Error (ITAE) under load**	**Mean Square Error (MSE)**
	Starting			Loading			Reversing				
	Torque ripple (N-m)	Speed ripple (rpm)	%Speed overshoot (rpm)	Torque ripple (N-m)	Speed ripple (rpm)	%Speed undershoot/ overshoot (rpm)	Torque ripple (N-m)	Speed ripple (rpm)	%Speed undershoot (rpm)		
PI-Controller	4.5	0.1	8.3	4.5	0.1	1.7	4.5	0.06	9	1.7	------
Conventional NFC	0.5	0.005	0	0.5	0.005	1.4	0.5	0.005	0	0.5	0.00187
Proposed NFC	**0.3**	**0.003**	**0**	**0.3**	**0.003**	**1.4**	**0.3**	**0.003**	**0**	**0.38**	**0.00175**

Since variable frequency IM is extensively used, the issue of power quality is the major concern in real practice, which is another aspect of the research area of IM drive. However, in the proposed NFC-based drive, the total harmonic distortion (THD) for supply current harmonics with the load of 10 N-m is found to be 5.15%, which is lower as compared to the conventional NFC and PI-controller based drive having THD of 9.25% and 20.47%, respectively. This indicates that the power quality in case of the proposed drive is improved as the current harmonic is drastically reduced compared to the PI-controller-based drive. These results are evident from Fig. 4.13. The reason of less THD in the NFC-based drive is the optimum selection of rules by learning method of artificial neural network. Also, the NFC-based drive has the significant advantage of controlling pulse signal, which is independent of sampling time. This leads to improved firing strength of the inverter and better power quality of induction motor drive. Fig. 4.14 represents the current THD vs. load for different controllers of linearized IM drive. The current THD gets reduced as the load increases from no-load to full-load.

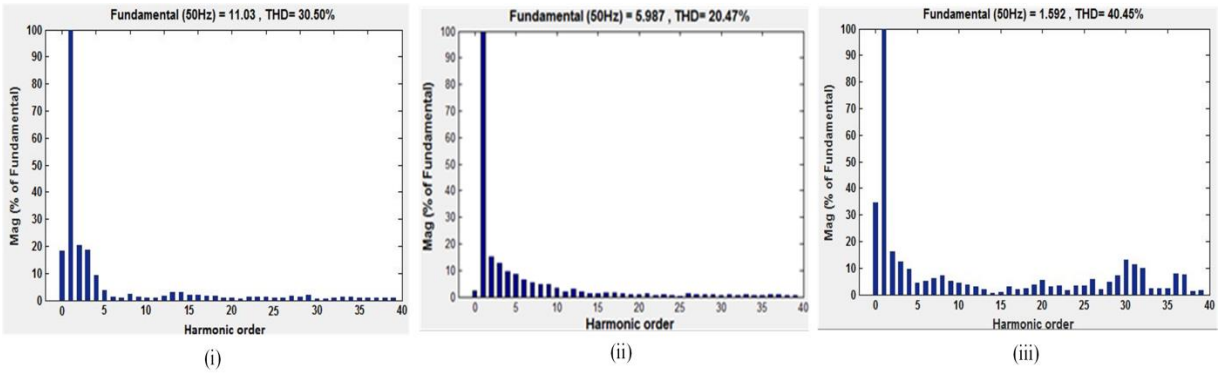

(i) (ii) (iii)

(a)

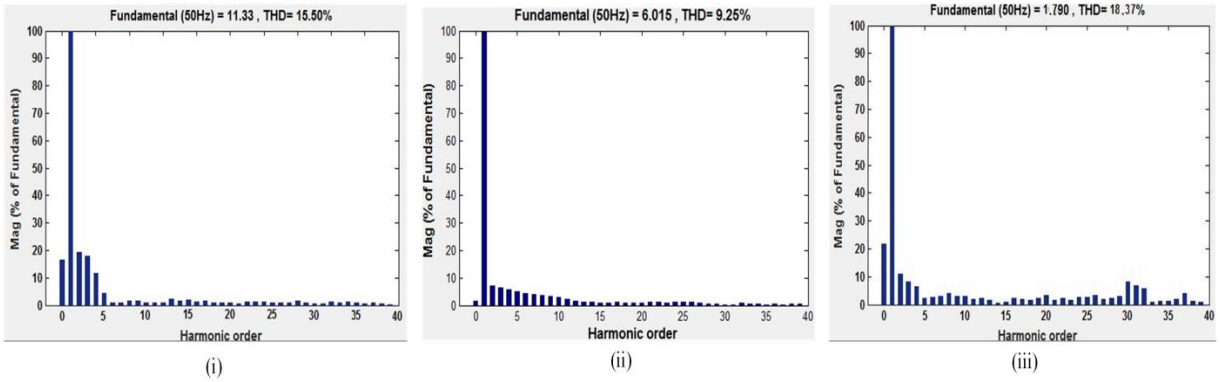

(i) (ii) (iii)

(b)

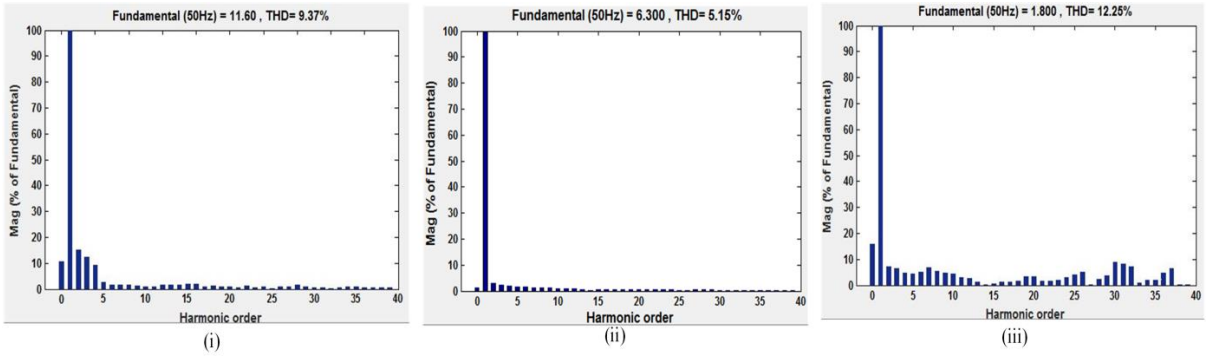

(c)

Fig. 4.13 The harmonic spectrum of supply current of linearized induction motor drive for current harmonics (a) PI-controller: (i) starting, (ii) 50% load (10N-m), (iii) free running, (b) conventional two-input NFC: (i) starting, (ii) 50% load (10N-m), (iii) free running, and (c) proposed simplified NFC: (i) starting, (ii) 50% load (10N-m), (iii) free running.

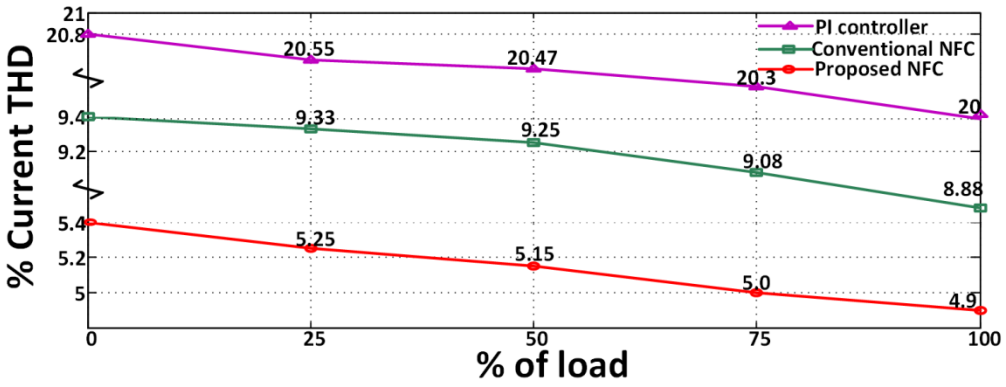

Fig. 4.14 Graph of %THD vs. %load for FBL IM for different controllers.

4.5 Experimental Setup

The simulation results of proposed auto-tuned NFC-based feedback linearized IM drive system are validated in real-time using the platform of 32-bit fixed point DSP TMS320F2812. The details of the experimental setup are described in Chapter 3. The developed real-time Simulink model of the proposed NFC with the auto-tuning algorithm is compiled and transferred to DSP board using an emulator as in Fig. 3.14 (a) of Chapter 3. The tuning rate of the weight (η_{wi}) and the tuning rate of the MFs (η_{ai}, η_{bi}) are adjusted to 0.05 and 0.005, respectively. However, these tuning rates are chosen to be very small by trial and error as they smoothen the transition. A conventional two-input NFC and PI-controller based linearized drive systems are also validated experimentally in order to have a fair comparison. As the structure of the proposed NFC is simplified one, to conduct this

operation, the lowest sampling time required is 100 μs whereas it is 250 μs for conventional NFC. The PI speed and torque controller tuning is done as given in Chapter 2 with regard to zero steady-state error, settling time, and speed overshoot and undershoot of the response so that it gives a fair comparison with that of the NFCs. It is possible to make the PI-controller [147] as critically damped, but it gave extremely sluggish response, which can't be even comparable with the proposed NFC-based drive scheme.

4.6 Experimental Validation

The efficacy of the proposed NFC-based drive is verified and compared in the real-time analysis under different operating modes as shown in Figs. 4.15-4.18 with the experimental setup as in Fig. 3.14. It is observed that the performance of the proposed simple adaptation of NFC is similar to that of conventional NFC, but it has the advantage of significantly reduced computational time, which is found to be 100 μs. The details of the experimental performance under various operating conditions are mentionedin Table 4.2.

Case1: Initially, the experimental responses of starting dynamics and forward motoring are carried out under 800 rpm without any load perturbation as illustrated in Fig. 4.15 (a) – (c). The feedback linearized IM accelerates from rest condition to target speed 800 rpm in 1.38 s using PI-controller with the overshoot, whereas it smoothly settles at 1.08 s and 1.15 s using the conventional NFC and the proposed NFC, respectively. Moreover, the torque ripple of the proposed NFC like conventional NFC is remarkably reduced to 0.5 N-m, which improves the torque response significantly as compared to PI-controller where the ripple is found to be 5N-m as shown in Fig. 4.15 (ii). The stator current responses using all controllers are shown in Fig. 4.15 (iii). The magnitude of steady-state stator current is less (3.2 A) with less distortion using the proposed NFC as compared to PI-controller based drive. The rotor *d-q* components of flux are observed as a constant peak magnitude of 0.6 Wb from starting to steady-state without losing its decoupling behavior which is evident from Fig. 4.15 (iv).

Case2: While IM operates at steady-state speed of 800 rpm, a sudden load of 10 N-m is applied and withdrawn at instants 1.5 s and 2 s, respectively as shown in Fig. 4.16 (a). This leads to a speed undershoot and overshoot of 2.16 rpm at the instants mentioned above and settles down in 0.34 s using PI-controller. The load perturbation makes the motor peak current to increase to 12.8 A at 1.51 s and decrease down at 2.01 s. The proposed NFC-based feedback linearized drive preserves quick and robust response of conventional NFC-based linearized IM drive. Also, there is a remarkable reduction of torque ripple by around 90%, and reduction of speed undershoot/overshoot by 33% over PI-controller-based drive during

load perturbation which is shownin Fig. 4.16 (c) (i) and (ii). Apart from this, the settling times of speed during load changes are 0.16 s which are improved by around 50% over PI-torque controller. Nevertheless, the flux components for controllers remain constant throughout the operation which is evident from Fig. 4.16 (iv).

Case3: Subsequently, the experimental responses in reversal mode of IM are observed in Fig. 4.17 (a) – (c). The responses of the proposed NFC-based drive resemble with that of conventional NFC, and simultaneously it shows the superiority over PI-controller-based drive. Speed reversal took place at 2.5 s with uniform deceleration, reaching command speed of -400 rpm at 3.85 s, 3.55 s and 3.64 s using PI-controller, conventional NFC, and proposed NFC based drive, respectively as shown in Fig. 4.17 (i). Fig. 4.17 (ii) also reveals that the distortion in torque is drastically reduced by using the proposed NFC-based drive. The rotor flux component is observed as constant throughout the operations as shown in Fig. 4.17 (iii).

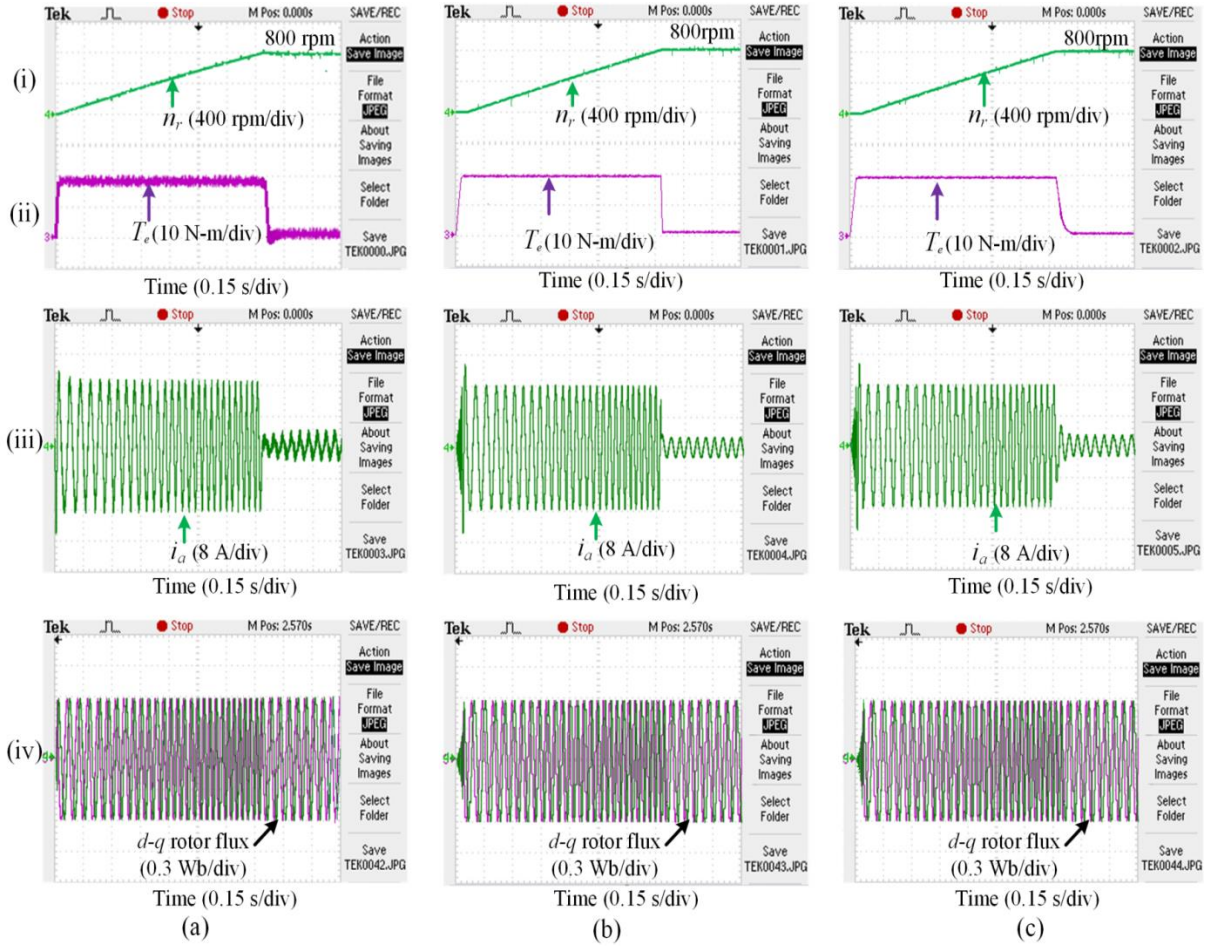

Fig. 4.15 The experimental results no load starting responses of FBL controlled motor drive for 800 rpm using (a) PI-controller: (i) speed (n_r), (ii) torque (T_e), (iii) stator current (i_a), and (iv) rotor *d-q* flux (ψ_{dqr}), (b) conventional NFC: (i) n_r, (ii) T_e, (iii) i_a, and (iv) ψ_{dqr}, (c) proposed simplified NFC: (i) n_r, (ii) T_e, (iii) i_a, and (iv) ψ_{dqr}.

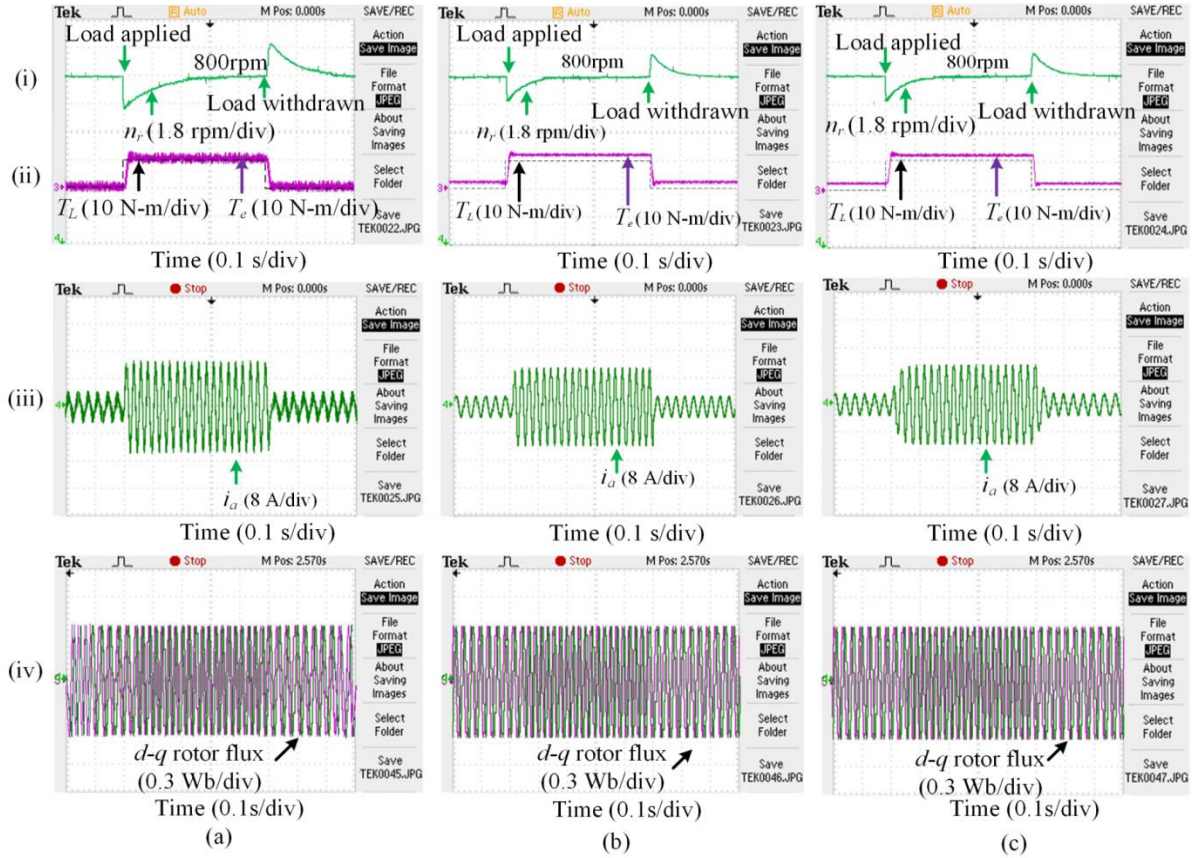

Fig. 4.16 The experimental load perturbation responses of FBL controlled motor drive for 50% (10 Nm) step load from 1.5 s to 2 s using (a) PI-controller: (i) speed (n_r), (ii) torque (T_e), (iii) stator current (i_a), and (iv) rotor *d-q* flux (ψ_{dqr}), (b) conventional NFC: (i) n_r, (ii) T_e, (iii) i_a, and (iv) ψ_{dqr}, (c) proposed simplified NFC: (i) n_r, (ii) T_e, (iii) i_a, and (iv) ψ_{dqr}.

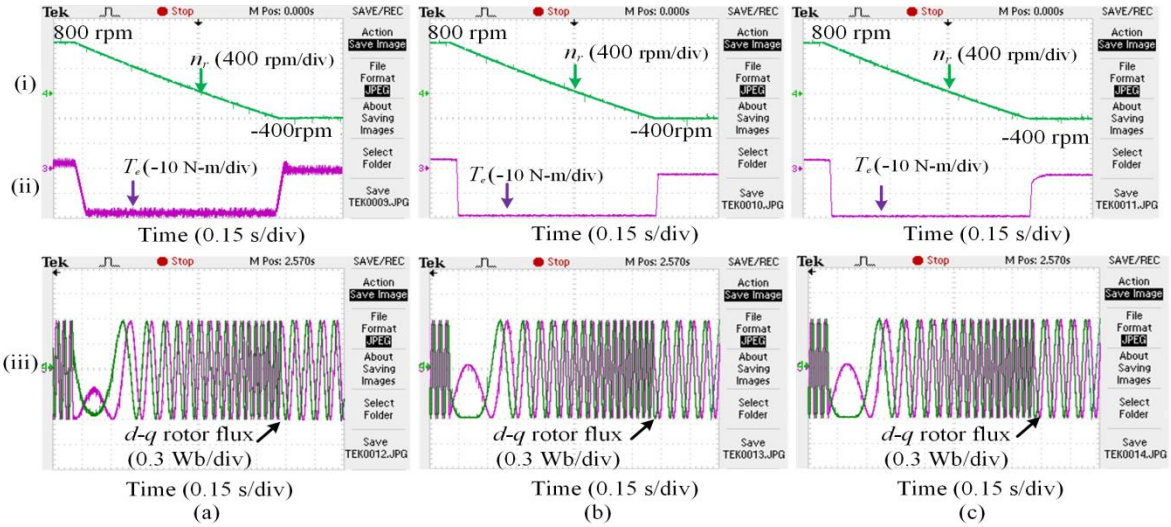

Fig. 4.17 Experimental responses for speed reversal characteristics of FBL-based IM drive using (a) PI-controller: (i) speed (n_r), (ii) torque (T_e), and (iii) rotor *d-q* flux (ψ_{dqr}), (b) conventional NFC: (i) n_r, (ii) T_e, and (iii) ψ_{dqr}, (c) proposed simplified NFC: (i) n_r, (ii) T_e, and (iii) ψ_{dqr}.

Table 4.2 Comparison of simulation and experimental results

Controller	**Speed (rpm)**		**Torque ripples (N-m)**		**Settling time (s)**		
	% Undershoot and Overshoot during load of 10N-m from 1.5s to 2s		Simulation	Experiment	Initiated time (s)	Simulation	Experiment
	Simulation	Experiment				$t_s(n_r)$	$t_s(n_r)$
PI-Controller	1.7	2.16	4.5	5	0	1.1	1.38
					1.5	0.3	0.34
					2	0.3	2034
					2.5	1.3	1.35
Conventional NFC	1.4	1.44	0.5	0.7	0	0.79	1.08
					1.5	0.1	0.12
					2	0.1	0.12
					2.5	1.01	1.05
Proposed NFC	**1.4**	**1.44**	**0.3**	**0.5**	**0**	**0.86**	**1.15**
					1.5	**0.13**	**0.16**
					2	**0.13**	**0.16**
					2.5	**1.1**	**1.14**

The flux remains uniform through every working mode regardless of the speed for the various controllers, which is obvious from the results of Fig. 4.18. Further, the robustness of the feedback linearized IM drive with the proposed simplified NFC is investigated through experiment with doubling of inertia and the responses are illustrated in Fig. 4.19. The rotor inertia is increased by coupling the existing motor with another motor, and it is observed that the rotor takes more time as compared to Fig. 4.15 (i) to reach the command value smoothly unlike PI-controller as the inertia is doubled.

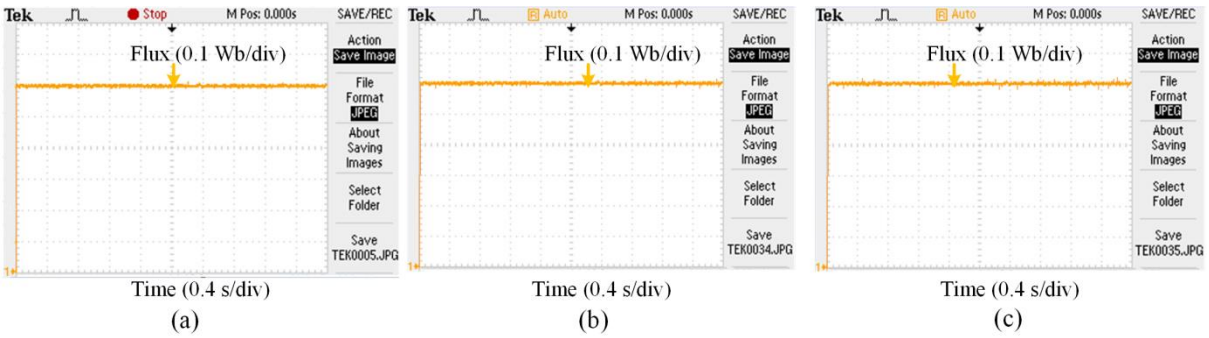

Fig. 4.18 Experimental flux response (starting, step load of 50% from 1.5 s to 2 s, and reversal) of FBL controlled IM for using (a) PI-controller, (b) conventional two-input NFC, and (c) proposed simplified NFC.

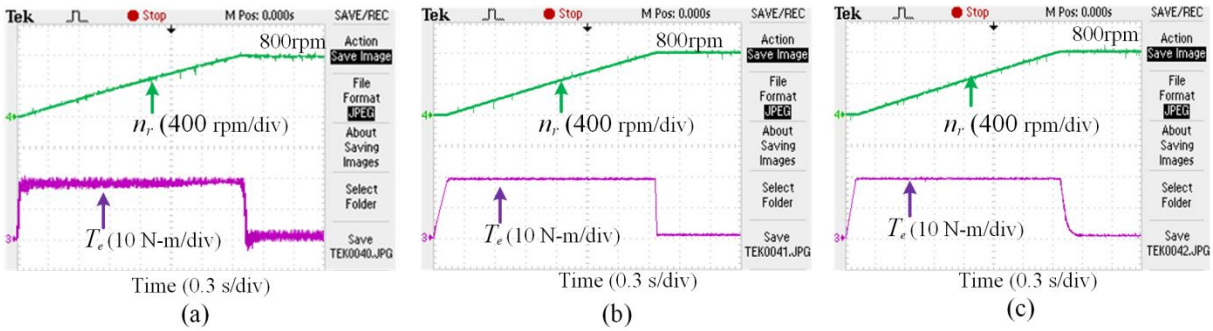

Fig. 4.19 Experimental starting responses of FBL controlled IM drive with twice of rotor inertia for (a) PI-controller: (i) speed (n_r), (ii) torque (T_e), (b) conventional NFC: (i) n_r, (ii) T_e, and (c) proposed NFC: (i) n_r, (ii) T_e.

4.7 Sensitivity Analysis and Robustness Study of Controller

The response of the closed-loop system under the deviation of the system parameters are studied in this Section and depicted in Figs. 4.19-4.21. The main objective of this Section is to verify the robust stability and error sensitivity of the proposed controller-based drive scheme rather than the dynamic behavior of the response under the conditions mentioned above that are confronted while the real-time analysis is carried out. The nominal motor

parameters are used for execution of the FBL, and the controller is so designed that the system achieves robust stability as the parameter varies during the operation. The impact of flux and torque error on FBL is not considered here as the torque and flux estimator provides comparatively good results.

Taking consideration of the uncertainties, the errors of the control signals are symbolized as Δi_{ds}^{*} and Δi_{qs}^{*}. The equation (2.37) is used to evaluate these errors in terms of parameter error and to analyze the impact of uncertainties in the case of NFC design. So (2.37) can be written as

$$i_s = i_{ds}^{*} + j i_{qs}^{*} = u_1 - j\frac{u_2}{\psi_r} \tag{4.32}$$

The (4.32) can be written in terms of the equivalent error Δu as

$$i_s = \left(u_1 + \Delta u_1\right) - \frac{j}{\psi_r}\left(u_2 + \Delta u_2\right) \tag{4.33}$$

Equations (4.32) and (4.33) give the equivalent error Δu as

$$\Delta u = \Delta u_1 + j\Delta u_2 = -\frac{u_2}{\psi_r} - j u_2 \tag{4.34}$$

Now using (4.34) and with the error $\left(u_1 - \Delta u_1\right)$ and $\left(u_2 - \Delta u_2\right)$, (2.34) and (2.35) can be written as

$$\frac{d\psi_r}{dt} = -\frac{R_r}{L_r}\psi_r + \frac{L_m R_r}{L_r}\left(u_1 + \frac{u_2}{\psi_r}\right) \tag{4.35}$$

$$\frac{d\omega_r}{dt} = -\frac{B}{J}\omega_r + \frac{1}{J}\frac{3}{2}\frac{L_m}{L_r}P 2u_2 - \frac{1}{J}T_l \tag{4.36}$$

Since u_2 is produced by the NFC, it has no uncertainty. So, in (4.35), the rotor resistance R_r is the most predominantly variable parameter as it changes with temperature. However, the FBL has the advantage of not affecting the rotor speed dynamics, but affecting the rotor flux dynamics, which is shown in Fig. 4.20. It shows that as the R_r increases, the rate of change of flux increases, i.e., it reaches the steady-state flux faster which is evident from (4.35). The maximum uncertainty of R_r considered here is 100%. Further, R_r uncertainty dynamic does not change the steady-state behavior, indicating the robustness of operation.

Equation (4.36) reveals that the change in rotor inertia J has a substantial impact on speed dynamics. Fig. 4.19 illustrates that with the proposed NFC the motor can track the target

speed smoothly unlike PI-controller-based drive, but the settling time response is more that of the result shown in Fig. 4.15 (i) as the rotor inertia is doubled.

Further, the robustness of the proposed NFC is also investigated by reducing the load torque to 4.5 N-m for the same time instants of 1.5 s to 2 s. An experimental analysis is performed by altering the gain of the speed-PI controller from (K_p, K_i) from (20, 0.02) to (17, 0.01) as shown in Fig. 4.21. It reveals that even if the K_p and K_i values of the PI-speed controller are altered, unlike PI-controller as in Fig. 4.21 (a) (i) and (b) (i), there is no such difference of speed response in terms of undershoot/overshoot and settling time by NFC torque controller-based feedback linearized drive as presented in Fig. 4.21 (a) (ii) and (b) (ii). Therefore, the proposed NFC provides substantial torque ripple minimization and less dip in speed subjected to quick dynamic response than that of the PI-controller-based drive with the deviation of PI-speed controller gain. This shows robustness of the proposed scheme because the gains of PI controllers are tuned with proper optimization of rule by NFC using the center-of-gravity method.

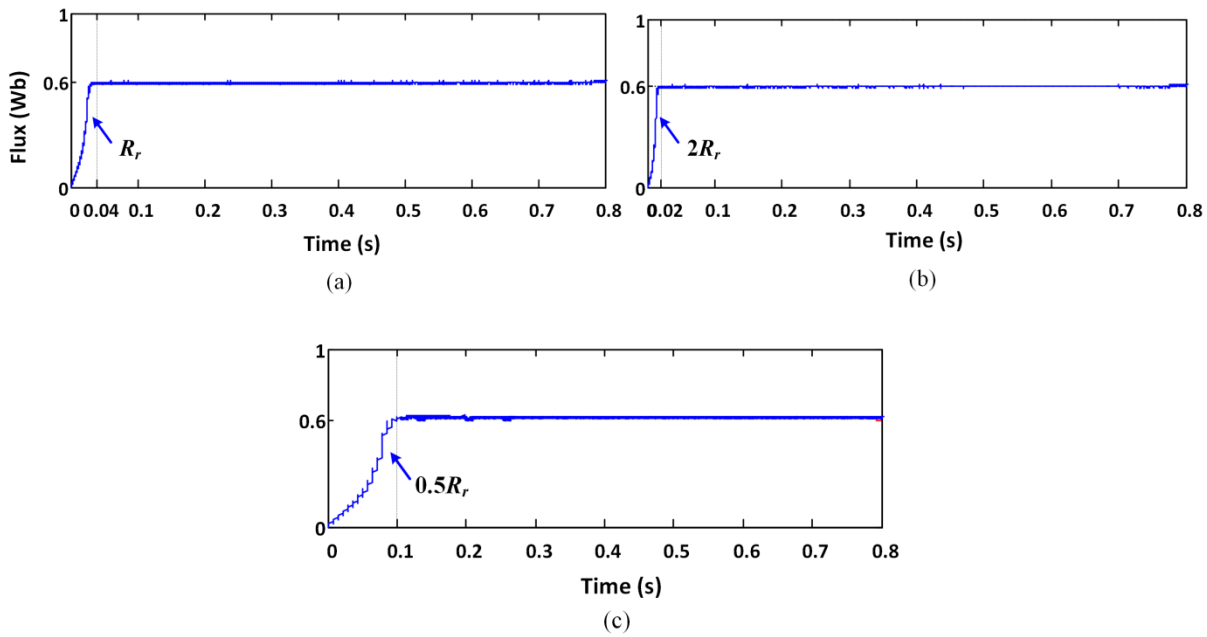

Fig. 4.20 Flux responses during starting with the proposed NFC-based FBL IM drive with the uncertainties of R_r: (a) R_r, (b) +100% R_r error, and (c) -50% R_r error.

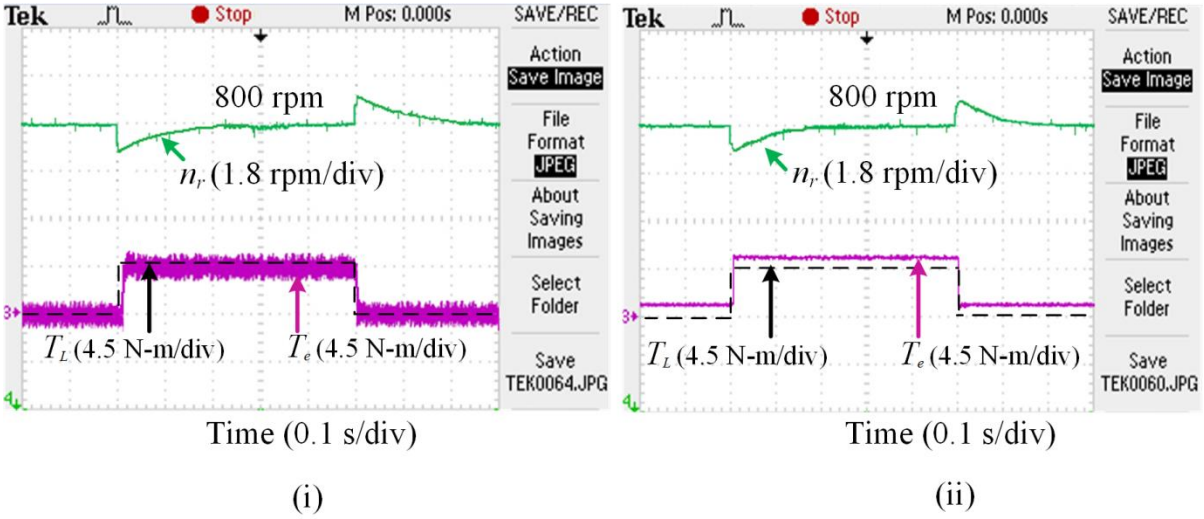

(i) (ii)

(a)

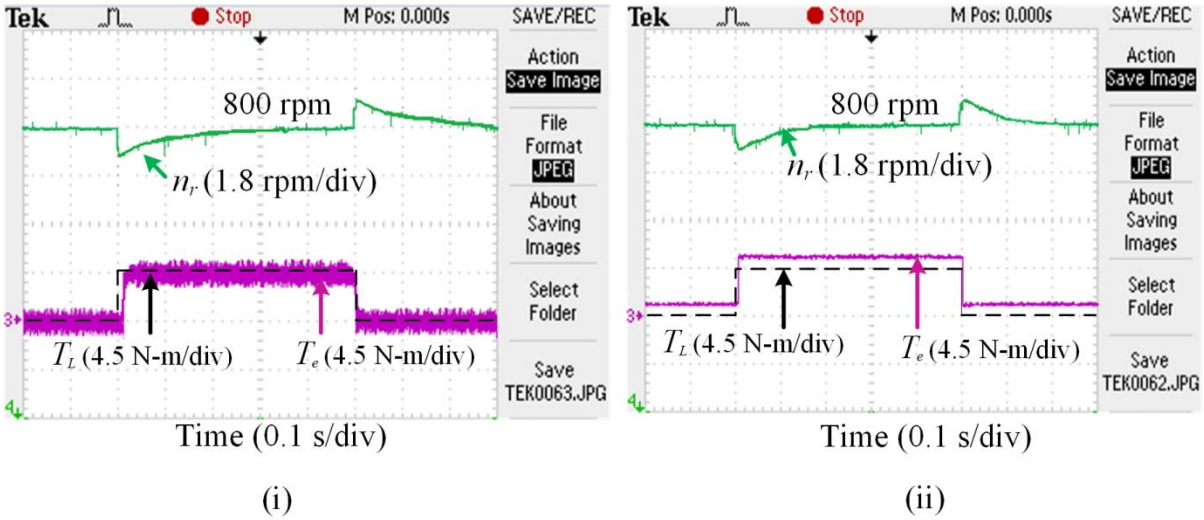

(i) (ii)

(b)

Fig. 4.21 The experimental load perturbation responses of FBL controlled motor drive for 4.5 N-m load from 1 s to 1.5 s for different gains of PI-speed controller with (a) K_p = 20 and K_i = 0.02: (i) PI-controller-based drive and (ii) proposed NFC-based drive, (b) K_p = 17 and K_i = 0.01: (i) PI-controller-based drive and (ii) proposed NFC-based drive.

4.8 Conclusion

The design of the specific NFCs as implemented on the FBL modeled IM drive is presented here. Comprehensive and systematic algorithm is developed with stepwise procedure followed for self-tuning of the proposed NFC. The proposed NFC incorporated with theintuitive FBL based IM drive system is designed, modeled, and simulated in MATLAB software, and experimentally investigated in the real-time hardware setup using DSP TMS320F2812 processor.

The FBL-based IM drive with the proposed NFC demonstrates fast and robust performance with remarkably reduced torque ripple compared to the PI-controller in terms of starting, load perturbation, and speed reversal operations. The flux response with the proposed NFC is almost constant throughout all the operating modes without deteriorating the decoupling issue.

The sensitivity and robustness of the controller are tested in terms of parameter variations like rotor resistance, moment of inertia, and external load disturbances. Further, the robustness and versatility of the proposed NFC are investigated experimentally by varying the P and I gains of the speed controller. The flux response shows good tracking performance with perfect decoupling behavior. It is concluded from the results that the performance of the proposed simplified NFC is almost similar to that of the conventional NFC, but it has the main advantage of significantly reduced computational burden, which is obtained as 100 μs compared to 250 μs in case of the conventional NFC. The comparative analysis as evident from Table 4.1 and 4.2 shows that the system behavior with the proposed NFC does not deteriorate compared to the conventional NFC. Additionally, it outperforms PI-controller with regard to transient and steady-state performance. Thus, the proposed controller is suitable for implementation in high-performance drive applications.

In Chapter 5, some efforts have been made to improve some performances of the linearized drive system further by using simplified neuro-fuzzy sliding-mode controller (NFSMC). The simulation and experimental results are provided, and a comparative study is carried out with the conventional one for the FBL IM drive system. Further, the proposed controller is integrated with the fuel cell powered FBL IM drive system as a stand-alone application which gives huge advantage during interruption of main supply and voltage outages.

Chapter 5

DESIGN AND INVESTIGATION OF A FEEDBACK LINEARIZED INDUCTION MOTOR DRIVE USING HYBRID SIMPLIFIED NEURO-FUZZY SLIDING-MODE CONTROLLER AND ITS APPLICATION TO FUEL CELL OPERATED DRIVE SYSTEM

CHAPTER 5
DESIGN AND INVESTIGATION OF A FEEDBACK LINEARIZED INDUCTION MOTOR DRIVE USING HYBRID SIMPLIFIED NEURO-FUZZYSLIDING-MODE CONTROLLER AND ITS APPLICATION TO FUEL CELL OPERATED DRIVE SYSTEM

5.1 Introduction

The advantages of simplified neuro-fuzzy control (NFC) and robust sliding-mode control (SMC) are combined in this Chapter to make the feedback linearized drive robust against all uncertainties and to improve the transient performance further. SMC is one of the effective robust control techniques for the plant, where inaccurate dynamic modeling with parameter uncertainties and disturbances are present. It has been largely applied to IM drives in servo applications, where a complex trajectory has to be tracked by the actuator. Most often, SMC introduces chattering effect in the control signal and the system states. So, the main objective of the adaptive hybrid simplified neuro-fuzzy sliding-mode control (NFSMC) proposed in this Chapter is to incorporate adaption law based on a sliding surface that updates the parameters of the simplified NFC against external disturbances, parameter variations, and system uncertainties. The sensitivity of the feedback linearized IM model to parameter detuning and uncertainties, and high computational burden imposed by the conventional NFC lead to the development of simplified NFSMC. Apart from being insensitive to the motor parameter variations, plant uncertainties, and outer load perturbation, the proposed simplified NFC reduces the computational burden by reducing the rules and membership functions (MFs) compared to the conventional two-input NFC. The adaptive mechanism and the cost function used to optimize the simplified NFC parameters are based on the sliding surface of SMC concept. Generally, inverter fed IM drive takes power from a grid, but during power interruption and voltage outages, the power is supplied directly from a separate DC source to improve efficiency of the system. Therefore, fuel cell driven FBL IM drive incorporated with the proposed NFSMC is used for the stand-alone applications. The implementation of SMC with the modified NFC makes the system chattering-free, effective, and robust for every

working state of linearized IM drive. An estimation strategy based flux and speed observer is presented in Section 5.2. In Section 5.3, the design methodology of the simplified NFC pertaining to sliding-mode approach for a speed sensorless linearized IM drive is presented. The self-tuning algorithm for the proposed NFSMC is derived and based on the mentioned update rules, the steps employed for updating parameters is depicted in Section 5.4. In Section 5.5, hybrid fuel cell-energy storage power system for the linearized IM drive is modeled. Extensive simulation results with its analysis followed by experimental implementation and validation are explained in Section 5.6, 5.7, and 5.8. Section 5.9 depicts the design and robustness test of the proposed controller. Finally, the conclusion part is presented in Section 5.10.

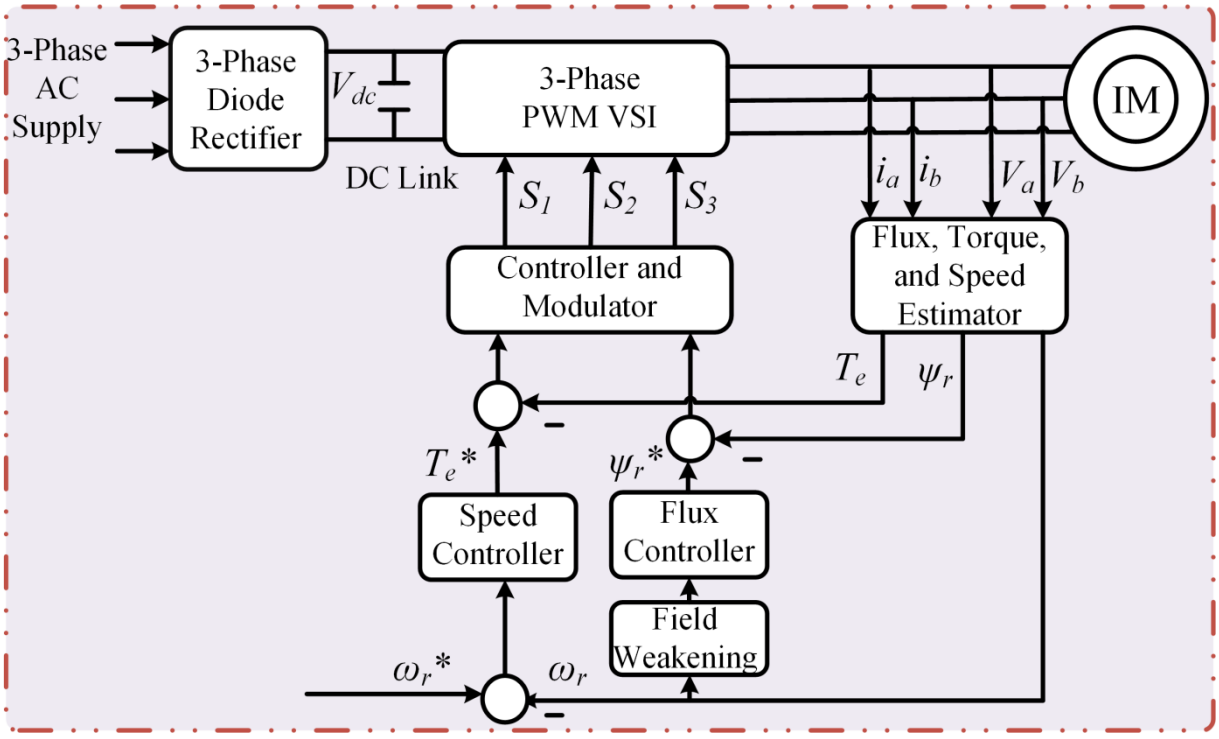

(a)

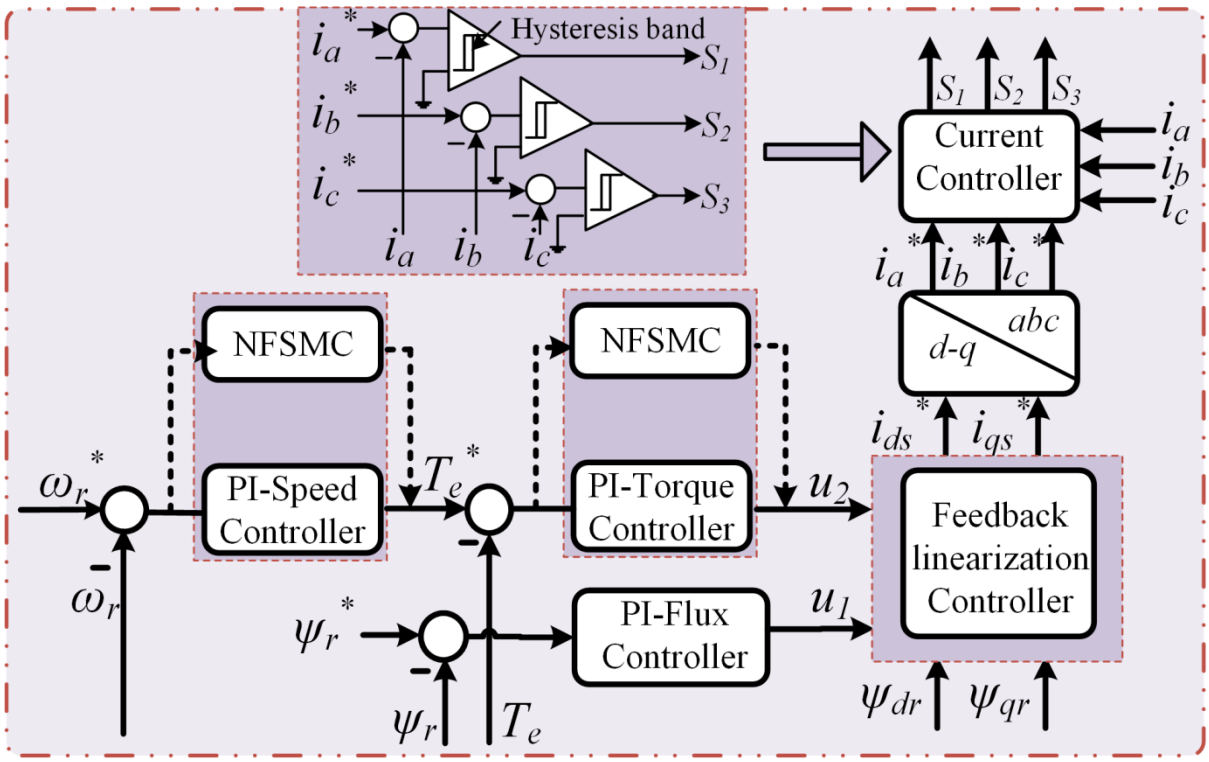

(b)

Fig. 5.1 (a) Proposed simplified sensorless FBL controlled IM drive, (b) speed and torque NFSMC for linearized IM drive.

5.2 Rotor Flux and Speed Estimator

In order to minimize the speed and flux estimation error in the realistic situation, simple flux and speed observers are chosen here purposefully to test the controller robustness [4], [58]. An estimation based sensorless strategy is adapted based on voltage model, where the stator voltages and currents are sensed, and the fluxes are estimated from the *d-q* stationary reference frame using *d-q* modeling of induction motor drive and voltage equations as stated in equations (3.3) and (3.4). The rotor flux and torque components can be obtained by using equation (2.5), (3.3), and (3.4).

From equations (3.3) and (3.4), the *d-q* components of flux, ψ_{dr} and ψ_{qr} can be obtained by integration operation which interduces DC offsets. Though these DC components are very small, they drive the integrators to saturation [141]. During low-speed operations, to observe the *d-q* component of flux accurately, a simple high pass filter is introduced here after integration operation as it eliminates DC offset that arises due to the integration. The cutoff frequency ω_0 must be selected properly to remove the DC component so that the flux

observer gives fast and accurate results at low speeds. In this Chapter, based on experience, the ω_0 is chosen to be 5 rad/s. The estimated rotor speed can be given as $\omega_{rest} = \omega_{\psi_r est} - \omega_{slest}$, where $\omega_{\psi_r est} = \frac{d\theta_{\psi_r}}{dt}$ is the speed of rotor flux and $\omega_{slest} = \frac{2}{3}\frac{1}{P}\frac{R_r}{\psi_r^2}T_e$ is the slip speed [4].

5.3 Design Methodology of the Adaptive NFSMC

The combined advantages of the adaptive simplified NFC and robust SMC are proposed here to deal with uncertainties that arise in the feedback linearized drive control. The main priority given in this adaptive NFSMC is to propose sliding surface-based adapting rules that tune the parameters of the simplified NFC under system and parameters uncertainties, as well as external disturbances. However, unoptimized and uncertain fuzzy logic control as well as the computational burden imposed by the conventional NFC motivates us to develop a more simplified NFC. The proposed NFSMC-based feedback linearized drive is illustrated in Fig. 5.1.

5.3.1 Simplified NFC

The proposed simple modified version of NFC design combines fuzzy logic control (FLC) with a four-level artificial neural network (ANN) structure, as shown in Fig. 4.2 (a) of Chapter 4. The two inputs speed error and acceleration (change in speed error) of the conventional NFC give rise to more number of membership functions and updating rules. The robustness of the controller can be improved by adopting acceleration as one of the inputs [135], [136]. However, the difficulty in measuring fast and accurate acceleration [137] worsens the ability of NFC by increasing the computational burden and also, makes the measurement of acceleration useless. Therefore, the proposed NFC is modified by a simple control algorithm in order to achieve the required performance of the IM drive system. The parameter of the third layer is modified by tuning to control any deviation of control effort. The single input speed error in the simplified NFC, is the difference between the desired speed ω_r^* and the actualspeed ω_r of the NFC which details are given in Chapter 4.

5.3.2 Conventional NFC

The conventional two-input NFC is also designed as shown in Fig 4.3 in order to have a comparative performance with the proposed simplified NFC. Also, the MFs of both conventional NFC and proposed NFC are kept identical as in Fig 4.2 (b) in order to make a fair comparison. But, the MFs parameters are fixed in the conventional NFC. The two inputs

of the conventional NFC are normalized speed error and change in speed error. Both NFCs are also tuned by the same auto-tuning methods as described in Section 5.4.

Similarly, the NFC for rotor torque dynamics is designed as the same method of the NFC for rotor speed dynamics. Moreover, the MFs of the neuro-fuzzy torque controller is kept same as the neuro-fuzzy speed controller as depicted in Fig. 5.2 (b), but it has different input and output crisp values as in Fig. 5.1 (b).

Fig. 5.2 (a) signifies the surface view of the change in control output of NFC. The dependency of the output on a single input, error (E) is displayed by using the surface viewer. Also, the surface viewer is defined as the change in control output surface mapping of the system. Fig. 5.2 (b) represents applied input MFs for the proposed simplified NFC.

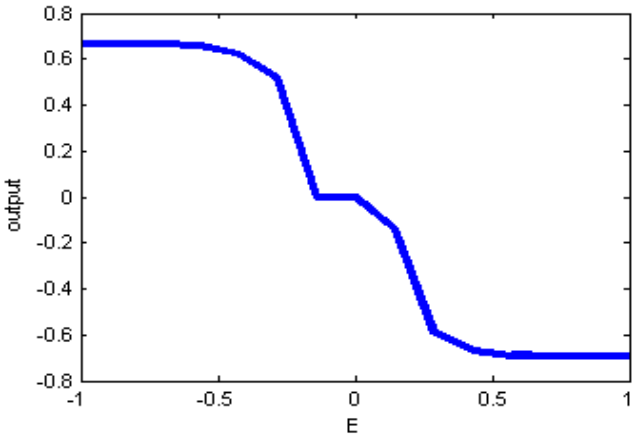

(a)

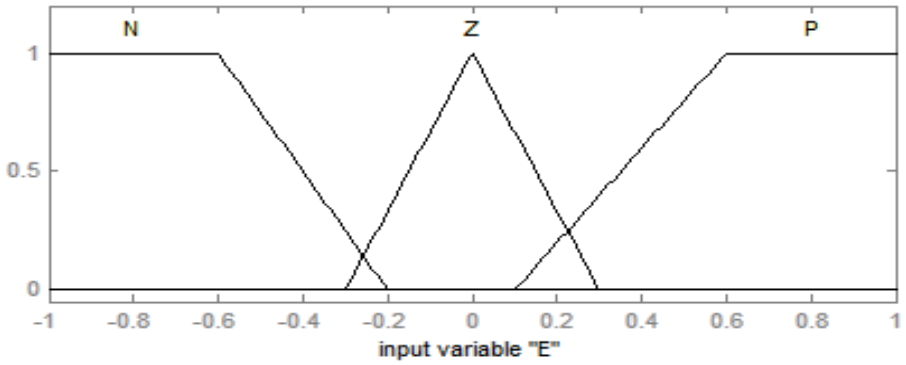

(b)

Fig. 5.2 Proposed simplified NFC: (a) output vs. error and (b) input MFs.

5.3.3 Proposed Sliding-mode Based Simplified NFC

Fig. 5.3 depicts the structure of the proposed simplified NFSMC for interfacing with FBL IM drive. The error (e) and change in error (Δe) are processed through the sliding surface whereas only error input is applied to the fuzzifier block of the simplified NFC, unlike conventional NFC. In sliding-mode controller (SMC), the sliding surface parameters govern

the entire system dynamics. The response of the system is not affected by parameter variations and external perturbations. The classical PI controllers are not able to handle such problem. Over the years, a lot of research work has been reported using SMC instead of PI-controller. Robustness of system with SMC is inherent as its control technique is independent of system model and is insensitive to outer disturbances upto certain range. As the IM has nonlinear and coupled dynamics and it encounters with various disturbances during real-time implementation, SMC based controllers have been applied effectively for the IM performance enhancement.

In SMC, the system is so controlled that the error and change in error of both speed and torque dynamics drive the system trajectories along the sliding surface, which is defined as [58]

$$S = \left(\frac{d}{dt} + \lambda_{\omega r} \right) e \tag{5.1}$$

where $\lambda_{\omega r}$ is the design parameter which is greater than zero.

The sliding surface considered here to design SMC for the linearized system of (2.35) as the speed error

$$S = \omega_r - \omega_r^* \tag{5.2}$$

where ω_r^* is the reference speed and ω_r is the observed speed. The SMC law used for selecting of sliding line

$$\%u_2 = -\hat{k}_{\omega r} - \beta_{\omega r} \operatorname{sgn}(S), \beta_{\omega r} > 0 \tag{5.3}$$

where $\%u_2 = \frac{1}{J}\frac{3}{2}\frac{L_m}{L_r} P u_2 \approx T_e^*$, $k_{\omega r}$ is the uncertain dynamics of FBL speed dynamics, which is not exactly known; from (2.35) the estimated dynamics of the uncertainties is obtained as $\hat{k}_{\omega r} = -\frac{B}{J}\omega_r$. $\beta_{\omega r}$ is the switching control gain and $\beta_{\omega r} \operatorname{sgn}(S)$ represents the corrective switching control which is discrete and ensures the sliding. Here, the load torque T_l is assumed to be zero for simplicity.

The trajectory of the system shifts to the sliding surface if the following condition holds true.

$$\frac{1}{2}\frac{d}{dt} S^2 \le -\eta_{\omega r} |S| \tag{5.4}$$

where $\frac{S^2}{2}$ is the chosen Lyapunov function 'V' and $\eta_{\omega r}$ is positive constant which controls the convergence speed to the SMC. Now

$$\frac{1}{2}\frac{d}{dt}S^2 = S\frac{d\omega_r}{dt} \tag{5.5}$$

Substituting (2.35) in (5.5), the following equation is obtained.

$$\begin{aligned}\frac{1}{2}\frac{d}{dt}S^2 &= S\left(-\frac{B}{J}\omega_r + \frac{1}{J}\frac{3}{2}\frac{L_m}{L_r}Pu_2\right)\\ &= S\left(k_{\omega r} + \%u_2\right)\\ &= S\left(k_{\omega r} - \hat{k}_{\omega r} - \beta_{\omega r}\,\mathrm{sgn}(S)\right)\\ &= S\left(k_{\omega r} - \hat{k}_{\omega r}\right) - S\beta_{\omega r}\,\mathrm{sgn}(S)\\ &= S\left(k_{\omega r} - \hat{k}_{\omega r}\right) - \beta_{\omega r}|S|\end{aligned} \tag{5.6}$$

The above equation must be negative during uncertainties in order to have robust convergence. Here, the switching control gain $\beta_{\omega r}$ is considered as in (5.7) to satisfy the condition in (5.4).

$$\beta_{\omega r} = K_{\omega r} + \eta_{\omega r} \tag{5.7}$$

The switching control gain $\beta_{\omega r}$ of (5.7) includes the first term $K_{\omega r}$ to ensure robust stability. A larger value of $\eta_{\omega r}$ makes the trajectory of the system to reach faster but with the cost of more chattering. Also, $\left|\hat{k}_{\omega r} - k_{\omega r}\right| \le K_{\omega r}$ is assumed to be estimated bounded error.

A boundary layer around the sliding surface to make the system response chattering-free is defined as

$$L_{\omega r}(t) = \left\{x, |S(x)| \le \phi_{\omega r}\right\} \tag{5.8}$$

where a boundary layer of thickness $\phi_{\omega r} > 0$ is introduced here for a chattering-free response. Inside the boundary layer, a proportional term is introduced to the control of (5.3), which is given by (5.9) as follows:

$$\%u_2 = -\hat{k}_{\omega r} - \beta_{\omega r}\,\mathrm{sgn}(S) + \lambda_{\omega r}\left(\omega_r - \omega_r^*\right), \beta_{\omega r} > 0 \tag{5.9}$$

Above the boundary layer $\left(|S(x)| > \phi_{\omega r}\right)$, the corrective switching control drives the system to move along the sliding surface.

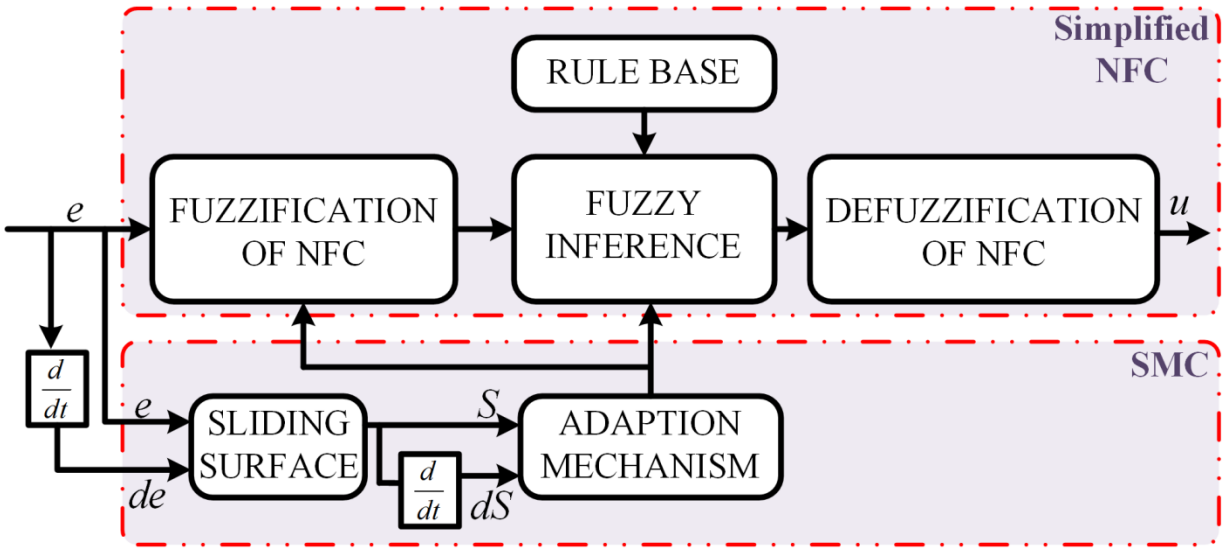

Fig. 5.3 Proposed simplified NFSMC structure.

5.4 Auto-tuning Algorithm for Proposed NFSMC

The value of the sliding surface *S* is used here for the adaptive mechanism, which is based on the gradient descent algorithm to update the parameters of the proposed NFC [148]. However, it is a very tough task to find out the required NFC output and offline trained data under different dynamic operating conditions. Therefore, an unsupervised auto-tuning online method based on Back-propagation algorithm is proposed here whose assignment is to upgrade the MFs parameters and weight in order to have minimized error signal. The cost function to be optimized is defined as

$$E = \frac{1}{2}(\dot{S} + \lambda_{\omega r} S)^2 \tag{5.10}$$

In order to achieve the desired control performance, the parameters of the NFC to be updated are as follows:

$$a_i(k+1) = a_i(k) - \eta_{ai} \frac{\partial}{\partial a_i} E(k) \tag{5.11}$$

$$b_i(k+1) = b_i(k) - \eta_{bi} \frac{\partial}{\partial b_i} E(k) \tag{5.12}$$

$$w_i(k+1) = w_i(k) - \eta_{wi} \frac{\partial}{\partial w_i} E(k) \tag{5.13}$$

where k is the sampling instant, a_i and b_i are the i^{th} node values of a and b, and $\eta_{ai}, \eta_{bi}, \eta_{wi}$ are their learning rates.

Using (5.10), the differential terms of aforesaid equations are described by the following equations.

$$\frac{\partial}{\partial a_i}E(k) = (\dot{S} + \lambda_{\omega r} S)\frac{\partial S}{\partial \omega_r}\frac{\partial \omega_r}{\partial v}\frac{\partial v}{\partial O_i^1}\frac{\partial O_i^1}{\partial a_i} \tag{5.14}$$

$$\frac{\partial}{\partial b_i}E(k) = (\dot{S} + \lambda_{\omega r} S)\frac{\partial S}{\partial \omega_r}\frac{\partial \omega_r}{\partial v}\frac{\partial v}{\partial O_i^1}\frac{\partial O_i^1}{\partial b_i} \tag{5.15}$$

$$\frac{\partial}{\partial w_i}E(k) = (\dot{S} + \lambda_{\omega r} S)\frac{\partial S}{\partial \omega_r}\frac{\partial \omega_r}{\partial v}\frac{\partial v}{\partial w_i} \tag{5.16}$$

The differential terms common to (5.14) – (5.16) are given by

$$\frac{\partial S}{\partial \omega_r} = -1 \tag{5.17}$$

$$\frac{\partial \omega_r}{\partial v} = \text{constant } K \tag{5.18}$$

The value of K is greater than zero for the proposed induction motor drive scheme [74], [137]. The other terms of equations (5.14) – (5.16) are determined from equations (4.2) – (4.7) as

$$\frac{\partial v}{\partial O_i^1} = \frac{v_i(k)}{\sum w_i(k)} \tag{5.19}$$

$$\left.\begin{aligned} &\frac{\partial O_i^1}{\partial a_i} = \frac{\partial O_1^1}{\partial a_1} = \frac{x_1^{\,1} - b_1}{(b_1 - a_1)^2} = -\frac{1 - O_1^1(k)}{b_1(k) - a_1(k)} \text{ for } i = 1 \\ &\frac{\partial O_3^1}{\partial a_3} = -\frac{1 - O_3^{\,1}(k)}{b_3(k) - a_3(k)} \text{ for } i = 3 \end{aligned}\right\} \tag{5.20}$$

$$\left.\begin{aligned} &\frac{\partial O_i^1}{\partial b_i} = \frac{\partial O_1^1}{\partial b_1} = -\frac{x_1^{\,1} - a_1}{(b_1 - a_1)^2} = -\frac{O_1^1(k)}{b_1(k) - a_1(k)} \text{ for } i = 1 \\ &\frac{\partial O_2^1}{\partial b_2} = \frac{(x_2^{\,1} - a_2)}{b_2^{\,2}} = \frac{1 - O_2^1(k)}{b_2(k)} \text{ for } i = 2 \\ &\frac{\partial O_3^1}{\partial b_3} = -\frac{O_3^1(k)}{b_3(k) - a_3(k)} \text{ for } i = 3 \end{aligned}\right\} \tag{5.21}$$

$$\frac{\partial v}{\partial w_i} = \frac{v_i(k)}{\sum w_i(k)} \tag{5.22}$$

Substituting (5.19) – (5.22) in (5.11) – (5.13), the following update rules are obtained as:

$$a_1(k+1) = a_1(k) - \eta_{a1}(\dot{S} + \lambda_{\omega r} S)K \frac{v_1(k)}{\sum w_i(k)} \frac{1 - O_1^1(k)}{b_1(k) - a_1(k)} \tag{5.24}$$

$$a_3(k+1) = a_3(k) - \eta_{a3}(\dot{S} + \lambda_{\omega r} S)K \frac{v_3(k)}{\sum w_i(k)} \frac{1 - O_3^1(k)}{b_3(k) - a_3(k)} \tag{5.25}$$

$$b_1(k+1) = b_1(k) - \eta_{b1}(\dot{S} + \lambda_{\omega r} S)K \frac{v_1(k)}{\sum w_i(k)} \frac{O_1^1(k)}{b_1(k) - \mathrm{a}_1(k)} \tag{5.26}$$

$$b_2(k+1) = b_2(k) + \eta_{b2}(\dot{S} + \lambda_{\omega r} S)K \frac{v_2(k)}{\sum w_i(k)} \frac{1 - O_2^1(k)}{b_2(k)} \tag{5.27}$$

$$b_3(k+1) = b_3(k) - \eta_{b3}(\dot{S} + \lambda_{\omega r} S)K \frac{v_3(k)}{\sum w_i(k)} \frac{O_3^1(k)}{b_3(k) - a_3(k)} \tag{5.28}$$

$$w_i(k+1) = w_i(k) + \eta_{wi}(\dot{S} + \lambda_{\omega r} S)K \frac{v_i(k)}{\sum w_i(k)} \tag{5.29}$$

The steps to be followed for tuning the parameters based on update rules mentioned by (5.24) – (5.29) are given as follows:

Step 1: First, fuzzy rules of the simplified NFSMC and the parameters a_1, a_3, b_1, b_2, b_3, and w_i are initialized.

Step 2: The normalized input speed error is obtained by using (4.1)

Step 3: The MFs values O_i^1 are then calculated by using equations (4.2) – (4.4).

Step 4: By using (5.29), tuning of the weight w_i is done.

Step 5: The error signal from step 2, O_i^1 values from step 3, and the tuned weight w_i from step 4 are used in equations (5.24) – (5.29) to update the parameters a_i and b_i.

Step 6: Repeat step 3 till the error signal is minimized.

Similarly, the SMC operation is also adopted to update the NFC parameters of the motor torque dynamics, where the error signal is defined as

$$e = (T_e^* - T_e) \tag{5.30}$$

where T_e^* is the reference torque, which is the output of the neuro-fuzzy speed controller and T_e is the actual or estimated torque.

The error of the proposed simplified NFSMC is found to be the least value 0.00125 as shown in Fig. 5.4. These errors were displayed by taking 30 iterations but, prior to five iterations, the controllers are settled down to the minimum error of 0.00137 and 0.00125 for the conventional NFSMC and the proposed NFSMC, respectively.

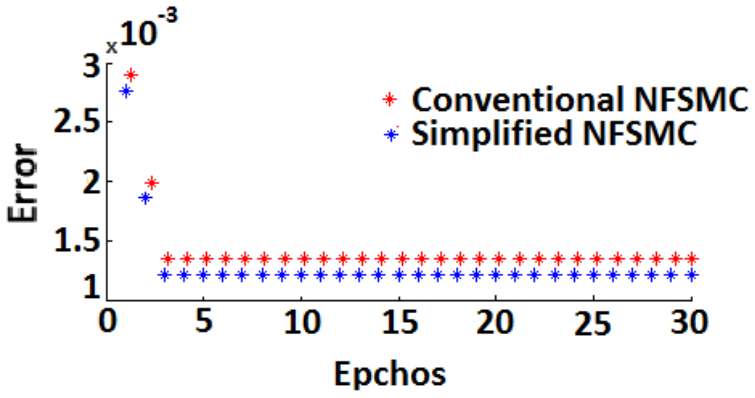

Fig. 5.4 Error of the proposed NFSMC.

5.5 Modeling of Hybrid Fuel cell-Energy Storage Power System for FBL IM Drive

Usually, IM requires power from a grid followed by a rectifier and an inverter. But, to make the system more efficient during power failure and voltage outages, the power is delivered directly from DC as a stand-alone application which shows a big advantage. This Section focuses on the design of a hybrid fuel cell (FC) supply system to deliver the power demanded by the FBL-based IM drive. A hybrid FC energy storage (ES) based drive system has the advantages of providing fast responses, additional power during acceleration, and recovery of energy during regenerative braking through a braking chopper, which improves the drive efficiency [134]. The FC system as a clean and continuous source of electrical energy provides an effective and eco-friendly approach to be used as a separate external source. Fig. 5.5 (a) shows the proposed hybrid fuel cell-energy storage system for the linearized IM drive as a stand-alone application. This system comprises of 1) FC with dc/dc boost converter; 2) battery as an energy storage system; 3) braking chopper; and 4) IM drive.

FC is the primary energy source which is connected with a boost converter to boost the voltage level to the standard dc link voltage level. A battery is used as an ESS which supplements the FC during different modes of the drive operations. Finally, the unabsorbed energy due to some battery limitations is dissipated in the braking chopper during regenerative braking.

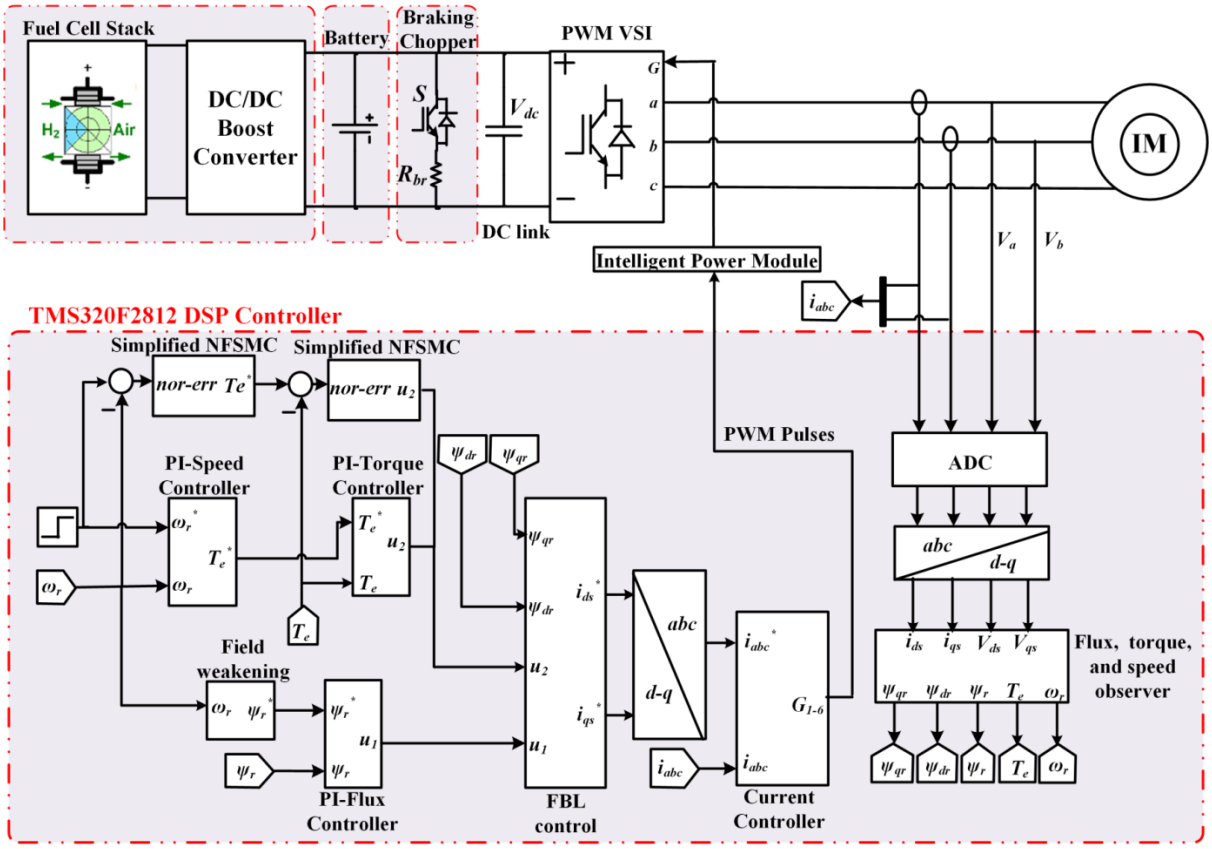

(a)

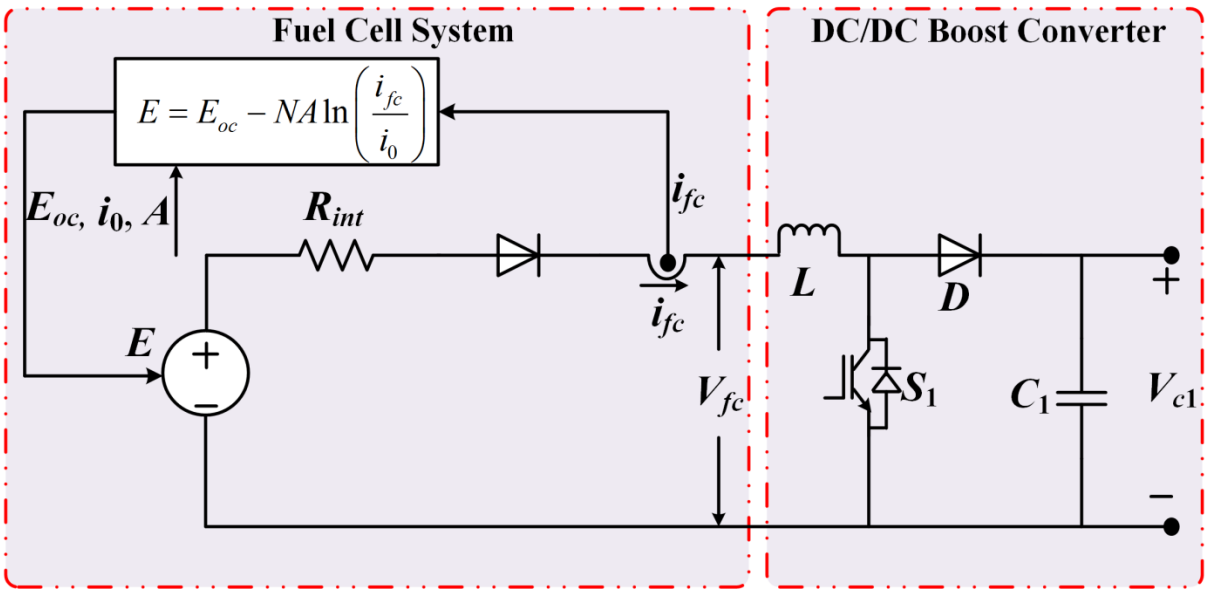

(b)

Fig. 5.5 (a) Overall configuration of the proposed fuel cell-based linearized sensorless IM drive using simplified NFSMC, (b) fuel cell system model with a boost converter.

5.5.1 Fuel cell System with dc/dc Boost Converter

The fuel cell (FC) is a DC-voltage generator based on an electrochemical process which can produce energy in electrical form from chemical energy (H_2 and O_2) [149]. The proton exchange membrane (PEM) is one of the most suitable technologies and broadly used FC. The PEM-FC has the special characteristic of having low temperature and high power density. The efficiency of the PEM-FC stack-based on H_2 and air at normal operation is observed to be nearly 50%. The overall operation of the FC can be listed as

- The output of the FC is low DC voltage which is not fixed based on the operational conditions;
- The FC never allows regenerative braking as it provides positive DC current.

To encounter with fast load transient and to offer regenerative braking, a hybrid FC system is incorporated as described above. A conventional dc/dc boost converter [150] is required to increase the FC voltage to meet the DC link voltage requirement of the three-phase inverter for IM drive system as observed in Fig. 5.5 (b). Detailed specifications of the boost converter are given in Appendix A.2.

The simplified FC stack model implemented here is based on the equivalent circuit as shown in Fig. 5.5 (b). This specific FC stack model operating at normal pressure and temperature conditions is given by [149]:

$$V_{fc} = E_{oc} - NA\ln\left(\frac{i_{fc}}{i_0}\right) - i_{fc}R_{\text{int}} \tag{5.31}$$

where V_{fc}, i_{fc} are the PEM-FC stack output voltage and current, respectively, E_{oc} is the open circuit voltage, i_0 is the exchange current, R_{int} is the FC internal resistance, N is the number of cells, and A is the Tafel slope. Here, a diode is used to avoid the negative current into the stack. Also, the diode voltage drop is neglected here.

The typical polarization curve (V-I characteristic) and power curve of the FC stack are obtained here as in Fig. 5.6 which represent its normal operating point. This curve can be classified into three parts. The first part indicates the activation voltage drop due to the slow reactions of the chemical process at electrode surfaces. The second part represents the ohmic losses due to the FC stack internal resistance. Finally, the third region represents the mass transport losses because of the variation in concentration of reactants as the fuel is used.

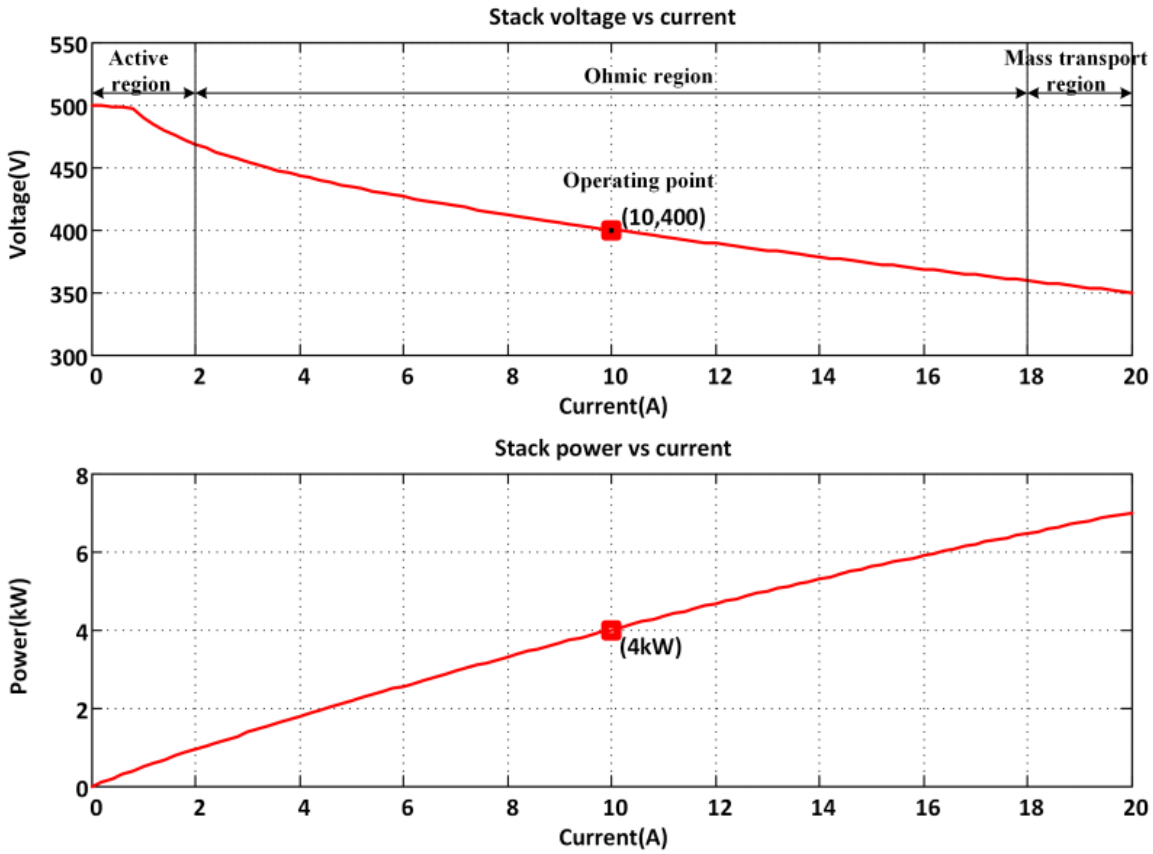

Fig. 5.6 FC stack polarization curve and power curve.

5.5.2 Braking Chopper

During regenerative braking, some part of the energy must be dissipated through the resistance (R_{br}) of the braking chopper as it is not absorbed by the battery because of its some constraints. Also, it absorbs the energy produced by a motor deceleration when desired. Braking Chopper is modeled by an IGBT (S) series with the resistance (R_{br}), connected parallel with the DC link as in Fig. 5.5 (a). The R_{br} in this context is calculated as $R_{br} = \frac{V^2_{act}}{P_n}$, where P_n is the IM nominal rated power as given in Appendix A.1 and V_{act} is the activation voltage in order to limit the increase in voltage during regenerative braking. V_{act} is set to be higher value than the shutdown voltage (V_{sh}) of the braking chopper. Again the V_{sh} should be slightly higher value than the DC bus peak voltage which is given by $V_{peak} = V_n\sqrt{2} = 415\sqrt{2} = 587$ V. So, V_{sh} and V_{act} are considered to be 600 V and 650 V, respectively. In this case, the effective resistance R_{br} to be calculated to dissipate the power

for 5 hp IM drive system as $R_{br} = \frac{V^2_{act}}{P_n} = 113.3\,\Omega$. The braking chopper hysteresis logic is illustrated in Fig. 5.7 (a).

5.5.3 DC Link

The DC link voltage ripple can be reduced by taking suitable bus capacitance which is calculated as [151] $C_{dc} = \frac{P_n}{12 f_n . \Delta v . V_{dc}} = 221\,\mu\text{F}$, where Δv is the desired voltage ripple which is considered to be 50 V here, V_{dc} is the average DC link voltage which is given by $V_{dc} = 1.35 V_n = 560.25\,\text{V}$, and other parameters P_n and f_n are givenin the Appendix A.1.

Further, the braking chopper is controlled by a voltage control loop as demonstrated in Fig. 5.7 (b). The DC link voltage is considered as a reference signal and is compared with the activation voltage of the braking chopper. The error is processed through a proportional controller in order to produce the desired switching signal for energy dissipation in the braking chopper during regenerative braking.

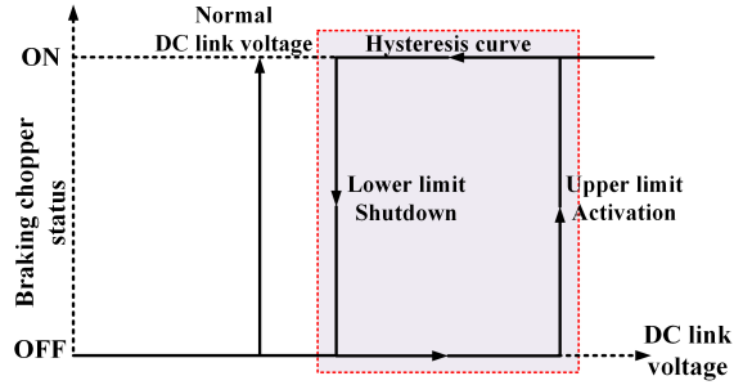

(a)

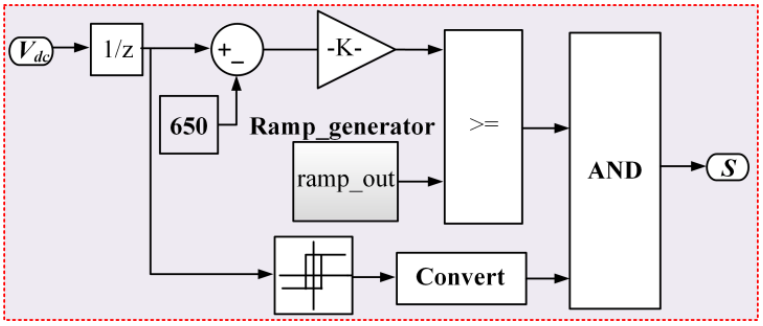

(b)

Fig. 5.7 (a) Braking Chopper hysteresis curve and (b) controller for switching signal of the braking chopper.

5.6 Simulation Results and Performance Assessment

The performance of the proposed simple modified NFSMC via FBL IM drive is examined by simulation as well as by experiment for a 3.7 kW IM. The responses under various working modes as in Figs. 5.8-5.10 are analyzed and compared with the conventional PI-controller, and the details are illustrated in Fig. 5.11. The parameters of IM drive system are given in the Appendix A.1. As the structure of the proposed NFSMC is simplified one, the lowest sampling time required is 150 μs whereas it is 300 μs for the conventional NFSMC. It is observed from the results that the proposed less computationally burdened simplified NFSMC does not deteriorate the system behavior compared to the conventional NFSMC. Simultaneously, it gives an enhanced performance compared to the conventional PI-controller, which is seen from Fig. 5.11 and Table 5.2. The detail comparison of performance analysis for different controllers and its summary is provided in Table 5.1.

Case 1: The FBL IM drive without load at 800 rpm using various controllers is performed under MATLAB simulation, and the responses for this starting operation are shown in Fig. 5.8. The less distorted stator current (18 A) improves the starting torque response of the proposed NFSMC based FBL IM drive by significantly reduced ripples compared to the conventional PI-controller based drive. However, with the proposed NFSMC, the spike in capacitor voltage V_{dc} (742 V) is observed at starting as the capacitor charges and settles down later within 5 to 6 cycles by discharging through properly selected switching path as in Fig. 5.8 (c) (iv). It is evident from the results that the low computational proposed NFSMC based drive bears a resemblance compared to the conventional NFSMC. On the other hand, it shows superior performance compared to the classical PI-controller based drive with regard to ripples, overshoot, and settling time which are demonstrated in Fig. 5.11 and Table 5.2.

Case 2: The response of the external load perturbation by increasing the step load to 50% (T_l = 10 N-m) from 1.5 s to 2 s is illustrated in Fig. 5.9. It reveals that the speed response of the proposed simplified NFSMC has very good load disturbance rejection in terms of undershoot and overshoot. The torque ripples with the proposed NFSMC are extensively reduced compared to the PI-controller, thereby decreasing the magnitude and distortion of the motor current. In fact, the oscillation in speed is almost disappeared by using the proposed NFSMC based drive as shown in Fig. 5.9 (c) (i) compared to the conventional NFSMC, which still can have small oscillations. Further, the capacitor voltage is reduced to 644 V during the sudden increase of stator current at 1.5 s as the energy stored in the capacitor gets released when the large current is drawn by motor through the capacitor and comes to the

steady state after half cycle (0.01 s). Likewise, the capacitor starts discharging and charging during application and removal of the load, which is evident from Fig. 5.9 (iv).

Case 3: Subsequently, the linearized IM drive is undergoing speed reversal from 800 rpm to -400 rpm at 2.5 s as shown in Fig. 5.10. This leads to large negative motor torque and large stator current. During reversing, the frequency of the current reduces first by the controller using regenerative braking followed by phase reversal and the responses replicate the responses of the starting operation as shown in Fig. 5.8. The details of all above three cases are compared in Fig. 5.11.

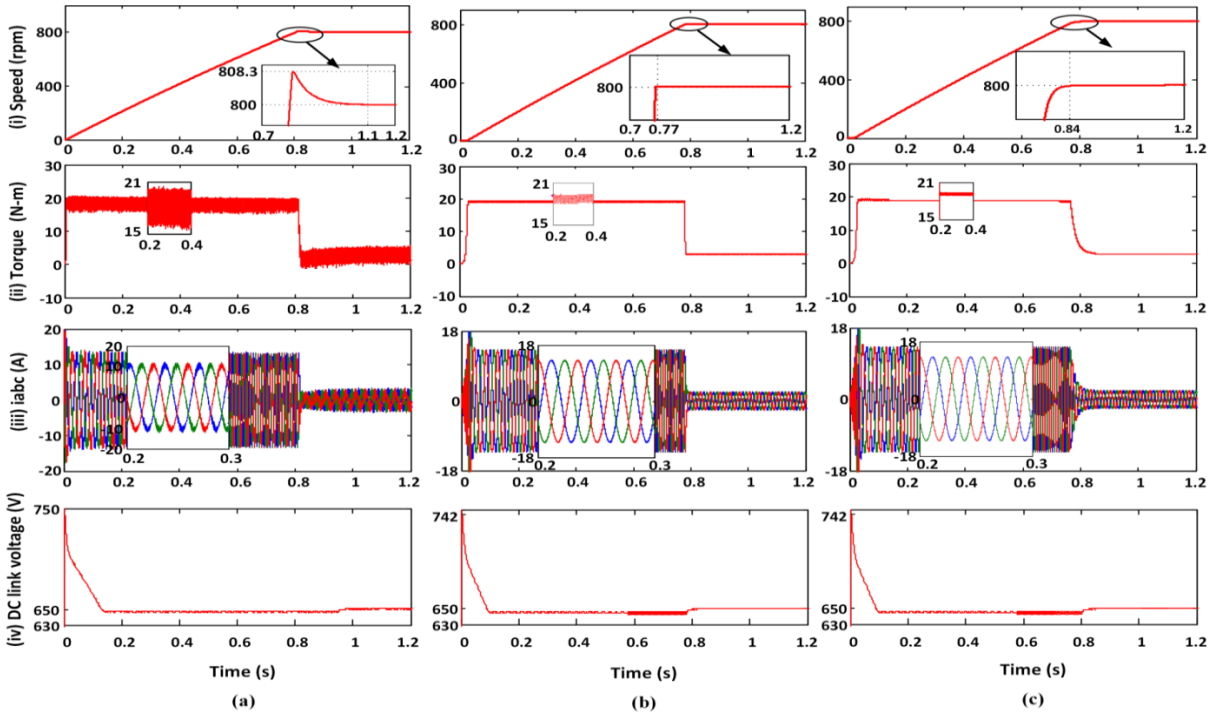

Fig. 5.8 Simulation responses of FBL IM drive during starting using (a) PI-controller: (i) speed (n_r), (ii) torque (T_e), (iii) stator current (i_{abc}), (iv) DC link voltage (V_{dc}), (b) conventional NFSMC: (i) n_r, (ii) T_e, (iii) i_{abc}, (iv) V_{dc}, (c) proposed simplified NFSMC: (i) n_r, (ii) T_e, (iii) i_{abc}, (iv) V_{dc}.

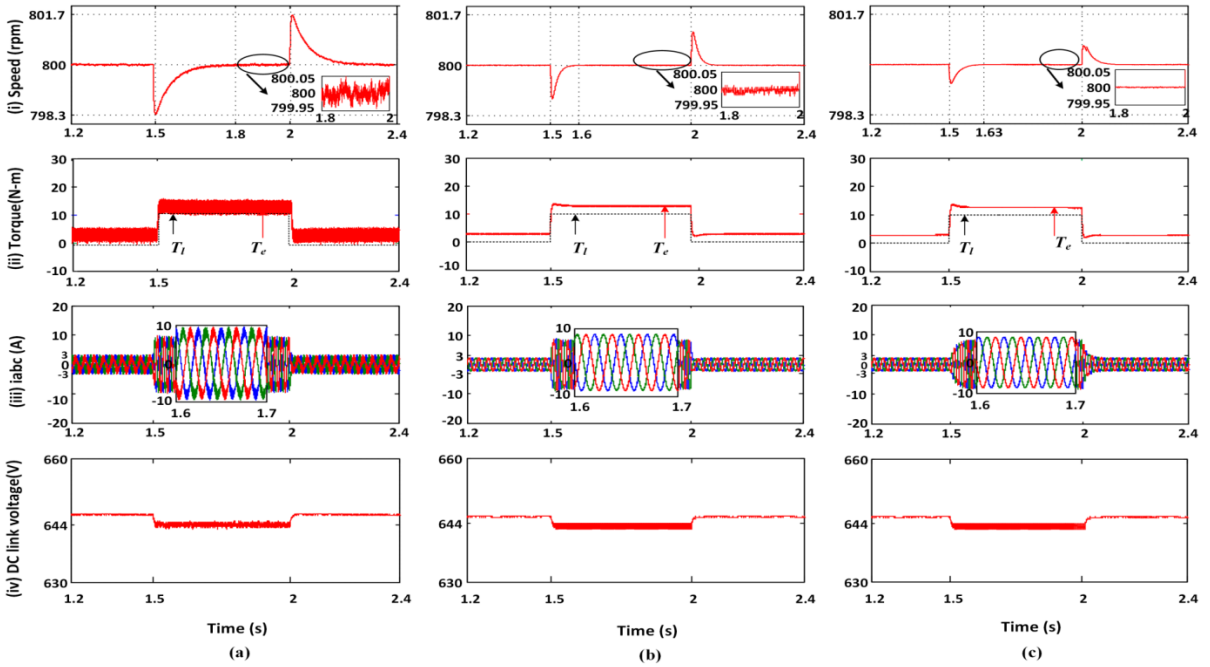

Fig. 5.9 Simulation responses for load perturbation with a step increase of load to 50% using (a) PI-controller: (i) speed (n_r), (ii) torque (T_e), (iii) stator current (i_{abc}), (iv) DC link voltage (V_{dc}), (b) conventional NFSMC: (i) n_r, (ii) T_e, (iii) i_{abc}, (iv) V_{dc}, (c) proposed simplified NFSMC: (i) n_r, (ii) T_e, (iii) i_{abc}, (iv) V_{dc}.

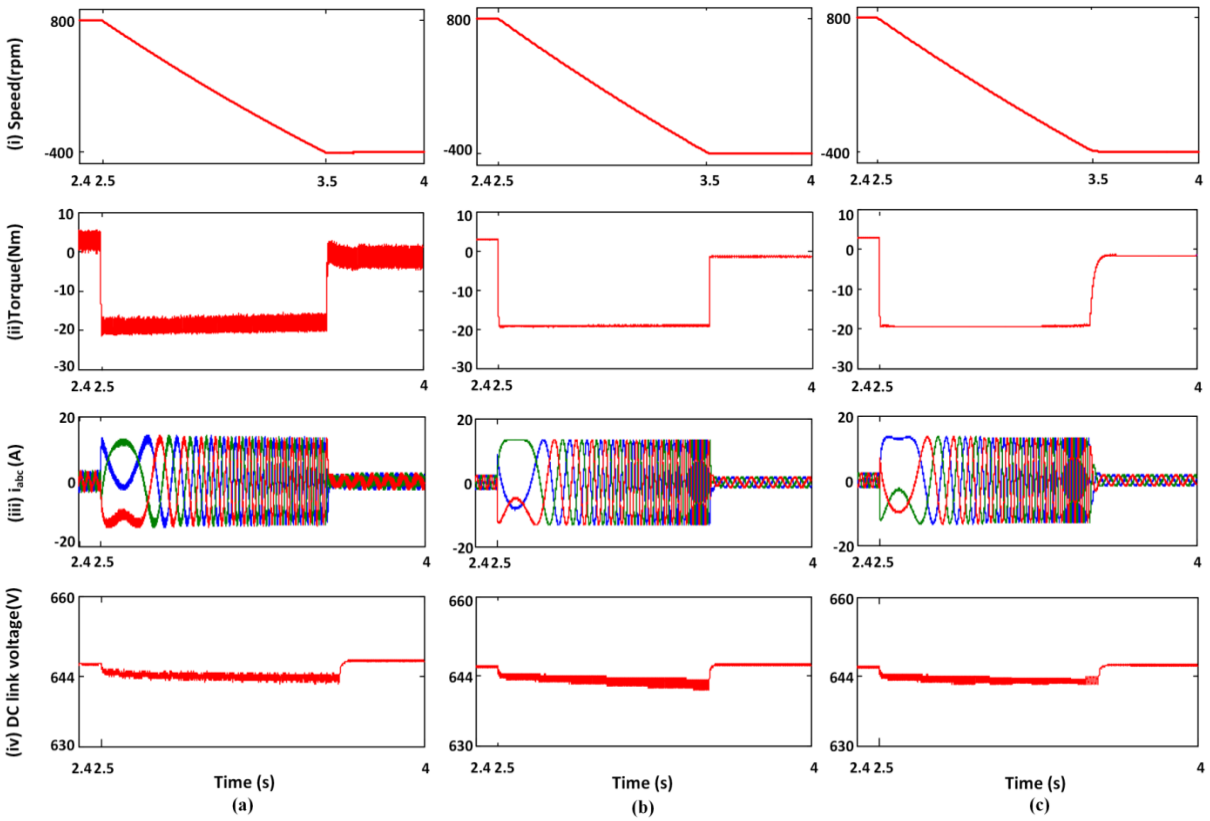

Fig. 5.10 Speed reversal responses of FBL controlled IM drive using (a) PI-controller: (i) speed (n_r), (ii) torque (T_e), (iii) stator current (i_{abc}), (iv) DC-link voltage (V_{dc}), (b) conventional NFSMC: (i) n_r, (ii) T_e, (iii) i_{abc}, (iv) V_{dc}, (c) proposed simplified NFSMC: (i) n_r, (ii) T_e, (iii) i_{abc}, (iv) V_{dc}.

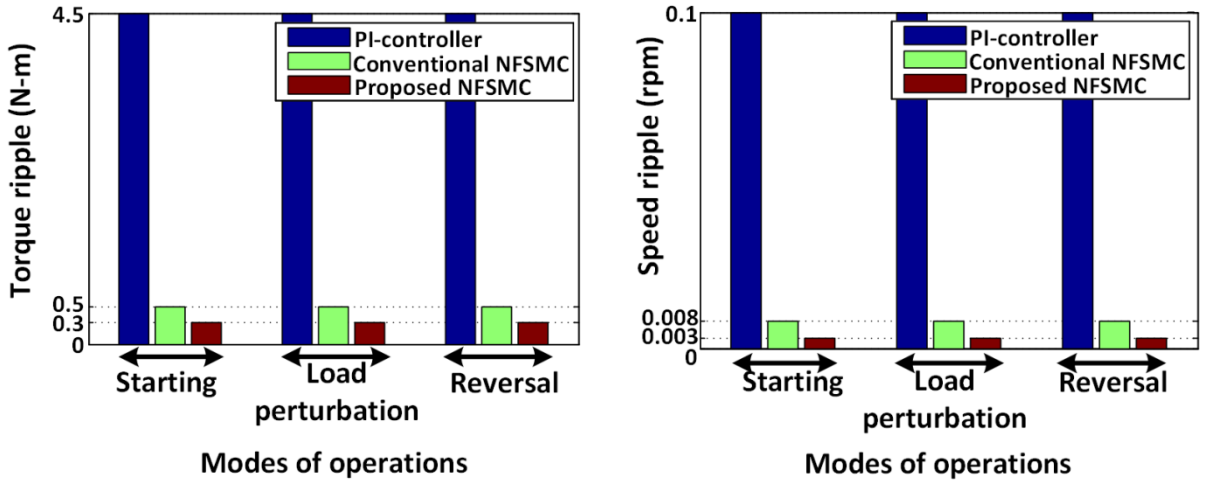

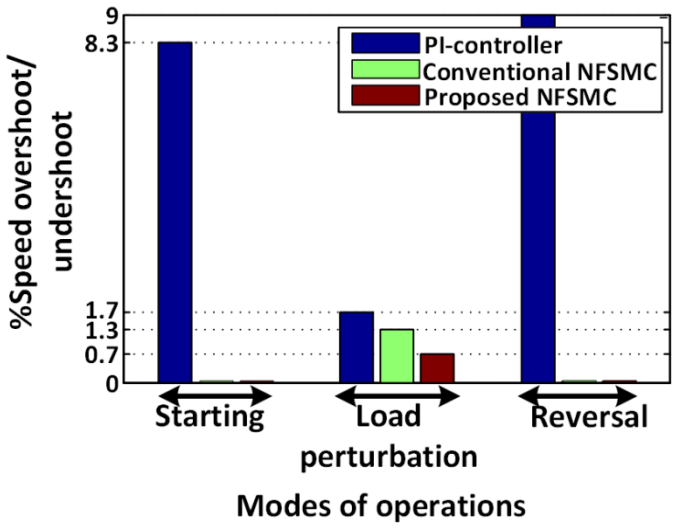

Fig. 5.11 Comparison of various controllers for FBL IM drive.

Fig. 5.11 shows the comparison of the performance of the proposed NFSMC based FBL IM drive with the conventional NFSMC and PI-controller based drive. The performance of the proposed simplified NFSMC in terms of speed and torque ripple with or without load, and % undershoot and overshoot of speed are observed to be superior compared to the conventional NFSMC and PI-controller.

Moreover, the proposed controller based FBL IM has less dip in capacitor voltage with less speed and torque distortion. Since sufficient evidences are provided from extensive simulation results in support of proposed NFSMC, the conventional NFSMC is not considered further from Fig. 5.12-5.16. Fig. 5.12 reveals that the rotor flux is steady with fast and perfect reference tracking throughout every operating mode regardless of the speed. From Fig. 5.12 (i) and Fig. 5.13, it is observed that the proposed low computational NFSMC establishes the perfect decoupling without compromising the system behavior. Instead, it exhibits superior performance compared to the classical PI-controller based drive. Fig. 5.14 demonstrates the circular flux trajectory evolution with respect to time which clearly exhibits the optimal variation of flux.

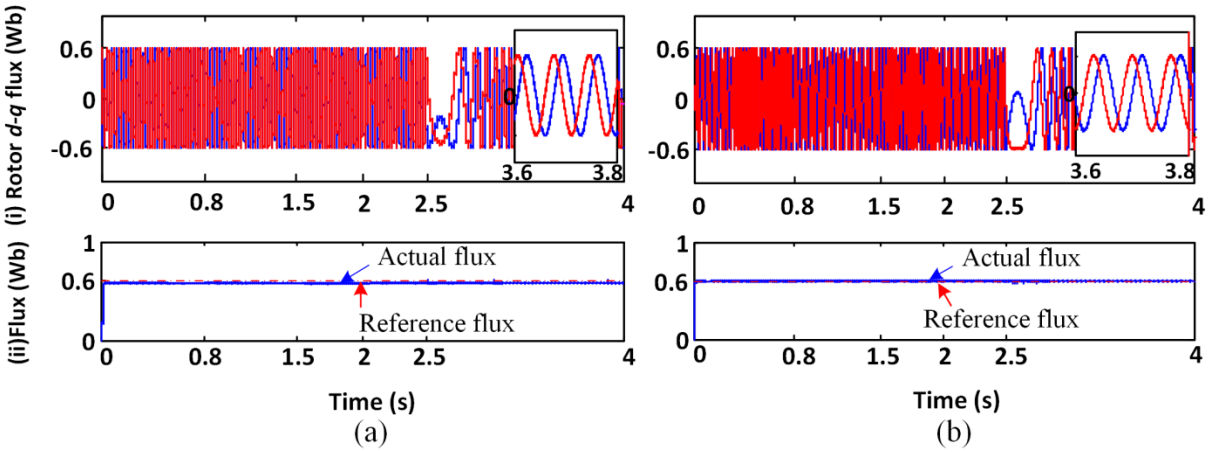

Fig. 5.12 Simulation responses (starting, 50% loading from 1.5 s to 2 s and reversal) of FBL IM drive using (a) PI-controller: (i) rotor *d-q* flux (ψ_{dqr}), (ii) flux, (b) proposed NFSMC: (i) ψ_{dqr}, (ii) flux.

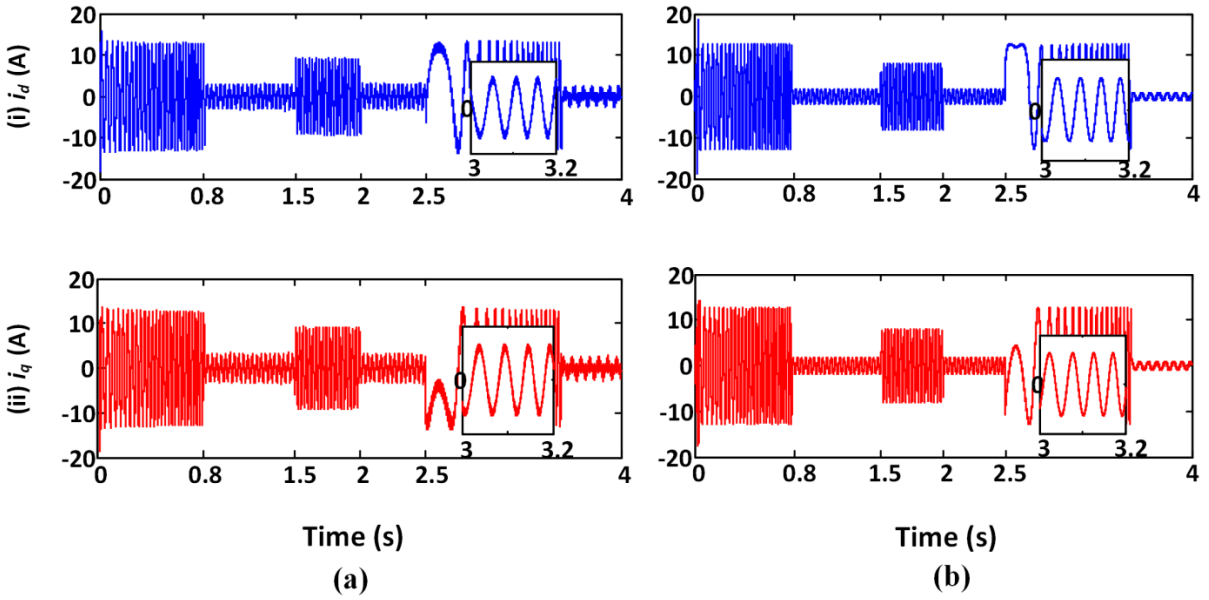

Fig. 5.13 Simulation responses (starting, 50% loading from 1.5s to 2 s and reversal) of FBL IM drive by (a) PI-controller: (i) i_d, (ii) i_q, (b) proposed NFSMC: (i) i_d, (ii) i_q.

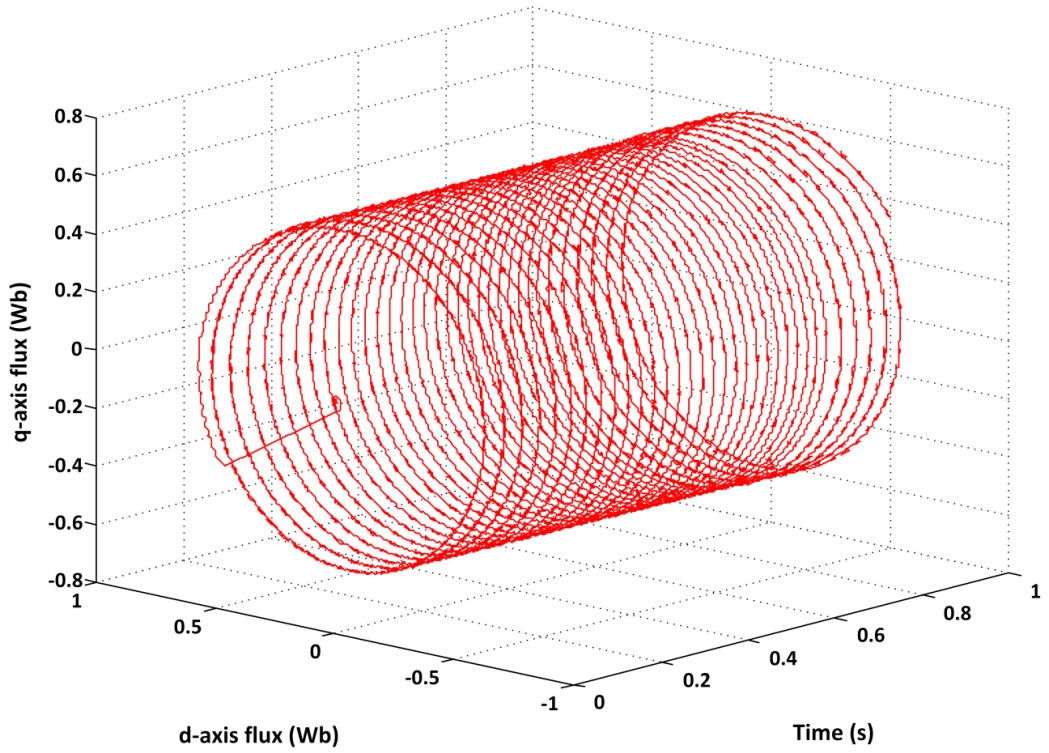

(a)

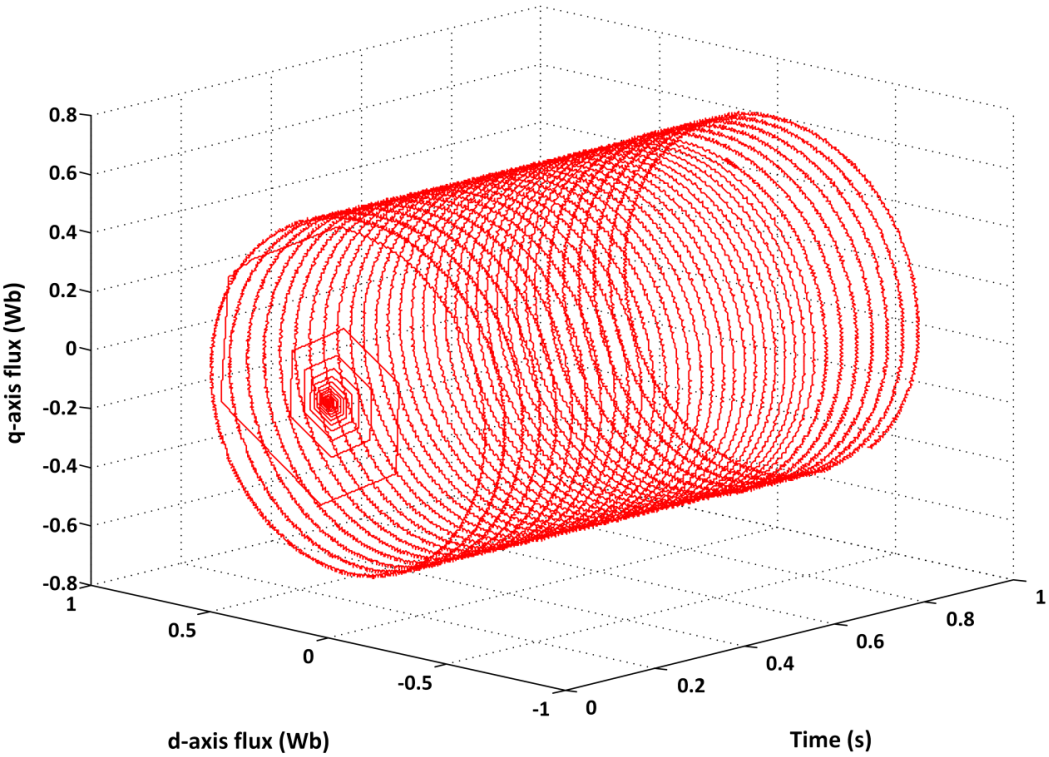

(b)

Fig. 5.14 Rotor flux linkage trajectory of FBL IM drive using (a) PI-controller and (b) proposed NFSMC.

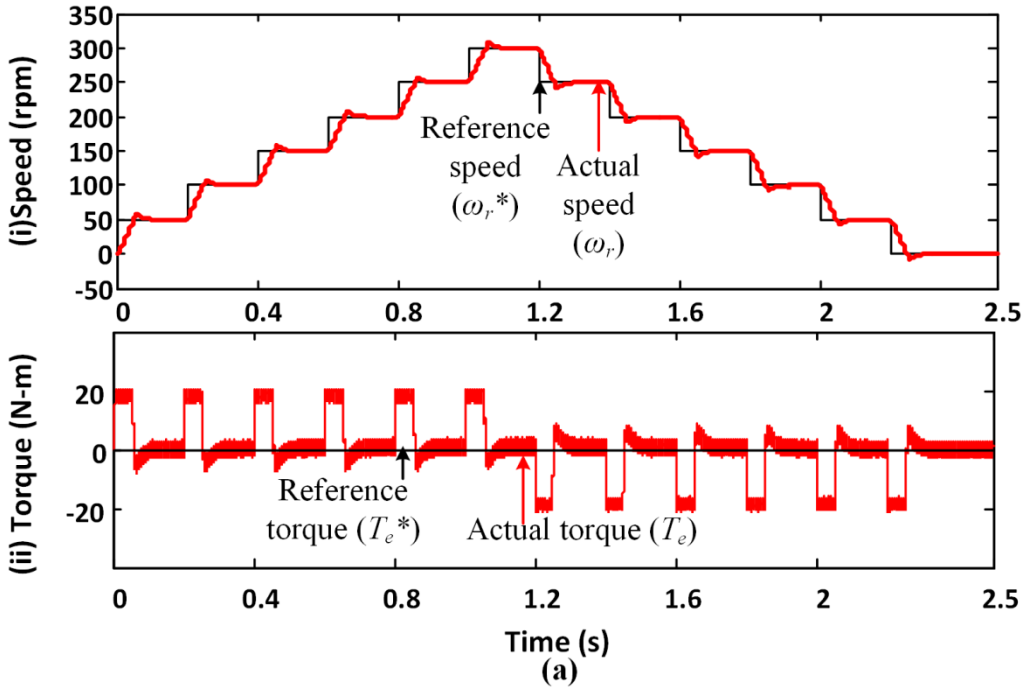

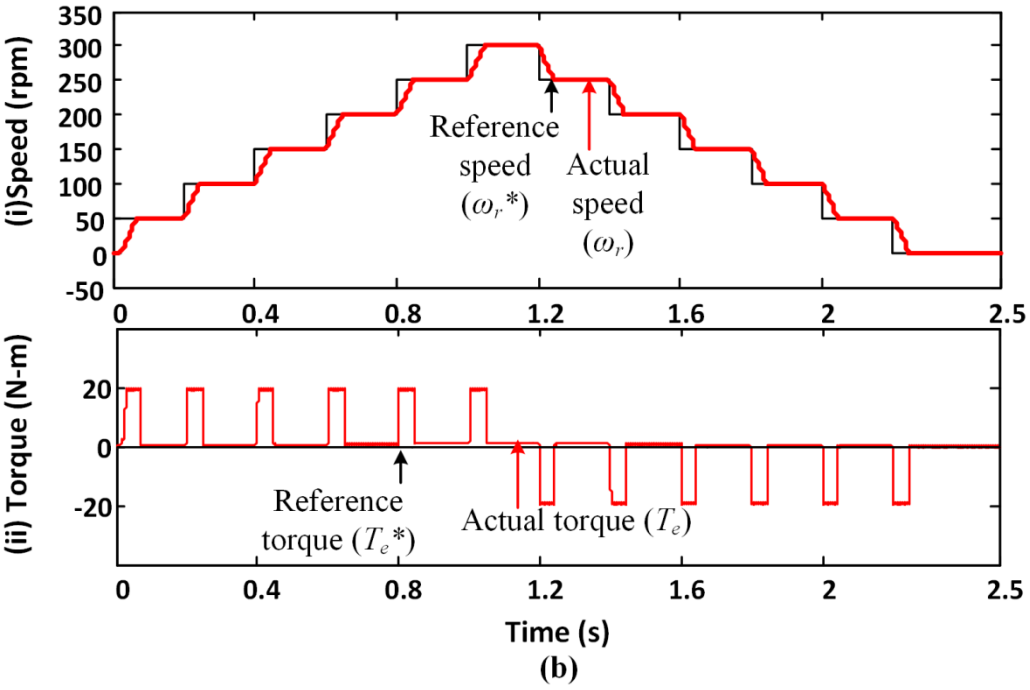

Fig. 5.15 Simulation responses of FBL IM drive under low-speed operation (from 3% to 20% of rated speed and vice versa in staircase form) using (a) PI-controller and (b) proposed NFSMC.

Case 4: Fig. 5.15 represents the low-speed operation of FBL IM drive with both controllers from 50 rpm (about 3% of rated speed) to 300 rpm (about 20% of rated speed) in staircase form and vice versa. It is observed that, unlike conventional PI-controller based FBL IM drive, the proposed NFSMC based drive demonstrates good speed response in terms of fast and good reference tracking and good torque response in terms of reduced ripples in transient as well as steady-state conditions.

Case 5: The robustness of the proposed NFSMC-based feedback linearization controller in the face of parameter variation is examined with the doubled rotor inertia and rotor resistance as shown in Fig. 5.16. The settling time response is almost doubled as the rotor inertia is doubled. The responses demonstrate the robustness of the proposed NFSMC compared to the PI-controller based drive.

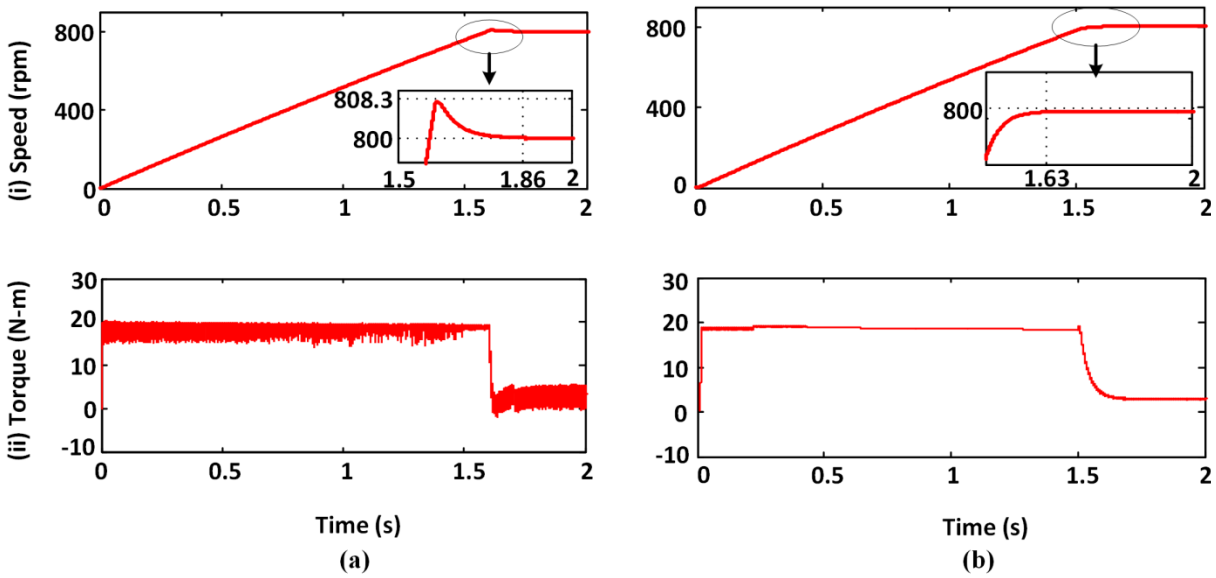

Fig. 5.16 Starting behavior of FBL IM drive with doubled rotor inertia and rotor resistance using (a) PI-controller: (i) speed (n_r), (ii) torque (T_e), (b) proposed NFSMC: (i) n_r (ii) T_e.

The power quality issue in terms of total harmonic distortion (THD) is one of the major challenges in inverter-fed IM drive. However, the total current harmonic distortion at 50% of load is observed to be 4.12% using the proposed NFSMC-based linearized drive, which is less compared to the conventional NFSMC and PI-controller based drive having THD of 8.28% and 20.47%, respectively. This shows the improved power quality in the proposed IM drive, and the results are evident from Fig. 5.17. The less THD in the NFSMC-based drive is

because of the fact that the sliding surface based optimized adapting rules tune the parameters of the NFC under load perturbation. The plots of current THD with respect to different loads using various controllers are demonstrated in Fig. 5.17. This shows that the current THD decreases as the load increases from no-load to full-load.

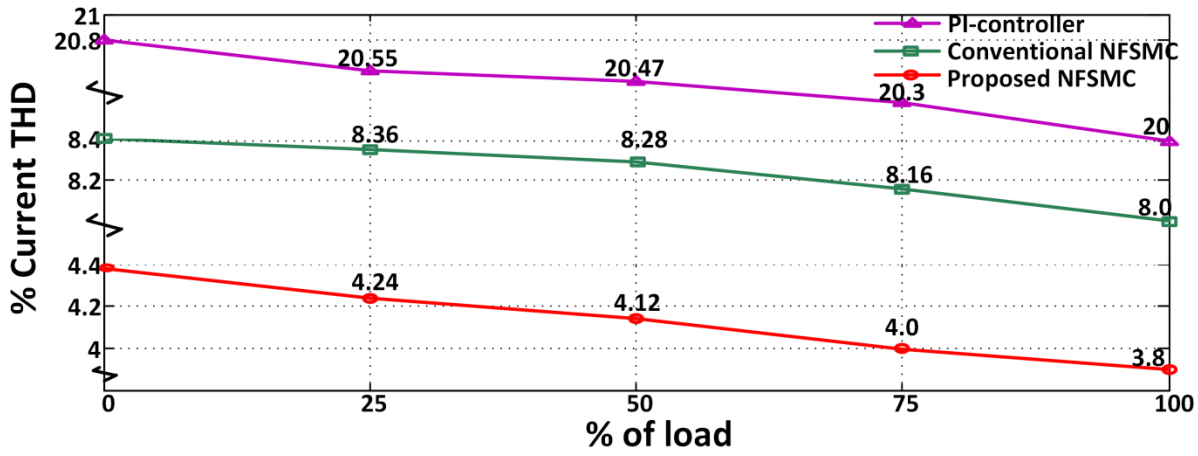

Fig. 5.17 Comparison of %THD vs. load of FBL IM for different controllers.

Table 5.1 Performance comparison of different controllers for FBL IM drive

Modes of operation	Parameters	PI-controller	Proposed NFSMC
Starting	% Speed overshoot	High	No overshoot
	Torque and speed ripple	Very high	Significantly reduced
	Settling time of speed	More	Less
	Stator current	More distorted	Distortion free
	Rotor flux	Decoupling in steady-state with good tracking	Perfect decoupling in both steady-state and transient state with better tracking
Load perturbation	% Speed overshoot	High	Small
	Torque and speed ripple	Very high	Significantly reduced
	Settling time of speed	More	Less
	Stator current	More distorted	Distortion free
	Rotor flux	Decoupling with good tracking	Perfect decoupling with better tracking
Reversal	% Speed overshoot	High	No overshoot
	Torque and speed ripple	Very high	Significantly reduced
	Settling time of speed	More	Less
	Rotor flux	Decoupling with good tracking	Perfect decoupling with better tracking
Low-speed	Torque ripple	Very high	Significantly reduced
	% Speed overshoot	High	No overshoot

It is summarized from the above table that the proposed simplified NFSMC-based FBL IM drive outperforms their counterpart in every respect in both dynamic as well as steady-state operation without compromising the decoupling behavior of the system.

5.6.1 Fuel cell Efficiency of the Simulated Model

As the relation between input chemical energy and output electrical energy is not properly defined, it is very difficult to obtain the energy relation with a fuel cell. However, the emf *E* of the hydrogen cell can be written as [132]

$$E = -\frac{\Delta \tilde{g}_f}{2F} \tag{5.32}$$

where $\Delta \tilde{g}_f$ is Gibb's free energy discharged and *F* is the Faraday constant.

If the hydrogen fuel cell chemical energy is converted to electrical energy form, then the emf is given by

$E = -\frac{\Delta \tilde{h}_f}{2F} = 1.25$ V relative to the low heating value (LHV) of the water.

where $\Delta \tilde{h}_f$ is the enthalpy of formation (calorific value).

The voltage above is considered to be reference voltage for that of a system with 100% efficiency. The nominal (actual) efficiency of the fuel cell stack is given by

$$\eta_{fc} = \frac{V_{cell}}{1.25} \times 100\% \text{ relative to the LHV.} \tag{5.33}$$

where V_{cell} is the actual operating voltage of the single cell.

So, for this simulated model used here,

$$\eta_{fc} = \frac{400/500}{1.25} \times 100\% = 64\%.$$

Here, 400 V is the total operating voltage of the fuel cell stack as obtained from polarization curve of Fig. 5.6 and 500 is the number of cells (*N*) in the fuel cell stack.

5.7 Experimental Setup

The proposed auto-tuned NFSMC-based feedback linearized IM drive system is validated in real-time using the 32-bit fixed point DSP TMS320F2812. The photograph of the prototype FBL IM drive experimental setup is shown in Fig. 5.18. Since only the experimental implementation of the simplified NFSMC algorithm is demonstrated, the control loop for switching the braking chopper is excluded and the FC stack with the converter is replaced by a constant DC source, which is input to the inverter. This DC is obtained from an autotransformer followed by a three-phase rectifier circuit. Hall-effect voltage sensor and current sensor sense the actual motor line voltages and currents, which are

fed to the DSP board through A/D channels. The hysteresis current controlled PWM signals are generated by the DSP board which are required to be fed to the switches of 3-phase voltage source inverter. In order to get the load perturbation for torque analysis, IM is coupled to a DC machine shaft. Then by introducing resistance on its armature circuit, the load torque is varied. Other than the current, all the variables of this test are observed through a D/A converter, and these are displayed on a digital oscilloscope.

The developed real-time Simulink model of the proposed NFSMC with the auto-tuning algorithm is compiled and dumped into DSP board using a JTAG emulator. The tuning rate of the weight η_{wi} and the tuning rate of the MFs (η_{ai}, η_{bi}) are set to 0.04 and 0.004, respectively. These are chosen to be very small by trial and error as it smoothens the transition. A PI-controller based linearized IM drive system is also validated experimentally in order to have a comparison. As the structure of the proposed NFSMC is simplified one, to conduct this operation, the lowest sampling time required is 150 μs, whereas it is 300 μs for the conventional NFSMC. In order to have a fair comparison with the proposed NFSMC, the PI controller tuning was done by using the conventional second-order single-variable linear system theory as it provides simple mathematical analysis approach [138]. The gains of the PI controllers are obtained by using SISO tool in MATLAB environment. Thus, the calculated values of K_p and K_i are 19.5 and 0.025, respectively for PI-speed controller, and 9.4 and 0.01 for PI-torque controller, respectively.

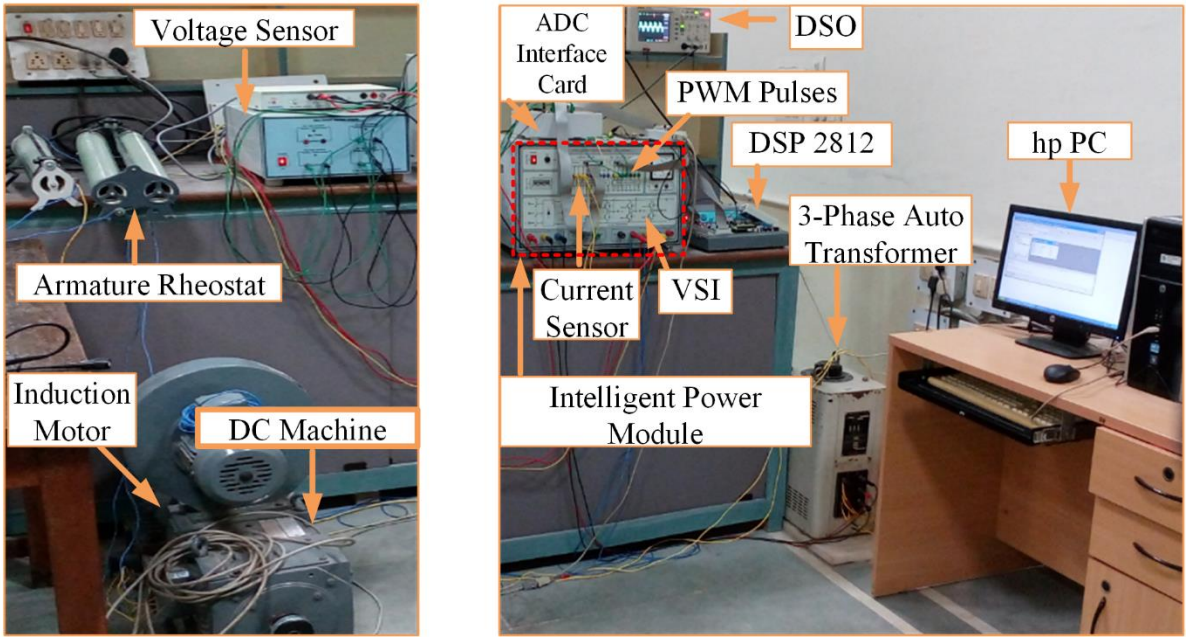

Fig. 5.18 Photograph of the experimental setup.

5.8 Experimental Results and Discussions

The efficacy of the proposed NFSMC based FBL IM drive is verified and compared in real-time platform as in Fig. 5.18 using DSP2812 under load perturbation of 10 N-m (50% of rated torque) by coupling a DC machine to an IM shaft. The waveforms are shown in Fig. 5.19, which reveals that the proposed simplified NFSMC based FBL drive shows superior dynamic response and reduced ripples as compared to the classical PI-controller based drive. Also, it has the advantage of significantly reduced computational burden, which was found to be 150 μs and suitable for industrial application. The details of the experimental performance are compared in Table 5.2.

While IM operates at a steady-state speed of 800 rpm, a sudden load of 10 N-m (T_l = 10 N-m) is applied and withdrawn at instants 1.5 s and 2 s, respectively as shown in Fig. 5.19 (a). This leads to a speed undershoot and overshoot of 1.8 rpm at the instants mentioned above and settles down at 1.84 s and 2.34 s, respectively using a PI-controller. The load perturbation makes the peak motor current to increase to 12.8 A at 1.51 s and decrease down at 2.01 s.

The proposed NFSMC-based feedback linearized IM drive preserves quick and robust response of conventional NFSMC based linearized IM drive. In addition, the less distorted stator current (19.6 A) improves the torque response by significantly reducing ripple by around 92% compared to the conventional PI-controller based drive as evident from Fig. 5.19 (ii) and (iii). Further, there is a good reduction of speed undershoot/overshoot by around 50% over PI-controller based drive during load perturbation as shown in Fig. 5.19 (i) and (ii). Further, the settling time of speed responses during load perturbations are 0.2 s using proposed simplified NFSMC, which is reduced by around 41% over PI-controller based drive. Since the stator current increases at 1.5 s, there is a sudden dip in DC link voltage (capacitor voltage) as shown in Fig. 5.19 (iii) and (vii). This is because of the discharging of the capacitor while motor draws large current due to the application of load. Similarly, the capacitor gets charged during removal of the load at 2 s, which is shown in Fig. 5.19 (vii). Nevertheless, the flux components remain constant with good reference tracking throughout the operation as shown in Fig. 5.19 (vi). The proposed low computational burdened NFSMC based FBL IM drive preserves the good features of the conventional PI-controller based IM drive without deteriorating the system behavior which is evident from Fig. 5.19 (iv) and (v).

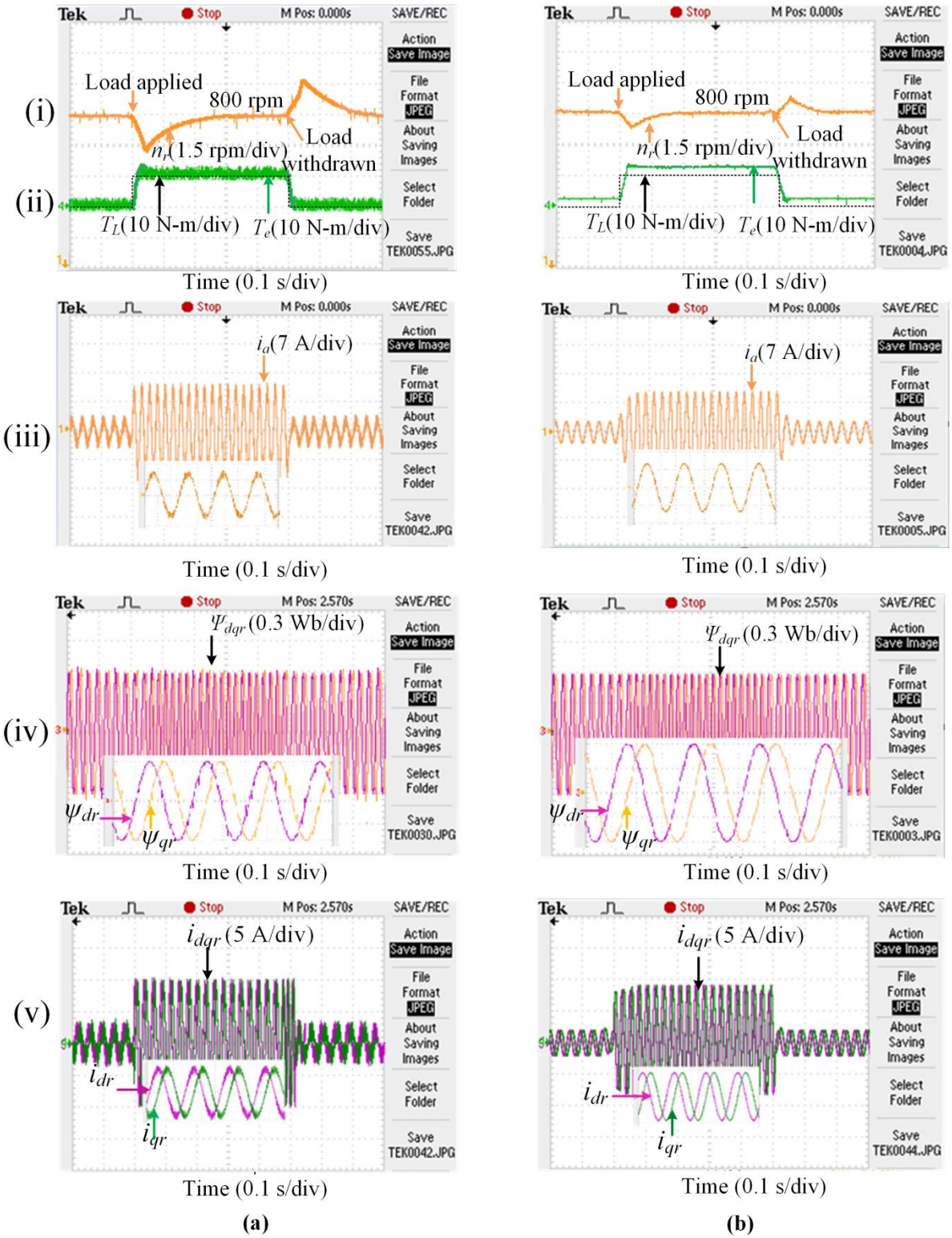

Fig. 5.19 Experimental waveforms with load perturbation of FBL IM drive for 50% step load from 1.5 s to 2 s using (a) PI-controller: (i) speed (n_r), (ii) torque (T_e) (iii) stator current (i_a), (iv) rotor *d-q* flux (ψ_{dqr}), (v) i_{dqr}, (vi) rotor flux, and (vii) DC link voltage (V_{dc}), (b) proposed simplified NFSMC: (i) n_r, (ii) T_e, (iii) i_a, (iv) ψ_{dqr}, (v) i_{dqr}, (vi) rotor flux, and (vii) V_{dc}.

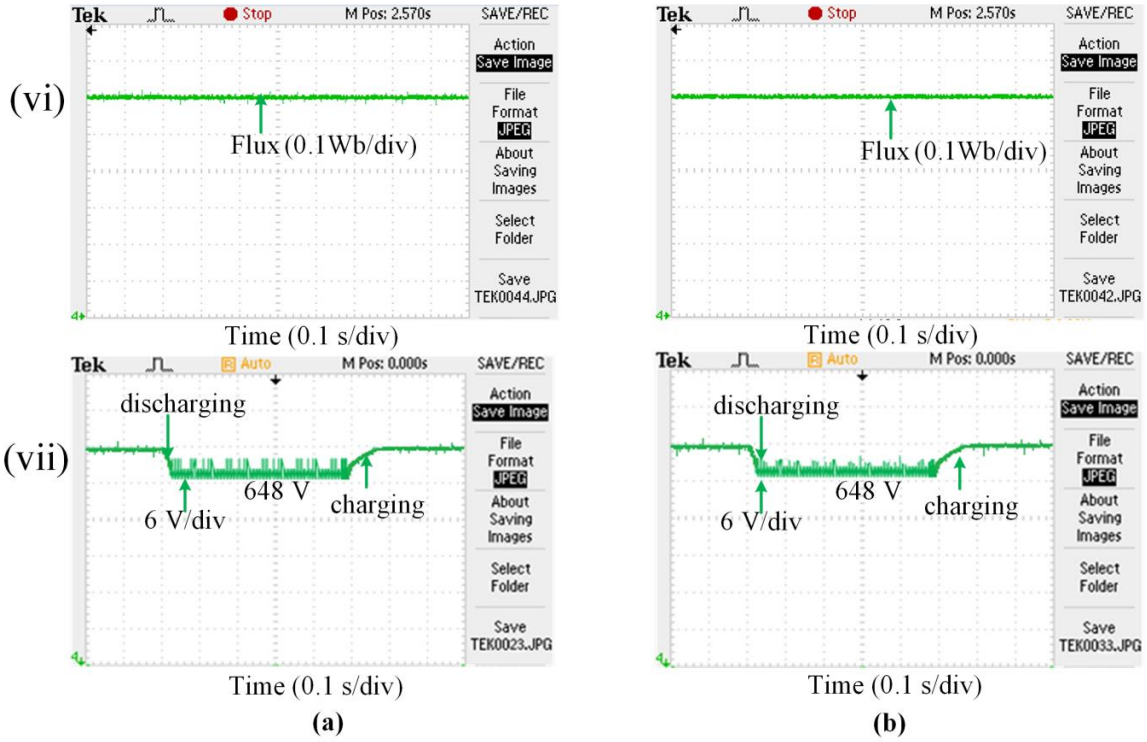

Fig. 5.19 (continued)

Further, the robustness of the FBL IM drive with the proposed simplified NFSMC is investigated by experiment through parameter variation and the responses are illustrated in Fig. 5.20. The rotor inertia is increased by coupling the existing motor with another motor, and it is observed that the rotor takes longer time to track the command value smoothly, unlike PI-controller as the inertia is doubled. In fact, the PI-controller shows an overshoot of 11.2 rpm before it reaches a steady-state speed.

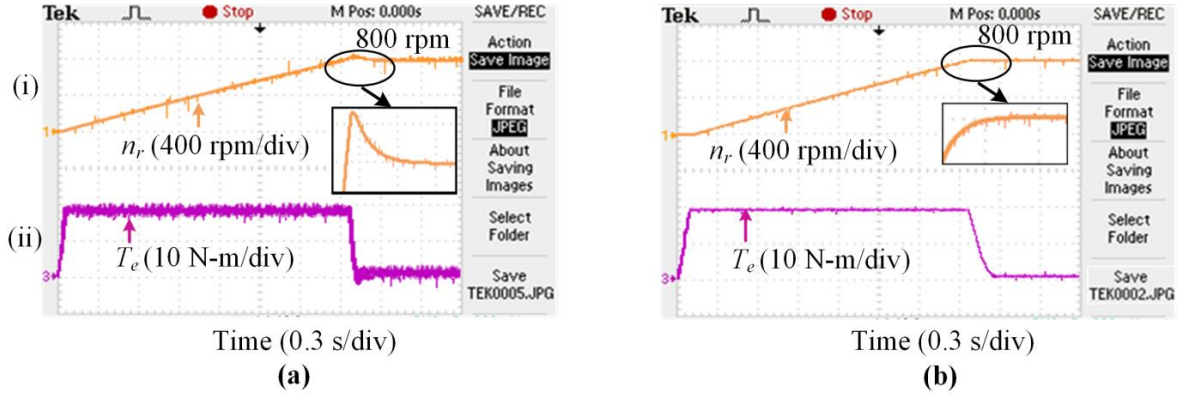

Fig. 5.20 Experimental starting responses of FBL IM drive with doubled rotor inertia using (a) PI-controller: (i) speed (n_r), (ii) torque (T_e), (b) proposed NFSMC: (i) n_r, (ii) T_e.

Table 5.2 Comparison of simulation and experimental performance

Controller	**% Speed undershoot and overshoot during 50% of rated load from 1.5 s to 2 s**		**Torque ripples (N-m)**		**Settling time (s)**		
					Different initiated time (s)	Simulation	Experiment
	Simulation	Experiment	Simulation	Experiment		$t_s(n_r)$	$t_s(n_r)$
PI-Controller	1.7	1.8	4.5	5	0	1.1	
					1.5	1.8	1.84
					2	2.3	2.34
					2.5	3.8	
Proposed NFSMC	**0.7**	**0.9**	**0.3**	**0.4**	**0**	**0.84**	
					1.5	**1.63**	**1.7**
					2	**2.13**	**2.2**
					2.5	**3.6**	

Table 5.2 shows the performance comparison of the proposed NFSMC based FBL IM drive with the conventional PI-controller-based drive. The slight discrepancy in experimental and simulation results are observed as certain constraints like dead band, fluctuation of temperature, hard switching effect, variation of supply, electromagnetic interference phenomena, etc., have not been considered in theoretical approach.

5.9 Robustness study and design of controller

This Section provides a design for the proposed controller that attains robustness and stability of the linearized drive system. The response of the closed-loop system under the deviation of the system parameter is investigated here and is depicted in Fig. 5.20 and Fig. 5.21. Here, the robust stability of the proposed controller-based drive scheme is given more priority than the dynamic response under the conditions of uncertainties that are encountered in the real-time practice. The constant motor parameter values are used here for FBL execution, and the controller used here is so designed that the system achieves robust stability as the parameter varies during the operation. On the other side, the impact of flux and torque error on FBL is not discussed here as the torque and flux observer provides fairly good results.

The control error signals due to the consideration of these uncertainties are symbolized as Δi_{ds}^{*} and Δi_{qs}^{*}. The equation (2.37) is used to estimate these errors in terms of parameter error and to analyze the impact of uncertainties on the NFSMC design. So (2.37) can be written as

$$i_s = i_{ds}^{\ *} + j i_{qs}^{\ *} = u_1 - \frac{u_2}{\psi_r} \tag{5.34}$$

Considering the equivalent error as Δu , (5.34) can be written as

$$i_s = \left(u_1 + \Delta u_1\right) - \frac{j}{\psi_r}\left(u_2 + \Delta u_2\right) \tag{5.35}$$

Using equations (5.34) and (5.35), the equivalent error Δu can be expressed as

$$\Delta u = \Delta u_1 + j\Delta u_2 = -\frac{u_2}{\psi_r} - j u_2 \tag{5.36}$$

Now using (5.36) and with the error $\left(u_1 - \Delta u_1\right)$ and $\left(u_2 - \Delta u_2\right)$, (2.34) and (2.35) can be written as

$$\frac{d\psi_r}{dt} = -\frac{R_r}{L_r}\psi_r + \frac{L_m R_r}{L_r}\left(u_1 + \frac{u_2}{\psi_r}\right) \tag{5.37}$$

$$\frac{d\omega_r}{dt} = -\frac{B}{J}\omega_r + \frac{1}{J}\frac{3}{2}\frac{L_m}{L_r}P 2u_2 - \frac{1}{J}T_l \tag{5.38}$$

However, no uncertainty is considered in u_2 as the NFSMC produces it. So, from (5.37), the rotor resistance R_r is the most dominant parameter subjected to variation as it changes with temperature. The proposed FBL has the advantage of not changing the rotor speed dynamics abruptly, but it affects the rotor flux dynamics, which is shown in Fig. 5.21. It shows that as the R_r increases, the rate of change of flux increases, i.e., it reaches the steady-state flux faster which is evident from (5.37). The maximum uncertainty of R_r considered here is 100%. Further, R_r uncertainty dynamic does not change the steady-state behavior, making the operation robust. The flux dynamic behavior of the proposed one is faster under uncertainty of R_r compared to both the conventional NFSMC and PI-controller as shown in Fig. 5.21.

Again, the change in rotor flux dynamics due to change in R_r has an impact on the estimated speed, which in fact, determines the value of corrective switching control gain $\beta_{\omega r}$ of SMC. Thus, the change in speed equation from (2.35) to (5.39) is as follows.

$$\frac{d\omega_r}{dt} = -\frac{B}{J}\left(\omega_{rest} - \omega_r\right) + \frac{1}{J}\frac{3}{2}\frac{L_m}{L_r}P u_2 - \frac{1}{J}T_l \tag{5.39}$$

The switching control gain can ensure the robust performance if the maximum estimation error of speed is known. Therefore, by assuming maximum speed estimation error of 10

rad/s, we get $\left|\frac{B}{J}\left(\omega_{rest}-\omega_r\right)\right|<2.1$, which determines $K_{\omega r}$ to be 2.1 and $\beta_{\omega r} = K_{\omega r} + \eta_{\omega r} = 12.1$. Here, $\eta_{\omega r}$ is considered to be 10 in this context in order to have a realistic speed dynamic response and $\frac{B}{J}=0.21$ as per the values of B and J given in the Appendix A.1. In our experiment, the $\beta_{\omega r}$ is chosen to be 15 (>12.1), which gives even good result at the expense of large errors.

Equation (5.38) reveals that the change in rotor inertia J has a substantial impact on speed dynamics as the rate of change of speed is inversely proportional to the J. It means that the rotor takes a longer time to be settled at target speed. Fig. 5.20 illustrates that with the proposed NFC the motor can track the target speed smoothly unlike PI-controller-based drive, but the settling time response is almost twice as the rotor inertia is doubled.

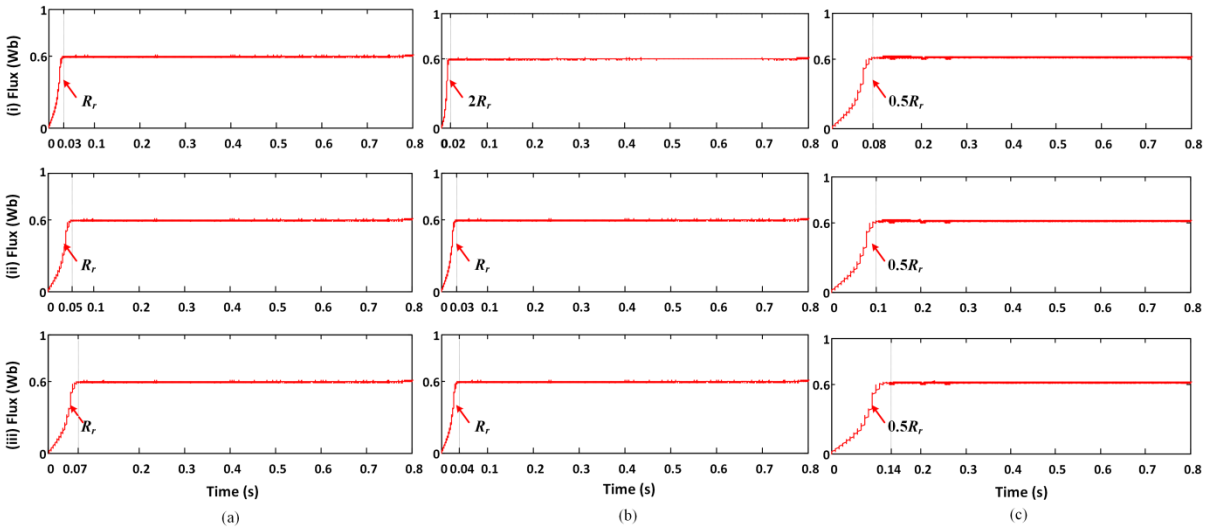

Fig. 5.21 Flux responses during starting of FBL IM drive with (i) proposed NFSMC: (a) R_r, (b) uncertainties of +100% R_r, (c) uncertainties of -50% R_r, (ii) conventional NFSMC: (a) R_r, (b) uncertainties of +100% R_r, (c) uncertainties of -50% R_r, (iii) PI-controller: (a) R_r, (b) uncertainties of +100% R_r, (c) uncertainties of -50% R_r.

5.10 Conclusion

The design approach which incorporates simplified NFSMC with the fuel cell back-up supply system based FBL IM drive is articulated in this Chapter. The fuel cell system interfaced with the VSI fed FBL IM drive is used for a stand-alone application during disruption of supply and thereby, making the system more reliable. A systematic control algorithm is developed and stepwise procedure is illustrated for auto-tuning of the proposed

NFSMC. The overall drive system is designed and modeled in MATLAB software, and the proposed controller is experimentally investigated in real-time prototype hardware setup using low cost, high computational power DSP TMS320F2812 processor.

An experimental analysis has been conducted for the proposed IM control algorithm, and the results authenticate the potentiality of the proposed NFSMC algorithm. The proposed simplified NFSMC based FBL IM drive preserves quick and robust response of conventional NFSMC based drive. In addition, the proposed control algorithm has the benefit of considerably reduced computational burden due to low computational complexity. Thus, the proposed technique can be implemented in IM drive control applications with small execution time. Further, the proposed algorithm can also be implemented in motors of different sizes only by adjusting the tuning rates online. Moreover, it is evident from the comparative analysis data that the proposed simplified NFSMC outperforms their counterparts with regard to dynamic as well as steady-state response. The proposed controller has faster flux dynamic response under uncertainty of rotor resistance compared to both the conventional NFSMC and PI-controller. Also, the steady-state flux responses all through these operations are maintained almost constant with good reference tracking and with perfect decoupling. Thus, this robust performance of simplified NFSMC is found to be suitable for a realistic situation like high-performance industrial drive, robotics system, etc., where the control is more accurate in spite of parametric uncertainties and load perturbations.

Chapter 6

CONCLUSIONS AND FUTURE SCOPE

CHAPTER 6

CONCLUSIONS AND FUTURE SCOPE

6.1 General

Induction motor (IM) drives have been tremendously evolving as a focused area of investigation work. The implementation of field oriented control in IM drive has remarkable impact on industrial applications. The progressive advance in the technology of DSP processor makes it easy for applying advance control techniques like feedback linearization control (FBL), variable structure control, adaptive control, and emerging control like fuzzy logic, neural network, neuro-fuzzy control in the domain of power electronics and drives. It has been seen in the course of the literature review that the aforementioned control techniques are used to enhance the performance of the drive system. So, this research work is focused on the development and implementation of robust adaptive hybrid intelligent techniques and its comparison with the conventional controllers in order to have a comparative analysis of performance. This comparative study of some controllers for the linearized IM drive may be helpful for selecting the proper drive system for different applications. This Chapter summarizes various aspects of design and implementation of controllers for a voltage source inverter (VSI) fed linearized IM drive. A possible scope for future research is also outlined here.

6.2 Conclusion

The current research topic is mainly focused on study, development, and implementation of some advance controllers and their comparative performance analysis in order to assess properly the controllers for the IM drive performance and its better utilization. The assessments of the work are summarized as follows:

- Initially, a systematic and comprehensive nonlinear mathematical model of the IM drive is developed in stationary reference frame with stator current, rotor flux components, and rotor speed as state variables. The control techniques of linear system are not applied directly to the IM drive and alternative methods have been introduced by transforming the nonlinear system to linear using linearization technique.

- The dynamic state feedback linearization concept [27] has been used for decoupling feedback linearization control of the IM drive in the stationary reference frame. With this control approach, the IM drive model has been divided into two linear decoupled Electrical and Mechanical subsystems
- First of all, systematic procedure is developed to design and tune PI controllers for both the subsystems. Over a large range of operation, the system provides satisfactory performance using the PI-controller. However, under various disturbance cases like sudden change in speed and load torque, the PI-controller performance may not be satisfactory. Moreover, the controller configuration requires exact mathematical model, and constant tuning of controller gains to accomplish high performance drive system.
- To overcome the demerits of parameter variations, a robust adaptive control strategy based on hybrid smart control technique is used to enhance the performance of the linearized IM drive system further even at various disturbances. The development and implementation of an adaptive neuro-fuzzy inference system (ANFIS) based controller are presented to enhance the performance, and disturbance rejection of the feedback linearized IM drive system. A comprehensive and systematic tuning algorithm of the ANFIS controller is developed for the mechanical subsystem. A simple sensorless flux and torque estimator has been developed and used here purposely to test the controller robustness.
- The proposed FBL IM drive system is designed and modeled in the MATLAB/SIMULINK environment and is experimentally investigated in the real-time hardware setup using DSP TMS320F2812 processor. The robust performance and fast response with considerably low torque ripple compared to the PI-torque controller are demonstrated by using ANFIS controller incorporated with the FBL IM drive. The robustness of ANFIS scheme isalso tested experimentally by taking different gain values of the PI-speed controller. Some noticeable features of the ANFIS controller are observed from the comparative study which may be beneficial for implementation in high precision drive applications.
- Despite satisfactory performances of this intelligent controller, many industries have been still reluctant to implement these controllers for commercial drive because of high computational burden. Low sampling frequency due to this high computational burden is not sufficient for real-time applications. Thus, a simple

modified neuro-fuzzy controller (NFC) method with a decoupled FBL approach of IM model is presented.

- The design of the self-tuned simplified NFC as implemented on the feedback linearized drive has been given here in order to overcome the aforesaid problem. The proposed NFC-based FBLIM drive system is developed and experimentally implemented to show its potentiality in the real-time applications.
- It is concluded from the results that the performance of the proposed simplified NFC bears a resemblance to that of the conventional one, but it has the main benefit of considerably reduced computational burden.
- The comparative study shows that the system response using proposed NFC does not deteriorate compared to the conventional NFC. Simultaneously, it shows superiortransient and steady-state performance compared to PI-controller. Thus, the proposed controller is suitable for high-performance drive for industrial applications.
- There are some performances of the linearized drive system which need to be improved further. Thus, a hybrid intelligent technique is developed using the concept of sliding surface-based adapting rules that update parameters of the simplified NFC. This hybrid control system is known as simplified neuro-fuzzy sliding-mode control (NFSMC) technique.
- Further, the performance of the drive system is investigated in parallel by integrating fuel cell-energy storage system with the NFSMC-based FBL IM drive system. This has the main advantage for stand-alone application of the drive system during voltage disruption and outages and thereby, making the system more reliable.
- The simulation results are shown and a comparative study is carried out with the conventional NFSMC for the FBL IM drive system. As the NFC in the proposed NFSMC is simplified one, this has the main advantage of reduced computational burden compared to conventional one, which is the major concern of the industry. Moreover, the proposed simplified NFSMC outperforms its counterparts in both dynamic as well as steady-state response. Further, in the lower speed zone and staircase type speed changes, unlike PI-controller, the proposed NFSMC-based drive performs well in terms of first and good reference tracking with reduced torque chattering in both dynamic and steady-state conditions. Thus, this robust

performance of the simplified NFSMC is found to be suitable for real-time applications as follows:

- As a torque and speed regulator, it is implemented in high-performance industrial drive applications where the control is more accurate in spite of parametric uncertainties and load perturbations.
- Further, torque ripple is one of the major factor for the industrial drive as large ripple leads to acoustic noise, torsional oscillations, etc., that may lead to damage of the motor shaft. Therefore, the proposed low computationally burdened simplified NFSMC may be suitable for the real-time industrial purpose as the torque ripple is drastically reduced.

- The experimental hardware setup is developed in the laboratory and used to implement all proposed control schemes mentioned above. Extensive results are provided and compared with the simulated responses in order to establish the superiority of the control algorithms. The real-time results clearly validated the proposed scheme with certain restrictions due to noise, parameter variations, nonlinearity behavior of inverter, and saturation in voltages. Also, there are slight deviations between simulated and experimental results due to some constraints like dead band, fluctuation of temperature, hard switching effect, variation of supply, electromagnetic interference phenomena, etc., which have not been considered in theoretical approach.

6.3 Limitations and Scope for Future Work

The design, development, and implementation of some controllers for induction motor drive and their comparative performance analysis are successfully carried out in the present research work. But, there is no end of research. A number of possible investigations may be undertaken as a future work of this research topic to update and enhance the drive system further.

1. Since sensitivity of parameters is major constraint of IM drive, parameter adaptation method can be used for state feedback linearization control approach in order to achieve good dynamic response.
2. Modeling and design of model reference adaptive system (MRAS) based sensorless linearized IM drive with different adaptation mechanism.

3. Some other advanced artificial intelligence method with the proposed method can be incorporated as an extension work of this thesis for the optimal performance of IM drive.
4. Further, this research work can be extended in future by implementing different training methods like recursive least square and extended Kalman filter methods for simplified NFC as well as simplified type-2 NFC.
5. Still, there is a scope for improving the performance of linearized IM drive with regard to chattering reduction by using second-order sliding-mode scheme and its combination with simplified NFC as an intelligent hybrid controller.
6. The present work can be extended in terms of power quality improvement at supply system for the IM drive by using different types of power filters such as active, passive, and hybrid power filters.
7. The model predictive approach can be used with the FBL IM drive to improve the performance and power quality of IM drive system.
8. Since the present work is based on balanced IM drive system, the validity of this research work can also be performed under unbalanced or faulty condition of IM drive.
9. The proposed method can also be integrated with the different renewable energy systems to expand its applications.

REFERENCES

[1] W. Leonhard, "Microcomputer control of high dynamic performance as drives – a survey," *Automatica*, vol. 22, no.1, pp.1-19, 1986.

[2] J. J. E. Slotine and W. Li, *Applied Nonlinear Control,* Prentice Hall, Englewood Cliffs, NJ, 1991.

[3] S. Lekhchine, T. Bahi, I. Abadlia, H. Bouzeria, "PV-battery energy storage system operating of asynchronous motor driven by using fuzzy sliding mode control," *International journal of hydrogen energy*, vol. 42, no. 13, pp. 8756-8764, Mar. 2017.

[4] B. K. Bose, *Modern Power Electronics and AC Drives*, Prentice Hall Of India, New Delhi, 2008.

[5] F. Blaschke, "The principle of field orientation as applied to the new transvector closed-loop control system for rotating-field machines," *Siemens review*, vol. 34, no. 3, pp. 217-220, May 1972.

[6] G. S. Kim, I. J. Ha, and M. S. Ko, "Control of induction motors for both high dynamic performance and high power efficiency," *IEEE Trans. Industrial Electronics*, vol. 39, no. 4, pp. 323-333, Aug. 1992

[7] D. I. Kim, I. J. Ha, and M. S. Ko, "Control of induction motors via feedback linearization with input-output decoupling," *Int. Journal of Control*, vol. 51, no. 4, pp. 863-883, 1990.

[8] Y. R. Kim, S. K. Saul, and M. H. Park, "Speed sensorless vector control of induction motor using extended Kalman filter," *IEEE Trans. Industry Applications*., vol. 30, no. 5, pp. 1225-1233, Sep./Oct. 1994.

[9] A. Isidori, A. J. Krener, C. Gori-Giorgi, and S. Monaco, "Nonlinear decoupling via feedback: A differential-geometric approach," *IEEE Trans. Automatic Control*, vol. 26, no. 2, pp. 331-345, April 1981.

[10] Z. Krezminski, "Nonlinear control of induction motor," in *Proc.10th IFAC World Congress on Automatic Control,* vol. 3, Munich, Germany, 1987, pp. 357-362.

[11] G. Luckjiff, I. Wallace, and D. Divan, "Feedback linearization of current regulated induction motors," in *Proc. IEEE 32nd Annual Power Electronics Specialists Conference*, Vancouver, Canada, June 2001, pp. 1173-1178.

[12] Z. Zhang, R. Tang, B. Bai, and D. Xie, “Novel direct torque control based on space vector modulation with adaptive stator flux observer for induction motors,” *IEEE Trans. Magnetics*, vol. 46, no. 8, pp. 3133-3136, June 2010.

[13] F. Alonge, M. Cirrincione, M. Pucci, and A. Sferlazza, “Input-output feedback linearization control with on-line MRAS-based inductor resistance estimation of linear induction motors including the dynamic end effects,” *IEEE Trans. Industry Applications*, vol. 52, pp. 254–266, Jan./Feb. 2016.

[14] C. Lascu, I. Boldea, and F. Blaabjerg, “Variable-structure direct torque control – A class of fast and robust controllers for induction machine drives,” *IEEE Trans. Industrial Electronics*, vol. 51, no. 4, pp. 785-792, Aug. 2004.

[15] A. Isidori and J. W. Grizzle, “Fixed modes and nonlinear noninteracting control with stability,” *IEEE Trans. Automatic Control*, vol. 33, no. 10, pp. 907-913, Nov. 1988.

[16] A. Isidori and C. I. Byrnes, “Output regulation of nonlinear systems,” *IEEE Trans. Automatic Control*, vol. 35, no. 2, pp. 131-140, Feb. 1990.

[17] C. I. Byrnes and A. Isidori, “Asymptotic stabilization of minimum phase nonlinear systems,” IEEE *Trans. Automatic Control*, vol. 36, no. 10, pp. 1122-1137, Oct. 1991.

[18] Z. Krezminski, “Nonlinear control of induction motor,” in *Proc. 10th IFAC World Congress on Automatic Control*, vol. 3, Munich, Germany, 1987, pp. 349-354.

[19] A. De Luca and G. Ulivi, “Design of exact nonlinear controller for induction motors,” *IEEE Trans. Automatic Control*, vol. 34, no. 12, pp. 1304-1307, Dec. 1989.

[20] A. De Luca and G. Ulivi, “Dynamic decoupling of voltage frequency controlled induction motors,” in *Analysis and Optimization of Systems, Lecture Notes in Control and Information Sciences*, vol. 111, Springer, Berlin, Heidelberg, 1988.

[21] R. Marino, S. Peresada, and P. Valigi, “Adaptive partial feedback linearization of induction motor,” in *Proc. 29th Conf. Decision and Control*, Honolulu, USA, Dec. 1990, pp. 3313-3318.

[22] R. Marino, S. Peresada, and P. Valigi, “Nonlinear control of induction motors: a simulation study,” in *Proc. European Control conference*, Grenoble, France, Jul. 1991, pp. 1057-1062.

[23] R. Marino, S. Peresada, and P. Valigi, “Adaptive input-output linearizing control of induction motors,” *IEEE Trans. Automatic Control*, vol. 38, no. 2, pp. 208-221, Feb. 1993.

[24] R. Marino and P. Tomei, "Global adaptive output-feedback control of nonlinear systems, part1: Linear parameterization," *IEEE Trans. Automatic Control*, vol. 38, no.1, pp. 18-32, Jan. 1993.

[25] R. Marino and P. Tomei, "An adaptive output feedback control for a class of nonlinear systems with time varying parameters," *IEEE Trans. Automatic Control*, vol. 44, no. 11, pp. 2190-2194, Nov. 1999.

[26] R. Marino, S. Peresada, and P. Tomei, "Output feedback control of current-fed induction motors with unknown rotor resistance," *IEEE Trans. Control Systems Technology*, vol.4, no. 4, pp. 336-346, July 1996.

[27] S. Liuzzo, R. Marino, and P. Tomei, "Adaptive learning control of nonlinear systems by output error feedback," *IEEE Trans. Automatic Control*, vol. 52, no. 7, July 2007.

[28] J. Chiasson, A. Chaudhari, and M. Bodoson, "Nonlinear controllers for the induction motor," *in Proc. IFAC Nonlinear Control System Design Symp.*, Bordeaux, France, June 1992, pp. 150-155.

[29] J. Chiasson, "Dynamic feedback linearization of the induction motor," *IEEE Trans. Automatic Control*, vol. 38, no. 10, pp. 1588-1594, Oct. 1993.

[30] J. Chiasson, "A new approach to dynamic feedback linearization control of an induction motor," *IEEE Trans. Automatic Control*, vol. 43, no. 3, pp. 391-397, Mar. 1998.

[31] R. Ortega and G. Espinosa, "A controller design methodology for systems with physical structures: applications to induction motors," in *Proc. 30th Conf. Decision and Control*, Brighton, England, Dec. 1991, pp. 2345-2349.

[32] R. Ortega, C. Canudas, and S. I. Seleme, "Nonlinear control of induction motors: torque tracking with unknown load disturbances," *IEEE Trans. Automatic Control*, vol. 38, no. 11, pp. 1675-1680, Nov. 1993.

[33] C. C. Chan, W. S. Leung, and C. W. Ng, "Adaptive decoupling control of induction motor drives," *IEEE Trans. Industrial Electronics* , vol. 35, no. 1, pp. 41-47, Feb. 1990.

[34] K. B. Mohanty and N. K. De, "Nonlinear controller for induction motor drive," in *Proc. IEEE Int. Conf. on Industrial Technology* (*ICIT*), Goa, Jan. 2000, pp. 382-387.

[35] A. De Luca and G. Ulivi, "Full linearization of induction motors via nonlinear state-feedback," in *Proc. 26th Conf. Decision and Control*, Los Angeles, California, USA, Dec. 1987, pp. 1765-1770.

[36] B. Charlet, J. Levine, and R. Marino, “Two sufficient conditions for dynamic feedback linearization,” in *Analysis and Optimization of Systems*, Lecture Notes in Control and Information Sciences, vol. 111, 1988.

[37] X. Chaoying and G. Haiyu, “Feedback linearization control approach for brushless doubly-fed machine,” *International Journal of Precision Engineering and Manufacturing* (*Springer*), vol. 16, no. 8, pp. 1699-1709, 2015.

[38] M. Illic Spong, R. Marino, S. M. Peresada, and D. G. Taylor, “Feedback linearizing control of switched reluctance motors,” *IEEE Trans. Automatic Control*, vol. 32, no. 5, pp. 371-379, May 1987.

[39] Y. S. Choi, H. H. Choi, and J. W. Jung, “Feedback linearization direct torque control with reduced torque and flux ripples for IPMSM drives,” *IEEE Trans. Power Electronics*, vol. 31, no. 5, pp. 3728-3737, May 2016.

[40] K. H. Kim, Y. C. Jeung, D. C. Lee, and H. G. Kim, “LVRT scheme of PMSG wind power system based on feedback linearization,” *IEEE Trans. Power Electronics*, vol. 27, no. 5, pp. 2376-2384, May 2012.

[41] X. Bao, F. Zhuo, Y. Tian, and P. Tan, “Simplified feedback linearization control of three-phase photovoltaic inverter with an LCL filter,” *IEEE Trans. Power Electronics*, vol. 23, no. 3, pp. 2739-2752, June 2013.

[42] P. Liutanakul, S. Pierfederici, and F. M. Tabar, “Application of SMC with I/O feedback linearization to the control of the cascade controlled rectifier/inverter-motor drive system with small dc link capacitor,” *IEEE Trans. Power Electronics*, vol. 23, no. 5, pp. 2489-2499, Oct. 2008.

[43] H. A. Zarchi, J. Soltani, and G. A. Markadeh, “Adaptive input-output feedback-linearization-based torque control of synchronous reluctance motor without mechanical sensor,” *IEEE Trans. Industrial. Electronics*, vol. 57, no. 1, pp. 375-384, Jan. 2010.

[44] D. E. Kim and D. C. Lee, “Feedback linearization control of three-phase UPS inverter systems,” *IEEE Trans. Industrial Electronics*, vol. 57, no. 3, pp. 963-968, Mar. 2010.

[45] J. Matas, M. Castilla, J. M. Guerrero, L. G. de Vicuña, and J. Miret, “Feedback linearization of direct drive synchronous wind turbines via a sliding mode approach,” *IEEE Trans. Power Electronics*, vol. 23, no. 3, pp. 1093-1103, May 2008.

[46] J. Matas, L. G. de Vicuña, J. Miret, J. M. Guerrero, M. Castilla, “Feedback linearization of a single-phase active power filter via sliding mode control,” *IEEE Trans. Power Electronics*, vol. 23, no. 1, pp. 116-125, Jan. 2008.

[47] G. W. Chang, G. Espinosa-Perez, E. Mendes, and R. Ortega, “Tuning rules for the PI gains of field-oriented controllers of induction motors,” *IEEE Trans. Industrial Electronics*, vol. 47, no. 3, pp. 592–602, Jun. 2000.

[48] M. N. Uddin, T. S. Radwan, and M. A. Rahman, “Performances of fuzzy-logic-based indirect vector control for induction motor drive,” *IEEE Trans. Industry Applications*, vol. 38, no. 5, pp. 1219-1225, Sep./Oct. 2002.

[49] E. C. Shin, T. S. Park, W. H. Oh, and J. Y. Yoo, “A design method of PI controller for an induction motor with parameter variation,” in *Proc. IEEE IECON*, Roanake, USA, vol. 1, Nov. 2003, pp. 408–413.

[50] A. Miloudi and A. Draou, “Variable gain PI controller design for speed control and rotor resistance estimation of an indirect vector controlled induction machine drive,” in *Proc. IEEE IECON*, Sevilla, Spain, vol. 1, Nov. 2002, pp. 323–328.

[51] R. Krishnan and A. S. Bharadwaj, “A review of parameter sensitivity and adaptation in indirect vector controlled induction motor drive systems,” *IEEE Trans. Power Electronics*, vol. 6, no. 4, pp. 695–703, Oct. 1991.

[52] T. K. Boukas and T. G. Habetler, “High-performance induction motor speed control using exact feedback linearization with state and state derivative feedback,” *IEEE Trans. Power Electronics*, vol. 19, no. 4, pp. 1022-1028, July 2004.

[53] R. J. Wai, “Adaptive sliding-mode control for induction servomotor drives,” *IEE Proc. Electric Power Applications*, vol. 147, no. 6, pp. 553–562, Nov. 2000.

[54] L. Fan & L. Zhang, “Fuzzy based flatness control of an induction motor,” *Journal of Power Electronic and Engineering Application*, vol. 23, pp. 72–76, 2011.

[55] B. Dandil, “Fuzzy neural network IP controller for robust position control of induction motor drive” *Expert Systems with Applications*, vol. 36, no. 3, pp. 4528–4534, Apr. 2009.

[56] H. A. Yousef and M. A. Wahba, “Aptive fuzzy MIMO control of induction motors,” *Expert Systems with Applications*, vol. 36, no. 3, pp. 4171–4175, Apr. 2009.

[57] R. J. Wai, R. Y. Duan, W. K. Liu, and S. P. Yu, “Nonlinear decoupled control for linear induction motor servo drive,” in *Proc. IEEE IECON*, vol. 1, Feb. 2001, pp. 1635-1640.

[58] C. Lascu, S. Jafarzadeh, S. Fadali, and F. Blaabjerg, “Direct torque control with feedback linearization for induction motor drives,” *IEEE Trans. Power Electronics*, vol. 32, no. 3, pp. 2072-2080, Mar. 2017.

[59] S. D. Swain, P. K. Ray, and K. B. Mohanty, “Improvement of power quality using a robust hybrid series active power filter,” *IEEE Trans. Power Electronics*, vol. 32, no. 5, pp. 3490-3498, May 2017.

[60] V. M. Panchade, R. H. Chile, and B. M. Patre, “A survey on sliding mode control strategies for induction motors,” *Annual Reviews in Control*, vol. 37, no. 2, pp. 289–307, Dec. 2013.

[61] B. C. Toledo, S. D. Gennaro, A. G. Loukianov, and J. Rivera, “Discrete time sliding mode control with application to induction motors,” *Automatica*, vol. 44, no.12, pp. 3036–3045, Dec. 2008.

[62] J. Soltani, N. R. Abjadi, G. R. A. Markadeh, and H. W. Ping, “Adaptive Sliding-Mode control of a two five-phase series-connected induction motors drive,” in *Proc. Int. Conf. on Electrical Machines and Systems*, Seoul, South Korea, Oct. 2007, pp. 1496-1501.

[63] J. Soltani and M. A. Abbasian, “Robust nonlinear control of linear induction motor taking into account the primary end effects,” in *Proc. 5th Int. Power Electronics and Motion Control Conf*., Shanghai, China, vol. 2, Aug. 2006, pp. 1043-1048.

[64] J. Soltani, N. R. Abjadi, and G. R. A. Markadeh, “Nonlinear decoupled control for a six-phase series-connected two induction motor drive using the sliding-mode technique,” in *Proc. Int. Conf. on Power Electronics and Drive Systems*, Bangkok, Thailand, Nov. 2007, pp. 1267-1273.

[65] G. R. A. Markadeh and J. Soltani, “A current-based output feedback Sliding Mode control for speed sensorless induction machine drive using adaptive sliding Mode flux observer,” *International Journal of Engineering, Transactions A: Basics*, vol. 19, no. 1, pp. 21-34, Nov. 2006.

[66] J. Soltani, Y. Abdolmaleki, and M. Hajian, “Adaptive fuzzy sliding-mode control of speed sensorless universal field oriented induction motor drive with on-line stator resistance tuning,” *Iranian Journal of Science and Technology, Transaction B*: Engineering, vol. 29, no. 4, pp. 425-442, 2005.

[67] A. Markadeh, G. R. Yazdanpanah, and J. Soltani, “Input-output feedback linearization control of induction motor with adaptive backstepping observer,” *European Power Electronics and Drives Journal*, vol. 18, no. 2, pp. 33-40, April 2008.

[68] R. Yazdanpanah, J. Soltani, and G. R. Arab Markadeh, “Nonlinear torque and stator flux controller for induction motor drive based on adaptive input-output feedback

linearization and sliding mode control," *Energy Conversion and Management*, vol. 49, no. 4, pp. 541-550, April 2008.

[69] N. R. Abjadi, G. R. A. Markadeh, and J. Soltani, "Model following sliding-mode control of a six-phase induction motor drive," *Journal of Power Electronics*, vol. 10, no. 6, pp. 694-701, Nov. 2010.

[70] S. M. N Hassan and I. Hussain, "A laurenberger sliding mode observer for on line parameter estimation and adaptation in high performance induction motor drives," *IEEE Trans. Industry Applications*, vol. 45, no. 2, pp. 772-781, Mar./Apr. 2009.

[71] O. Kowalska, T. M. Dybkowski, and K. Szabat, "Adaptive sliding–mode neuro-fuzzy control of the two-mass induction motor drive without mechanical sensors," *IEEE Trans. Industrial Electronics*, vol. 57, pp. 553-564, Feb. 2010.

[72] S. A. Mir, D. S. Zinger, and M. E. Elbuluk, "Fuzzy controller for inverter fed induction machines," *IEEE Trans. Industry Applications*, vol. 30, no. 1, pp. 78-84, Jan./Feb. 1994.

[73] M. N. Uddin, M. A. Abido, and M. A. Rahman, "Development and implementation of a hybrid intelligent controller for interior permanent magnet synchronous motor drive," *IEEE Trans. Industry Applications*, vol. 40, no. 1, pp. 68–76, Jan./Feb. 2004.

[74] C. T. Lin and C. S. G. Lee, *Neural Fuzzy Systems: A Neuro–Fuzzy Synergism to Intelligent Systems*, Prentice Hall, Englewood Cliffs, NJ, 1996.

[75] M. N. Uddin and H. Wen, "Development of a self-tuned neuro–fuzzy controller for induction motor drives," *IEEE Trans. Industry Applications*, vol. 43, no. 4, pp. 1108–1116, Jul. 2007.

[76] M. N. Uddin and M. I. Chy, "A novel fuzzy logic controller based torque and flux controls of IPM synchronous motor," *IEEE Trans. Industry Applications*, vol. 46, no. 3, pp. 1220–1229, May/June 2010.

[77] N. Venkataramana Naik and S. P. Singh, "A comparative analytical performance of F2DTC and PIDTC of induction motor using DSPACE DS-1104," *IEEE Trans. Industrial Electron*ics, vol. 62, no. 12, pp. 7350 – 7359, Dec. 2015.

[78] T. Ramesh and A. K. Panda, "Type-2 fuzzy logic control based MRAS speed estimator for speed sensorless direct torque and flux control of an induction motor drive," *ISA Transactions*, vol. 57, pp. 262-275, July 2015.

[79] T. C. Huang and M. A. El-Sharkawi, "High performance speed and position tracking of induction motors using multi-layer fuzzy control," *IEEE Trans. Energy Conversion*, vol. 11, no. 2, pp. 353–358, Jun. 1996.

[80] C. C. Lee, "Fuzzy Logic in Control Systems: Fuzzy Logic Controller–Part I," *IEEE Trans. Systems, Man, and Cybernetics*, vol. 20, no. 2, pp. 404-418, Mar./Apr. 1990.

[81] P. Z. Grabowski, M. P. Kazmierkowski, B. K. Bose, and F. Blaabjerg, "A simple direct torque neuro fuzzy control of PWM inverter fed induction motor drive," *IEEE Trans. Industrial Electronics*, vol. 47, no. 4, pp. 863-870, Aug. 2000.

[82] J. S. R. Jang, "ANFIS: Adaptive-network-based fuzzy inference system," *IEEE Trans. Systems, Man, and Cybernetics*, vol. 23, no. 3, pp. 665-685, May/June 1993.

[83] M. N. Uddin, Z. R. Huang, and A. B. M. S. Hossain, "Development and implementation of a simplified self-tuned neuro–fuzzy-based IM drive," *IEEE Trans. Industry Applications*, vol. 50, no. 1, pp. 51–59, Jan./Feb. 2014.

[84] G. W. Chang, G. Espinosa-Perez, E. Mendes, and R. Ortega, "Tuning rules for the PI gains of field-oriented controllers of induction motors," *IEEE Trans. Industrial Electronics*, vol. 47, no. 3, pp. 592–602, June 2000.

[85] K. B. Mohanty, "Study of different controllers and implementation for an inverter-fed induction motor drive," Ph.D. dissertation, Dept. Elect. Eng., IIT Kharagpur, Kharagpur, India, 2005.

[86] C. W. De Silva, *Intelligent Control: Fuzzy Logic Applications*, CRC Press, Boca Raton, FL, 1995.

[87] J. Nie and D. Linkens, *Fuzzy-Neural Control: Principles, Algorithms and Applications*, Prentice-Hall, Englewood Cliffs, NJ, 1995.

[88] C. T. Lin and C. S. L. George, *Neural Fuzzy Systems*, Prentice-Hall, Englewood Cliffs, NJ, 1996.

[89] L. X. Wang, *A Course in Fuzzy Systems and Control*, Prentice-Hall, Englewood Cliffs, NJ, 1997.

[90] O. Omidvar and D. L. Elliott, *Neural Systems for Control*, Academic Press, Elsevier, USA, MA, 1997.

[91] F. J. Lin, R. J. Wai, and H. P. Chen, "A PM synchronous servo motor drive with an on-line trained fuzzy neural network controller," *IEEE Trans. Energy Conversion*, vol. 13, no. 4, pp. 319–325, Dec. 1998.

[92] F. J. Lin, W. J. Hwang, and R. J. Wai, "A supervisory fuzzy neural network control system for tracking periodic inputs," *IEEE Trans. Fuzzy Systems*, vol. 7, no. 1, pp. 41–52, Feb. 1999.

[93] F. J. Lin, R. F. Fung, and R. J. Wai, "Comparison of sliding mode and fuzzy neural network control for motor-toggle servomechanism," *IEEE Trans. Mechatronics*, vol. 3, no. 4, pp. 302–318, Dec. 1998.

[94] A. Rubaai, D. Ricketts, and M. D. Kankam, "Development and implementation of an adaptive fuzzy-neural-network controller for brushless drives," *IEEE Trans. Ind. Appl.*, vol. 38, no. 2, pp. 441–447, Mar./Apr. 2002.

[95] W. Y. Wang, Y. G. Leu, and C. C. Hsu, "Robust adaptive fuzzy-neural control of nonlinear dynamical systems using generalized projection update law and variable structure controller," *IEEE Trans. Systems, Man, and Cybernetics B*, vol. 31, no. 1, pp. 140–147, Feb. 2001.

[96] C. H. Wang, H. L. Liu, and T. C. Lin, "Direct adaptive fuzzy-neural control with state observer and supervisory controller for unknown nonlinear dynamical systems," *IEEE Trans. Fuzzy Systems*, vol. 10, no. 1, pp. 39–49, Feb. 2002.

[97] W. Y. Wang, M. L. Chan, C. C. Hsu, and T. T. Lee, "H Tracking-based sliding mode control for uncertain nonlinear systems via an adaptive fuzzy-neural approach," *IEEE Trans. Systems, Man, and Cybernetics B*, vol. 32, no. 4, pp. 483–492, Aug. 2002.

[98] Y. G. Leu, W. Y. Wang, and T. T. Lee, "Robust adaptive fuzzy-neural controllers for uncertain nonlinear systems," *IEEE Trans. Robotics and Automation*, vol. 15, no. 5, pp. 805–817, Oct. 1999.

[99] F. J. Lin and R. J. Wai, "Hybrid control using recurrent fuzzy neural network for linear induction motor servo drive," *IEEE Trans. Fuzzy Systems*, vol. 9, no. 1, pp. 102–115, Feb. 2001.

[100] R. J. Wai, "Hybrid fuzzy neural-network control for nonlinear motor-toggle servomechanism," *IEEE Trans. Control Systems Technology*, vol. 10, no. 4, pp. 519–532, Jul. 2002.

[101] R. J. Wai and C. C. Chu, "Robust Petri Fuzzy-Neural-Network Control for Linear Induction Motor Drive," *IEEE Trans. Industrial Electronics*, vol. 54, no. , pp. 177–188, Feb. 2007.

[102] A. Consoli, E. Cerruto, A. Raciti, and A. Testa, “Adaptive vector control of induction motor drives based on a neuro-fuzzy approach,” in *Proc. IEEE Power Electronics Specialists Conference (PESC)*, Taipei, Taiwan, June 1994, pp. 225–232.

[103] B. K. Bose, N. R. Patel, and K. Rajashekara, “A neuro-fuzzy based online efficiency optimization control of a stator flux-oriented direct vector controlled induction motor drive,” *IEEE Trans. Industrial Electronics*, vol. 44, no. 2, pp. 270–273, Apr. 1997.

[104] F. Rashidi, “Sensorless speed control of induction motor drives using a robust and adaptive neuro-fuzzy based intelligent controller,” in *Proc. IEEE Int. Conf. Industrial Technology (ICIT)*, Hammamet, Tunisia, Dec. 2004, pp. 617–627.

[105] P. Z. Grabowski and F. Blaabjerg, “Direct torque neuro-fuzzy control of induction motor drive, DSP implementation,” in *Proc. IEEE IECON*, Aachen, Germany, Aug. 1998, pp. 657–662.

[106] F. Lima, W. Kasier, I. N. da Silva, A. A. Azauri, and D. Oliveira, “Open-loop neuro-fuzzy estimator applied to vector and scalar induction motor drives,” *Applied Soft Computing*, vol. 21, pp. 469-480, April 2014.

[107] M. N. Uddin and H. Wen, “Model reference adaptive flux observer based neuro-fuzzy controller for induction motor drive,” in *Proc. Industry Applications Conference, IAS IEEE*, Hong Kong, China, Oct. 2005, pp. 1279–1285.

[108] M. Hafeez, M. N. Uddin, N. A. Rahim, and H. W. Ping “Self-tuned NFC and adaptive torque hysteresis-based DTC scheme for IM drive,” *IEEE Trans. Industry Applications*, vol. 50, no. 2, pp. 1410–1420, March/April 2014.

[109] V. I. Utkin, “Variable structure systems with sliding mode: A survey,” *IEEE Trans. Automatic Control*, vol. 22, no. 2, pp. 212-222, Apr. 1977.

[110] V. I. Utkin, “Sliding mode control design principles and applications to electric drives,” *IEEE Trans. Industrial Electronics*, vol. 40, no. 1, pp. 23-36, Feb. 1993.

[111] R. Soto and K. S. Yeung, “Sliding mode control of an induction motor without flux measurement,” *IEEE Trans. Industry Applications*, vol. 31, no. 4, pp. 744-751, July/Aug. 1995.

[112] K. K. Shyu and H. J. Shieh, “A new switching surface sliding mode speed control for induction motor drive systems,” *IEEE Trans. Power Electronics*, vol. 11, no. 4, pp. 660-667, July 1996.

[113] C. C. Chan and H. Q. Wang, "New scheme of sliding mode control for high performance induction motor drives," *IEE Proc. Electric Power Applications*, vol. 143, no. 3, pp. 177-185, May 1996.

[114] C. M. Young and C. H. Liu, "Discrete integral variable structure model following control for induction motor drives," *IEE Proc. Electric Power Applications*, vol. 143, no. 6, pp. 467-474, Nov. 1996.

[115] T. G. Park and K. S. Lee, "SMC-based adaptive input-output linearizing control of induction motors," *IEE Proc. Control Theory Applications*, vol. 145, no. 1, pp. 55-62, Jan. 1998.

[116] H. J. Shieh and K. K. Shyu, "Nonlinear sliding-mode torque control with adaptive backstepping approach for induction motor drive," *IEEE Trans. on Industrial Electronics*, vol. 46, no. 2, pp. 380-389, Apr. 1999.

[117] V. I. Utkin, J. guldner, and J. Shi, *Sliding mode control of electromechanical systems*, CRC Press, Taylor & Fransis, London, 1999.

[118] K. Jezernik, J. Korelic, and R. Horvat, "PMSM sliding mode FPGA based control for torque ripple reduction," *IEEE Trans. Power Electronics*, vol. 28, no. 7, pp. 3549-3556, Jul. 2013.

[119] R. Ling, D. Maksimovic, and R. Leyva, "second order sliding mode controlled synchronous buck dc-dc converter," *IEEE Trans. Power Electronics*, vol. 31, no. 3, pp. 2539-2549, Mar. 2016.

[120] H. U. Rehman and R. Dhaouadi, "A fuzzy learning–sliding mode controller fordirect field-oriented induction machines," *Neuro computing*, vol. 71, pp. 2693–2701, Aug. 2008.

[121] S. M. Gadoue, D. Giaouris, and J. W. Finch, "MRAS sensorless vector control of an induction motor using new sliding-mode and fuzzy-logic adaptation mechanisms," *IEEE Trans. Energy Conversion*, vol. 25, no. 2, pp. 394–402, June 2010.

[122] F. Barrero, A. Gonzalez, A. Torralba, E. Galvan, and L. G. Franquelo, "Speed control of induction motors using a novel fuzzy sliding-mode structure," *IEEE Trans. Fuzzy Systems*, vol. 10, pp. 375–383, June 2002.

[123] C. I. Huang, K. C. Hsu, H. H. Chiang, K. K. Kou, and T. T. Lee, "Adaptive fuzzy sliding-mode control of linear induction motors," in *Proc. Int. Conf. on Advanced Mechatronic Systems*, Tokyo, Japan, Sep. 2012, pp. 626–631.

[124] T. O. Kowalska, M. Dybkowski, and K. Szabat, “Adaptive sliding-mode neurofuzzy control of the two-mass induction motor drive without mechanical sensors,” *IEEE Trans. Industrial Electronics*, vol. 57, no. 2, pp. 553–564, Feb. 2010.

[125] R. J. Wai, “Adaptive enhanced fuzzy sliding-mode control for electrical servo drive,” *IEEE Trans. Industrial Electronics*, vol. 53, no. 2, pp. 569–580, Apr. 2006.

[126] O. Cerman and P. Husek, “Adaptive fuzzy sliding mode control for electrohydraulic servo mechanism,” *Expert Systems with Applications*, vol. 39, no. 11, pp. 10269–10277, Sep. 2012.

[127] C. C. Kung and K. H. Su, “Adaptive fuzzy position control for electrical servo drive via total-sliding-mode technique,” *IEE Proc. Electric Power Applications*, vol. 152, no. 6, pp. 1489–1502, Nov. 2005.

[128] R. J. Oentayo, M. J. Er, S. Linn, and X. Li, “Online probabilistic learning for fuzzy inference system,” *Expert Systems with Applications*, vol. 41, no. 11, pp. 5082–5096, Sep. 2014.

[129] R. Shahnazi, H. M. Shanechi, and N. Pariz, “Position control of induction and DC servomotors: A novel adaptive fuzzy PI sliding mode control,” *IEEE Trans. on Energy Conversion*, vol. 23, no. 1, pp. 138–147, Mar. 2008.

[130] A. Chitra and S.Himavathi, “Investigation and analysis of high performance green energy induction motor drive with intelligent estimator,” *Renewable Energy*, vol. 87, pp. 965-976, Mar. 2016.

[131] S. Jia-Min, J. Hurng-Liahng, W. Jinn-Chang, and W. Kuen-Der, “Single-phase three-wire grid-connected power converter with energy storage for positive grounding photovoltaic generation system*,” Int. Jour. of Electrical Power & Energy Systems*, vol. 54, pp. 134-143, Jan. 2014.

[132] A. K. Panda and N. Patnaik, “Combined operation of a new power angle control unit vector template based unified power quality conditioner and fuel cell stack supply with effective utilization of shunt and series inverter,” *Electric Power Components and Systems*, vol. 44, no.18, pp. 2048–2058, Oct. 2016.

[133] L. M. Fernandez, P. Garcia, C. A. Garcia, and F. Jurado, “Hybrid electric system based on fuel cell and battery and integrating a single dc/dc converter for a tramway,” *Energy Conversion and Management*, vol. 52, no. 5, pp. 2183–2192, May. 2011.

[134] Q. Li, W. Chen, S. Liu, Z. You, and S. Tao, "Power management strategy based on adaptive neuro-fuzzy inference system for fuel cell-battery hybrid vehicle," *J. Renewable and Sustainable Energy*, vol. 4, pp. 013106, Feb. 2012.

[135] S. J. Ovaska and S. Valiviita, "Angular acceleration measurement: A review," *IEEE Trans. Instrumentation and Measurement*, vol. 47, no. 5, pp. 1211–1217, Oct. 1998.

[136] P. B. Schmidt and R. D. Lorenz, "Design principles and implementation of acceleration feedback to improve performance of DC drives," *IEEE Trans. Industry Applications*, vol. 28, no. 3, pp. 594–599, May/June 1992.

[137] K. P. Venugopal, R. Sudhakar, and A. S. Pandya, "An improved scheme for direct adaptive control of dynamical systems using back propagation neural networks," *J. Circuits, Systems and Signal Processing*, vol. 14, no. 2, pp. 213–236, Mar. 1995.

[138] M. H. N. Talib, Z. Ibrahim, N. A. Rahim, A. S. A. Hasim, "Comparison analysis of indirect FOC induction motor drive using PI, anti-windup and pre-filter schemes," *Int. Jour. of Power Electronics and Drive Systems*, vol. 5, no. 2, pp. 219-229, 2014.

[139] *Matlab*, Simulink User Guide, The MathWorks Inc., Natick, MA, USA, 2003.

[140] H. Kubota, K. Matsuse, and T. Nakano, "DSP-based speed adaptive flux observer of induction motor*," IEEE Trans. Industry Applications*, vol. 29, pp. 344-348, Mar./Apr. 1993.

[141] A. Ammar, A. Bourek, and A. Benakcha, "Nonlinear SVM-DTC for induction motor drive using input-output feedback linearization and high order sliding mode control," *ISA Transactions*., vol. 67, pp. 428–442, Mar. 2017.

[142] G. Durgasukumar and M. K. Pathak, "Comparison of adaptive neuro-fuzzy based space vector modulation for two-level inverter," *Int. Jour. of Electrical Power & Energy Systems*, vol. 38, no. 1, pp. 9-19, Jun. 2012.

[143] N. Venkataramana Naik, J. Thankachan, and S. P. Singh, "A neuro-fuzzy direct torque control using bus-clamped space vector modulation," *IETE Technical Review*, vol. 33, no. 2, pp. 205-217, Aug. 2015.

[144] X. Duan, H. Deng, H. Li, and H. xiong, "A Saturation-based tuning method for fuzzy PID controller," *IEEE Trans. Industrial Electronics*, vol. 60, no. 11, pp. 577–585, Nov. 2013.

[145] *DSP controllers reference guide*, System and Peripherals, Texas, USA, 2001.

[146] A. Rubaai, J. Jerry, and S. T. Smith, "Performance evaluation of fuzzy switching position system controller for automation and process industry control," *IEEE Trans. Industry Applications*, vol. 47, no. 5, pp. 2274–2282, Sept./Oct. 2011.

[147] K. J. Astrom and T. Hagglund, *PID Controllers: Theory, Design, and Tuning*," Sec. Ed., Research Triangle Park, Instrument Society of America, The International Society for Measurement and Control, pp. 166, 1995.

[148] S. Masumpoor, H. Yaghobi, M. A. Khanesar, "Adaptive sliding-mode type-2 neuro-fuzzy control of an induction motor," *Expert Systems with Applications*, vol. 42, no. 19, pp. 6635-6647, Nov. 2015.

[149] H. A. Sher and K. E. Addoweesh, "Power storage options for hybrid electric vehicles-A survey," *J. of Renewable and Sustainable Energy*, vol. 4, no. 5, pp. 052701, Sept. 2012.

[150] M. K. Kazimierczuk, *Pulse-width modulated DC-DC power converters*, John Wiley & Sons, Chichester, UK, 2008.

[151] MathWorks, Electric Drives, "file:///C:/Program%20Files/MATLAB/R2013a/help/physmod/powersys/ug/advanced-users-retune-the-drive-parameters.html".

[152] J. Dalei, and K. B. Mohanty, "An approach to estimate and control SEIG voltage and frequency using CORDIC algorithm," *Transaction of the Institute of Measurement and Control*, (DOI: 10.1177/0142331215621374).

Appendix A

Ratings and Specifications of the Drive System

A.1 Induction Motor

Table A.1 Induction motor nominal parameters

Rated power	P_n	3.7 kW
Rated line voltage	V_n	415 V
Rated speed	n_r	1445 rpm
Rated frequency	f_n	50 Hz
No. of pole pairs	P	2
Stator resistance	R_s	7.34 Ω
Stator leakage inductance	L_{ls}	0.021 H
Rotor resistance	R_r	5.64 Ω
Rotor leakage inductance	L_{lr}	0.021 H
Mutual inductance	L_m	0.5 H
Friction coefficient	B	0.035 kg-m^2/s
Inertia coefficient	J	0.16 kg-m^2

A.2 Fuel Cell based Drive

Table A.2 Fuel cell parameters

Rating	P_{fr}-V_{fdc}	4kW-175 V
Operating voltage	V_{fo}	400 V
No of FC stack	N	500

Table A.3 DC/DC Boost converter parameters

Inductance	L	3 mH
Capacitance	C_1	200 μF
Switching frequency	f_{sw}	5 kHz
Duty cycle	D	50%

Table A.4 Braking chopper parameters

Shutdown voltage	V_{sh}	600 V
Activation voltage	V_{act}	650 V
Braking resistance	R_{br}	113.3 Ω

Table A.5 DC link parameters

DC link voltage	V_{dc}	560.25 V
DC link capacitor	C_{dc}	221 μF

Appendix B

Devices used for Experimental Prototype

B.1 Intelligent Power Module (IPM)

IPM is based on third-generation IGBT and DIODE technology and is designed for motor control applications.

Table B.1 Nominal parameters IPM (PEC16DSM01)

3-phase supply	460 V
DC link voltage	750 V
IGBT	1200 V/25 A
IGBT for over voltage breaking	1200 V/10 A
DIODE	1200 V/60 A
Dead time	6 μs
Fault terminal max. output voltage	3.3 V
Max. speed terminal voltage	2.6 V
PWM amplitude	5 V
Output fault current	20 mA

- **Features of IPM:**
  - AC-DC power conversion by bridge converter
  - Hall Effect voltage sensor (1 No) and current sensors (4 Nos) for sensing DC link voltage and currents, respectively
  - Bridge inverter three output currents
  - Opto Isolator to isolate all PWM signals
  - Overcurrent protection circuit
  - Independent power supplies for all isolated circuits
  - Interfacing with DSP controllers by FRC connector

B.2 Digital Signal Processor (DSP) Controller

The control strategies of the drive system are implemented by a cost-effective, algorithm developed based motor control application 32-bit fixed point DSP Processor. The current controlled PWM signals are generated by the DSP board which are required to be fed to the six switches of the IPM through the connector provided on the front panel.

Table B.2 Specifications of DSP (TMS320F2812) controller

Clock frequency	150 MHz
Resolution of ADC	16 channel, 12-bit
Input voltage range of ADC	0-3 V

- **Features of DSP:**
  - Useful peripherals such as ADC, DAC, Timer and PWM generation block
  - PWM outputs (16 Nos)
  - Quadrature encoder interface (2 Nos)
  - User program development and debugging
  - Compatible serial port (1 No RS232)
  - Inputs of ADC are protected and terminated at 26 pin FRC connector
  - On Board 12-bit DAC
  - Parallel interface with the controller
  - ±5 V bipolar output

B.3 Voltage Sensor

Hall Effect voltage sensor (LEM LV 25-P) senses the terminal voltage of IM and scales down to the ADC input voltage range, i.e., 0-3 V. A current signal proportional to the measured voltage is collected across the external resistance. The output of voltage sensor is processed through an ADC interface card and is fed to the input of on-chip ADC of DSP controller.

Table B.3 Specifications of Voltage sensor

Nominal primary current	10 mA
Nominal secondary current	25 mA
Supply voltage	±12-15 V
Conversion ratio	2500:1000
Response time	40 μs

B.4 Current Sensor

Hall-effect current sensors (LEM LTS 25-NP) sense the actual motor line currents, which are fed to the DSP board through A/D channels.

Table B.4 Specifications of Current sensor

Nominal primary current	50 A
Nominal secondary current	50 mA
Supply voltage	± 12-15 V
Conversion ratio	1:1000
Response time	< 1 μs
Reaction time	< 500 μs

B.5 Speed Sensor

Table B.5 Specifications of Speed sensor

Supply voltage	± 4.5-5.5 V
Supply current	50-70 mA
Amplitude of pulse output	512 ppr

Dissemination

Journals:

[1] **R. N. Mishra** and K. B. Mohanty, "Design and realization of an auto-tuned modified neuro-fuzzy sliding-mode-based IM drive deploying feedback linearization," *European Power Electronics and Drives* (*Taylor and Francis*), vol. 28, no. 1, pp. 28-42, Jan. 2018.

[2] **R. N. Mishra** and K. B. Mohanty, "Design and implementation of a feedback linearization controlled IM drive via simplified neuro-fuzzy approach," *IETE Journal of Research* (*Taylor and Francis*), vol. 64, no. 2, pp. 209-230, July 2017.

[3] **R. N. Mishra** and K. B. Mohanty, "Development of a hybrid fuel cell system operated simplified neuro-fuzzy sliding-mode control based IM drive deploying linearization approach: An effort to enhance the performance," *Journal of Renewable and Sustainable Energy* (*American Institute of Physics*), DOI: 10.1063/1.4989796, Dec. 2017.

[4] **R. N. Mishra** and K. B. Mohanty, "Implementation of feedback linearization modelled induction motor drive through an adaptive simplified neuro-fuzzy approach," *Sadhana* (*Springer*), vol. 42, no. 12, pp. 2113-2135, Dec. 2017.

[5] **R. N. Mishra** and K. B. Mohanty, "Real time implementation of an ANFIS-based induction motor drive via feedback linearization for performance enhancement," *Engineering Science and Technology, an International Journal* (*Elsevier*), vol. 19, no. 4, pp. 1714-1730, Dec. 2016.

Conferences:

[1] K. B. Mohanty and **R. N. Mishra**, "Robust modified structured NFC integrating with GA for linearized induction motor drive," in *Proc. 15th IEEE International Workshop on Advanced Motion Control (AMC)*, Tokyo, Japan, 2018, pp. 193-197.

[2] **R. N. Mishra**, K. B. Mohanty, K. Thakre, and A. K. Nayak, "Modelling and design of a modified neuro-fuzzy control-based IM drive via feedback linearization," in *Proc. 7th Power India Int. Conf.* (*PIICON*), Bikaner, 2016, pp. 1-6.

[3] **R. N. Mishra**, K. B. Mohanty, P. Ray, and D. P. Mishra, "A reduced MF-based self-tuned robust neuro-fuzzy control of a decoupling linearized IM Drive," in *Proc. Int. Conf. on Next Generation Intelligent Systems* (*ICNGIS*), Kerala, 2016, pp. 1-6.

[4] **R. N. Mishra** and K. B. Mohanty, "Performance enhancement of a linearized induction motor drive using ANFIS based torque controller," in *Proc. 12th Annual IEEE India Conf.* (*INDICON*), New Delhi, 2015, pp. 1-6.

[5] **R. N. Mishra**, K. B. Mohanty, K. Thakre, and P. R. Sahu, "Design of a simplified neuro-fuzzy-GA-based IM drive deploying linearization approach," presented at the *14th Annual IEEE India Conf. (INDICON)*, IIT, Roorkee, Dec. 15-17, 2017.